BIOSURFACTANTS: FROM RENEWABLE RESOURCES TO INNOVATIVE APPLICATIONS

EDITED BY: Murat Ozdal, Tomasz Janek and Surekha K. Satpute
PUBLISHED IN: Frontiers in Bioengineering and Biotechnology

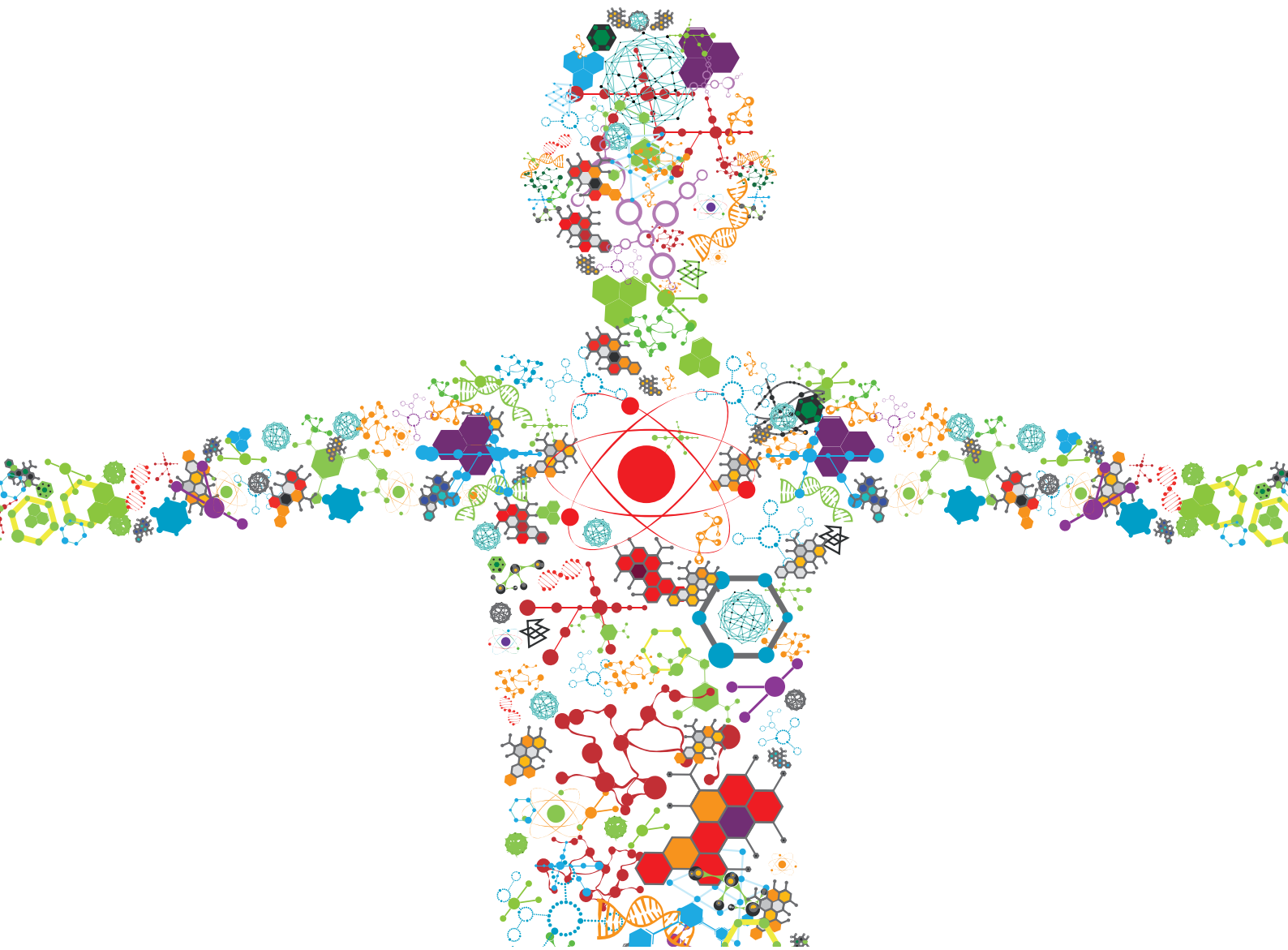

frontiers Research Topics

ISSN 1664-8714
ISBN 978-2-83250-031-6
DOI 10.3389/978-2-83250-031-6

About Frontiers

Frontiers is more than just an open-access publisher of scholarly articles: it is a pioneering approach to the world of academia, radically improving the way scholarly research is managed. The grand vision of Frontiers is a world where all people have an equal opportunity to seek, share and generate knowledge. Frontiers provides immediate and permanent online open access to all its publications, but this alone is not enough to realize our grand goals.

Frontiers Journal Series

The Frontiers Journal Series is a multi-tier and interdisciplinary set of open-access, online journals, promising a paradigm shift from the current review, selection and dissemination processes in academic publishing. All Frontiers journals are driven by researchers for researchers; therefore, they constitute a service to the scholarly community. At the same time, the Frontiers Journal Series operates on a revolutionary invention, the tiered publishing system, initially addressing specific communities of scholars, and gradually climbing up to broader public understanding, thus serving the interests of the lay society, too.

Dedication to Quality

Each Frontiers article is a landmark of the highest quality, thanks to genuinely collaborative interactions between authors and review editors, who include some of the world's best academicians. Research must be certified by peers before entering a stream of knowledge that may eventually reach the public - and shape society; therefore, Frontiers only applies the most rigorous and unbiased reviews.
Frontiers revolutionizes research publishing by freely delivering the most outstanding research, evaluated with no bias from both the academic and social point of view. By applying the most advanced information technologies, Frontiers is catapulting scholarly publishing into a new generation.

What are Frontiers Research Topics?

Frontiers Research Topics are very popular trademarks of the Frontiers Journals Series: they are collections of at least ten articles, all centered on a particular subject. With their unique mix of varied contributions from Original Research to Review Articles, Frontiers Research Topics unify the most influential researchers, the latest key findings and historical advances in a hot research area! Find out more on how to host your own Frontiers Research Topic or contribute to one as an author by contacting the Frontiers Editorial Office: frontiersin.org/about/contact

BIOSURFACTANTS: FROM RENEWABLE RESOURCES TO INNOVATIVE APPLICATIONS

Topic Editors:
Murat Ozdal, Atatürk University, Turkey
Tomasz Janek, Wroclaw University of Environmental and Life Sciences, Poland
Surekha K. Satpute, Savitribai Phule Pune University, India

Citation: Ozdal, M., Janek, T., Satpute, S. K., eds. (2022). Biosurfactants: From Renewable Resources to Innovative Applications. Lausanne: Frontiers Media SA. doi: 10.3389/978-2-83250-031-6

Table of Contents

frontiers | Frontiers in Bioengineering and Biotechnology

TYPE Editorial
PUBLISHED 11 August 2022
DOI 10.3389/fbioe.2022.988646

OPEN ACCESS

EDITED AND REVIEWED BY
Georg M. Guebitz,
University of Natural Resources and Life Sciences Vienna, Austria

*CORRESPONDENCE
Murat Ozdal,
mozdal@atauni.edu.tr,
murat.ozdal@yahoo.com
Tomasz Janek,
tomasz.janek@upwr.edu.pl
Surekha K. Satpute,
satputesk@unipune.ac.in,
drsurekhasatpute@gmail.com

SPECIALTY SECTION
This article was submitted to Industrial Biotechnology, a section of the journal Frontiers in Bioengineering and Biotechnology

RECEIVED 07 July 2022
ACCEPTED 20 July 2022
PUBLISHED 11 August 2022

CITATION
Ozdal M, Janek T and Satpute SK (2022), Editorial: Biosurfactants: From renewable resources to innovative applications.
Front. Bioeng. Biotechnol. 10:988646.
doi: 10.3389/fbioe.2022.988646

Editorial: Biosurfactants: From renewable resources to innovative applications

Murat Ozdal[1]*, Tomasz Janek[2]* and Surekha K. Satpute[3]*

[1]Department of Biology, Science Faculty, Ataturk University, Erzurum, Turkey, [2]Department of Biotechnology and Food Microbiology, Wrocław University of Environmental and Life Sciences, Wrocław, Poland, [3]Department of Microbiology, Savitribai Phule Pune University, Pune, India

KEYWORDS

biosurfactant, applications, pathogens, fermentation, nanoparticle

Editorial on the Research Topic
Biosurfactants: From renewable resources to innovative applications

The Research Topic entitled "*Biosurfactants: From Renewable Resources to Innovative Applications*" has meticulously contributed original research and review articles towards pioneering applications of biosurfactant/s (BSs) in plentiful areas like medical, pharmaceutical, agriculture, bioremediation, waste-water treatment, etc.

The multifarious functional potential, phase behaviour, huge structural diversity, biodegradable and eco-friendly nature of BSs offer enormous opportunities to explore them for innovative applications. Emphasis on employment of appropriate, precise, accurate methodologies are mandatory to achieve effective isolation, production, extraction and characterization of BSs. Continuous efforts are desirable in the BSs fermentation processes to develop commercially sound technology. Nevertheless, challenges like requirement of desirable microbial strains, growth substrates, high monetary inputs, downstream processing etc. hinder the economical production of BS. Legalizing the BSs production technology through vigorous experimental conditions are indispensable. Genome mining studies offer new-fangled avenues of BSs producers for benefit of mankind.

The various articles published under this Research Topic deliver guiding principles and vital operating protocols to elevate the production of BSs from diverse microorganisms. Contributors have portrayed putative ground-breaking applications of BSs in varied industries. Review article of Salek et al. showcased extensive uses of rhamnolipids (RL), sophorolipids (SL), mannosylerythritol lipids (MEL) and cellobiose lipids (CL) in medical, agriculture, bioremediation, food, detergent, household-care agents and clean-up strategies.

Regardless of the empathetic knowledge of BS molecule; there is a prerequisite to investigate the process at the bioreactors level to establish economical level production. Beck et al. reported MEL fermentation from *Moesziomyces aphidis* in a bioreactor with monitoring of kinetics for process parameters (substrate consumption rates, product formation rates). An enhanced level of biomass along with yield of MEL has been achieved

successfully through an exponential fed-batch approach. Another research group of Oraby et al. has optimized fermentation process for CL from Ustilaginaceae sp. using modelling and techno-economic studies.

The purification process of microbial metabolites has a prodigious impact on monetary inputs and further their applicability. Till today, plentiful procedures have been employed to produce and purify BS. Conventionally, the freeze-drying technique is employed to produce lipopeptides from *Bacillus subtilis*. Vassaux et al. have operated the spray-drying process to purify three lipopeptides - surfactin, mycosubtilin and plipastatin without affecting their antimicrobial and surfactant potential. Therefore, the proposed innovative technique can replace the conventional freeze-drying steps from an industrial perspective.

Indigenous microbes dwelling in oil/hydrocarbon/metal-polluted sites attain incredible potential to utilize those resources as compared to non-native entities. The genomic analysis of BS producing microbes from such habitats is imperious to improve future production processes and discovery of bioactive compounds of industrial interest. Yasmin et al. reported genome studies of BS producing *B. subtilis* strains. Researches have revealed protein-coding genes responsible for virulence, metal or multidrug resistance, flagella assembly, biosynthesis of secondary metabolites along with their role in emulsification, utilization and degradation of oil. The distinctness in gene operons and their involvement in the biosynthesis of surfactin along with their efficiency in degradation of oil has been explained in this article.

Removal of inorganic-based contaminants from soils and water bodies is extremely challenging. The existing remediation techniques are insufficient to manage and remove the pollutants completely. Nanoparticles (NPs), due to their extraordinary physico-chemical and functional properties have been utilized for remediation purposes. Moura et al. have demonstrated an attractive and low-cost green approach for remediation of contaminated water. Researchers have presented the functionalization of zero-valent iron (nZVI) with RL to remove inorganic pollutants from simulated groundwater. The role of RL in reducing the aggregation tendency of NP and removal of nitrate form contaminated water has been explained deeply.

BSs pose their candidature to deal with dreaded diseases like cancer. Till today, several studies have been reported for anticancer activity of RL. However, few studies have included triple-negative breast cancer. Additionally, the mechanistic role of RLs detailing molecular aspects has not been revealed completely. Mishra et al. have demonstrated noticeable anticancer activity of *Pseudomonas aeruginosa* origin RL against breast cancer cell lines. The radical scavenging activity of RL affects the cell line through the inhibition of p38 MAPKs. Targeting p38 for anticancer therapy is imperative due to its involvement in signalling pathways. Around 12 different congeners have been explored for anticancer activity of RL.

Worldwide, the agriculture sector is under continuous coercion to enhance productivity and meet the ever-rising food demands of the escalating population. The various factors (climate change, pesticide resistance etc.) lead to the emergence of pathogens in plants and reduce crop productivity. Additionally, humans are adversely impacting the environment through the use of enormous amounts of agrochemicals and intensive agronomic practices. Therefore, it is obligatory to develop an eco-friendly sustainable approach to deal the challenges. Karamchandani et al. has demonstrated antimicrobial activities of chitosan, chitosan NPs and BS singly and in combinations against selected phytopathogens. This work has led a strong hope to develop nano-formulation for sustainable and green agriculture. Like bacteria, filamentous fungi also proficiently produce several fungicidal compounds including BSs. Piegza et al. have used *Trichoderma citrinoviride* for production of BS in media accompanied by lytic enzymes inducers. Biocontrol potential of fungal derived BS has been demonstrated in this research article.

In summary, the valuable research presented in this thematic issue clearly demonstrated that breakthrough approaches are mandatory in the isolation, extraction and recovery of BS from various microbial sources. Selection of suitable microbial producers along with cheap or renewable agro-industrial substrates under precise optimizing fermentation parameters could lead not only great success at large-scale but also an economical production of BS. Further, BSs can be used singly or in combinations due to their functional potential in defeating dreaded pathogens or against cancer. Elucidation of mechanisms at biochemical, cellular levels along with preclinical or nonclinical studies is mandatory to broaden the applications of BSs. Information on the structure and function relationship of pure and/or a mixture of BSs would be undoubtedly obliging to recommend their many more extraordinary applications. Overall, the considerate knowledge about the innovative production technology, detailed physicochemical properties, innovative applications, molecular level studies of BSs have been contributed magnificently by the scientific fraternity.

Author contributions

MO was a guest associate editor of the Research Topic. TJ was a guest associate editor of the Research Topic and edited the text. SS was a guest associate editor of the Research Topic and wrote the paper text.

Funding

TJ gratefully acknowledge the financial support from the National Science Centre, Poland, project 2020/37/B/NZ9/01,519. SKS acknowledge the financial support from Savitribai Phule Pune University, India and Rashtriya Uchchatar Shiksha Abhiyan, Maharashtra, India RUSA-CBS-TH-3.2.

Acknowledgments

We thank authors of the papers published in this Research Topic for their valuable contributions and the referees for their rigorous review.

Conflict of interest

The authors declare that the research was conducted in the absence of any commercial or financial relationships that could be construed as a potential conflict of interest.

Publisher's note

frontiers in Bioengineering and Biotechnology

ORIGINAL RESEARCH
published: 23 November 2021
doi: 10.3389/fbioe.2021.778701

Trichoderma citrinoviride: Anti-Fungal Biosurfactants Production Characteristics

Michał Piegza, Kamil Szura and Wojciech Łaba*

Department of Biotechnology and Food Microbiology, Wrocław University of Environmental and Life Scinces, Wrocław, Poland

The mechanism of direct impact of *Trichoderma* fungi on other organisms is a multilayer process. The level of limiting the growth of other microorganisms is determined by the strain and often by the environment. Confirmation of the presence of extracellular biosurfactants in certain strains of *Trichoderma* considered as biocontrol agents was regarded as a crucial topic complementing the characterization of their interactive mechanisms. Selected strains of *T. citrinoviride* were cultured in media stimulating biosurfactant biosynthesis, optionally supplemented with lytic enzyme inducers. Results confirmed the anti-fungal properties of surface-active compounds in the tested culture fluids. Preparations that displayed high fungal growth inhibition presented marginal enzymatic activities of both chitinases and laminarinases, implying the inhibitory role of biosurfactants. Fractions from the foam of the culture fluid of the C1 strain, cultured on Saunders medium, and HL strain on MGP medium, without an additional carbon source, exhibited the most prominent ability to inhibit the growth of phytopathogens. Filamentous fungi capable of producing fungicidal compounds, including surfactants, may find applications in protecting the plants against agri-food pathogenic molds.

Keywords: T. citrinoviride, biosurfactant, biocontrol, anti-fungal activities, surface, active agent

OPEN ACCESS

Edited by:
Murat Ozdal,
Atatürk University, Turkey

Reviewed by:
Andrew Spiers,
Abertay University, United Kingdom
Sonja Kubicki,
Heinrich Heine University of Düsseldorf, Germany

****Correspondence:***
Michał Piegza
michal.piegza@upwr.edu.pl

Specialty section:
This article was submitted to Industrial Biotechnology, a section of the journal Frontiers in Bioengineering and Biotechnology

Received: *17 September 2021*
Accepted: *02 November 2021*
Published: *23 November 2021*

Citation:
Piegza M, Szura K and Łaba W (2021) Trichoderma citrinoviride*: Anti-Fungal Biosurfactants Production Characteristics. Front. Bioeng. Biotechnol. 9:778701. doi: 10.3389/fbioe.2021.778701*

INTRODUCTION

In recent years, plant protection has become the dominant field for biological control. The application of living organisms as pesticides has become a vital alternative to the standard use of their chemical equivalents. The use of traditional pesticides tends to be severely limited due to numerous undesirable effects on human health and the environment (Thomas and Willis, 1998). Some of the microorganisms inhabiting the soil, in particular the rhizosphere, displayed the ability to control the expansion of plant pathogens (Sjingh et al., 2007). The term "biological control" has been diversely defined by various biologists, and the first definitions focused on the use of predators and insect parasites to combat other organisms. In the agricultural industry, the activity limiting the development of pathogens has been noticed among many species of bacteria and filamentous fungi. The ability of biological control over microorganisms is attributed not only to the competition for nutrients or the biosynthesis of lytic enzymes (Piegza et al., 2014) but also to other compounds secreted into the medium, including those of a biosurfactant nature (Banat et al., 2000).

The genus *Trichoderma* itself was proposed for the application in biocontrol due to the fact that these fungi are effective producers of extracellular hydrolases, including chitinases and glucanases (Harman, 2006). Majority of *Trichoderma* species have been extensively evaluated in terms of both the produced compounds and their genome sequences (Schuster and Schmoll, 2010). The *Trichoderma citrinoviride* C1 strain, formerly known as *T. hamatum* C1, has been the target of

research on the directional use in the protection of plants against pathogens for many years. The beginning of this type of experiments dates back to the 1980s, and the results indicated the antagonistic behavior of *T. hamatum* in relation to other species of filamentous fungi (Chet et al., 1981). In subsequent years, the research focused mainly on determining the ability of this strain to produce lytic enzymes (CWDE—cell wall degrading enzymes), predominantly chitinases and β-1,3-glucanases, causing the degradation of pathogen cell walls as the main mechanisms of interaction with fungal pathogens (Witkowska and May 2002; Witkowska et al., 2009; Piegza et al., 2015; Piegza et al., 2016). It is worth to emphasize that *T. citrinoviride* C1 can facilitate efficient biotransformation, e.g., cortexolone to 1-dehydrocortexolone through 1-dehydrogenation (Bartmańska and Dmochowska-Gładysz, 2007). Recent studies have also indicated the mycoparasite activity of this species against the pathogens of the ginseng plant (*Panax ginseng*). The inhibitory effect concerning *Botrytis cinerea* is probably due to its ability to inhibit the expression of *B. cinerea* genes responsible for growth and virulence. On the other hand, stimulating the expression of ginseng genes is related to the response to pathogens, and the production of phytohormones and extracellular enzymes that degrade the pathogen cell walls is also considered (Park et al., 2019). *Trichoderma citrinoviride* exhibits a potential towards biological control as its high larvicidal and ovicidal activity has been verified against the parasitic cotton root nematode *Meloidogyne incognita* (Fan et al., 2020). Moreover, there is available reference that confirms the ability of *T. citrinoviride* isolated from rotting algae to inhibit and inactivate the toxic cyanobacteria *Microcystis aeruginosa* (Mohamed et al., 2014). The complexity of biocontrol mechanisms means that the discovery of any additional factor that may affect the correlation between organisms inspires thorough study. Such a factor was the confirmation that *T. citrinoviride* strains are capable of biosurfactants biosynthesis (Piegza et al., 2021).

The antibiotic activity of biosurfactants produced by microorganisms may play the role in competition, pathogenesis, and self-protection. At the same time, however, deepening knowledge of their chemical structure and mode of action seems important for medicine or industry. Also, information on their antiprotozoal, anti-cancer, and potentially weakening biofilms is relatively sparse (Markande et al., 2021). By modifying the liquid surface tension, biosurfactants may enhance the bioavailability of exogenous compounds, such as nutrients, by increasing their absorption, and endogenous metabolites, including phenazine antibiotics, resulting in their increased biological activity. Additionally, microbial surface-active compounds may help to protect plants against pathogens (D'aes et al., 2010). Due to their amphiphilic nature, they can interact with biological membranes, which also consist essentially of amphiphilic lipid bilayers. This enables the activity of biosurfactants as cytolytic agents with a broad spectrum of activity, due to the capability of cell membrane disruption and, as a result, inactivation of bacteria, fungi, oomycetes, and neutralization of viruses (Hutchinson and Johnstone, 1993). Microbial biosurfactants are usually characterized by the specificity of action towards particular microorganisms. These differences in the activity are attributed to the structural properties of both the surfactant and the cell membrane of the affected microorganism (D'aes et al., 2010). The first experimental observations of brown spots induced on edible mushrooms by *P. tolaasii*, as a result of pore formation in cell membranes and surface-active properties of tolaasin, indicated that these compounds may be responsible for antagonistic interactions between microorganisms (Hutchinson and Johnstone, 1993; Saikia et al., 2021).

The aim of the study was to assess the ability of selected *Trichoderma citrinoviride* strains towards the production of biosurfactants that accompany lytic enzymes, with properties limiting the development of pathogenic filamentous fungi. For this purpose, the surface tension was evaluated in culture fluids, enzymatic activities were determined, and inhibitory potential was assessed against phytopathogenic fungi, in relation to the composition of culture media.

MATERIALS AND METHODS

The research involved filamentous fungi from the collection of the Department of Biotechnology and Food Microbiology of the Wrocław University of Environmental and Life Sciences: *T. citrinoviride* C1, *T. citrinoviride* HL, and *T. citrinoviride* B3 (Piegza et al., 2021).

Cultures were carried out in 250 ml Erlenmeyer flasks containing 50 ml of medium. Each tested strain was cultured in Mineral-Glucose-Peptone (MGP) (M) medium (Piegza et al., 2021) or Saunders medium (S), optionally supplemented with 6 g/L yeast biomass (dry biomass of *Saccharomyces* sp. and *Yarrowia* sp. equal) and 10 g/L mushroom biomass (dry biomass of champignon and *Fusarium* sp—4:1) that served as an inducer and a source of carbon (Mx and Sx, respectively). The cultivation was carried out for 5 days under agitation at 160 rpm, at 25°C (Advanced ADS10000, VWR, USA), and the post-culture fluids of each variant were collected.

Surface tension measurements were performed immediately after the collection of culture fluids. For this purpose, the tear-off method was used, based on the measurement of force necessary to detach the ring from the surface of the liquid (Rakowska and Porycka, 2009; Piegza et al., 2021). The measurements were performed on a Krüss K6 manual tensiometer, at room temperature.

From each culture fluid variant three fractions were analyzed: the raw culture fluid (R), foam obtained from a culture fluid (F), and the residue after foaming (FR).

Phytopathogenic fungi (*Lecanicillium lecanii*, *Fusarium sporotrichioides*, *Penicillium* spp, *Rhizopus nigricans*, *Aspergillus niger CZ*, *Paecilomyces variotii DSM 1961*, *Botrytis cinerea 5s*, *Fusarium culmorum*, *Mucor hiemalis*, *Epicoccum nigrum*, *and Fusarium poae 1*) were deep inoculated into PDA medium (Difco). The 6-mm-diameter wells were cut into each plate with a plug, and 100 µL of a specific culture fluid fraction was introduced into the wells. The test was performed for the fluids of each of the three tested *Trichoderma citrinoviride* strains, obtained in Saunders medium (S), Saunders medium enriched

TABLE 1 | Surface tension measurements (mN/m) in post-culture fluid, (M) MGP medium, (S) Saunders medium, (Mx) MGP medium with inductors, (Sx) Saunders medium with inductors.

Trichoderma citrinoviride	Culture medium [mN/m]			
Strain	S	Sx	M	Mx
C1	32	34	37	35
HL	36	34	37,5	35
B3	32	35	38	35
H_2O	72	72	72	72
Control	68	67	68	67

with yeast biomass (inductors) (Sx), MGP medium (M), and MGP medium enriched with yeast biomass (inducers) (Mx). The plates were incubated for 7 days at 4°C. After incubation, the effect of metabolites present in the culture fluids on the growth inhibition of phytopathogenic fungi was determined. For this purpose, clear zones were measured around the wells in which no fungal growth was observed. The zone of inhibition was compared with the growth of filamentous fungi around the wells of the plates where 100 µL of distilled water was introduced into the wells.

Laminarinases and chitinases activities were assayed in each fluid fraction with the DNS method, using laminarin and chitin, respectively, substrates, by running the enzymatic reaction for 30 min at 50 °C and pH 5.0. Reaction products, i.e., glucose in the case of laminarinases and glucosamine in the case of chitinases, were determined colorimetrically using dinitrosalicylic acid (Sigma) (Piegza et al., 2016), in order to determine the effect of enzymes on the inhibition of the test filamentous fungi.

Statistical analysis: One-way analysis of variance (ANOVA) was applied along with Duncan's test to determine statistically homogeneous groups. Statistica 13 (TIBCO Software, Inc.) software was used.

RESULTS

The post-culture fluids of *Trichoderma citrinoviride* C1, HL, and B3 cultivated on Saunders (S, Sx) and MGP media (M, Mx) with and without yeast biomass were subjected to a series of tests to determine their ability to produce biosurfactants with fungicidal characteristics. The first measurements of surface tension were carried out in order to assess whether the metabolites present in the tested fluids exhibit surface-active properties. In all post-culture fluids, a reduction in surface tension was found (**Table 1**). It is worth emphasizing that in the case of C1 and B3 strains, the addition of fungal and yeast biomass did not affect the final result. Conversely, in the case of the HL strain, the Saunders medium with the addition of biomass turned out to be more effective. The obtained results indicate the possible occurrence of surface-active compounds, which allowed continuing the research in order to determine their characteristics.

In order to determine the fungicidal properties of the obtained preparations, the diffusion test was carried out against 11 species of phytopathogenic fungi (**Table 2**). Majority of crude culture fluids demonstrated an intense inhibitory effect towards *Fusarium sporotrichioides* and *Paecilomyces variotii* DSM 1961. On the contrary, no clear zones were observed for in tests with *Lecanicillium lecanii* and *Epicoccum nigrum*.

The comparison of the inhibitory effect of individual post-culture fluid fractions revealed the highest fungicidal properties of foam preparations. In the vast majority of cases, the compounds present in the F fraction induced the largest inhibition zones. Foam fractions from cultures of the C1 strain in MGP and HL in Saunders medium exhibited significant activity against the majority of the tested phytopathogens. Clear zones in plate tests occurred in 8 out of 11 species of filamentous fungi tested (**Table 2**).

For selected culture variants (S, M), the foam fraction was separated with ultrafiltration, on a membrane with a 10 kDa cutoff, to separate the low molecular weight biosurfactants from larger accompanying proteins, including enzymes (**Table 3**). The well diffusion test was repeated with 20 µL of fractions <10 kDa and 50 µL of the residual fraction <10 kDa. As a result, it turned out that low molecular weight biosurfactants derived from the foam after culturing the HL and C1 strains restricted the growth of *Fusarium* and *Aspergillus* strains. The extent of inhibition was moderate due to the use of the lowest possible amount of the preparation. Furthermore, the >10 kDa fractions of foam containing high molecular weight compounds retained their antifungal activity (**Table 3**).

The addition of yeast and fungal biomass to cultures of *Trichoderma* strains, as an inducer of the biosynthesis of lytic enzymes, resulted in the appearance of the inhibitory effect on a greater number of species of tested fungi. However, in a few cases, supplementation caused an opposite effect and reduced the zones of inhibition.

In all tested samples, a dominant activity of laminarinases over that of chitinases was observed. As expected, higher activities were achieved generally in cultures with the addition of inducers. Moreover, it is worth noting that the biosynthesis level of laminarinases did not differ significantly depending on the producer strain.

The enzymatic activities were determined in three fractions of culture fluids. The highest value of laminarinases activity was 0.481 U/ml, observed in the R fraction of the C1 strain grown in Saunders medium with the addition of biomass. The following highest values of activity, at the level of ca. 0.3 U/ml, were found for the HL strain in MGP and Saunders medium, as well as the B3 strain in Saunders medium, in each case with the addition of inducing biomass. The lowest activities were recorded for the C1 strain grown in Saunders medium without biomass enrichment, for all three fractions, especially R and FR (**Figures 1–3**).

Comparison of culture medium variants and fractions for each separate strain allowed distinguishing Saunders medium supplemented with biomass as favorable for laminarinases biosynthesis by the C1 and B3 strain. Importantly, enzymatic activity in the raw culture fluid (R) of the B3 strain compared to both F and FR fractions remained at a similar level and also gave the C1 strain a comparable result. In the case of the HL strain, the activity of laminarinases in the foam fraction (F) from the Saunders (Sx) medium was higher than in both F and FR fractions.

TABLE 2 | The clear zones (cm) around the wells, raw fluid (R), foam (F), and residue after foaming (FR). "-"—no inhibition, (M) MGP medium, (S) Saunders medium, (Mx) MGP medium with inducers, (Sx) Saunders medium with inducers. *E. nigrum* and *L. lecanii* did not produce inhibition zones.

Trichoderma fluid/ pathogen	*F. sporotrichioides*	*Penicillium* spp.	*R. nigricans*	*A. niger* CZ	*F. culmorum*	*B. cinerea* 5s	*M. hiemalis*	*P. variotii*	*F. poae 1*
C1 S; R	-	1.9	-	-	-	-	-	0.6	-
C1 Sx; R	0.4	-	0.4	0.2	-	-	-	0.8	-
C1 M; R	0.3	-	-	-	-	-	-	0.8	-
C1 Mx; R	0.4	0.2	0.4	-	0.2	0.1	0.9	0.5	-
HL S; R	0.5	-	-	-	0.5	-	-	0.5	-
HL Sx; R	0.3	0.2	-	-	-	-	-	0.5	-
HL M; R	-	-	0.2	-	-	-	-	0.5	1.6
HL Mx; R	-	-	-	-	-	-	-	-	-
B3 S; R	0.7	0.2	0.4	0.2	0.6	-	-	-	-
B3 Sx; R	0.4	-	0.3	-	0.7	-	0.4	0.5	-
B3 M; R	0.3	-	-	-	-	-	-	0.9	-
B3 Mx; R	0.3	-	-	-	1.2	-	-	0.5	-
C1 S; F	-	2.1	-	-	-	-	-	-	-
C1 Sx; F	0.5	0.1	0.5	-	-	-	-	0.9	-
C1 M; F	0.6	0.5	0.3	0.6	1.9	0.3	0.3	1.1	-
C1 Mx; F	0.4	0.1	0.3	-	-	-	0.7	0.7	-
HL S; F	0.6	0.2	0.4	0.2	0.7	0.2	-	1	0.5
HL Sx; F	0.4	0.1	-	-	-	-	-	0.9	-
HL M; F	0.4	-	0.3	-	-	0.3	0.3	0.7	1.9
HL Mx; F	-	-	-	-	-	-	-	-	-
B3 S; F	0.5	0.2	0.4	0.1	-	-	-	-	-
B3 Sx; F	0.3	-	0.4	-	0.4	-	0.5	0.7	-
B3 M; F	0.4	-	0.4	-	-	-	-	0.8	-
B3 Mx; F	0.4	-	-	-	0.9	-	-	0.7	-
C1 S; FR	-	2.1	-	-	-	-	-	-	0.1
C1 Sx; FR	0.5	-	0.4	0.3	-	-	-	0.7	-
C1 M; FR	0.2	-	-	-	0.5	-	-	0.7	-
C1 Mx; FR	0.3	0.1	0.3	-	-	-	0.8	-	-
HL S; FR	0.5	-	-	0.1	0.5	-	-	0.7	-
HL Sx; FR	0.4	0.1	-	-	-	0.5	-	0.8	-
HL M; FR	-	-	-	-	-	-	-	0.7	-
HL Mx; FR	-	-	-	-	-	-	-	-	-
B3 S; FR	0.5	0.2	0.5	0.2	0.3	0.2	-	0.7	-
B3 Sx; FR	0.3	-	0.3	-	0.6	-	0.4	0.6	-
B3 M; FR	-	-	-	-	-	-	-	1.2	-
B3 Mx;FR	0.3	-	-	-	1.1	-	-	0.5	-

TABLE 3 | Clear zones diameter (cm) in inhibition test with foam fractions (F) after separation through ultrafiltration. "-"—no inhibition, (M) MGP medium, (S) Saunders medium. *E. nigrum* and *M. hiemalis* did not produce inhibition zones.

Trichoderma strain	Culture medium	Fraction	*R. nigricans*	*L. lecanii*	*Penicillium* spp.	*F. poae*	*F. sporotrichioides*	*A. niger* CZ
HL	S	<10 kDa	-	-	-	0.20	0.10	0.10
		>10 kDa	0.20	-	0.10	0.70	-	0.10
HL	M	<10 kDa	-	-	-	0.20	0.20	-
		>10 kDa	0.20	0.20	0.10	0.45	-	0.10
C1	M	<10 kDa	-	-	-	0.20	0.10	-
		>10 kDa	0.20	1.00	0.10	0.15	0.40	0.30
B3	S	<10 kDa	-	-	-	-	-	-
		>10 kDa	0.20	-	0.10	0.50	-	0.10

The biosynthesis of chitinases in media dedicated to the biosurfactants overproduction and supplemented with the biomass was characterized by a much greater differentiation than the biosynthesis of the previously discussed enzyme. While the highest activity was recorded for the C1 strain, its biosynthesis took place on a pure Saunders medium. More importantly, its high level was neither recorded in the F nor in the FR fraction. For this strain, it was also noted that the chitinases biosynthesized on Saunders medium with inducers remained in the FR fraction, while from the MGP medium with

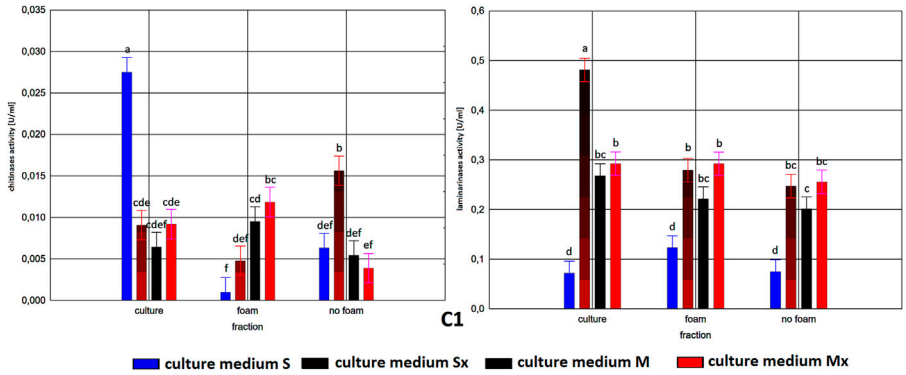

FIGURE 1 | Enzymatic activities in three fractions: raw (R), foam (F), foaming residue (FR), of *Trichoderma citrinoviride* B3 strain cultivated in different culture media, after separation with foaming technique (M) MGP medium, (S) Saunders medium, (Mx) MGP medium with inductors, (Sx) Saunders medium with inductors. One-way analysis of variance (ANOVA) was applied; a . . . i—homogeneous groups according to Duncan's test.

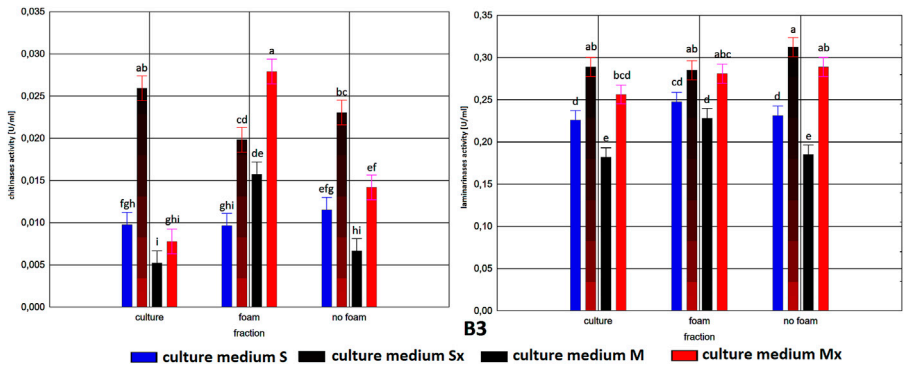

FIGURE 2 | Enzymatic activities in three fractions: raw (R), foam (F), foaming residue (FR), of *Trichoderma citrinoviride* C1 strain cultivated in different culture media, after separation with foaming technique (M) MGP medium, (S) Saunders medium, (Mx) MGP medium with inductors, (Sx) Saunders medium with inductors. One-way analysis of variance (ANOVA) was applied; a . . . i—homogeneous groups according to Duncan's test.

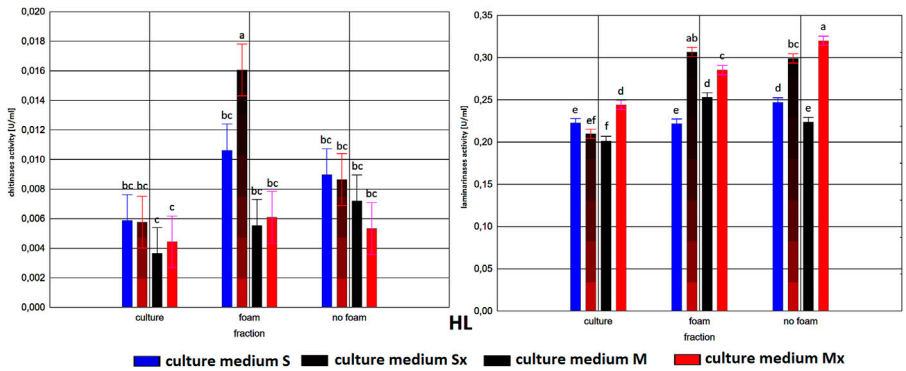

FIGURE 3 | Enzymatic activities in three fractions: raw (R), foam (F), foaming residue (FR), of *Trichoderma citrinoviride* HL strain cultivated in different culture media, after separation with foaming technique (M) MGP medium, (S) Saunders medium, (Mx) MGP medium with inductors, (Sx) Saunders medium with inductors. One-way analysis of variance (ANOVA) was applied; a . . . i—homogeneous groups according to Duncan's test.

inducers migrated to foam (F). For the B3 strain, where the highest levels of chitinase biosynthesis were recorded in Saunders medium with inducers, these activities were evenly distributed in both foaming and foaming residues (F and FR). The chitinases biosynthesis by the HL strain, as well as their activity in all three assessed fractions, with the exception of the high level of chitinase

obtained in Saunders culture with inducers, was practically equal. Certainly, the level of activity, as in all the cases, depended on the volume of foam obtained and thus the volume of the residual fraction, but in order to assess the inhibitory role of biosurfactants, this was not relevant as the main object of the study (**Figures 1–3**).

As to the fractions of C1 and HL strains that exhibited significant clear zones in the well test or the action against many fungal species, with the tested enzymatic activities, they are characterized by a very low activity of chitinases and relatively low of laminarinases. Due to low enzymatic activities and large inhibition zones, the obtained results may indicate the presence of fungicidal biosurfactants in the post-culture fluids, which were predominantly present in the F fraction. In terms of the production of these compounds, the *T. citrinoviride* C1 and HL strains cultivated in both Saunders and MGP media, without the addition of yeast and fungal biomass, deserve special consideration.

DISCUSSION

Biosurfactants produced by filamentous fungi using renewable substrates (sources) become a versatile and sustainable alternative to synthetic petroleum-based surfactants. The public attention is drawn to the use of environmentally safe products obtained with "green" methods is encouraged (da Silva et al., 2008). The results obtained in the experiment allowed us to conclude that the filamentous fungi of the *Trichoderma citrinoviride* species have the ability to secrete extracellularly not only hydrolytic enzymes but also presumably biosurfactants with antimicrobial characteristics. The latter may have a direct effect on the microbial cells and additionally support the action of hydrolases.

Leaving aside the basic theories of the phenomenon of *Trichoderma* fungi involved in biocontrol processes, based mainly on CWDE, the presented results may additionally constitute an important aspect in the discussion explaining the evolutionary purpose of microbial biosurfactants biosynthesis. The considered concepts of biosurfactants role indicate the emulsifying properties and solubility improvement of nutritive compounds in the immediate surroundings, changing environmental parameters, facilitating the attachment of fungal cells to cell walls of other organisms, but also their antibiotic activity to counteract competitors in the environment (da Silva et al., 2021).

The synthesis of surfactants can occur spontaneously or as a result of induction due to the presence of lipid compounds, temperature fluctuations, pH, stirring, cellular stress, and low concentration of nitrogen in the medium. Probably, the main source of biosurfactant synthesis is carbohydrates in the culture medium. Their availability regulates the course of glycolysis and lipogenesis, whereby the hydrophilic or hydrophobic components of surfactant are synthesized (da Silva et al., 2008; Kalyani et al., 2014).

The tested culture fluids exhibited a significantly reduced surface tension, even to the level of 32 mN/m, which can be considered a substantial result, especially when compared with the values obtained for other microorganisms. For example, Mennes et al. (2017) reported the capability of *Aureobasidium thailandense* LB01 to produce biosurfactants on waste materials such as olive oil mill wastewater. After partial purification, the biosurfactants present in the culture fluid could lower the surface tension to 31.2 mN/m. According to Fechter et al. (2017), the high-strength bacterial biosurfactant is capable of reducing surface tension maximally to the level 22–25 mN/m. On the other hand, Lima et al. (2016) out of eight filamentous fungi analyzed in terms of the production of biosurfactants picked a single *Phoma* sp. strain that exhibited a promising potential. The results indicated that the surface tension of the post-culture extract was 51.03 mN/m. The ability of the culture extract to emulsify diesel fuel was also demonstrated.

The emulsifying properties are a generally well-researched phenomenon; however, it may reflect some interactions between biosurfactant molecules and microorganisms. Hence, the focus was on a simple but highly effective method of assessing this relationship. The results of the diffusion tests performed revealed a great potential to inhibit the development of pathogenic fungi concerning the proportion of surfactants present in the tested post-culture fluids. The preceding separation of the obtained post-culture fluids into P, F, and FR fractions allowed us to initially determine the inhibitory potential of the tested biosurfactants against phytopathogens, rather than their characteristics, as they were obtained in earlier studies (Piegza et al., 2021).

Thus, particularly impressive inhibition was denoted in the separated fractions of foam (F). It was the foam fractions that caused both the largest extent of inhibition and the widest range of inhibited fungal strains. The visible clear zones in the diffusion plate tests occurred in 9 out of 11 species of phytopathogens tested in the experiment. Importantly, in many trials, the diameter of the inhibition zones was ca. 1.0 cm, and the highest values reached 1.9 cm. In the report that involved diffusion tests to determine the antibacterial activity of biosurfactants clear zones of the inhibited growth of pathogenic bacteria were notably less distinct (Wieczorek et al., 2014). In most cases, their diameter was below 0.5 cm, with occasional highest values of ca. 1.1 cm. At the same time, the additional separation of foam into two fractions (above and below 10 kDa) and the well diffusion test performance allowed to put forward the thesis about the combined action of lytic enzymes and biosurfactants, visible in the preceding test involving unseparated foam fractions and presenting clearly stronger inhibition of pathogens. This type of combined effect is also observed, e.g., with a cocktail of antibiotics and a biosurfactant (Hage-Hülsmann et al., 2018).

Other studies confirm the capability of different species of the genus *Trichoderma* to produce compounds of fungicidal nature. In the study by Witkowska et al. (2009), *T. harzianum* T33 was used in an inhibitory test against pathogenic *F. poae*, while *T. citrinoviride* T2 and C1 against *F. avenaceum*. The test showed distinct zones of pathogen growth inhibition around the discs with *Trichoderma* strains. In the mentioned report and in the results from the presented study, impressive zones of inhibition of

pathogen growth were obtained in the case of the *T. citrinoviride* C1 strain. This may signify the profound effectiveness of its prospective use in the protection of plants against phytopathogens. Comparable positive results of the plate tests were also observed in the trials with the use of HL and B3 strains. The number of positive results from the diffusion tests, as well as the satisfactory extent of the clear zones around the wells, may indicate the potential fungicidal characteristics of biosurfactants produced by the *T. citrinoviride* strains. The conclusions from this experiment allow us to imply that filamentous fungi of the *T. citrinoviride* species possess the ability to biosynthesize biosurfactants with anti-fungal characteristics. The abovementioned test results indicated the possibility of using *Trichoderma* fungi to produce natural surfactants, causing inhibition of other, especially pathogenic fungal species. Similar features of these compounds are described in the literature. Surfactants isolated from *Aspergillus ustus* MSF3 showed significant inhibitory activity against *Candida albicans* and gram-negative bacteria. Sophorolipids from the mutant strain *Candida bombicola* ATCC 22214 are used in the cosmetics industry due to their properties, including radical-scavenging, stimulating fibroblast metabolism, and hygroscopic properties supporting the physiological health of the skin (Bhardwaj et al., 2013). Rhamnolipids produced by few species are recognized as a plant protection against many different bacteria and fungi (Vatsa et al., 2010). The awareness that the fraction derived from the foam of *T. citrinoviride* post-culture fluids is characterized by the greatest intensity of inhibiting the development of pathogens may be of great importance in further directional research and facilitate the use of these compounds in industry. Also, the knowledge that the fraction derived from the foam of *T. citrinoviride* culture fluids is characterized by the greatest intensity of inhibitory effect against phytopathogens may be of great importance in further research and facilitate the use of these compounds in industry.

Demonstrating the complexity of Trichoderma secondary metabolites may further affirm the importance of their introduction in environmentally friendly agricultural cultivation. Because of the recent emphasis on their antimicrobial properties and plant growth promotion, biosurfactants gain exceptional significance. Surface-active compounds are already used to remediate soil of trace elements and toxic residues. However, typical surfactants of chemical origin contradict the concept of ecological neutrality. Hence, the application of microbiological surfactants could have a positive impact on halting soil degradation with simultaneous support of plant development and maintenance of natural microbial balance (Kumar et al., 2021).

The possibility of using ecological fungicides may be of great importance, in particular for the agrotechnical industry. In the era of constant struggle to replace chemical pesticides, their natural equivalents that do not pose an environmental burden and effectively inhibit the development of pathogenic fungi turn out to be a favorable research object. The properties of *T. citrinoviride* involved in this study may contribute to the broader use of this species in the search for new solutions for the biological control of plant pathogens.

CONCLUSION

The complexity of processes involved in microbial coexistence, especially in the context of their competition for living space, is still a boundless field for further discoveries. Previous findings regarding *Trichoderma* fungi indicated the participation of CWDE, a broadly understood competition mechanism, or antibiosis based on peptaibols or terpenes. However, within the same species, differences in the biocontrol mechanisms were pointed out. The finding that the most active strains in this regard additionally produce biosurfactants, of which synergistic action with other compounds is confirmed in the literature, appears to be an important contribution to the understanding of the biology of *Trichoderma* fungi.

DATA AVAILABILITY STATEMENT

The raw data supporting the conclusions of this article will be made available by the authors, without undue reservation.

AUTHOR CONTRIBUTIONS

All authors contributed to the writing of this manuscript and gave their approval for the final version. All authors have read and agreed to the published version of the manuscript.

REFERENCES

Banat, I. M., Makkar, R. S., and Cameotra, S. S. (2000). Potential Commercial Applications of Microbial Surfactants. *Appl. Microbiol. Biotechnol.* 53, 495–508. doi:10.1007/s002530051648

Bartmańska, A., and Dmochowska-Gładysz, J. (2007). Transformation of Steroids by Trichoderma hamatum. *Enzyme Microb. Technology.* 40, 1615–1621. doi:10.1016/j.enzmictec.2006.11.011

Bhardwaj, G., Cameotra, S. S., and Chopra, H. K. (2013). Biosurfactants From Fungi: a Review. *J. Pet. Environ. Biotechnol.* 4, 6. doi:10.4172/2157-7463.1000160

Chet, I., Harman, G. E., and Baker, R. (1981). Trichoderma Hamatum: Its Hyphal Interactions With Rhizoctonia Solani and Pythium Spp. *Microb. Ecol.* 7, 29–38. doi:10.1007/bf02010476

da Silva, A. F., Banat, I. M., Giachini, A. J., and Robl, D. (2021). Fungal Biosurfactants, From Nature to Biotechnological Product: Bioprospection, Production and Potential Applications. *Bioproc. Biosyst Eng.* 44, 2003–2034. doi:10.1007/s00449-021-02597-5

da Silva, S. A., dos Santos, N. P., e Silva, L. T., Andrade, R. F. S., and Campos-Takaki, G. M. (2008). Biosurfactant Production by Fungi as a Sustainable Alternative. *Arq. Inst. Biol.* 85, 1–12. doi:10.1590/1808-1657000502017

D'aes, J., De Maeyer, K., Pauwelyn, E., and Höfte, M. (2010). Biosurfactants in Plant–*Pseudomonas Interactions* and Their Importance to Biocontrol. *Environ. Microbiol. Rep.* 2 (3), 359–372. doi:10.1111/j.1758-2229.2009.00104.x

Fan, H., Yao, M., Wang, H., Zhao, D., Zhu, X., Wang, Y., et al. (2020). Isolation and Effect of *Trichoderma Citrinoviride* Snef1910 for the Biological Control of Root-Knot Nematode, *Meloidogyne incognita*. *BMC Microbiol.* 20–299. doi:10.1186/s12866-020-01984-4

Fechtner, J., Cameron, S., Deeni, Y. Y., Hapca, S. M., Kabir, K., Mohammed, I. U., et al. (2017). Limitation of Biosurfactant Strength Produced by Bacteria. In ed. R. Upton, *Biosurfactants: Occurrences, Applications and Research*. Hauppauge New York, Nova Publisher. 2–19.

Hage-Hülsmann, J., Grünberger, A., Thies, S., Santiago-Schübel, B., Klein, A. S., Pietruszka, J., et al. (2018). Natural Biocide Cocktails: Combinatorial Antibiotic Effects of Prodigiosin and Biosurfactants. *PLoS One.* 19 (137), e0200940. doi:10.1371/journal.pone.0200940

Harman, G. E. (2006). Overview of Mechanisms and Uses of *Trichoderma* Spp. *Phytopathology.* 96, 190–194. doi:10.1094/phyto-96-0190

Hutchison, M. L., and Johnstone, K. (1993). Evidence for the Involvement of the Surface Active Properties of the Extracellular Toxin Tolaasin in the Manifestation of Brown Blotch Disease Symptoms by Pseudomonas Tolaasii on Agaricus Bisporus. *Physiol. Mol. Plant Pathol.* 42, 373–384. doi:10.1016/s0885-5765(05)80013-x

Kalyani, A. L. T., Sireesha, G. N., Sankar, G. G. G., and Prabhakar, T. (2014). Isolation of Bio Surfactant Producing *Actinomycetes* From Terrestrial and marine Soils. *Inter. J.of Pharm. Scien.. Res.* 5 (9), 4015. doi:10.13040/ijpsr.0975-8232.5(9).4015-22

Kumar, A., Singh, S. K., Kant, C., Verma, H., Kumar, D., Singh, P. P., et al. (2021). Microbial Biosurfactant: a New Frontier for Sustainable Agriculture and Pharmaceutical Industries. *Antioxidants.* 10–1472. doi:10.3390/antiox10091472

Lima, J. M. S., Pereire, J. O., Batista, I. H., Costa Neto, P. Q., dos Santos, J. C., de Araujo, S. P., et al. (2016). Potential Biosurfactant Producing Endophytic and Epiphytic Fungi, Isolated From Macrophytes in the Negro River in Manaus, Amazonas, Brazil. *Afr. J. Biotechnol.* 15 (24), 1217–1223. doi:10.5897/AJB2015.15131

Markande, A. R., Patel, D., and Varjani, S. (2021). A Review on Biosurfactants: Properties, Applications and Current Developments. *Bioresour. Technology.* 330, 124963. doi:10.1016/j.biortech.2021.124963

Menses, D. P., Gudina, E. J., Fernandes, F., Goncavle, s. L. R. B., Rodrigues, L. R., and Rodrigues, S. (2017). The Yeast-Like Fungus *Aureobasidium Thailandense* LB01 Produces a New Biosurfactant Using Olive Oil Mill Wastewater as an Inducer. *Microbiol. Res.* 204, 40–47. doi:10.1016/j.biortech.2021.124963

Mohamed, Z. A., Hashem, M., and Alamri, S. A. (2014). Growth Inhibition of the Cyanobacterium *Microcystis Aeruginosa* and Degradation of its Microcystin Toxins by the Fungus *Trichoderma Citrinoviride*. *Toxicon.* 86, 51–58. doi:10.1016/j.toxicon.2014.05.008

Park, Y.-H., Chandra Mishra, R., Yoon, S., Kim, H., Park, C., Seo, S.-T., et al. (2019). Endophytic *Trichoderma Citrinoviride* Isolated From Mountain-Cultivated Ginseng (Panax Ginseng) Has Great Potential as a Biocontrol Agent Against Ginseng Pathogens. *J. Ginseng Res.* 43 (3), 408–420. doi:10.1016/j.jgr.2018.03.002

Piegza, M., Łaba, W., Kancelista, A., Witkowska, D., and Kawa-Rygielska, J. (2015). Evaluation of brewer's Spent Grain as a Substrate for *Trichoderma* Hydrolytic Enzymes Production and Source of Majorly Fermentable Sugars. *Acta Sci. Pol. Biotechnol.* 14 (3), 17–31. Available at: http://www.ejpau.media.pl/volume18/issue4/art-04.html.

Piegza, M., Pietrzykowska, J., Trojan-Piegza, J., and Łaba, W. (2021). Biosurfactants from Trichoderma Filamentous Fungi-A Preliminary Study. *Biomolecules.* 11–519. doi:10.3390/biom11040519

Piegza, M., Szlączka, K., Łaba, W., and Witkowska, D. (2014). Effect of Carbon Source on the Production of Lytic Enzymes by Filamentous Fungi of the *Tichoderma* Genus. *EJPAU.* 17 (2). Avilable at: http://www.ejpau.media.pl/volume17/issue2/art-06.html.

Piegza, M., Witkowska, D., Łaba, W., and Siepka, E. (2016). *Trichoderma* Lytic Enzymes Induced by *Yarrowia Lypolytica* Cell wall Biopolimers. *Acta Sci. Pol. Biotechnol.* 15 (2), 31–42.

Rakowska, J., and Porycka, B. (2009). Badania Związane Z Określeniem Aktywności Powierzchniowej Podstawowych Składników Środków Zwilżających. *Bezpieczeństwo i Technika Pożarnicza.* 2, 65–80.

Saikia, R. R., Deka, S., and Sarma, H. (2021). Biosurfactants from Bacteria and Fungi Perspectives on Advanced Biomedical Applications. In *Biosurfactants for a Sustainable Future: Production and Applications in the Environment and Biomedicine*. Edited by H Sarma and M N V Prasad, 293–315.

Schuster, A., and Schmoll, M. (2010). Biology and Biotechnology of *Trichoderma*. *Appl. Microbiol. Biotechnol.* 87, 787–799. doi:10.1007/s00253-010-2632-1

Sjingh, A., Van Hamme, J., and Ward, O. P. (2007). Surfactants in Microbiology and Biotechnology: Part 2. Application Aspects. *Biotechnol. Adv.* 25, 99–121. doi:10.1016/j.biotechadv.2006.10.004

Thomas, M. B., and Willis, A. J. (1998). Biocontrol-Risky but Necessary. *Trends Ecol. Evol.* 13 (8), 325–329. doi:10.1016/s0169-5347(98)01417-7

Vatsa, P., Sanchez, L., Clement, C., Baillieul, F., and Dorey, S. (2010). Rhamnolipid Biosurfactants as New Players in Animal and Plant Defense against Microbes. *Int. J. Mol. Sci.* 11, 5095–5108. doi:10.3390/ijms11125095

Wieczorek, D., Gwiazdowska, D., Michocka, K., Kwaśniewska, D., and Kluczyńska, K. (2014). Antibacterial Activity of Selected Surfactants. *Towaroznawcze problemy jakości.* 2, 142–149.

Witkowska, D., and Maj, A. (2002). Production of Lytic Enzymes byTrichoderma Spp. And Their Effect on the Growth of Phytopathogenic Fungi. *Folia Microbiol.* 47, 279–282. doi:10.1007/bf02817652

Witkowska, D., Stolaś, J., Kancelista, A., and Piegza, M. (2009). Uzdolnienia Lityczne Grzybów Z Rodzaju *Trichoderma* W Obecności Biomasy Fitopatogenów. *Acta Sci. Pol. Biotechnologia.* 8 (2), 17–25.

Conflict of Interest: The authors declare that the research was conducted in the absence of any commercial or financial relationships that could be construed as a potential conflict of interest.

Publisher's Note: All claims expressed in this article are solely those of the authors and do not necessarily represent those of their affiliated organizations, or those of the publisher, the editors, and the reviewers. Any product that may be evaluated in this article, or claim that may be made by its manufacturer, is not guaranteed or endorsed by the publisher.

frontiers in Bioengineering and Biotechnology

ORIGINAL RESEARCH
published: 30 November 2021
doi: 10.3389/fbioe.2021.761266

Characterization and Cytotoxicity of *Pseudomonas* Mediated Rhamnolipids Against Breast Cancer MDA-MB-231 Cell Line

Neelam Mishra[1], *Kavita Rana*[2], *Siva Deepthi Seelam*[1], *Rakesh Kumar*[3], *Vijyendra Pandey*[4], *Bharathi P. Salimath*[5,6] *and Dayanand Agsar*[1]*

[1]Department of Microbiology, Gulbarga University, Gulbarga, India, [2]Department of Toxicology, Chaudhary Charan Singh University, Meerut, India, [3]Department of Life Science, School of Life Sciences, Central University of Karnataka, Kadaganchi, India, [4]Department of Psychology, School of Social and Behavioural Sciences, Central University of Karnataka, Kadaganchi, India, [5]Department of Biotechnology, University of Mysore, Mysore, India, [6]Sanorva Biotech Pvt. Ltd., Mysuru, India

A biosurfactant producing bacterium was identified as *Pseudomonas aeruginosa* DNM50 based on molecular characterization (NCBI accession no. MK351591). Structural characterization using MALDI-TOF revealed the presence of 12 different congeners of rhamnolipid such as Rha-C8-C8:1, Rha-C10-C8:1, Rha-C10-C10, Rha-C10-C12:1, Rha-C16:1, Rha-C16, Rha-C17:1, Rha-Rha-C10:1-C10:1, Rha-Rha-C10-C12, Rha-Rha-C10-C8, Rha-Rha-C10-C8:1, and Rha-Rha-C8-C8. The radical scavenging activity of rhamnolipid (DNM50RL) was determined by 2, 3-diphenyl-1-picrylhydrazyl (DPPH) assay which showed an IC_{50} value of 101.8 µg/ ml. The cytotoxic activity was investigated against MDA-MB-231 breast cancer cell line by MTT (4,5-dimethylthiazol-2-yl-2,5-diphenyl tetrazolium bromide) assay which showed a very low IC50 of 0.05 µg/ ml at 72 h of treatment. Further, its activity was confirmed by resazurin and trypan blue assay with IC_{50} values of 0.01 µg/ml and 0.64 µg/ ml at 72 h of treatment, respectively. Thus, the DNM50RL would play a vital role in the treatment of breast cancer targeting inhibition of p38MAPK.

Keywords: MDA-MB-231 cell lines, rhamnolipid, MTT, trypan blue, p38MAPK, TNBC, resazurin, cytotoxic

OPEN ACCESS

Edited by:
Surekha K. Satpute, Savitribai Phule Pune University, India

Reviewed by:
Nurul Farahana Kamaludin, National University of Malaysia, Malaysia
Deepansh Sharma, Amity University Jaipur, India

***Correspondence:**
Dayanand Agsar
dayanandagsar@gmail.com

Specialty section:
This article was submitted to Industrial Biotechnology, a section of the journal Frontiers in Bioengineering and Biotechnology

Received: *19 August 2021*
Accepted: *27 October 2021*
Published: *30 November 2021*

Citation:
Mishra N, Rana K, Seelam SD, Kumar R, Pandey V, Salimath BP and Agsar D (2021) Characterization and Cytotoxicity of Pseudomonas *Mediated Rhamnolipids Against Breast Cancer MDA-MB-231 Cell Line. Front. Bioeng. Biotechnol. 9:761266. doi: 10.3389/fbioe.2021.761266*

INTRODUCTION

Biosurfactants are a group of amphipathic compounds that moderate the surface and interfacial tension of liquids (De almeida et al., 2016; Gudiña et al., 2016). They harbor saturated and unsaturated fatty acids as hydrophobic moieties along with polysaccharides, peptides, amino acids, and anions/cations as hydrophilic moieties. There are different groups of biosurfactants, out of which glycolipids are the most preferred due to their low molecular weight (Banat et al., 2014a). Also, they can be synthesized using hydrocarbons, agro-industrial waste, frying and olive oil wastes (Inès and Dhouha, 2015). Rhamnolipids (RLs) are the extensively studied glycolipid based biosurfactant due to its properties such as low critical micellar concentration (CMC: 10–200 mg/ L), surface tension reduction (up to 28–31 mN/ m), high emulsification index (60–70%), and high production in a short period of time (Gudiña et al., 2016).

Different microorganisms can produce different congeners or homologs of RLs by using a variety of sugars, hydrocarbons, and other oil/dairy product wastes (Shao et al., 2017; Pathania and Jana,

2020). *Pseudomonas aeruginosa*, a predominant microbial species, can produce various RL congeners with the most common ones as Rha-Rha-C10-C10, Rha-C10, Rha-C10-C10, and Rha-Rha-C10 (Hošková et al., 2015). RLs have gained importance in various industries such as food, healthcare, pharmaceuticals, and petrochemicals due to their wide range of properties along with enhanced oil recovery, biodegradation, and bioremediation. RLs are known to inhibit proliferation of cancer cells by inducing apoptosis. They regulate humoral and cellular immune response by acting as immunomodulators. They act as antimicrobial agents as they can lower the surface hydrophobicity, thus destroying the cytoplasmic membrane causing killing of bacterial cells. They are also involved in synthesis of nanoparticles. Thus, RLs have high biological applications because of its antimicrobial, anticancer, antioxidant, immunomodulatory property and their capability of nanoparticles synthesis (Banat et al., 2014b; Thakur et al., 2021).

Rhamnolipid is recovered from cell free culture broth by solvent extraction or acid precipitation method in partially purified form. Structural elucidation of any surface-active compound is of utmost importance and cannot be confirmed merely with TLC and FTIR as both of them carries some drawbacks and hence it should be accompanied by other methods such HPLC-MS/UPLC-MS and NMR spectroscopy (Twigg et al., 2020). MALDI-TOF is the emerging technology and can be used to characterize biosurfactants (Price et al., 2009). As RLs are composed of mono-RLs and di-RLs along with different congeners, MALDI-TOF has emerged as the screening strategy where new congeners can be determined at intimal stages (Sato et al., 2019).

Breast cancer is one of the most prominent malignant diseases in the world. Worldwide, there are 3,465,951 incidences and 1,121,413 deaths respectively, according to GLOBOCAN 2020. In 2020, 1,204,532 new cases and 436,417 deaths were recorded in India (Sung et al., 2021). Breast cancer affecting the female population continues to increase annually and there is no ideal treatment for the disease (Wu et al., 2017). Doxorubicin, etoposide, and mitoxantrone are some of the widely prescribed anticancer drugs. One of the major causes of high mortality in people with cancer is resistance developed to the classical chemotherapeutic agent, which is being considered to be a major hindrance, leading to major obstructions in cancer treatment (Housman et al., 2014; Wambang et al., 2016; Wang et al., 2019). Besides this, the limited solubility, stability, bio-distribution, and cytotoxic effect on normal cells significantly reduces the effectiveness of chemotherapeutic drugs. Thus, it is essential to create efficient alternative formulations, selectively targeting cancer cells without causing substantial harm to healthy cells (Haque et al., 2021). The life expectancy of cancer patients would be significantly influenced by the development of new chemotherapeutic/chemical substances/agents. RLs have recently been discovered as a promising antitumor agent interfering with the proliferation of cancer cells of different origins (Chen et al., 2017).

Rhamnolipids have shown a significant effect on human as well as animal cancer cells in the recent past. It is reported that di-RLs produced from *Pseudomonas aeruginosa* B189 inhibit the proliferation of a breast cancer cell line MCF-7 and an insect cell line C6/36 (Thanomsub et al., 2006). This anticancer property of RLs was further tested on various cell lines such as BV-173, SKW-3, HL-60, and JMSU-1 derived from tumors of different origin with IC_{50} values of 50–140 μM (Christova et al., 2013). RLs isolated from *Pseudomonas aeruginosa* MR01 inhibited HeLa cancer cells growth at the concentration of 5 μg/ ml (Loftabad et al., 2010). Burgos-Díaz et al. (2013) reported anticancer activity of glycolipid from *Sphinobacterium detergens* against colorectal cancer cell line. Trehalose lipid, a glycolipid from *Mycobateria,* was used as an antitumor agent (Fracchia et al., 2015).

Similarly, Rahimi et al. (2019) investigated the cytotoxic effect of RL-1 and RL-2 isolated from *Pseudomonas aeruginosa* MR01 against MCF-7, a breast cancer cell line. The results clearly indicate the antiproliferative effect of RLs, emphasizing induction of apoptosis. They reported increased expression of p53 gene in mRNA levels, indicating induction of cell cycle control by RLs in cancer cells. All these reports give insight into the use of RLs as a potential therapeutic antitumor agent.

TNBC, commonly referred to as triple negative breast cancer cell line, lacks expression of ER–a estrogen receptor, PR–a progesterone receptor, and HER 2-a human epidermal growth factor receptor 2 (Chavez et al., 2010). Poor long-term outcomes are associated with it, as compared to other breast cancer (Li et al., 2017). The MDA-MB-231 cell line also lacks expression of these receptors and thus is an aggressive and invasive breast cancer cell line (Cailleau et al., 1978). It is insensitive to anti-hormone-based therapies, including tamoxifen due, to the absence of ER expression (Osborne and Schiff, 2011). It accounts for approximately 15% of breast cancer diagnosed worldwide, which amounts to almost 200,000 cases each year. It is more commonly diagnosed in women younger than 40 years, compared with hormone receptor-positive breast cancer (Swain, 2008). These types of breast cancer have limited treatment options and thus it is commonly used for development of novel therapeutic approaches by exploring molecular basis of this type of breast cancer (Mohammed et al., 2020).

The involvement of p38MAPK signaling pathway, a group of stress-activated kinases in apoptotic cell death phenomenon, makes this pathway striking for cancer researchers (García-Cano et al., 2016). The inhibition of p38MAPK plays a remarkable role in cancer therapy. P38MAPK is a crucial player in response to chemotherapy, as apoptosis is the main mechanisms associated with it (Sanchez-Prieto et al., 2000; Cai et al., 2006). In few cases of colorectal cancer, experimental evidence supports the fact that p38MAPK inhibition by itself is a promising target in cancer therapy (Gupta et al., 2015; Igea and Nebreda 2015). In primary acute myeloid leukemia, the p38MAPK inhibition overcomes the resistance to compounds such as Birinpant (Lalaoui et al., 2016). Ongoing trials showed these inhibitors safety for ralimetinib and ARRY-614 (Garcia-

Manero et al., 2015; Patnaik et al., 2016). The implication of active p38MAPK in cancer is not a genetic alteration in the MAPK, instead a pathological context of a tumor. Thus, it is advisable to search for P38MAPK inhibitor for cancer researchers (Pritchard and Hayward 2013). Hence, the use of p38MAPK can be considered as a potential target for cancer therapy. A new era of better prognosis and personalized treatment can be led by a deep understanding of the role of p38MAPK in cancer therapy.

The DNM50RL (a mixture of mono-RL and di-RL congeners) used in the present study was produced using *Pseudomonas aeruginosa* DNM50. MALDI-TOF was used to characterize RLs in view to identify its different congeners. Radical scavenging activity was assessed though DPPH assay. Cytotoxic effect of DNM50RL was assessed against MDA-MB-231 triple negative cell line through MTT, Resazurin, and Trypan blue assay. Since p38 plays a crucial role in anticancer therapy, inhibition of phosphorylated p38 was examined using Western blot analysis.

MATERIALS AND METHODS

Chemicals Used

Chemicals and media used in the present study were obtained from Himedia (Mumbai, India), Sigma Aldrich Pvt. Ltd. (United States), and Merck and Co. Inc. (United States).

Characterization of Microbial Strain

Pseudomonas aeruginosa DNM50 used in the present study was previously isolated from oil contaminated soil sourced from railway tracks of Wadi, Kalaburagi, Karnataka, India, in A-DBT Research Laboratory, Gulbarga University, Kalaburagi. Seven different screening methods were used to confirm its efficiency for biosurfactant production, and the data was reported in our earlier study (Mishra et al., 2021).

Pseudomonas aeruginosa DNM50 was identified and characterized using 16 S rRNA sequencing. Spin column kit (Qiagen, Hilden, Germany) was used to extract chromosomal DNA while purification of bacterial 16 S rRNA (1500) was done by using exonuclease I-Shrimp Alkaline phosphatase (Exo-SAP) (Darby et al., 2005). For the amplification of 200 ng/ μL of 16 S rRNA genes, PCR technique was applied using universal primers, 27F (AGAGTTTGATC(C/A)TGGCTCAG) and 1492R (TACGG (C/T) TACCTTGTTACGACTT) (Clarridge 2004; Mulla et al., 2016; 2018). Amplicons of PCR amplified genes were sequenced by following the method of Sanger (Sanger et al., 2000) using ABI 3500xL genetic analyzer (Life Technologies, United States). Sequencing files (.ab1 format) were edited with CHROMASLITE (version1.5) and then analyzed with the Basic Local Alignment Search Tool (BLAST) against the closest culture sequence retrieved from the National Centre for Biotechnology Information (NCBI) database, which identifies regions of local similarity between sequences. The evolutionary history and evolutionary analysis were deduced by Neighbor-Joining method and MEGA 6, respectively (Altschul et al., 1990; Tamura et al., 2013).

Characterization of Rhamnolipids

The RLs produced by *Pseudomonas aeruginosa* DNM50 under submerged process was subjected for its chemical characterization. The production medium used was neem oil cake extract (19.5%), as a sole source of nutrition. The extract of neem oil cake (pH 7.5) was prepared (Amena et al., 2010), sterilized and inoculated with 10% of 24 h culture followed by incubation at 40°C with agitation of 200 rpm for 5 days. Growth stages of the culture, production levels of RL, and surface tension (SFT) reduction of the production medium were recorded for a period of 5 days. All experiments were carried out in triplicates. The mean values were plotted along with standard deviation (Hazra et al., 2010; Samykannu and Achary, 2017; Chopra et al., 2020).

Cell free broth was used for extraction of RLs as per the modified procedure described by Chandankere et al. (2013). After 3 days of fermentation, culture broth was centrifuged for 10 min at 10,000 rpm. The cell free broth was filtered through 0.45 μM filter and extracted three times with equal volume of chloroform. The organic phase was collected, and solvent evaporated using a rotavapour. The resulting brownish semisolid compound was dried in an oven at 70°C and subjected to TLC (compared with reference standard of RLs from AGAE technologies, USA). The extracted RL (DNM50RL) was further analyzed by HPLC (not reported here) and MALDI—TOF.

Thin Layer Chromatography

For thin layer chromatography, a sample of DNM50RL was dissolved in chloroform and 20 μL of the aliquot was applied to pre-coated silica gel (F 1500 LS. 254; Schleicher-Schull, Germany). A mixture of butanol:acetic acid:water in the ratio of 2:1:1 (v/v/v) was used as the mobile phase. Molisch reagent (α-naphthol in ethanol with 10% H_2SO_4), ninhydrin reagent, and iodine vapors were used for detection of carbohydrate, proteins, and lipids, respectively (Loftabad et al., 2010).

Matrix Assisted Laser Desorption/Ionization Time of Flight

To elucidate the structure of RLs, MALDI-TOF was performed using an Applied Biosystem Ultraflextreme, Bruker Daltonic Germany Mass Spectrometer in reflection mode (Maiqian et al., 2010).

Antioxidant Activity

DPPH Assay

The 2,2,-diphenyl-1-picrylhydrazyl (DPPH) free radical scavenging potential of DNM50RL was examined according to the method described by Li et al. (2014). A concentration range of 0.00625–5 mg/ml was used for both DNM50RL and ascorbic acid (standard). The absorbance at 517 nm determines the reduction of DPPH radical and the calculation for radical scavenging activity was done as follows,

DPPH radical scavenging % = $[(A_0\text{-}A_1)/A_0]$ x 100. where DPPH absorbance is denoted by A_0 and absorbance of sample is denoted by A_1.

The antioxidant property is measured in % radical scavenging activity and the results are presented as the average of three independent experiments.

The IC_{50} (effective concentration to scavenge DPPH radical) value of DNM50RL was determined by GraphPad prism software version 9.1.0.221. The dose response curve is plotted between DPPH radical scavenging activity and the concentration.

Cytotoxic Activity

Cell Cultures

MDA-MB-231, a tumorigenic, invasive, metastatic, and TNBC representative cell line was procured and authenticated from National Centre for Cell Sciences (NCCS), Pune, India. The cells were cultured in L-15 (Leibovitz's 15) medium with 2 mM L-glutamine and 10% FBS (fetal bovine serum) and were maintained at 37°C.

MTT Assay

5×10^4 cells (MDA-MB-231) were cultured in 96-well plate (Nunc MicroWell™) in complete Dulbecco's Modified Eagle Medium (DMEM) medium and incubated overnight at 37°C in 5% CO_2. Cells were exposed to different concentrations (0.01, 0.05, 0.1, 0.5, 1.0, and 5.0 μg/ ml) of compound in triplicates with vehicle control (0.05% DMSO served as negative control) and positive control (Etoposide in the concentration range of 1—1000 μM). 24 h of post-treatment, 10 μL of 4,5-dimethylthiazol-2-yl-2,5-diphenyltetrazolium bromide (MTT) (5 mg/ ml) was added in each well and incubated for 4 h at 37°C. The resultant purple formazan crystals were solubilized in 150 μL of DMSO. The color development was recorded at a test wavelength of 570 nm and a reference wavelength of 630 nm (Varioskan™ Flash Multimode Reader, Thermo Scientific, Switzerland). The cytotoxicity in percentage was derived against control cells as 100% (Riss et al., 2016; Byrappa et al., 2017). The cytotoxicity measurements were depicted in the dose-response curve for a period of 24, 48, and 72 h. The IC_{50} value (half-maximal inhibition concentration) was determined using GraphPad Prism software version 9.1.0.221 using nonlinear regression (curve fit).

Resazurin Assay

5×10^4 MDA-MB-231 cells were grown in 96-well plate (Nunc MicroWell™) in complete L-15 medium and incubated overnight at 37°C. Cells were treated with increasing concentrations (0.01, 0.05, 0.1, 0.5, 1.0, and 5.0 μg/ml) of the compound in triplicates with vehicle control (0.05% DMSO served as negative control) and a positive control (Etoposide in the concentration range of 1—1000 μM). After 24 h of treatment, cells were incubated with 100 μL of resazurin sodium salt (0.01 g/2 ml sterile PBS—phosphate buffered saline) at 37°C for 4 h. The resultant change from blue to pink color indicates the presence of viable cells. The optical density of the colored solution was determined at a reference wavelength of 630 nm and test wavelength of 570 nm (Infinite Pro Tecan Multimode reader, Thermo Scientific, Finland). The percentage of cytotoxicity was calculated against control cells as 100% (Riss et al., 2016; Byrappa et al., 2017). The cytotoxicity measurements were analyzed in the dose-response curve for 24, 48, and 72 h. The IC_{50} value (half-maximal inhibition concentration) was demonstrated using GraphPad Prism software version 9.1.0.221 using nonlinear regression (curve fit).

Trypan Blue Assay

5×10^4 MDA-MB-231 cells were seeded in 6-well plate in complete L-15 medium and cells were treated with increasing concentrations (0.01, 0.05, 0.1, 0.5, 1.0, and 5.0 μg/ ml) of the compound with control. After 24 h of treatment, cells were stained with trypan blue (0.4% trypan blue in PBS—phosphate buffered saline, pH 7.2–7.3). A mixture of treated cells (10 μL), trypan blue (10 μL), and PBS (980 μL) were resuspended and 10 μL of the mixture was loaded from the edge of a coverslip placed on a hemocytometer. The number of viable cells/mL was enumerated by using the following formula.

Average of cells counted from four squares x 10,000 x dilution factor (i.e., 100)

= Average cells count x 10^6 cells.

Cell viability (%) = (Number of live cells ÷ Number of total cells) × 100.

Three independent readings were taken. All the measurements were depicted in the dose-response curve for 24, 48, and 72 h (Phillips, 1973). Etoposide in the concentration range of 1–1000 μM served as the positive control along with 0.05% DMSO as negative control. The IC_{50} value (half-maximal inhibition concentration) was determined using GraphPad Prism software version 9.1.0.221 using nonlinear regression (curve fit).

Western Blotting for Regulation of P38

MDA-MB-231 cells were revived and grown until 80% confluent, the cells were trypsinized (trypsin-EDTA 0.25%), split, and then seeded into sterile Petri dishes. After 80–90% confluency, the media was aspirated, and cells were starved overnight with basal media. MDA-MB 231 cells were treated with 2 mM sodium orthovanadate for 2 h, followed by 5 μg of compound for 24, 48, and 72 h. The cell lysate was prepared using chilled lysis RIPA buffer. Cell lysate of 24, 48, and 72 h was collected. After estimating protein (Bradford, 1976), the supernatant was loaded on gel (150 μg/well) and processed for Western blotting using a semidry blotter. The unwanted protein binding sites on the membrane were blocked by incubating membrane in 5% bovine serum albumin (BSA) for 2 h at room temperature with moderate agitation. Blot was washed three times with TBST buffer (tris-buffered saline, 0.1% tween 20) for 10 min each. Membrane was incubated overnight at 4°C with moderate agitation in primary antibody (phosphorylated p38, polyclonal rabbit antibody), diluted as 1: 1000 ratio in blocking buffer. After washing the blot, the blot was incubated with secondary goat anti-rabbit HRP tagged antibody in 1:3000 ratio for 2 h at room temperature with gentle agitation. Following washing, the blot was developed using enhanced chemiluminescence (ECL). Blot was stripped and re-probed with total p38 antibody to show equal loading in

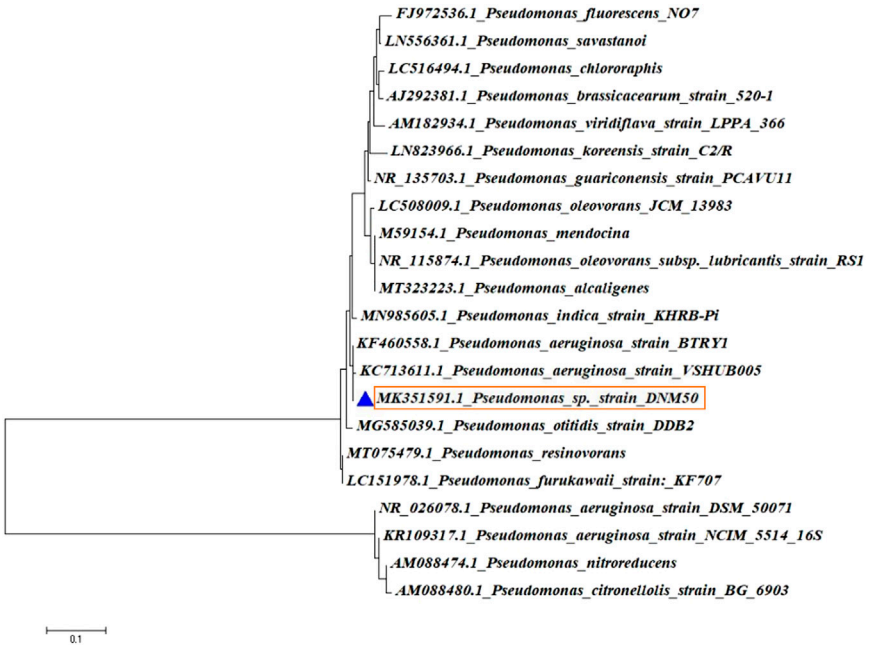

FIGURE 1 | Phylogenetic tree of the isolate DNM50.

all blots. β actin served as the loading control. Membrane was washed with TBST extensively and continued with blocking procedure. Quantification of protein bands were determined by ImageJ software (Towbin et al., 1979).

Statistical Analysis

All the results were expressed as the Mean ± SD values obtained in triplicate from three independent tests. SPSS version 22.0 was used to perform all statistical analysis. One-way ANOVA followed by Tukey's HSD Post-Hoc test and Student's t test were used to make multiple comparisons with control groups. $^{*}p < 0.05$ represents statistically significant values.

RESULTS AND DISCUSSION

Strain Characterization

The isolated genomic DNA of the potential isolate was amplified to obtain a PCR product, which was further purified. It was then subjected to 16SrRNA gene sequencing and identified by phylogenetic analysis. The consensus sequences available from National Centre for Biotechnology Information (NCBI) were used to perform Nucleotide Blast (Blast-n). Sequence alignment was done using CLUSTAL–W and a phylogenetic tree was constructed using MEGA 6 software as shown in **Figure 1**. The potential isolate DNM50 was identified based on phylogenetic analysis and designated as *Pseudomonas aeruginosa* DNM50 (99% similarity with *Pseudomonas aeruginosa*). The sequence was submitted to NCBI and the GenBank accession number MK351591 was obtained.

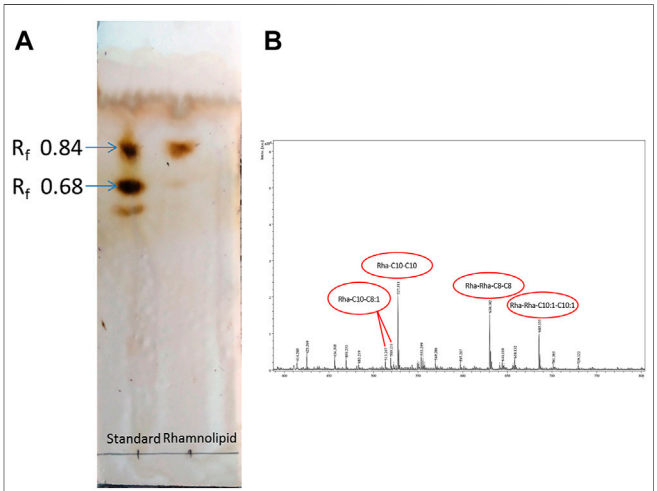

FIGURE 2 | Chemical characterization of Rhamnolipid (DNM50RL) produced from *Pseudomonas aeruginosa* DNM50 by **(A)** thin-layer chromatography (TLC): TLC plate run in a solvent system of butanol:acetic acid:water (2:1:1), developed with Molisch reagent (α—naphthol in ethanol and H_2SO_4) showing typical brown color spots of Rhamnolipid. **(B)** MALDI TOF peaks.

Characterization of Rhamnolipids

A linear increase in the growth of the culture was observed up to 60 h and was declined further. Maximum production of RLs (2.9 g/ L) was achieved at 72 h with no significant increase up to 120 h. A consistent decrease in SFT (from 62 mN/ m to 30 mN/ m) of the medium was recorded up to 120 h (**Supplementary Figure S1**).

TABLE 1 | Molecular ions observed in MALDI-TOF for Rhamnolipids produced by *Pseudomonas aeruginosa* DNM50.

Rhamnolipids	Molecular formula	Calcd mass units [M]	$[M + Na]^+$		$[M + K]^+$		$[M-H+2Na]^+$		Observed
			Obsd	Calcd	Obsd	Calcd	Obsd	Calcd	
Rha-C8-C8:1	$C_{22}H_{38}O_9$	446.2	469	469.2	483-2H	485.2	–	491.2	
Rha-C10-C8:1	$C_{24}H_{42}O_9$	474.2	–	497.2	513	513.2	519	519.2	
Rha-C10-C10	$C_{26}H_{48}O_9$	504.3	527	527.3	–	543.2	–	549.3	
Rha-C10-C12:1	$C_{28}H_{50}O_9$	530.3	553	555.3	569	569.3	–	575.3	
Rha-C16:1	$C_{22}H_{38}O_7$	414.2	–	437.2	–	453.2	–	459.2	414
Rha-C16	$C_{22}H_{40}O_7$	416.2	–	439.2	456 + H	455.2	–	461.2	
Rha-C17:1	$C_{23}H_{40}O_7$	428.2	–	451.2	–	467.2	–	473.2	425
Rha-Rha-C10:1-C10:1	$C_{32}H_{54}O_{13}$	646.3	–	669.3	685	685.3	–	691.3	
Rha-Rha-C10-C12	$C_{34}H_{62}O_{13}$	678.4	701	701.4	–	717.3	–	723.4	
Rha-Rha-C10-C8	$C_{30}H_{54}O_{13}$	622.3	644-H	645.3	–	661.3	–	667.3	
Rha-Rha-C10-C8:1	$C_{30}H_{52}O_{13}$	620.3	–	643.3	658 -H	659.3	–	665.3	
Rha-Rha-C8-C8	$C_{28}H_{50}O_{13}$	594.3	–	617.3	630-3H	633.2	–	639.2	597−3H

Thin layer chromatogram (**Figure 2A**) of RLs produced by *Pseudomonas aeruginosa* DNM50 showed two characteristic spots corresponding to standard RLs on reaction with Molisch reagent with retardation factor (R_f) values of 0.84 and 0.68 confirming the presence of mono-RLs and di-RLs, respectively. Positive reaction with Molisch reagent and iodine vapors ratifies glycolipid nature of RLs. No spots were observed with ninhydrin reagent indicating absence of amino acids/proteins. Many researchers reported similar RLs mixture with varying composition (Haba et al., 2003; Silva et al., 2010; Abbasi et al., 2012).

MALDI-TOF (**Figure 2B**) confirmed the presence of mono-RL and di-RL congeners, specifically Rha-C8-C8:1, Rha-C10-C8:1, Rha-C10-C10, Rha-C10-C12:1, Rha-C16:1, Rha-C16, Rha-C17:1, Rha-Rha-C10:1-C10:1, Rha-Rha-C10-C12, Rha-Rha-C10-C8, Rha-Rha-C10-C8:1, and Rha-Rha-C8-C8 as shown in **Table 1**. The spectrum was characterized by molecular ions for mono-RLs (m/z 470-575) and di-RLs (m/z 640-730). Major ions at m/z 527 were attributed to $[M + Na]^+$ adduct ions of the major mono-RL, Rha-C10-C10 and m/z 630 and 685 were attributed to $[M + K]^+$ adduct ions of the major di-RLs, Rha-Rha-C8-C8, and Rha-Rha-C10:1-C10:1, respectively. These findings were in accordance with the work previously reported for analysis of RLs produced by different strains of *Pseudomonas aeruginosa* (Price et al., 2009; Sarachat et al., 2010; Abeer Mohammed et al., 2018).

Based on chromatographic and spectroscopic analyses, it can be inferred that the biosurfactant produced by *Pseudomonas aeruginosa* DNM50 is comprised of congeners of mono-RLs and di-RLs.

Radical Scavenging Attribute

DPPH assay was developed to examine the antioxidant activity, which relies on the measurement of scavenging ability of antioxidants to a stable free radical, DPPH. Electron of nitrogen atom from DPPH was reduced to corresponding hydrazine by a hydrogen atom from the antioxidant. Reduced form of DPPH shows a color change from deep violet to yellow, thus assessing antioxidant activity of the given compound (Kedare and Singh, 2011). The DPPH radical scavenging activity of DNM50RL and ascorbic acid was as shown in **Figures 3A,B**.

At 5 mg/ml concentration, DNM50RL and ascorbic acid showed a radical scavenging activity of 84.25 and 98.4%, respectively. This activity increases with an increase in concentration. The IC_{50} value was 101.8 μg/ml for DNM50RL and 2.064 μg/ml for ascorbic acid as determined from GraphPad Prism software. At 1 mg/ml, MCTG107b and MCTG214 (3b1) derived biosurfactant exhibited only 9.67 ± 3.27% and 15.46 ± 4.03% inhibition for DPPH assay (Voulgaridou et al., 2021).

DPPH radical scavenging activity of 69.1 and 73.5% were reported at 5.0 mg/ml of BS-VSG4 and BS-VS16 biosurfactants from *Bacillus* strains (Giri et al., 2019). An IC_{50} value of 4.15 mM for RLs from *Pseudomonas aeruginosa* was deduced (Abdollahi et al., 2020). Similarly, IC_{50} value of 357 μg/ml was observed for DCS1 lipopeptide biosurfactants produced from *Bacillus methylotrophicus* (Jemil et al., 2017). The DNM50RL has shown weak antioxidant activity than standard ascorbic acids but is better than the activity reported by other related studies. The radical scavenging activity for biosurfactants was due to the transfer of protons or electrons, thus neutralizing free radicals. This activity was enhanced by hydrocarbon fatty acid in RLs and was not affected by their variation in chain length (Tofani et al., 2010; Tabbene et al., 2012).

Cytotoxic Attribute

Cell viability assays such as dye exclusion, colorimetric, fluorometric, luminometric, and flowcytometric are being used by various researchers. However, measurement of cell viability/proliferation cannot be examined by only one method, since it is influenced by types and origins of cell lines and the mechanism of action of the cytotoxic agents explored. Thus, it is recommended to apply more than one assay for cell viability/proliferation (Kamiloglu et al., 2020).

MTT assay was performed to assess the antiproliferative effect of different concentrations of DNM50RL against MDA-MB-231 cell lines. There is a linear relationship between cell activity and absorbance measuring growth rate of cells, thus MTT is a quantitative and sensitive detection of cell proliferation (Mahajan et al., 2012). MTT can be reduced through the

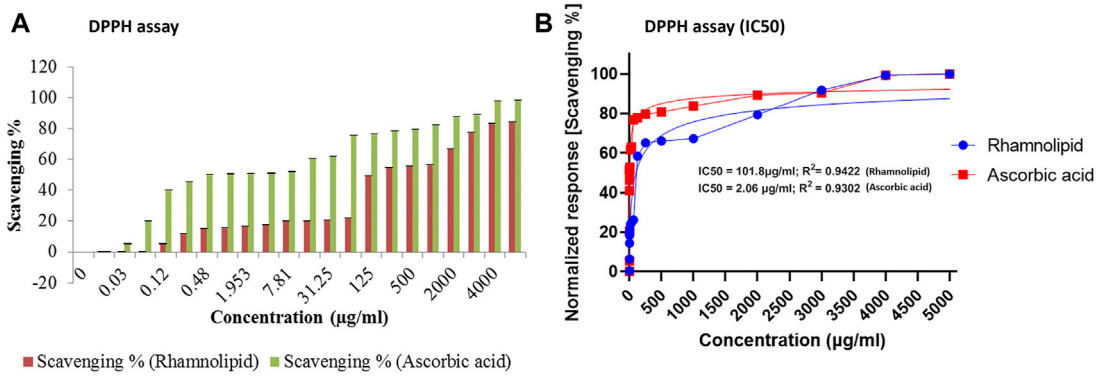

FIGURE 3 | The DPPH radical scavenging activity of DNM50RL and ascorbic acid **(A)** Scavenging %. Values represented as mean ± SD of three independent experiments. Error bars represent SD (*$p < 0.05$). **(B)** Non-linear regression curve fit (DPPH assay). IC_{50} determined by nonlinear regression (curve fit [Inhibitor] vs. normalized response–Variable slope) using GraphPad prism software.

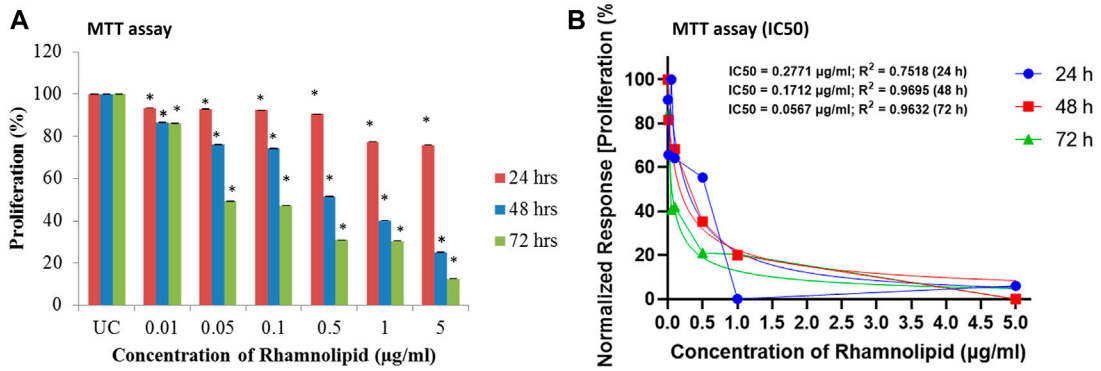

FIGURE 4 | Antiproliferative effect of DNM50RL on MDA-MB 231 cell line by MTT assay after 24, 48, and 72 h of treatment. **(A)** Dose dependent inhibition. Values represented as mean ± SD of three independent experiments. Error bars represent SD (*$p < 0.05$). **(B)** IC_{50} determination by nonlinear regression [curve fit (Inhibitor) vs. normalized response–Variable slope] using GraphPad prism software.

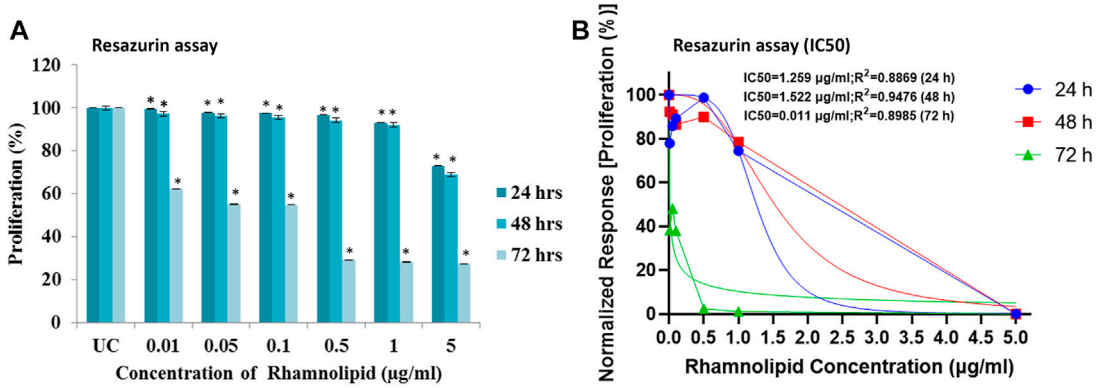

FIGURE 5 | Antiproliferative effect of DNM50RL on human breast cancer cell lines MDA-MB- 231 cell line by resazurin assay after 24, 48, and 72 h of treatment. **(A)** Dose dependent inhibition. Values represented as mean ± SD of three independent experiments. Error bars represent SD (*$p < 0.05$). **(B)** IC_{50} determined by nonlinear regression [curve fit (Inhibitor) vs. normalized response–Variable slope] using GraphPad prism software.

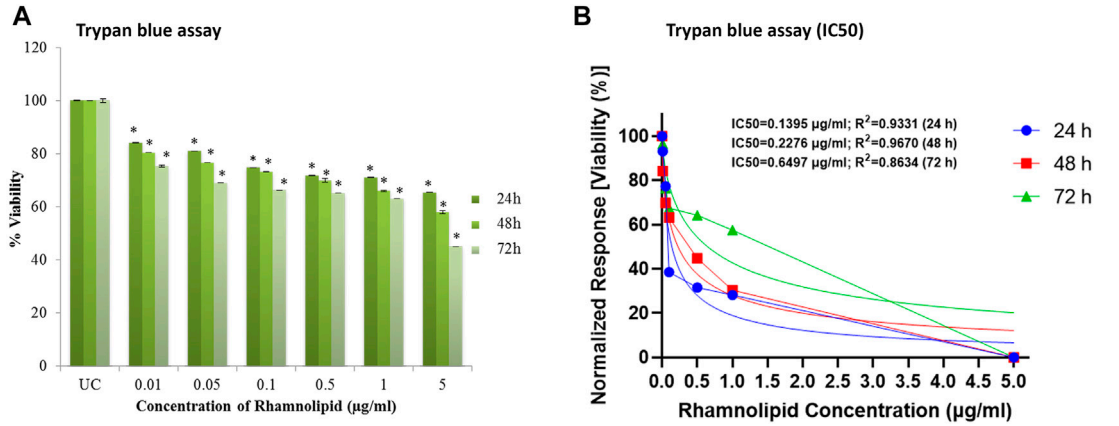

FIGURE 6 | Cell viability efficacy of DNM50RL on human breast cancer cell lines MDA-MB-231 cell line by trypan blue assay after 24, 48, and 72 h of treatment. **(A)** Dose dependent inhibition. Values represented as mean ± SD of three independent experiments. Error bars represent SD (*$p < 0.05$). **(B)** IC_{50} determined by nonlinear regression [curve fit (Inhibitor) vs. normalized response–Variable slope] using GraphPad prism software.

mitochondrial enzyme, which is possible only in the cells with active metabolism. Hence, measurement of cell proliferation is indicated directly by the number of metabolically active/viable cells. With an increase in the concentration of DNM50RL, there is an increase in inhibition of cell proliferation at 24 h. Similar dose-dependent inhibition was observed at 48 and 72 h, with the best results obtained when treatment was given for 72 h showing an IC_{50} value of 0.05 µg/ml (**Figures 4A,B**).

In resazurin assay, viable cells with active metabolism cause reduction of resazurin to resofurin product, which is pink and fluorescent (Riss et al., 2016). The assay is more sensitive than the MTT assay (Shum et al., 2008), hence it is used to confirm further the antiproliferative activity of DNM50RL against MDA-MB-231 cell lines. A dose dependent trend was observed with IC_{50} value of 1.5 µg/ml at 48 h of treatment, though the best effect was observed at 72 h of treatment with IC_{50} of 0.01 µg/ml (**Figures 5A,B**).

Trypan blue dye exclusion assay was further used for evaluation of cytotoxicity activity of DNM50RL. This assay easily differentiates live and dead cells as the dead cells take up the dye and live cells exclude trypan blue, hence the name. It is because live cells will retain their membrane intact and dead cells will lose membrane integrity due to apoptosis/necrosis (Farghadani et al., 2017). **Figure 6A** shows the decrease in cell viability in 72 h by DNM50RL in a dose dependent manner confirming its role in cytotoxicity activity against MDA-MB-231 cell line (**Figure 6B**). When the treatment was given for 72 h, the IC_{50} value was 0.64 µg/ml. The IC_{50} value of DNM50RL was lower than the positive control, Etoposide (IC_{50} value of 20.65, 25.77, 51.10 µM by MTT, resazurin and Trypan blue assay at 72 h of treatment) (**Supplementary Figure S2**).

A number of researchers worked on cytotoxic effect of different glycolipid based biosurfactants against different cell lines (**Table 2**). However, there is limited data available on the cytotoxic effect of RLs against MDA-MB-231 cell line.

It can be inferred from the results of all cell proliferation/viability assays that DNM50RL is inhibiting proliferation of MDA-MB-231 cell line in a dose dependent and time dependent manner. Moreover, few reports showed that mono-RLs are more effective for inhibition of breast cancer cells and some emphasize di-RLs to be more effective (Thanomsub et al., 2006; Jiang et al., 2014; Rahimi et al., 2019). Due to such variations found in the biological potentials of purified mono-RLs and di-RLs from previous reports, the present study was aimed to reveal the biological attributes of natural RLs in their native form. This is because an appropriate proportion/mixture of mono-RLs and di-RLs may have much pronounced activity than the individual congeners. Many researchers reported a lack of cytotoxic activity of RLs against normal human cells, e.g., Vero cells, PBMN-peripheral blood mononuclear cells. This may be due to the presence of more negatively charged functional groups on cancer cells and its variation in fatty acid profiles with respect to normal cells, which facilitates greater endocytosis activity of cancer cells (Gudiña et al., 2013; Dwivedi et al., 2015). Reports from various studies on RLs against different cancerous and normal healthy cells show discrete results. This may be due to the nature of normal and cancerous cells studied, purity and types of RL variants, and the degree of surface tension reduction (Rahimi et al., 2019).

Downregulation of P38MAPK

Western blot analysis was done to compare the phosphorylated (p-p38MAPK) and total (t-p38MAPK) p38MAPK protein levels after treatment with DNM50RL (5 µg/ ml). This was done to determine whether p38MAPK is responsible for DNM50RL cytotoxicity in triple negative breast cancer cell line MDA-MB-231. As shown in **Figures 7A,B**, the protein levels of total p38 were higher in these cells until 72 h in control and treated cells (lower panel) while the phosphorylated p38 was downregulated (upper panel).

Several studies showed that p38 mitogen activated protein kinases (MAPKs) play a critical role in cellular responses, proliferation, survival, cell cycle, and migration in cancer. As DNM50RL can downregulate p38 phosphorylation, it can be proposed as a novel and potent anticancer agent with its effectiveness at a very low concentration. RL a (Rha-Rha-C10-

TABLE 2 | IC_{50} values of few glycolipid based biosurfactants against different cell lines.

Biosurfactant	Source	Cell line	Cytotoxic assay	IC50/LC50/GI50/ EC50	Treatment time	References
Rhamnolipid 1; Rhamnolipid 2	*Pseudomonas sp.*	HepG2 liver cancer cell line; A549 lung cancer cell line; MDA-MB-231 cell line; HeLa cell line	MTT assay	140 μM, 154 μM, 86 μM, 123 μM; 79 μM, 98 μM, 58 μM, 88 μM	48 h	Kamal et al. (2012)
Glycolipid biosurfactant S9BS	*Lysinibacillus fusiformis* S9	HEK-293, a human embryonic kidney cancer cell	MTT assay	75 μg/ ml (LC50)	24 h	Pradhan et al. (2014)
Monorhamnolipid (NDYS-4E)	*Streptomyces coelicoflavus* NBRC (15399^T)	MCF-7, a breast cancer cell line	MTT assay	88.60 μg/ ml	48 h	Allada et al. (2015)
BS1a; BS1b	R−95^{TM} RL; R−90 ^{TM} RL	MCF−7, a breast cancer cell line	MTT assay	153.40 μg/ ml,98.27 μg/ ml,33.08 μg/ ml; 168.50 μg/ ml, 42.85 μg/ ml,30.05 μg/ ml	24 h, 48 h, 72 h	Akiyode et al. (2016)
Rhizoleucinoside, a RL - amino-alcohol hybrid	*Bradyrhizobium sp.* BRAil	Murine microglia; Rat microglia	CellTiter-Glo 2.0 (CTG 2.0) assay	6.9 μM; 22 μM	24 h	Chen et al. (2016)
Biosurfactant	*Lactobacillus casei*	HEp-2 cell line	MTT assay	109.1 ± 0.84 mg/ ml to 129.7 ± 0.52 mg/ ml	48 h	Merghni et al. (2017)
Dokdolipids A, B, C	*Actinoalloteichus hymeniacidonis* 179DD-027	MDA-MB-231 breast cancer cell line	Sulforhodamine (SRB) assay	30.6, 40.4, 25.5 μM (GI50)	48 h	Choi et al. (2019)
Monorhamnolipids; Dirhamnolipids	*Pseudomonas aeruginosa* MR01	MCF-7 breast cancer cell line	MTT assay	25.87 μg/ ml; 31 μg/ ml	48 h	Rahimi et al. (2019)
L-SL (Lactonic form of sophorolipids); Glucolipids	*Starmerella bombicola* MTCC1910 *Candida bombicola*	Human lung adenocarcinoma epithelial cell line A549; MDA-MB-231 breast cancer cell line;	MTT assay	50 μg/ ml, 40 μg/ ml, 880 μg/ ml, 400 μg/ ml; 50 μg/ ml, 40 μg/ ml, 900 μg/ ml, 400 μg/ ml; 40 μg/ml, 35 μg/ml, 600 μg/ml, 100 μg/ml	24 h, 48 h	Haque et al. (2021)
MCTG107b (mixture of rhamnolipid analogues); MCTG214 (3b1) (dirhamnolipids congeners)	*Marinobacter* strain *Pseudomonas* strain	Mouse skin melanoma cell line B16F10 HaCat keratinocyte cell Line THLE3 liver cell line	Almar blue assay	1.3 ± 0.4 mg/ ml, 0.73 ± 0.1 mg/ ml, 0.76 ± 0.1 mg/ ml (EC50); 1.28 mg/ ml±0.2, 1.04 ± 0.1 mg/ ml, 0.96 ± 0.1 mg/ ml (EC50); 1.35 ± 0.1 mg/ ml, 0.78 ± 0.1 mg/ ml, 0.55 ± 0.1 mg/ml (EC50); 2.3 ± 0.2 mg/ml, 0.99 ± 0.1 mg/ml, 0.84 ± 0.1 mg/ ml (EC50);	24, 48, 72 h	Voulgaridou et al. (2021)
RL1; RL2	*Pseudomonas aeruginosa* BN10	MCF-7, breast cancer cell line; MDA-MB-231 breast cancer cell lines	MTT assay	8.68 μg/ ml, 8.67 μg/ ml; 6.99 μg/ ml, 8.60 μg/ ml	48 h	Semkova et al. (2021)
DNM50RL (a mixture of mono and dirhamnolipids)	*Pseudomonas aeruginosa* DNM50	MDA-MB-231 breast cancer cell line	MTT assay Resazurin assay Trypan blue assay	0.27 μg/ ml.,0.17 μg/ ml,0.05 μg/ ml 1.25 μg/ ml, 1.52 μg/ ml, 0.01 μg/ ml 0.13 μg/ ml,0.22 μg/ ml,0.64 μg/ ml	24, 48, 72 h	Present study
Etoposide	Standard anticancer drug	MDA-MB-231 cell line	MTT assay, Resazurin assay Trypan blue assay	46.59, 25.22, 20.65 μM 88.32, 60.94, 25.77 μM 70.25, 56.01, 51.10 μM	24h, 48h, 72 h	Present study

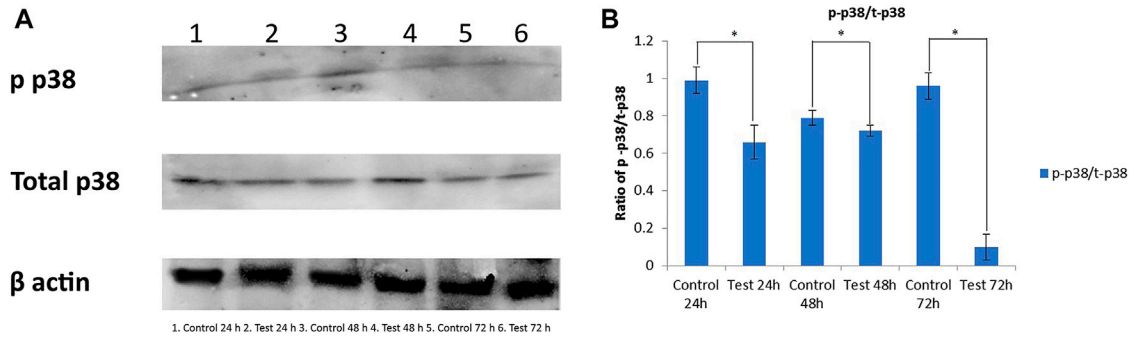

FIGURE 7 | (A) Western blot for antibody phosphorylated p38 and total p38. β actin served as loading control. **(B)** Graph representing the ratio of phosphorylated p38 (p-p38)/total p38 (t-p38). The intensity related to expression of p-p38 and t-p38 was analyzed using ImageJ software. All the results are presented as the means ± SD of three independent measurements. Error bars represent standard deviation. (*) Differences were considered significant at $p < 0.05$ as compared with control groups.

C10) isolated from *Pseudomonas aeruginosa* B189 inhibited the proliferation of MCF-7 cells, human breast cancer cell lines with a MIC of 6.25 μg/ml, whereas RL b (Rha-Rha-C10-C12) did not exhibit significant cytotoxic activity. At 50 μg/ml, Rha-Rha-C10-C10 or Rha-Rha-C10-C12 did not show cytotoxic effect against Vero cells, a normal cell line. Thus, this report demonstrates the toxic sensitivity of different congeners of these RLs to other cell lines used (Thanomsub et al., 2006).

Di-rhamnolipids (Rha-Rha-C10-C10 as a major component) produced by *Pseudomonas aeruginosa* M14808 showed antiproliferative efficiency against MCF-7 and H460, a human non-small lung cancer line with a MIC of 1 μg/ml and 5 μg/ml, whereas mono-RLs (Rha-C10-C10 as a major component) and crude extract did not show any antiproliferative activity (Zhao et al., 2013).

Similar sensitivity of RLs (mono-RLs and di-RLs) against two cancer cell lines, HepG2 (a human hepatocellular carcinoma cell line), Caco-2 (a human colon carcinoma cell line), and a normal cell HK-2 (a human proximal tubular epithelial cell line) were reported (Jiang et al., 2014). Mono-RLs presented higher cytotoxicity than di-RLs, which is due to large surface tension reduction by mono-RLs than di-RLs. They stated that similar sensitivity was observed for normal as well as cancerous cell lines with or without fetal bovine serum (FBS). Addition of FBS attenuates the cytotoxic effect of RLs. These observations revealed that RLs reduce surface tension of the culture medium, eliciting its cytotoxic effect, instead of causing any modification in molecular structure. Further, mainly decreased cytotoxic effect was observed *in vivo* as RLs get dissolved in simulated gastric juice. Thus, further research to illustrate high level of biosafety of RLs *in vivo* offers valuable suggestions for cancer researchers (Jiang et al., 2014).

An efficient cytotoxic potency of RLs (Rha-Rha-C10-C10 and Rha-Rha-C10) isolated from *Pseudomonas sp.* strain ICTB -745 was reported against different human cancer cell lines, e.g., lung adenocarcinoma, hepatocellular liver carcinoma, breast adenocarcinoma, and cervical cancer cell lines (Kamal et al., 2012). Mono-RLs (Rha-C10-C10, as a major component) from *Pseudomonas aeruginosa* BN10 had noticeable cytotoxic activity against human urinary bladder carcinoma cell line, human promyelocytic leukemia cell line, human pre-B leukemia cell line, and T-cell chronic lymphocytic leukemia cell line. The probable reason may be the structure of mono-RLs molecule, causing high penetration in tumor cell, leading to cell viability reduction. Mono-RLs induced cell death, are mediated by induction of apoptosis, inactivation of cellular oncogenes or activation/alteration of tumor suppressor process. The dose dependent apoptotic progression of mono-RLs may be due to efflux pump or the receptors present on cell membrane gets saturated, interfering with the permeation of active molecules within the cancerous cells (Christova et al., 2013). *Bcl-2* and *c-myc* gene overexpression in human BV-173 pre-B leukemia cell line were observed with high doses of mono-RLs, resulting in high proliferative and anti-apoptotic effect, which is overcome by prolonged incubation period (≥72 h). Low cytotoxicity against Balb/c 3T3, a non-tumorigenic mouse fibroblast cell line was confirmed by Balb/c 3T3 neutral red uptake test (Christova et al., 2013).

RL-AgNPs from *Pseudomonas aeruginosa* JS-11, at concentration of 10 μg/ ml, showed a remarkable decrease in cell viability of MCF-7 breast cancer cell lines and no significant effect on PBMN—a normal human peripheral blood mononuclear cell was reported. It might be because the anionic metal nanoparticles cause greater attachment into plasma membrane of MCF-7 cells due to the presence of a negatively charged group on the cancer cell surface. This causes greater endocytic activity causing internalization of metal nanoparticles through vesicular transport pathway. Thus, the RL-AgNPs attachment to the cell surface leads to oxidative stress and cell membrane disruption, which assures it as a primary candidate for novel cancer therapy (Dwivedi et al., 2015).

Although many reports are available showing the anticancer activity of the RLs against various other cancer cell lines, there is limited studies available on MDA-MB-231 cell lines. Also, the mechanism of action of RLs at the molecular level is still insufficiently understood. A future study to elucidate the mechanism is needed to learn its biochemical and cellular interaction followed by preclinical studies and clinical trials at different stages (Abbasi et al., 2013; Abalos et al., 2017). The structure and activity relationship studies of pure or mixture of RLs would also offer advantages for researchers to elucidate their biological characterization and predict the biological function of various RL congeners in combination or in particular (Chen et al., 2017).

CONCLUSION

Lower toxicity and higher biodegradability attributes of biosurfactants are always advantageous over chemical surfactants for significant biotechnological applications. Isolated and identified strain of *Pseudomonas aeruginosa* DNM50 in the present study is novel due to the significant cytotoxic effect of its RL against triple negative breast cancer cell lines. Twelve different congeners were detected by MALDI-TOF, which contributes to the functional efficiency of RLs. DNM50RL seems to be a potential molecule in the future for cancer therapy due to its very low IC_{50} value against MDA-MB-231 cell line and its significant role in inhibition of p38MAPK. Therefore, the DNM50RL can be a prospective natural, therapeutic anticancer agent.

DATA AVAILABILITY STATEMENT

The datasets presented in this study can be found in online repositories. The names of the repository/repositories and accession number(s) can be found in the article/**Supplementary Material**.

AUTHOR CONTRIBUTIONS

NM, DA, and BS designed the experiments. NM, SD, and KR performed the experiments. NM, RK, and VP performed the data analysis and wrote the manuscript. DA and BS critically reviewed the whole manuscript. All the authors read and approved the final manuscript.

FUNDING

This work was supported by the Department of Science and Technology, Women Scientist Scheme-A (SR/WOS-A/LS-262/2017).

ACKNOWLEDGMENTS

NM and DA thank BS, Department of Biotechnology, University of Mysuru, Manasgangothri, Mysuru for extending laboratory facilities. NM and DA thank NCIM, Pune for extending support for sequencing. The authors also wish to acknowledge Proteomics facility, Molecular Biophysics Unit (IISC Bangalore) for MALDI-TOF facility.

SUPPLEMENTARY MATERIAL

The Supplementary Material for this article can be found online at: https://www.frontiersin.org/articles/10.3389/fbioe.2021.761266/full#supplementary-material

Supplementary Figure 1 | Growth curve and production of rhamnolipids by Pseudomonas aeruginosa DNM50 in neem oil cake extract as the production medium.

Supplementary Figure 2 | Antiproliferative effect of Etoposide (Positive control) on MDA-MB 231 cell lines for 24, 48, and 72 h of treatment by **(A)** MTT assay showing dose dependent inhibition **(B)** IC50 representative graph for MTT assay **(C)** Resazurin assay showing dose dependent inhibition **(D)** IC50 representative graph for Resazurin assay **(E)** Trypan blue assay showing dose dependent inhibition **(F)** IC50 representative graph for Trypan blue assay. For dose dependent inhibition, values are represented as mean ± SD of three independent experiments. Error bars represent SD. Differences with control groups were significant at $^*p < 0.05$. IC50 was determined by nonlinear (curve fit [Inhibitor] vs. normalized response-Variable slope) using GraphPad prism software.

REFERENCES

Abalos, A., Pinazo, A., Infante, M. R., Casals, M., García, F., and Manresa, A. (2001). Physicochemical and Antimicrobial Properties of New Rhamnolipids Produced by *Pseudomonas aeruginosa* AT10 from Soybean Oil Refinery Wastes. *Langmuir* 17, 1367–1371. doi:10.1021/la0011735

Abbasi, H., Hamedi, M. M., Lotfabad, T. B., Zahiri, H. S., Sharafi, H., Masoomi, F., et al. (2012). Biosurfactant-producing Bacterium, *Pseudomonas aeruginosa MA01* Isolated from Spoiled Apples: Physicochemical and Structural Characteristics of Isolated Biosurfactant. *J. Biosci. Bioeng.* 113, 211–219. doi:10.1016/j.jbiosc.2011.10.002

Abbasi, H., Noghabi, K. A., Hamedi, M. M., Zahiri, H. S., Moosavi-Movahedi, A. A., Amanlou, M., et al. (2013). Physicochemical Characterization of a Monorhamnolipid Secreted by *Pseudomonas aeruginosa* MA01 in Aqueous Media. An Experimental and Molecular Dynamics Study. *Colloids Surf. B: Biointerfaces* 101, 256–265. doi:10.1016/j.colsurfb.2012.06.035

Abdollahi, S., Tofighi, Z., Babaee, T., Shamsi, M., Rahimzadeh, G., Rezvanifar, H., et al. (2020). Evaluation of Anti-oxidant and Anti-biofilm Activities of Biogenic Surfactants Derived from *Bacillus Amyloliquefaciens* and *Pseudomonas aeruginosa*. *Iran J. Pharm. Res.* 19, 115–126. doi:10.22037/IJPR.2020.1101033

Abeer Mohammed, A. B., Tayel, A. A., and Elguindy, N. M. (2018). Production of New Rhamnolipids Rha C16-C16 by *Burkholderia sp.* Through Biodegradation of Diesel and Biodiesel. *Beni-Suef Univ. J. Basic Appl. Sci.* 7, 492–498. doi:10.1016/j.bjbas.2018.05.003

Akiyode, O., George, D., Getti, G., and Boateng, J. (2016). Systematic Comparison of the Functional Physico-Chemical Characteristics and Biocidal Activity of Microbial Derived Biosurfactants on Blood-Derived and Breast Cancer Cells. *J. Colloid Interf. Sci.* 479, 221–233. doi:10.1016/j.jcis.2016.06.051

Allada, L. T. K., Guntuku, G. S., Muthyala, M. K. K., Duddu, M. K., and Golla, N. S. (2015). Characterization of Bioactive Compound from *Streptomyces Coelicoflavus* NBRC (15399T) and its Anticancer Activity. *Int. J. Chem. Pharm. Anal.* 2, 1–13. https://www.ijcpa.in/articles/characterization-of-bioactive-compound-obtained-from-streptomyces-coelicoflavus-nbrc-15399t-and-its-anticancer-activity.pdf. https://www.ijcpa.in/abstract/characterization-of-bioactive-compound-obtained-from-streptomyces-coelicoflavus-nbrc-15399t-and-its-anticancer-activity-80732.html.

Altschul, S. F., Gish, W., Miller, W., Myers, E. W., and Lipman, D. J. (1990). Basic Local Alignment Search Tool. *J. Mol. Biol.* 215, 403–410. doi:10.1016/S0022-2836(05)80360-2

Amena, S., Vishalakshi, N., Prabhakar, M., Dayanand, A., and Lingappa, K. (2010). Production, Purification and Characterization of L-Asparaginase from *Streptomyces Gulbargensis*. *Braz. J. Microbiol.* 41, 173–178. doi:10.1590/S1517-83822010000100002510.1590/s1517-83822010000100025

Banat, I. M., De Rienzo, M. A. D., and Quinn, G. A. (2014a). Microbial Biofilms: Biosurfactants as Antibiofilm Agents. *Appl. Microbiol. Biotechnol.* 98, 9915–9929. doi:10.1007/s00253-014-6169-6

Banat, I. M., Satpute, S. K., Cameotra, S. S., Patil, R., and Nyayanit, N. V. (2014b). Cost Effective Technologies and Renewable Substrates for Biosurfactants Production. *Front. Microbiol.* 5, 697. doi:10.3389/fmicb.2014.00697

Bradford, M. M. (1976). A Rapid and Sensitive Method for the Quantitation of Microgram Quantities of Protein Utilizing the Principle of Protein-Dye Binding. *Anal. Biochem.* 72, 248–254. doi:10.1006/abio.1976.999910.1016/0003-2697(76)90527-3

Burgos-Díaz, C., Martín-Venegas, R., Martínez, V., Storniolo, C. E., Teruel, J. A., Aranda, F. J., et al. (2013). *In Vitro* study of the Cytotoxicity and Antiproliferative Effects of Surfactants Produced by *Sphingobacterium Detergens*. *Int. J. Pharm.* 453, 433–440. doi:10.1021/acsomega.0c04933

Byrappa, S., Harsha Raj, M., Kungyal, T., Kudva, N., and Narayana, U. (2017). Synthesis and Biological Evaluation of Novel Isoxazolines Linked via Piperazine to 2- Benzoisothiazoles as Potent Apoptotic Agents. *Eur. J. Med. Chem.* 126, 218–224. doi:10.1016/j.ejmech.2016.09.094

Cai, B., Chang, S. H., Becker, E. B. E., Bonni, A., and Xia, Z. (2006). p38 MAP Kinase Mediates Apoptosis through Phosphorylation of BimEL at Ser-65. *J. Biol. Chem.* 281, 25215–25222. doi:10.1074/jbc.M512627200

Cailleau, R., Olivé, M., and Cruciger, Q. V. J. (1978). Long-term Human Breast Carcinoma Cell Lines of Metastatic Origin: Preliminary Characterization. *In Vitro* 14, 911–915. doi:10.1007/BF02616120

Chandankere, R., Yao, J., Choi, M. M. F., Masakorala, K., and Chan, Y. (2013). An Efficient Biosurfactant-Producing and Crude-Oil Emulsifying Bacterium Bacillus Methylotrophicus USTBa Isolated from Petroleum reservoir *Bacillus methylotrophicus* USTBa Isolated from Petroleum Reservoir. *Biochem. Eng. J.* 74, 46–53. doi:10.1016/j.bej.2013.02.018

Chavez, K. J., Garimella, S. V., and Lipkowitz, S. (2011). Triple Negative Breast Cancer Cell Lines: One Tool in the Search for Better Treatment of Triple Negative Breast Cancer. *Breast. Dis.* 32, 35–48. doi:10.3233/BD-2010-0307

Chen, J., Sun, J., Deering, R. W., DaSilva, N., Seeram, N. P., Wang, H., et al. (2016). Rhizoleucinoside, a Rhamnolipid-Amino Alcohol Hybrid from the Rhizobial Symbiont *Bradyrhizobium sp.* BTAi1. *Org. Lett.* 18, 1490–1493. doi:10.1021/acs.orglett.6b00461

Chen, J., Wu, Q., Hua, Y., Chen, J., Zhang, H., and Wang, H. (2017). Potential Applications of Biosurfactant Rhamnolipids in Agriculture and Biomedicine. *Appl. Microbiol. Biotechnol.* 101, 8309–8319. doi:10.1007/s00253-017-8554-4

Choi, B.-K., Lee, H.-S., Kang, J. S., and Shin, H. J. (2019). Dokdolipids A–C, Hydroxylated Rhamnolipids from the Marine-Derived Actinomycete *Actinoalloteichus hymeniacidonis*. *Mar. Drugs* 17, 237. doi:10.3390/md17040237

Chopra, A., Bobate, S., Rahi, P., Banpurkar, A., Mazumder, P. B., and Satpute, S. (2020). *Pseudomonas aeruginosa* RTE4: A tea Rhizobacterium with Potential for Plant Growth Promotion and Biosurfactant Production. *Front. Bioeng. Biotechnol.* 8, 861. doi:10.3389/fbioe.2020.00861

Christova, N., Tuleva, B., Kril, A., Georgieva, M., Konstantinov, S., Terziyski, I., et al. (2013). Chemical Structure and *In Vitro* Antitumor Activity of Rhamnolipids from *Pseudomonas aeruginosa* BN10. *Appl. Biochem. Biotechnol.* 170, 676–689. doi:10.1007/s12010-013-0225-z

Clarridge, J. E. (2004). Impact of 16S rRNA Gene Sequence Analysis for Identification of Bacteria on Clinical Microbiology and Infectious Diseases. *Clin. Microbiol. Rev.* 17, 840–862. doi:10.1128/CMR.17.4.840-862.2004

Darby, A. C., Chandler, S. M., Welburn, S. C., and Douglas, A. E. (2005). Aphid-symbiotic Bacteria Cultured in Insect Cell Lines. *Appl. Environ. Microbiol.* 71, 4833–4839. doi:10.1128/AEM.71.8.4833-4839.2005

De Almeida, D. G., Soares Da Silva, R. d. C. F., Luna, J. M., Rufino, R. D., Santos, V. A., Banat, I. M., et al. (2016). Biosurfactants: Promising Molecules for Petroleum Biotechnology Advances. *Front. Microbiol.* 7, 1718. doi:10.3389/fmicb.2016.01718

Dwivedi, S., Saquib, Q., Al-Khedhairy, A. A., Ahmad, J., Siddiqui, M. A., and Musarrat, J. (2015). Rhamnolipids Functionalized AgNPs-Induced Oxidative Stress and Modulation of Toxicity Pathway Genes in Cultured MCF-7 Cells. *Colloids Surf. B: Biointerfaces* 132, 290–298. doi:10.1016/j.colsurfb.2015.05.034

Farghadani, R., Rajarajeswaran, J., Mohd Hashim, N. B., Abdulla, M. A., and Muniandy, S. (2017). A Novel β-diiminato manganese III Complex as the Promising Anticancer Agent Induces G0/G1 Cell Cycle Arrest and Triggers Apoptosis via Mitochondrial-dependent Pathways in MCF-7 and MDA-MB-231 Human Breast Cancer Cells. *RSC Adv.* 7, 24387–24398. doi:10.1039/c7ra02478a

Fracchia, L., Banat, J. J., J. Banat, J., Cavallo, M., Ceresa, C., and M. Banat, I. (2015). Potential Therapeutic Applications of Microbial Surface-Active Compounds. *AIMS Bioeng.* 2, 144–162. doi:10.3934/bioeng.2015.3.144

García-Cano, J., Roche, O., Cimas, F. J., Pascual-Serra, R., Ortega-Muelas, M., Fernández-Aroca, D. M., et al. (2016). p38MAPK and Chemotherapy: We Always Need to Hear Both Sides of the story. *Front. Cel Dev. Biol.* 4, 1–8. doi:10.3389/fcell.2016.00069

Garcia-Manero, G., Khoury, H. J., Jabbour, E., Lancet, J., Winski, S. L., Cable, L., et al. (2015). A Phase I Study of Oral ARRY-614, a P38 MAPK/Tie2 Dual Inhibitor, in Patients with Low or Intermediate-1 Risk Myelodysplastic Syndromes. *Clin. Cancer Res.* 21, 985–994. doi:10.1158/1078-0432.CCR-14-1765

Giri, S. S., Ryu, E., Sukumaran, V., and Park, S. C. (2019). Antioxidant, Antibacterial, and Anti-adhesive Activities of Biosurfactants Isolated from *Bacillus* Strains. *Microb. Pathogenesis* 132, 66–72. doi:10.1016/j.micpath.2019.04.035

Gudiña, E. J., Rangarajan, V., Sen, R., and Rodrigues, L. R. (2013). Potential Therapeutic Applications of Biosurfactants. *Trends Pharmacol. Sci.* 34, 667–675. doi:10.1016/j.tips.2013.10.002

Gudiña, E. J., Rodrigues, A. I., de Freitas, V., Azevedo, Z., Teixeira, J. A., and Rodrigues, L. R. (2016). Valorization of Agro-Industrial Wastes towards the Production of Rhamnolipids. *Bioresour. Tech.* 212, 144–150. doi:10.1016/j.biortech.2016.04.027

Gupta, J., Igea, A., Papaioannou, M., Lopez-Casas, P. P., Llonch, E., Hidalgo, M., et al. (2015). Pharmacological Inhibition of P38 MAPK Reduces Tumor Growth in Patient-Derived Xenografts from colon Tumors. *Oncotarget* 6, 8539–8551. doi:10.18632/oncotarget.3816

Haba, E., Pinazo, A., Jauregui, O., Espuny, M. J., Infante, M. R., and Manresa, A. (2003). Physicochemical Characterization and Antimicrobial Properties of Rhamnolipids Produced by *Pseudomonas aeruginosa* 47T2 NCBIM 40044. *Biotechnol. Bioeng.* 81, 316–322. doi:10.1002/bit.10474

Haque, F., Khan, M. S. A., and AlQurashi, N. (2021). ROS-mediated Necrosis by Glycolipid Biosurfactants on Lung, Breast, and Skin Melanoma Cells. *Front. Oncol.* 11, 622470. doi:10.3389/fonc.2021.622470

Hazra, C., Kundu, D., Ghosh, P., Joshi, S., Dandi, N., and Chaudhari, A. (2010). Screening and Identification of *Pseudomonas aeruginosa* AB4 for Improved Production, Characterization and Application of a Glycolipid Biosurfactant Using Low-Cost Agro-Based Raw Materials. *J. Chem. Technol. Biotechnol.* 86, 185–198. doi:10.1002/jctb.2480

Hošková, M., Ježdík, R., Schreiberová, O., Chudoba, J., Šír, M., Čejková, A., et al. (2015). Structural and Physiochemical Characterization of Rhamnolipids Produced by *Acinetobacter Calcoaceticus, Enterobacter Asburiae* and *Pseudomonas aeruginosa* in Single Strain and Mixed Cultures. *J. Biotechnol.* 193, 45–51. doi:10.1016/j.jbiotec.2014.11.014

Housman, G., Byler, S., Heerboth, S., Lapinska, K., Longacre, M., Snyder, N., et al. (2014). Drug Resistance in Cancer: An Overview. *Cancers* 6, 1769–1792. doi:10.3390/cancers6031769

Igea, A., and Nebreda, A. R. (2015). The Stress Kinase P38α as a Target for Cancer Therapy. *Cancer Res.* 75, 3997–4002. doi:10.1158/0008-5472.CAN-15-0173

Inès, M., and Dhouha, G. (2015). Glycolipid Biosurfactants: Potential Related Biomedical and Biotechnological Applications. *Carbohydr. Res.* 416, 59–69. doi:10.1016/j.carres.2015.07.016

Jemil, N., Ben Ayed, H., Manresa, A., Nasri, M., and Hmidet, N. (2017). Antioxidant Properties, Antimicrobial and Anti-adhesive Activities of DCS1 Lipopeptides from *Bacillus Methylotrophicus* DCS1. *BMC Microbiol.* 17, 144. doi:10.1186/s12866-017-1050-2

Jiang, L., Shen, C., Long, X., Zhang, G., and Meng, Q. (2014). Rhamnolipids Elicit the Same Cytotoxic Sensitivity between Cancer Cell and Normal Cell by Reducing Surface Tension of Culture Medium. *Appl. Microbiol. Biotechnol.* 98, 10187–10196. doi:10.1007/s00253-014-6065-0

Kamal, A., Shaik, A. B., Kumar, C. G., Mongolla, P., Rani, P. U., Krishna, K. V., et al. (2012). Metabolic Profiling and Biological Activities of Bioactive Compounds Produced by *Pseudomonas Sp.* Strain ICTB-745 Isolated from Ladakh, India. *J. Microbiol. Biotechnol.* 22, 69–79. doi:10.4014/jmb.1105.05008

Kamiloglu, S., Sari, G., Ozdal, T., and Capanoglu, E. (2020). Guidelines for Cell Viability Assays. *Food Front.* 1, 332–349. doi:10.1002/fft2.44

Kedare, S. B., and Singh, R. P. (2011). Genesis and Development of DPPH Method of Antioxidant Assay. *J. Food Sci. Technol.* 48, 412–422. doi:10.1007/s13197-011-0251-1

Lalaoui, N., Hänggi, K., Brumatti, G., Chau, D., Nguyen, N.-Y. N., Vasilikos, L., et al. (2016). Targeting P38 or MK2 Enhances the Anti-leukemic Activity of Smac-Mimetics. *Cancer Cell* 29, 145–158. doi:10.1016/j.ccell.2016.01.006

Li, H., Guo, W., Ma, X.-j., Li, J.-s., and Song, X. (2017). *In Vitro* and *In Vivo* Anticancer Activity of Sophorolipids to Human Cervical Cancer. *Appl. Biochem. Biotechnol.* 181, 1372–1387. doi:10.1007/s12010-016-2290-6

Li, S., Huang, R., Shah, N. P., Tao, X., Xiong, Y., and Wei, H. (2014). Antioxidant and Antibacterial Activities of Exopolysaccharides from *Bifidobacterium Bifidum* WBIN03 and *Lactobacillus Plantarum* R315. *J. Dairy Sci.* 97, 7334–7343. doi:10.3168/jds.2014-7912

Lotfabad, T. B., Abassi, H., Ahmadkhaniha, R., Roostaazad, R., Masoomi, F., Zahiri, H. S., et al. (2010). Structural Characterization of a Rhamnolipid-type Biosurfactant Produced by *Pseudomonas aeruginosa* MR01: Enhancement of Di-rhamnolipid Proportion Using Gamma Irradiation. *Colloids Surf. B: Biointerfaces* 81, 397–405. doi:10.1016/j.colsurfb.2010.06.026

Mahajan, S. D., Law, W.-C., Aalinkeel, R., Reynolds, J., Nair, B. B., Yong, K.-T., et al. (2012). Nanoparticle-mediated Targeted Delivery of Antiretrovirals to the Brain. *Methods Enzymol.* 509, 41–60. doi:10.1016/B978-0-12-391858-1.00003-4

Merghni, A., Dallel, I., Noumi, E., Kadmi, Y., Hentati, H., Tobji, S., et al. (2017). Antioxidant and Antiproliferative Potential of Biosurfactants Isolated from *Lactobacillus Casei* and Their Anti-biofilm Effect in Oral *Staphylococcus aureus* Strains. *Microb. Pathogenesis* 104, 84–89. doi:10.1016/j.micpath.2017.01.017

Mishra, N., Agsar, D., Seelam, S. D., Kattegauda, U. M., Shetty, P. R., and Pandey, V. (2021). Novel Application of *Nerium* Leaf and Image J Software in Drop Collapse Assay for Rapid Screening of Biosurfactant Producing Microorganism. *Indian J. Exp. Biol.* 59, 484–492. http://nopr.niscair.res.in/handle/123456789/57850.

Mohammed, F., Rashid-Doubell, F., Taha, S., Cassidy, S., and Fredericks, S. (2020). Effects of Curcumin Complexes on MDA MB 231 Breast Cancer Cell Proliferation. *Int. J. Oncol.* 57, 445–455. doi:10.3892/ijo.2020.5065

Mulla, S. I., Hu, A., Sun, Q., Li, J., Suanon, F., Ashfaq, M., et al. (2018). Biodegradation of Sulfamethoxazole in Bacteria from Three Different Origins. *J. Environ. Manage.* 206, 93–102. doi:10.1016/j.jenvman.201710.1016/j.jenvman.2017.10.029

Mulla, S. I., Wang, H., Sun, Q., Hu, A., and Yu, C.-P. (2016). Characterization of Triclosan Metabolism in *Sphingomonas sp.* Strain YL-Jm2c. *Sci. Rep.* 6, 21965. doi:10.1038/srep21965

Nie, M., Yin, X., Ren, C., Wang, Y., Xu, F., and Shen, Q. (2010). Novel Rhamnolipid Biosurfactants Produced by a Polycyclic Aromatic Hydrocarbon-Degrading Bacterium *Pseudomonas aeruginosa* Strain. *Biotechnol. Adv.* 28, 635–643. doi:10.1016/j.biotechadv.2010.05.013

Osborne, C. K., and Schiff, R. (2011). Mechanisms of Endocrine Resistance in Breast Cancer. *Annu. Rev. Med.* 62, 233–247. doi:10.1146/annurev-med-070909-182917

Pathania, A. S., and Jana, A. K. (2020). Improvement in Production of Rhamnolipids Using Fried Oil with Hydrophilic Co-substrate by Indigenous *Pseudomonas aeruginosa* NJ2 and Characterizations. *Appl. Biochem. Biotechnol.* 191, 1223–1246. doi:10.1007/s12010-019-03221-9

Patnaik, A., Haluska, P., Tolcher, A. W., Erlichman, C., Papadopoulos, K. P., Lensing, J. L., et al. (2016). A First-In-Human Phase I Study of the Oral P38 MAPK Inhibitor, Ralimetinib (LY2228820 Dimesylate), in Patients with Advanced Cancer. *Clin. Cancer Res.* 22, 1095–1102. doi:10.1158/1078-0432.CCR-15-1718

Phillips, H. J. (1973). "Dye Exclusion Tests for Cell Viability," in *Tissue Culture: Methods and Applications*. Editors P. F. KruseJr and M. K. PattersonJr (New York: Academic Press), 406–408. doi:10.1016/b978-0-12-427150-0.50101-7

Pradhan, A. K., Pradhan, N., Mohapatra, P., Kundu, C. N., Panda, P. K., and Mishra, B. K. (2014). Cytotoxic Effect of Microbial Biosurfactants against Human Embryonic Kidney Cancerous Cell: HEK-293 and Their Possible Role in Apoptosis. *Appl. Biochem. Biotechnol.* 174, 1850–1858. doi:10.1007/s12010-014-1168-8

Price, N. P. J., Ray, K. J., Vermillion, K., and Kuo, T.-M. (2009). MALDI-TOF Mass Spectrometry of Naturally Occurring Mixtures of Monorhamnolipids and Dirhamnolipids. *Carbohydr. Res.* 344, 204–209. doi:10.1016/j.carres.2008.10.013

Pritchard, A. L., and Hayward, N. K. (2013). Molecular Pathways: Mitogen-Activated Protein Kinase Pathway Mutations and Drug Resistance. *Clin. Cancer Res.* 19, 2301–2309. doi:10.1158/1078-0432.CCR-12-0383

Rahimi, K., Lotfabad, T. B., Jabeen, F., and Mohammad Ganji, S. (2019). Cytotoxic Effects of Mono- and Di-rhamnolipids from *Pseudomonas aeruginosa* MR01 on MCF-7 Human Breast Cancer Cells. *Colloids Surf. B: Biointerfaces* 181, 943–952. doi:10.1016/j.colsurfb.2019.06.058

Riss, T. L., Moravec, R. A., Niles, A. L., Duellman, S., Benink, H. A., and Worzella, T. J. (20162016). *Cell Viability Assays*. Assay Guidance Manual [Internet]. Maryland, United StatesEli Lilly & Company and the National Center for Advancing Translational Sciences. Available from: https://www.ncbi.nlm.nih.gov/books/NBK144065/.

Samykannu, M., and Achary, A. (2017). Utilization of Agro-Industry Residue for Rhamnolipid Production by *P. aeruginosa* AMB AS7 and its Application in Chromium Removal. *Appl. Biochem. Biotechnol.* 183, 70–90. doi:10.1007/s12010-017-2431-6

Sanchez-Prieto, R., Rojas, J. M., Taya, Y., and Gutkind, J. S. (2000). A Role for the P38 Mitogen-Acitvated Protein Kinase Pathway in the Transcriptional Activation of P53 on Genotoxic Stress by Chemotherapeutic Agents. *Cancer Res.* 60, 2464–2472.

Sanger, F., Nicklen, S., and Coulson, A. R. (1977). DNA sequencing with chain-terminating inhibitors. *Proc. Natl. Acad. Sci. United States of America* 74 (12), 5463–5467. doi:10.1073/pnas.74.12.5463

Sarachat, T., Pornsunthorntawee, O., Chavadej, S., and Rujiravanit, R. (2010). Purification and Concentration of a Rhamnolipid Biosurfactant Produced by *Pseudomonas aeruginosa* SP4 Using Foam. *Bioresour. Tech.* 101, 324–330. doi:10.1016/j.biortech.2009.08.012

Sato, S., Fukuoka, T., Saika, A., Koshiyama, T., and Morita, T. (2019). A New Screening Approach for Glycolipid-type Biosurfactant Producers Using MALDI-TOF/MS. *J. Oleo Sci.* 68, 1287–1294. doi:10.5650/jos.ess19177

Semkova, S., Antov, G., Iliev, I., Tsoneva, I., Lefterov, P., Christova, N., et al. (2021). Rhamnolipid Biosurfactants-Possible Natural Anticancer Agents and Autophagy Inhibitors. *Separations* 8, 92. doi:10.3390/separations8070092

Shao, B., Liu, Z., Zhong, H., Zeng, G., Liu, G., Yu, M., et al. (2017). Effects of Rhamnolipids on Microorganism Characteristics and Applications in Composting: a Review. *Microbiol. Res.* 200, 33–44. doi:10.1016/j.micres.2017.04.005

Shum, D., Radu, C., Kim, E., Cajuste, M., Shao, Y., Seshan, V. E., et al. (2008). A High Density Assay Format for the Detection of Novel Cytotoxic Agents in Large Chemical Libraries. *J. Enzyme Inhib. Med. Chem.* 23 (6), 931–945. doi:10.1080/14756360701810082

Silva, S. N. R. L., Farias, C. B. B., Rufino, R. D., Luna, J. M., and Sarubbo, L. A. (2010). Glycerol as Substrate for the Production of Biosurfactant by *Pseudomonas aeruginosa* UCP0992. *Colloids Surf. B: Biointerfaces* 79, 174–183. doi:10.1016/j.colsurfb.2010.03.050

Sung, H., Ferlay, J., Siegel, R. L., Laversanne, M., Soerjomataram, I., Jemal, A., et al. (2021). Global Cancer Statistics 2020: GLOBOCAN Estimates of Incidence and Mortality Worldwide for 36 Cancers in 185 Countries. *CA A. Cancer J. Clin.* 71, 209–249. doi:10.3322/caac.21660

Swain, S. (2008). *Triple-Negative Breast Cancer: Metastatic Risk and Role of Platinum Agents 2008 ASCO Clinical Science Symposium*. Alexandria, Virginia: American Society of Clinical Oncology.

Tabbene, O., Gharbi, D., Slimene, I. B., Elkahoui, S., Alfeddy, M. N., Cosette, P., et al. (2012). Antioxidative and DNA Protective Effects of Bacillomycin D-like Lipopeptides Produced by B38 Strain. *Appl. Biochem. Biotechnol.* 168, 2245–2256. doi:10.1111/j.1574-6968.2010.02199.x

Tamura, K., Stecher, G., Peterson, D., Filipski, A., and Kumar, S. (2013). MEGA6: Molecular Evolutionary Genetics Analysis Version 6.0. *Mol. Biol. Evol.* 30, 2725–2729. doi:10.1093/molbev/mst197

Thakur, P., Saini, N. K., Thakur, V. K., Gupta, V. K., Saini, R. V., and Saini, A. K. (2021). Rhamnolipid the Glycolipid Biosurfactant: Emerging Trends and Promising Strategies in the Field of Biotechnology and Biomedicine. *Microb. Cel Fact* 20, 1–15. doi:10.1186/s12934-020-01497-9

Thanomsub, B., Pumeechockchai, W., Limtrakul, A., Arunrattiyakorn, P., Petchleelaha, W., Nitoda, T., et al. (2006). Chemical Structures and Biological Activities of Rhamnolipids Produced by *Pseudomonas aeruginosa* B189 Isolated from Milk Factory Waste. *Bioresour. Tech.* 97, 2457–2461. doi:10.1016/j.biortech.2005.10.029

Tofani, D., Balducci, V., Gasperi, T., Incerpi, S., and Gambacorta, A. (2010). Fatty Acid Hydroxytyrosyl Esters: Structure/antioxidant Activity Relationship by ABTS and in Cell-Culture DCF Assays. *J. Agric. Food Chem.* 58, 5292–5299. doi:10.1021/jf1000716

Towbin, H., Staehelin, T., and Gordon, J. (1979). Electrophoretic Transfer of Proteins from Polyacrylamide Gels to Nitrocellulose Sheets: Procedure and Some Applications. *Proc. Natl. Acad. Sci.* 76, 4350–4354. doi:10.1073/pnas.76.9.4350

Twigg, M. S., Baccile, N., Banat, I. M., Déziel, E., Marchant, R., Roelants, S., et al. (2020). Microbial Biosurfactant Research: Time to Improve the Rigour in the Reporting of Synthesis, Functional Characterization and Process Development. *Microb. Biotechnol.* 14, 147–170. doi:10.1111/1751-7915.13704

Voulgaridou, G.-P., Mantso, T., Anestopoulos, I., Klavaris, A., Katzastra, C., Kiousi, D.-E., et al. (2021). Toxicity Profiling of Biosurfactants Produced by Novel marine Bacterial Strains. *Int. J. Mol. Sci.* 22, 2383. doi:10.3390/ijms22052383

Wambang, N., Schifano-Faux, N., Aillerie, A., Baldeyrou, B., Jacquet, C., Bal-Mahieu, C., et al. (2016). Synthesis and Biological Activity of Ferrocenyl Indeno [1,2-C]isoquinolines as Topoisomerase II Inhibitors. *Bioorg. Med. Chem.* 24, 651–660. doi:10.1016/j.bmc.2015.12.033

Wang, X., Zhang, H., and Chen, X. (2019). Drug Resistance and Combating Drug Resistance in Cancer. *Cancer Drug. Resist.* 2, 141–160. doi:10.20517/cdr.2019.10

Wu, D., Si, M., Xue, H.-Y., and Wong, H. L. (2017). Nanomedicine Applications in the Treatment of Breast Cancer: Current State of the Art. *I. J. Nano.* Vol. 12, 5879–5892. doi:10.2147/IJN.S123437

Zhao, J., Wu, Y., Alfred, A. T., Xin, X., and Yang, S. (2013). Chemical Structures and Biological Activities of Rhamnolipid Biosurfactants Produced by *Pseudomonas aeruginosa* M14808. *J. Chem. Pharm. Res.* 5, 177–182. https://www.jocpr.com/abstract/chemical-structures-and-biological-activities-of-rhamnolipid-biosurfactants-produced-by-pseudomonas-aeruginosa-m14808-2394.html.

Conflict of Interest: The authors declare that the research was conducted in the absence of any commercial or financial relationships that could be construed as a potential conflict of interest.

Publisher's Note: All claims expressed in this article are solely those of the authors and do not necessarily represent those of their affiliated organizations, or those of the publisher, the editors, and the reviewers. Any product that may be evaluated in this article, or claim that may be made by its manufacturer, is not guaranteed or endorsed by the publisher.

frontiers in Bioengineering and Biotechnology

ORIGINAL RESEARCH
published: 22 December 2021
doi: 10.3389/fbioe.2021.815337

Impact of the Purification Process on the Spray-Drying Performances of the Three Families of Lipopeptide Biosurfactant Produced by *Bacillus subtilis*

Antoine Vassaux[1], *Marie Rannou*[1], *Soline Peers*[2], *Théo Daboudet*[1], *Philippe Jacques*[2,3] *and François Coutte*[1,2]*

[1]Université de Lille, UMRt BioEcoAgro 1158-INRAE, Équipe Métabolites Secondaires d'Origine Microbienne, Institut Charles Viollette, Lille, France, [2]LIPOFABRIK, Villeneuve d'Ascq, France, [3]TERRA Teaching and Research Centre, Université de Liège, UMRt BioEcoAgro 1158-INRAE, Équipe Métabolites Secondaires D'origine Microbienne, MiPI, Gembloux Agro-Bio Tech, Gembloux, Belgium

OPEN ACCESS

Edited by:
Tomasz Janek,
Wroclaw University of Environmental and Life Sciences, Poland

Reviewed by:
Vivek Rangarajan,
Birla Institute of Technology and Science, India
Eduardo J. Gudiña,
University of Minho, Portugal

***Correspondence:**
François Coutte
francois.coutte@univ-lille.fr

Specialty section:
This article was submitted to Industrial Biotechnology, a section of the journal Frontiers in Bioengineering and Biotechnology

Received: 15 November 2021
Accepted: 23 November 2021
Published: 22 December 2021

Citation:
Vassaux A, Rannou M, Peers S, Daboudet T, Jacques P and Coutte F (2021) Impact of the Purification Process on the Spray-Drying Performances of the Three Families of Lipopeptide Biosurfactant Produced by Bacillus subtilis. Front. Bioeng. Biotechnol. 9:815337. doi: 10.3389/fbioe.2021.815337

Lipopeptides produced by *Bacillus subtilis* display many activities (surfactant, antimicrobial, and antitumoral), which make them interesting compounds with a wide range of applications. During the past years, several processes have been developed to enable their production and purification with suitable yield and purity. The already implemented processes mainly end with a critical drying step, which is currently achieved by freeze-drying. In this study, the possibility to replace this freeze-drying step with a spray-drying one, more suited to industrial applications, was analyzed. After evaluating their thermal resistance, we have developed a spray-drying methodology applicable for the three lipopeptides families produced by *B. subtilis*, i.e., surfactin, mycosubtilin (iturin family), and plipastatin (fengycin family). For each lipopeptide, the spray-drying procedure was applied at three steps of the purification process by ultrafiltration (supernatant, diafiltered solution, and pre-purified fraction). The analysis of the activities of each spray-dried lipopeptide showed that this drying method is not decreasing its antimicrobial and biosurfactant properties. The methodology developed in this study enabled for the first time the spray-drying of surfactin, without adjuvants' addition and regardless of the purification step considered. In the case of fengycin and mycosubtilin, only diafiltered solution and purified fraction could be successfully spray-dried without the addition of adjuvant. Maltodextrin addition was also investigated as the solution for the direct drying of supernatant. As expected, the performances of the spray-drying step and the purity of the powder obtained are highly related to the purification step at which the product was dried. Interestingly, the impact of mycosubtilin concentration on spray-drying yield was also evidenced.

Keywords: spray-drying, *Bacillus subtilis*, antimicrobial lipopeptides, biosurfactants, surfactin, fengycin, mycosubtilin

Abbreviations: CMC, critical micellar concentration; LPPs, lipopeptides; MIC, minimal inhibitory concentration; NRP, non-ribosomal peptide; NRPS, non-ribosomal peptide synthetase; PKS, polyketide synthase.

INTRODUCTION

Secondary metabolites, including those synthesized by multi-enzymatic modular complexes such as polyketide synthase (PKS), non-ribosomal peptide synthetase (NRPS), and hybrid PKS/NRPS structure, represent an almost inexhaustible source of interesting bioactive compounds (Demain, 2014). Non-ribosomal peptides (NRPs) notably show a large structural diversity mainly due to the diversity of monomers, which can compose them (proteogenic and nonproteogenic amino acids, carbohydrates, lipids, etc.). NRPs showing a fatty acid chain linked to a peptide moiety are classified as lipopeptides (LPPs) (Caboche et al., 2008).

Bacillus subtilis is naturally producing and secreting three different families of LPPs: surfactins, iturins, and fengycins. Surfactins (surfactins, pumilacidins, and lichenysins) are cyclic heptapeptides linked to a β-hydroxy fatty acid of C_{12} to C_{17}, known for their biosurfactant properties but also for their antiviral and antitumoral activities. Iturins (iturins A, C, D, and E; mycosubtilins; bacillomycins D, F, and L; and mojavensin) consist in a heptapeptide linked to β-amino fatty acid of C_{14} to C_{19}, whereas fengycins (fengycins A and B, plipastatins A and B, and agrastatins) show a C_{12} to C_{19} β-hydroxy fatty acid (saturated or not) linked to a decapeptide (Jacques, 2011; Coutte et al., 2017). In addition to their biosurfactant properties, fengycins and iturins are mainly studied for their antifungal properties (Jacques, 2011). LPPs as iturins and fengycins display antifungal properties and are thus used as biocontrol agents to fight against phytopathogens. Several studies have already demonstrated their efficiency on plant fungal pathogens such as *Bremia lactucae* (Deravel et al., 2014), *Zymoseptoria tritici* (Mejri et al., 2018), and *Venturia inaequalis* (Desmyttere et al., 2019) and on foodborne pathogens such as *Paecilomyces variotii*, *Byssochlamys fulva*, and *Candida krusei* (Kourmentza et al., 2021). On the other hand, the elicitor potential of surfactin and its ability to act in synergy with the two other families of LPPs also make it a good candidate for an efficient biocontrol agent (Ongena and Jacques, 2008). The application of these LPPs as biocontrol agents is highly dependent on our capacity to produce and purify them with high yields, suitable purities, and low costs. To achieve this goal, several research teams have already developed innovative processes, such as the disc bioreactor, the membrane bioreactor, or the trickle-bed biofilm reactor, enabling notably to limit the foam apparition due to the surfactant properties of LPPs (Coutte et al., 2017). Conversely, some studies focused on the foaming properties of LPPs to set up overflowing culture processes (Chen et al., 2006; Gong et al., 2009; Guez et al., 2021). In terms of purification, a downstream process encompassing several steps of ultrafiltration/diafiltration/evaporation has already been established and proved its worth in several studies (Coutte et al., 2010a; Kourmentza et al., 2021) (**Figure 1**). The final formulation of LPPs in powder form is an optional step that enables to concentrate the product to facilitate storage, while reducing the risk of product degradation, thus increasing its shelf-life. In surfactin, iturin, and fengycin cases, the transition from a liquid to a solid state is conventionally operated through a freeze-drying process (Coutte et al., 2010a; Kourmentza et al., 2021).

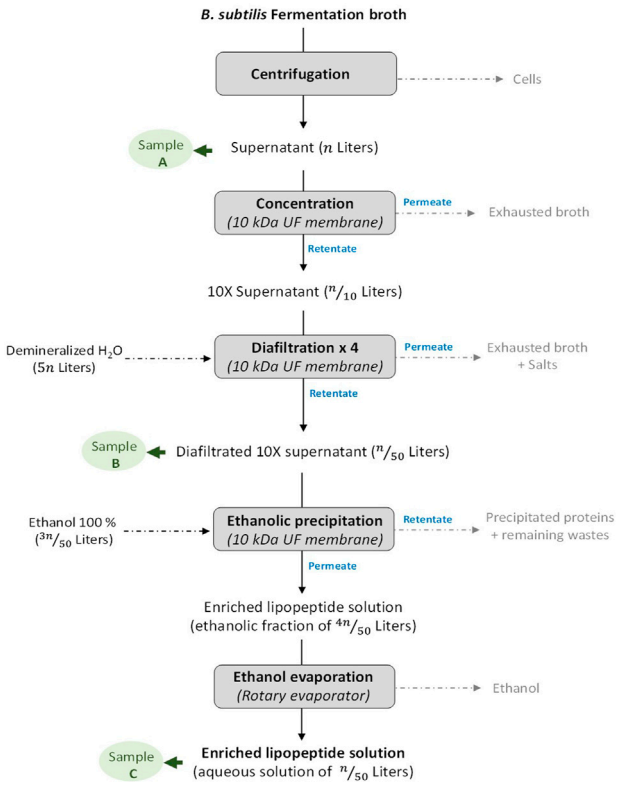

FIGURE 1 | Description of the workflow for the production and purification of lipopeptides from the fermentation of *Bacillus subtilis* to the enriched lipopeptide solution in an aqueous solution. The different steps where a sample has been taken for spray-drying experiments are highlighted as Sample **(A–C)**.

To dry compounds of interest, freeze-drying and spray-drying are the most used techniques in industrial processing. Due to its lower operating cost and its higher volume capacity, the spray-drying technique is often preferred by food and cosmetics industries (Vardanega et al., 2019). In a recent techno-economic study, authors have highlighted, in one of their scenarios, the requirement of a spray-drying step to set up a surfactin and lichenysin industrial-scale production derived from *Bacillus* fermentation (Czinkóczky and Németh, 2020). Therefore, to fit with industrial requirements, developing a methodology enabling LPPs to dry through spray-drying is of prime interest. The spray-drying technique has already been successfully used to formulate *B. subtilis* strains and its associated culture broth and led to a biocontrol product displaying long shelf-life, high viability, and capability to prevent peach brown rot and rice blast diseases (Yánez-Mendizábal et al., 2012; Meng et al., 2015). The antimicrobial LPPs produced by *Bacillus amyloliquefaciens* were encapsulated by spray-drying, with a limited loss of activity, thanks to the addition of maltodextrin and porous starch as composite wall materials (Wang et al., 2014). Regarding *B. subtilis* LPPs, a surfactin-like biosurfactant, isolated from B30 strain was

reported to be successfully spray-dried after a purification step by acid precipitation (Al-Wahaibi et al., 2014). Iturin A produced by *B. subtilis* was also spray-dried to be incorporated into microcapsules, with sodium alginate and poly(γ-glutamic acid) as wall materials, to improve the compound stability and facilitate its storage (Yu et al., 2017). The addition of a high amount of maltodextrin or kaolinite as drying adjuvants also enabled the spray-drying of surfactin without any loss in surfactant activity (Barcelos et al., 2014).

Although biosurfactant drying feasibility through a spray-drying approach has already been demonstrated, to the best of our knowledge, the addition of drying adjuvants has always been required to recover the bioactive compounds. This addition of drying adjuvant is deleterious, as it decreases the purity of the product, enhances the cost, and increases the storage volumes. In this study, we investigate for the first time and in a systemic way the spray-drying of the three families of LPPs. The methodology that enables the drying of *B. subtilis*-based biosurfactants without the addition of adjuvants is also presented. The molecules from the three main families of LPPs produced by *B. subtilis* (i.e., surfactin, mycosubtilin, and plipastatin) have been considered for spray-drying at three different steps of their purification process. The preservation of the surfactant and antimicrobial activities after drying was assessed for the three LPPs.

MATERIALS AND METHODS

Lipopeptides Production

Surfactin, mycosubtilin, and plipastatin (LPPs) were produced in 5-L shake flasks filled at 20% with Landy media, under orbital agitation at 160 rpm, as previously reported (Coutte et al., 2010a). Surfactin and plipastatin were respectively produced by *B. subtilis* BBG131 strain (Coutte et al., 2010a) and *B. subtilis* Bs2504 strain (Ongena et al., 2007). BBG131 and Bs2504 were grown for 72 h at 37°C in a modified Landy MOPS culture medium (composition: 20 g·L^{-1} of glucose, 5 g·L^{-1} of glutamic acid, 1 g·L^{-1} of yeast extract, 1 g·L^{-1} of K_2HPO_4, 0.5 g·L^{-1} of $MgSO_4{\cdot}7H_2O$, 0.5 g·L^{-1} of KCl, 16 mg·L^{-1} of L-tryptophan, 1.6 mg·L^{-1} of $CuSO_4{\cdot}5H_2O$, 1.2 mg·L^{-1} of $MnSO_4{\cdot}H_2O$, 0.4 mg·L^{-1} of $Fe_2(SO_4)_3{\cdot}7H_2O$, and 21 g·L^{-1} of 3-morpholinopropane-1-sulfonic acid MOPS, buffered at pH 7.0 using KOH 3 M). Mycosubtilin was produced by *B. subtilis* BBG125 strain (Béchet et al., 2013). BBG125 was grown for 72 h at 30°C in another modified Landy MOPS culture medium (Guez et al., 2021) (composition: 20 g·L^{-1} of glucose, 2 g·L^{-1} of glutamic acid, 1 g·L^{-1} of yeast extract, 1 g·L^{-1} of K_2HPO_4, 0.5 g·L^{-1} of $MgSO_4{\cdot}7H_2O$, 0.5 g·L^{-1} of KCl, 2.3 g·L^{-1} of $(NH_4)_2SO_4$, 32 mg·L^{-1} of $CuSO_4{\cdot}5H_2O$, 100 mg·L^{-1} of $MnSO_4{\cdot}H_2O$, 30 mg·L^{-1} of $Fe_2(SO_4)_3{\cdot}7H_2O$, and 21 g·L^{-1} of 3-morpholinopropane-1-sulfonic acid MOPS, buffered at pH 6.5 using KOH 3 M). In these culture conditions, BBG131, Bs2504, and BBG125 were able to produce respectively 1.2 ± 0.2 g·L^{-1} of surfactin, 0.4 ± 0.1 g·L^{-1} of plipastatin, and 0.05 ± 0.02 g·L^{-1} of mycosubtilin.

Lipopeptides Purification Process

The different steps undertaken for the production and the purification of LPP from a *B. subtilis* fermentation are shown in **Figure 1**. At the end of the culture, the broth medium was centrifuged in an Avanti J-E centrifugation unit (Beckman Coulter, Krefeld, Germany) at 8,000 *g* for 40 min at 10°C, and the cells were discarded. The supernatant was then 10-times concentrated through a 10-kDa Hydrosart ultrafiltration membrane (Sartorius, Goettingen, Germany). The resulting retentate was then supplemented with demineralized water (4 volumes of water for 1 volume of retentate) in order to perform four successive diafiltration processes through the ultrafiltration membrane described above. The de-salted resulting retentate was subsequently supplemented with ethanol 100% (3 volumes of ethanol for 1 volume of diafiltered retentate) to reach a final concentration in ethanol at 75%. On the one hand, the addition of ethanol precipitates most of the proteins included in the retentate, and on the other hand, it leads to the disruption of the LPP micelles into free LPP molecules (with a molecular weight <10 kDa). The ethanolic fraction obtained was subsequently filtrated through the same membrane described above in order to separate the precipitate fraction (retentate) from the pre-purified LPP fraction (permeate). Finally, the ethanol contained in the pre-purified LPP fraction was evaporated using a rotary evaporator (Rotavapor® R-300, Büchi Labortechnik AG, Flawil, Switzerland).

Evaluation of the Lipopeptides Thermal Resistance

Before proceeding to LPP spray-drying, a preliminary experiment has been carried out to determine the resistance of surfactin, mycosubtilin, and plipastatin to high-temperature treatment. LPPs (surfactin, mycosubtilin, and plipastatin) formulated in powder form were supplied by Lipofabrik (Lipofabrik, Villeneuve d'Ascq, France). LPP powders were solubilized with demineralized water at a concentration of 1 g·L^{-1} for surfactin and plipastatin and 0.5 g·L^{-1} for mycosubtilin. LPPs were held in an aqueous solution, in a closed container avoiding evaporation, in a sand bath (VWR, Fontenay-sous-Bois, France) heated at 20°C, 75°C, 92°C, 109°C, 126°C, 134°C, or 143°C for 1 min. Before and after the thermal treatment, the number of LPPs was quantified by ultra-high-performance liquid chromatography (UPLC) according to the method described in *Lipopeptide Quantification and Purity Determination*. LPPs were considered to be stable at the tested temperature when the same amount of LPPs was quantified before and after the thermal treatment.

Spray-Dried Materials

The characteristics of all the spray-dried LPP samples (LPP concentration and volume of the solution) of this study are presented in **Supplementary Table S1**. For each modality, the experiment (production, purification, and spray-drying) was performed in triplicate. Two types of LPP samples were spray-dried: either already formulated LPPs in powder forms

(**Supplementary Table S1A**) or LPPs in solution sampled at different steps of the LPP production and purification using membrane ultrafiltration workflow (**Figure 1**; **Supplementary Table S1B**). LPPs (surfactin, mycosubtilin, and plipastatin) formulated in powder form, supplied by Lipofabrik (Lipofabrik, Villeneuve d'Ascq, France), were resuspended with demineralized water before the spray-drying step. Surfactin, plipastatin, and mycosubtilin samples of various purities were sampled at different steps of the LPP purification process (A, untreated supernatant; B, concentrated and diafiltered LPP solution; C, enriched LPP solution after ethanol evaporation) before the spray-drying process. The addition of maltodextrin as an aid for spray-drying was also evaluated with mycosubtilin supernatant. Thus, supernatant from fermentation broth and containing 1 g·L^{-1} of mycosubtilin was also spray-dried after the addition of 2.5% and 5% w/v maltodextrin (Glucidex IT 12) supplied by Roquette (Lestrem, France).

Spray-Drying Conditions

The spray-drying of the solutions was carried out in the Büchi Mini Spray Dryer B-290 (Büchi Labortechnik AG, Switzerland) configured with an inlet temperature of 140°C and exhaust temperature of 70°C. The pressure of the spraying air was at 40-mm water column, and the pumping flow was maintained at 8.5 ml·min^{-1}. During the spray-drying procedure, inlet and outlet air characteristics (temperature, percentage of humidity, dew temperature, and wet bulb temperature) were analyzed using the Testo 625 psychrometer (Testo, Titisee-Neustadt, Germany). These values were used to establish a water balance as well as an energy balance.

Analysis of the Spray-Drying Performances

In order to calculate the yield of the spray-drying process, the dry matter of the obtained powder was determined with a desiccator (Presica XM60, Presica Instruments AG, Dietikon, Switzerland) set on 102°C. The yield (Y) and the specific LPP yield (Y_{LPP}), expressed in percent, were respectively calculated according to **Eqs 1**, **2**:

$$Y = \frac{DM_{powder} * m_{powder}}{DM_{solution} * m_{solution}} \quad (1)$$

$$Y_{LPP} = \frac{P_{lipopeptide} * m_{powder}}{C_{lipopetide} * V_{solution}} \quad (2)$$

with the following parameters:

DM_{powder} : the dry matter of the obtained spray-dried powder (%);
m_{powder} : the mass of the obtained spray-dried powder (g);
$DM_{solution}$: dry matter of the aqueous solution before spray-drying (%);
$m_{solution}$: mass of the aqueous solution before spray-drying (g);
$P_{lipopeptide}$: the LPP purity in the spray-dried obtained product (%);
$C_{lipopeptide}$: the LPP concentration in the spray-dried solution (g·ml^{-1});
$V_{solution}$: volume of the aqueous solution before spray-drying (ml).

Analysis of the Spray-Dried Products (Activity Assays)

In order to ensure that the spray-drying process is not altering LPP properties, several activity assays were carried out on the obtained spray-dried products. The surfactant properties of the three kinds of spray-dried LPPs (surfactin, mycosubtilin, and plipastatin) were evaluated by measuring the surface tension according to the Du Nouÿ method using a tensiometer TD1 (Lauda, Lauda-Königshofen, Germany) as described previously (Leclère et al., 2006). This was carried out in distilled water at pH 8. The values were compared with the surface tension measured on LPP solutions before spray-drying using the same methodology. The surfactant properties of LPPs are considered to be conserved if the values measured after spray-drying fit with those measured before spray-drying.

Anti-*Legionella* activity of surfactin was performed in a microtiter plate to evaluate the minimal inhibitory concentration (MIC) of surfactin against *Legionella pneumophila* strains. The strains *L. pneumophila* 2-15-1 and 2-15-2 used in this study were isolated and identified from sanitary water by the Institut Scientifique de Service Public of Liège and kindly made available to us for this study. The MIC has been determined following the standard protocol (Loiseau et al., 2015). Briefly, 100 µl of sterile liquid Buffered Yeast Extract (BYE) broth have been dispensed in each well of a 96-well plate. Then, 9 two-fold dilutions of surfactin (before spray-drying and after spray-drying) in BYE broth were made starting at a concentration of 50 mg·L^{-1}. Wells were inoculated by dispensing 5 µl of a 10^5 CFU·ml^{-1} of bacterial culture in the growth phase. Wells containing only 100 µl of BYE broth and wells inoculated BYE broth were used respectively as negative and positive controls. Plates were incubated at 37°C for 48 h. The MIC has been determined at the lowest concentration where no visible growth is observed in the wells. The mean value of MIC was presented.

The antifungal activities of plipastatin samples were determined against *V. inaequalis* S575 by measuring the EC_{50} as recently described (Desmyttere et al., 2019). The mean value of EC_{50} was presented.

The antifungal activity of mycosubtilin was evaluated using the microwell dilution method in a 96-well microplate. *Saccharomyces cerevisiae* DSM1333 strain was grown overnight at 37°C on Potato Dextrose Agar (PDA), dispersed in water, adjusted to a final OD_{600nm} of 0.04, and used as an inoculum. Mycosubtilin samples were dissolved in dimethyl sulfoxide (DMSO) and then diluted in Roswell Park Memorial Institute (RPMI) 2× media to reach a final concentration of 0.4 g·L^{-1}. Ninety-six-well microplates were prepared by dispensing 100 µl of RPM 2× media in all wells except in the negative control. Initially prepared mycosubtilin samples measuring 200 µl were added to the first wells. Two-fold serial dilutions of 100 µl were made from columns 1 to 10 in a concentration range from 0.8 to 400 mg·L^{-1}. The inoculum measuring 100 µl was added to each

well except in the negative control. Distilled sterile water measuring 100 µl was added to the negative control. The final volume of each well was 200 µl. The plate was incubated at 37°C for 12 h. After incubation, the lowest concentration of each extract showing no yeast growth or turbidity was taken as its MIC value. The mean value of MIC was presented.

For these three antimicrobial assays, mean values of MIC or EC_{50} and CIs ($\alpha = 0.05$) were calculated from three technical and three biological replicates using R software nlstools package (R version 3.5.3, R Core Team, 2019).

Lipopeptides Quantification and Purity Determination

The determination of the LPP concentration and purity in the samples before and after the spray-drying process was performed by UPLC. The LPPs in powder form, either those before spray-drying (surfactin, plipastatin, and mycosubtilin provided by Lipofabrik, Villeneuve d'Ascq, France) or those obtained after each spray-drying experiment, were solubilized in 100% methanol at a concentration of 1 $g{\cdot}L^{-1}$. Prior to being injected, all samples were centrifuged (10,000 *g*, 10 min). The high-concentrated samples such as those sampled at the late phase of the LPP purification process (diafiltered fraction and enriched LPP fraction) were diluted with demineralized water in order to be properly quantified by the apparatus. All the measurements have been done with an injection volume of 20 µl into an Interchim C18 column (UP5TP18-250/030 C18, Interchim, Montluçon, France) equipped on an ACQUITY UPLC system (Waters, Milford, MA, USA) coupled to a UV detector (detection at 215 nm). The solvents used, water of high-performance liquid chromatography (HPLC) grade with 0.1% trifluoroacetic acid (Solvent A) and acetonitrile of HPLC grade with 0.1% trifluoroacetic acid (Solvent B), were provided by Sigma Aldrich (St. Louis, MO, USA). The solvent flow was 0.6 $ml{\cdot}min^{-1}$ throughout the chromatography column.

To quantify surfactin, plipastatin, and mycosubtilin, the same analysis method was applied with the following gradient: from 0 to 5 min, 95% A/5% B; from 5 to 40 min, a linear gradient from 95% A/5% B to 0% A/100% B; from 40 to 45 min, 0% A/100% B; and from 45 to 56 min, 95% A/5% B. The concentration of the sample was determined by comparison with 98% surfactin, 95% iturin A, and 90% fengycin standards, all provided by Sigma Aldrich (St. Louis, USA). The elution time of surfactins, mycosubtilins (and iturin A), and plipastatins, under the above-described analysis conditions, were respectively 36–41, 24–26, and 27–33 min. The retention time and second derivative of the absorption spectrum between 200 and 400 nm were used to identify the eluted molecules (Empower Software, Waters).

The purity of the analyzed powders was determined by analogy with the corresponding LPP standard of known purity. Both the analyzed samples and the corresponding standard were solubilized at a concentration of 1 $g{\cdot}L^{-1}$ in 100% methanol. After analysis according to the method described above, the purity (P_{sample} in %) was determined according to the following equation (with $P_{standard}$ as the purity of the standard in %; A_{sample} as the total specific area of the sample in $\mu V{\cdot}s^{-1}$; and $A_{standard}$ as the total specific area of the standard in $\mu V{\cdot}s^{-1}$):

$$P_{sample} = \frac{P_{standard} * A_{sample}}{A_{standard}}$$

RESULTS AND DISCUSSION

Impact of Spray-Drying on Lipopeptides Activities

Prior to considering spray-drying as an appropriate method to formulate LPPs in powder form, it is important to ensure that this operation is not negatively impacting LPP activities. First of all, evaluation of the thermal resistance of the LPPs of *B. subtilis* was carried out. Commercial powders of the three LPPs (i.e., surfactin, plipastatin, and mycosubtilin, provided by Lipofabrik (Lipofabrik, Villeneuve d'Ascq, France)) were exposed 1 min to different temperatures (up to 143°C) in order to evaluate their thermal resistance and then were quantified by UPLC. Regarding the applied temperature, any degradation of the three LPPs tested was observed after exposure (*data not shown*). This result enables us to confirm that the structures of these LPPs are preserved after a short-time exposure at high temperatures (up to 143°C). This observation is in line with other previous studies that have demonstrated that the surfactant properties of surfactin for instance are preserved after a short-time exposure at temperatures of up to 170°C (Barcelos et al., 2014). Then, these different commercial LPPs in powder form have also been resuspended in demineralized water and subsequently spray-dried. Activities of the obtained dried LPPs have then been evaluated and compared with the activities of the non-spray-dried initial samples. The surfactant activity has been monitored for each LPP, while anti-*Legionella* activity was measured for surfactin samples, and antifungal activities were evaluated for both mycosubtilin and plipastatin samples.

Lipopeptide Surfactant Activity

In order to assess the preservation of the biosurfactant activities of the three spray-dried LPPs, a surface tension measurement was performed according to the Du Nouÿ method on samples before and after the drying process. The results obtained are presented in **Figure 2** for each LPP: surfactin (A), mycosubtilin (B), and plipastatin (C). No significant differences can be highlighted between the surface tension of mycosubtilin and plipastatin before and after spray-drying. Critical micellar concentrations (CMCs) of these molecules were calculated and are presented in **Table 1** in comparison with the values found in the literature. The micellization process of these amphiphilic molecules is dependent on the chemical structure (chemical composition, length, and isomery of the fatty acid chain) and on environmental parameters of the study (buffer, pH, and temperature) (Deleu et al., 2013). In the scientific literature, CMC of the different LPPs was measured in different aqueous solutions (water or saline buffer) and was from 10 $mg{\cdot}L^{-1}$ for surfactin in pH 8.5 in 5 mM of Tris–HCl or in 0.1 M of $NaHCO_3$ buffer (Thimon et al., 1992; Abdel-Mawgoud et al., 2008) to 25 $mg{\cdot}L^{-1}$ in water (Cooper et al., 1981), from

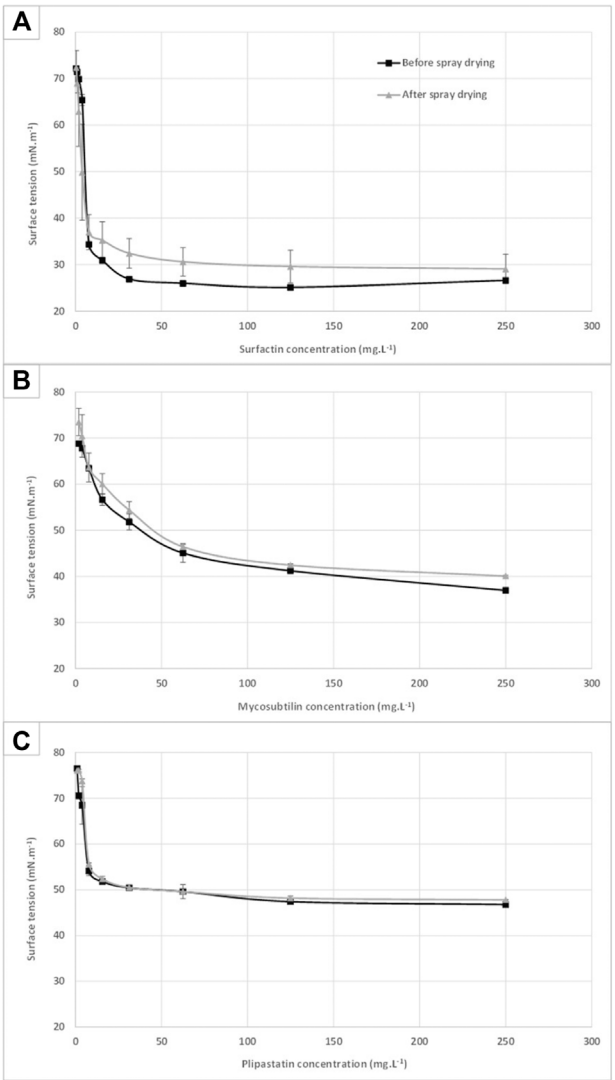

FIGURE 2 | Surface tension profiles of surfactin **(A)**, mycosubtilin **(B)**, and fengycin **(C)** samples before and after the spray-drying process. Each value is an average based on three distinct samples measured in triplicates according to the Du Nouÿ method.

39 mg·L^{-1} in 0.1 M of $NaHCO_3$ (Thimon et al., 1992) to 44 mg·L^{-1} for mycosubtilin in KCl 0.1 M (Maget-Dana et al., 1992) and from 2 mg·L^{-1} (Eeman et al., 2014) to 4 mg·L^{-1} for fengycin (plipastatin) in PBS buffer (Mantil et al., 2019). A slight impact can be observed on the surface tension profile of the surfactin with a surface tension approximately 10% higher in the surfactin samples, which has undergone a spray-drying step, from the concentration of 10 mg·L^{-1}. Nonetheless, the biosurfactant properties of the spray-dried surfactin samples have been preserved. The lower CMC value of mycosubtilin obtained here could be explained by the nature of the isoforms present, probably different from those tested in the literature, but also the difference in the ionic strength of the solution assay.

Lipopeptide Antimicrobial Activity

An antagonist antimicrobial assay was performed in order to determine whether the spray-drying procedure has an impact on the antibacterial activity of surfactin and on antifungal activities of mycosubtilin and plipastatin. The anti-*Legionella* activity of surfactin has been described for the first time several years ago by Loiseau et al. (2015). In this work, we investigated this specific antibacterial activity of surfactin against the opportunistic pathogen *L. pneumophila* before and after spray-drying. The results obtained are summarized in **Table 2**. The results obtained for surfactin against the two strains of *L. pneumophila* showed a different sensitivity of the LPP between them where the *L. pneumophila* 2-15-1 seems to be 1.6 times more sensitive than the strain *L. pneumophila* 2-15-2 (2.6–4.2 mg·L^{-1}). The MIC values obtained against these two strains are in agreement with those published by Loiseau et al. (2015) where MIC values between 2 and 4 mg·L^{-1} were found against these pathogen species (Loiseau et al., 2015). The spray-drying process seems to slightly reduce the activity of surfactin, as the MIC obtained for the two *L. pneumophila* strains are approximately 1.2 times higher than the surfactin before spray-drying. However, this is not significant in terms of the different confidence intervals.

The antimicrobial potential of mycosubtilin and plipastatin was respectively assessed through the determination of the MIC for *S. cerevisiae* (**Table 2**) and the EC_{50} for *Venturia inaequalis* (**Table 2**). The obtained results enable us to conclude that the spray-drying process did not impact the antifungal potential of the mycosubtilin toward *S. cerevisiae*, as the same MIC of 4.1 mg·L^{-1} [2.1–6.3] was obtained before and after the spray-drying process. A slight impact of the drying process can be noticed on the antifungal potential of plipastatin, which seems to be increased after spray-drying, but this is not significant regarding CIs obtained for both samples (before and after spray-drying; see **Table 2**). Nonetheless, taken as a whole, the results demonstrate that the antimicrobial properties of both mycosubtilin and plipastatin have been maintained after the drying process.

Performances of the Spray-Drying Process Regarding the Considered Purification Step

After demonstrating, on highly pure molecules, that spray-drying does not affect the activities of LPPs (surfactant and antimicrobial), we were interested in the performances of this drying process on different LPP preparations resulting from the different steps of the ultrafiltration purification process, namely, the cell-free supernatant, the diafiltered fraction, and finally the purified fraction. These different steps are presented in **Figure 1**. The dry matter of the spray-dried LPP solution and of the obtained powder, as well as the LPP purity in the dried product, is depicted in **Table 3**. From these first results, it can be concluded that spray-drying is a very efficient process to obtain LPPs in powder form with a high dry matter of 93.6% ± 2.2% whatever the considered family of LPPs is; nevertheless, the state of purification of the latter has an important impact.

TABLE 1 | Critical micellar concentration of the lipopeptides produced by *Bacillus subtilis* before and after spray-drying process.

Sample type	CMC ($mg{\cdot}L^{-1}$) before spray-drying	CMC ($mg{\cdot}L^{-1}$) after spray-drying	CMC ($mg{\cdot}L^{-1}$) from literature	References
Surfactin	10.1	8.4 ± 0.7	10 – 25	Cooper et al. (1981); Thimon et al. (1992); Abdel-Mawgoud et al. (2008)
Mycosubtilin	27.2	26.8 ± 1.5	39 – 44	Maget-Dana et al. (1992); Thimon et al. (1992)
Plipastatin	9.2	10.2 ± 0.8	2 – 4	Eeman et al. (2014); Mantil et al. (2019)

Note. CMC, critical micellar concentration.

TABLE 2 | Determination of the lipopeptide activities before and after the spray-drying process: anti-*Legionella* activity for surfactin samples **(A)**, antifungal activity against *Saccharomyces cerevisiae* for mycosubtilin samples **(B)**, and antifungal activity against *Venturia inaequalis* for plipastatin samples **(C)**.

Sample	A	MIC *L. pneumophila* 2-15-1 ($mg{\cdot}L^{-1}$)[a]	MIC *L. pneumophila* 2-15-2 ($mg{\cdot}L^{-1}$)[a]	B	MIC *S. cerevisiae* ($mg{\cdot}L^{-1}$)[a]	C	EC_{50} *V. inaequalis* ($mg{\cdot}L^{-1}$)[a]
Before spray-drying	Surf.	2.6 [1.6–3.6]	4.2 [2.1–6.2]	Myco.	4.1 [2.1–6.3]	Plip.	0.0124 [0.0062–0.0249]
After spray-drying		3.3 [1.9–4.7]	5.2 [3.4–7.0]		4.1 [2.1–6.3]		0.0077 [0.0066–0.0086]

Note. MIC, minimal inhibitory concentration.
[a]*Mean value and CIs are presented from three biological and three technical replicates.*

The results presented in **Table 3** show that the purification process has a significant impact on the purity of the dried LPPs obtained. This result was expected from our previous work on this purification process (Coutte et al., 2010b; Jauregi et al., 2013). The purity obtained with diafiltered solution of surfactin (between 50% and 60%) using the same ultrafiltration procedure is in accordance with that previously published by our team (Coutte et al., 2013). Nevertheless, a small decrease in the performance of the last purification step (enriched LPP fraction) can be noticed for surfactin and mycosubtilin in comparison with the ones previously obtained (82.4% ± 1.0% and 78.3% ± 12.6%, respectively) (Coutte et al., 2013; Deravel et al., 2014), but this remains in very high values compared with other studies using the ultrafiltration process (Wei et al., 2010). Regarding the purification of plipastatin alone, there is little work in the scientific literature because it is often combined with surfactin (Coutte et al., 2010b; Coutte et al., 2017). Our results obtained using a cut-off of 10 kDa are satisfactory with respect to the literature, not only at the diafiltration step where the purity of more than 30% is obtained (Ben Ayed et al., 2015) but also after the last purification step. Indeed, a work using a combination of ultrafiltration, acid precipitation, and nanofiltration has shown that it was possible to obtain fengycin with a purity close to 95%, which is close to the purity of our enriched plipastatin fraction (97.7%) (Sen and Swaminathan, 2005). It should also be noted here that there is a significant difference in the purity of surfactin and plipastatin (or mycosubtilin) after the diafiltration step. This can be explained by the fact that the concentrations of the solutions are very different between these molecules (4.73 $g{\cdot}L^{-1}$ for surfactin, 1.22 $g{\cdot}L^{-1}$ for mycosubtilin, and 1.46 $g{\cdot}L^{-1}$ for plipastatin).

The results presented in **Figures 3A,B** reveal, for the first time, that the yield of the spray-dried process is also related to the purity of the treated product. This is verified with spray-drying cell-free supernatant only, where the yield in LPP is quite low in the case of supernatant containing surfactin. For the latter two, a thick yellow paste is formed and sticks in an uncontrolled way all the parts of the spray-drier (data not shown). This phenomenon seems to be close to the one described by Barcelos et al. (2014), using crude LPP extract produced by *B. subtilis* LBBMA RI4914. A fermentation broth, even without cells, remains a complex matrix composed of numerous molecules that are more or less soluble in an aqueous solution (cell proteins, organic acids, biopolymers, sugars, etc.). This set of molecules (and particularly proteins) and the interactions they may have with each other when the solvent is removed can explain the formation of this sticky paste. Interestingly, in our study, this phenomenon does not appear when the supernatant contains only surfactin. Surfactin and plipastatin were produced by two strains derived from *B. subtilis* 168, thus showing a very similar potential of primary and secondary metabolite production profile (which is not the case for the mycosubtilin producing strain). Nevertheless, the overproduction of surfactin certainly limits the production of other metabolites by this strain, which may interfere with the spraying process. For surfactin, the yield of LPP recovered after the diafiltration step (diafiltered sample) is similar to the one obtained after the ethanol evaporation step (±80%). For plipastatin a slight decrease in the yield of LPP can be observed between the diafiltration and last purification steps (100%–78%). Nevertheless, for mycosubtilin, the yield of LPPs of the sample "purified fraction," obtained after the ethanol evaporation step, is two times lower than the one obtained before this last step of purification (95% compared with 52%). This result seems to correlate with a decrease in the global spray-drying yield after this step of purification (**Figure 3A**). This is a surprising result, which led us to investigate deeper the case of mycosubtilin.

The Specific Case of Mycosubtilin

As shown in **Figures 3A,B**, a decrease in the yield of spray-drying of mycosubtilin after the last step of the purification process (ethanol evaporation) is observed. For a better understanding of

TABLE 3 | Dry matter values measured for each spray-dried lipopeptide sample on the liquid solution before drying (Sample) and on the dried powder obtained (Product).

Sample type		Sample DM (%)	Product DM (%)	Product purity (%)
Surfactin	A—Supernatant	3.14 ±0.13	94.45 ±1.27	3.4 ±0.5
	B—Diafiltered LPP fraction	0.81 ±0.07	95.55 ±0.72	58.8 ±2.2
	C—Enriched LPP fraction	0.62 ±0.02	96.48 ±0.23	82.4 ±1.0
Mycosubtilin	B—Diafiltered LPP fraction	1.51 ±0.45	93.63 ±0.89	8.7 ±1.8
	C—Enriched LPP fraction	0.61 ±0.10	90.94 ±1.60	63.1 ±10.0
Plipastatin	B—Diafiltered LPP fraction	0.67 ±0.02	93.22 ±0.54	31.0 ±5.4
	C—Enriched LPP fraction	0.52 ±0.05	90.72 ±1.62	97.7 ±4.0

Note. The lipopeptide purity in each spray-dried product is also indicated.
DM, dry matter; LPP, lipopeptide.

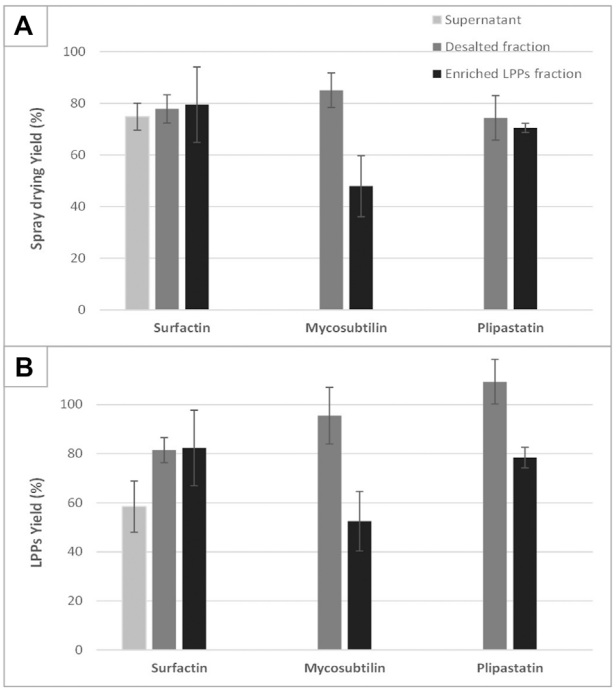

FIGURE 3 | Overview of the performances of the spray-drying process in terms of process yield **(A)** and lipopeptide specific yield **(B)**. The drying performances of the three lipopeptides sampled at different steps of the purification process (supernatant, diafiltered fraction, and enriched lipopeptides fraction) are compared with each other and with reference samples corresponding to spray-dried and resolubilized commercial lipopeptides. Any analyzable dry product was obtained after spray-drying of mycosubtilin or fengycin supernatant. Each drying experiment was performed on three distinct samples coming from different production batches; mean values and standard deviation are presented.

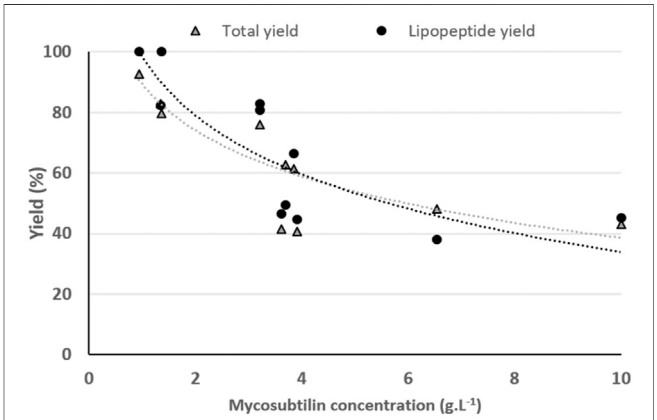

FIGURE 4 | Impact of the mycosubtilin concentration on the total yield and the lipopeptide yield of the spray-drying process. Gray triangle, total yield; black circle, lipopeptide yield. Each drying experiment was performed on distinct samples coming from different production batches.

this phenomenon, we studied the impact of the initial concentration of mycosubtilin in the solution to be spray-dried. Samples from 0.9 to 10 $g{\cdot}L^{-1}$ of mycosubtilin were spray-dried to mimic the concentration conditions obtained after the diafiltration or after the ethanol evaporation steps of purification. The results are presented in **Figure 4**. Interestingly, the total yield and the LPP yield decrease with the increase in the concentration of mycosubtilin, until a limit concentration of approximately 3.5 $g{\cdot}L^{-1}$. Indeed, results obtained for solutions below 3.5 $g{\cdot}L^{-1}$ are 90% ± 10% for LPP yield and 83% ± 5% for total yield. For solutions above 3.5 $g{\cdot}L^{-1}$, these results decrease to 50% ± 10% and 48% ± 10%. The ethanol evaporation process, which generates a high concentration, obviously has an important impact on the agglomeration phenomenon. The behavior of mycosubtilin in an aqueous solution is totally different from that of the other families of LPPs. It was shown that in the case of iturin A, micelles are formed at the CMC and larger vesicular structures at higher concentrations (Grau et al., 2001). In a more recent study, authors have investigated the behavior of the three families of LPPs using cryo-transmission electron microscopy, X-ray diffraction, and small-angle X-ray scattering. Their results confirm that mycosubtilin at high concentration has a distinct mode of self-assembly into extended nanotapes based on the stacking of LPP bilayers (Hamley et al., 2013). Moreover, Jauregi et al. (2013) have shown that mycosubtilin can interact with protein during the concentration/purification process by ultrafiltration (Jauregi et al., 2013). The amphiphilic,

tensioactive, and uncharged nature of mycosubtilin and its ability to interact with proteins are important parameters to consider in a drying process. Indeed, it is likely to adsorb at the air–water droplet interface, where inadequate surface energies may expose the hydrophobic region and induce LPPs to aggregation, as it is well known for proteins (Lee, 2002; Ameri and Maa, 2007). To prevent this phenomenon, excipients/surfactants are commonly used for the drying process (especially for protein), but they also make the preparation stickier, which leads to a higher wall deposition and yield losses (Ameri and Maa, 2007). Knowing the propensity of mycosubtilin to agglomerate and its surfactant properties, it does not seem surprising to observe this wall deposition. Wall deposition is a key processing problem during spray-drying. This phenomenon is greatly impacted by the technical parameters of the apparatus (size and geometry of spray dryer, wall surface energy, etc.) and the operational conditions (inlet–outlet temperature, feed rates, and excipients) but not exclusively (Keshani et al., 2015). The impact of the concentration of the feed solution on the spray-drying efficiency has already been observed in the case of carbohydrates (Elversson and Millqvist-Fureby, 2005). Indeed, the concentration influences the particle size, with an increase in particle size until a plateau is reached. The authors also showed that the solubility of the carbohydrates had an impact on the particle size, the less soluble they were and the larger the particle size (Elversson and Millqvist-Fureby, 2005). Thus, these results show that the success of the spray-drying of this particular LPP is therefore also dependent on its concentration. It is advisable to limit its concentration below 3.5 $g{\cdot}L^{-1}$ to obtain a good yield.

Finally, to deepen your knowledge on the direct spray-drying of the supernatant containing mycosubtilin (at low concentration), some additional trials were run to determine if the addition of charge (i.e., maltodextrin) can enable to obtain a dry product from a mycosubtilin-based supernatant. Maltodextrin is commonly used in spray-drying as a drying aid; it is used during the process to reduce not only the thermoplasticity and hygroscopicity but also the stickiness and product deposition (Keshani et al., 2015; Lee et al., 2018). Two proportions of maltodextrin were evaluated: 2.5% and 5% (w/v). In both cases, an analyzable dry product was obtained with the addition of maltodextrin. With 5% w/v of maltodextrin, the mycosubtilin supernatant containing 6.64% of dry matter was dried into a powder at 96.57% dry matter, with 1.39% LPP purity, and with a process yield of 70.18% and an LPP yield of 67.1%. With 2.5% w/v of maltodextrin, the mycosubtilin supernatant containing 4.33% of dry matter was dried into a powder at 91.32% dry matter, with 2.15% LPP purity, and with a process yield of 88.05% and an LPP yield of 89.76%. In both cases, the antifungal properties of mycosubtilin were only slightly impacted (compared with the value obtained with purified mycosubtilin, i.e., 4.1 $mg{\cdot}L^{-1}$ [2.1–6.3]) with a MIC against *S. cerevisiae* of 5.2 $mg{\cdot}L^{-1}$ [3.1–7.3]. This confirms the results obtained by Barcelos et al. (2014), who showed that the addition of maltodextrin at 10% is effective for the spray-drying of supernatant of *B. subtilis*-containing LPPs. Nevertheless, we demonstrated that 4 times less maltodextrin is sufficient as filler to make the spray-drying of these supernatant-containing LPPs easier.

CONCLUSION AND PROSPECTS

This study is the first one to systematically investigate the spray-drying of concentrated solutions of LPPs produced by *B. subtilis*. We have shown that this process produces a very high dry matter (up to 95%) and that surfactant and antimicrobial activities of the different LPPs are maintained. In addition, a more detailed study of the impact of the ultrafiltration purification process on the yield of the drying step demonstrated that this yield is directly impacted by the concentration of LPP, more particularly in the case of iturinic molecule such as mycosubtilin. Wall deposition phenomena were highlighted either when cell-free supernatants (for mycosubtilin and plipastatin) were used directly without additives or when the concentration of mycosubtilin was higher than 3.5 $g{\cdot}L^{-1}$. A specific study on the use of maltodextrin as an additive also showed its effectiveness for the direct drying of cell-free supernatants by limiting wall deposition phenomena. In the future, the impact of the operating conditions of the spray-drying process could be investigated (inlet temperature, feed concentration, and feed rate) in order to improve the yields of this process and constrain the phenomena of wall deposition. A granulometric study using microscopic means could also provide valuable information to characterize the formation of micellar aggregates, which can be involved in wall deposition phenomena.

DATA AVAILABILITY STATEMENT

The original contributions presented in the study are included in the article/**Supplementary Material**. Further inquiries can be directed to the corresponding author.

AUTHOR CONTRIBUTIONS

VA and CF conceptualized the experiments. VA, RM, DT, and PS took part in the investigation, methodology, and analysis. VA and CF wrote the manuscript. VA, JP, and CF helped in the critical review and the editing of the manuscript. JP and CF participated in the funding acquisition.

FUNDING

This work was supported by the project "BioSMART—Bio-based smart packaging for enhanced preservation of food quality"—Grant agreement No. 745762, funded by the Bio-based Industries Joint Undertaking (BBI-JU) under the European Union's Horizon 2020 Research and Innovation Programme. This work was also supported by the Universities of Lille and Liège from the European INTERREG V SmartBioControl/BioProd project and the Charles Viollette Institute by the ALIBIOTECH program

funding administered by the Hauts-de-France Region and for Lipofabrik by the SME Instrument Grant agreement No. 849713 under the European Union's Horizon 2020 Research and Innovation Programme. Met steun van het europees fonds voor regionale ontwikkeling. Avec le soutien du fonds européen de développement régional.

ACKNOWLEDGMENTS

The authors would like to thank Estelle Jans, Chloé Dupuis, and Papa Makhona Niang for their technical assistance during the lipopeptide production and purification steps and Aline Leconte for the test against *V. inaequalis*. The authors would also like to thank Robert Marmulla from Roquette for his donation of maltodextrins and also Dr. Nadine Burlion and Didier Schrooten from the Institut Scientifique de Service Public of Liège for the isolation, characterization and donation of the two strains of *L. pneumophila*.

SUPPLEMENTARY MATERIAL

The Supplementary Material for this article can be found online at: https://www.frontiersin.org/articles/10.3389/fbioe.2021.815337/full#supplementary-material

REFERENCES

Abdel-Mawgoud, A. M., Aboulwafa, M. M., and Hassouna, N. A.-H. (2008). Characterization of Surfactin Produced by Bacillus Subtilis Isolate BS5. *Appl. Biochem. Biotechnol.* 150, 289–303. doi:10.1007/s12010-008-8153-z

Al-Wahaibi, Y., Joshi, S., Al-Bahry, S., Elshafie, A., Al-Bemani, A., and Shibulal, B. (2014). Biosurfactant Production by Bacillus Subtilis B30 and its Application in Enhancing Oil Recovery. *Colloids Surf. B: Biointerfaces* 114, 324–333. doi:10.1016/j.colsurfb.2013.09.022

Ameri, M., and Maa, Y.-F. (2007). Spray Drying of Biopharmaceuticals: Stability and Process Considerations. *Drying Tech.* 24, 763–768. doi:10.1080/03602550600685275

Barcelos, G. S., Dias, L. C., Fernandes, P. L., Fernandes, R. d. C. R., Borges, A. C., Kalks, K. H., et al. (2014). Spray Drying as a Strategy for Biosurfactant Recovery, Concentration and Storage. *Springerplus* 3, 1–9. doi:10.1186/2193-1801-3-49

Béchet, M., Castéra-Guy, J., Guez, J.-S., Chihib, N.-E., Coucheney, F., Coutte, F., et al. (2013). Production of a Novel Mixture of Mycosubtilins by Mutants of Bacillus Subtilis. *Bioresour. Tech.* 145, 264–270. doi:10.1016/j.biortech.2013.03.123

Ben Ayed, H., Bardaa, S., Moalla, D., Jridi, M., Maalej, H., Sahnoun, Z., et al. (2015). Wound Healing and *In Vitro* Antioxidant Activities of Lipopeptides Mixture Produced by Bacillus Mojavensis A21. *Process Biochem.* 50, 1023–1030. doi:10.1016/J.PROCBIO.2015.02.019

Caboche, S., Pupin, M., Leclere, V., Fontaine, A., Jacques, P., and Kucherov, G. (2008). NORINE: A Database of Nonribosomal Peptides. *Nucleic Acids Res.* 36, D326–D331. doi:10.1093/nar/gkm792

Chen, C.-Y., Baker, S. C., and Darton, R. C. (2006). Continuous Production of Biosurfactant with Foam Fractionation. *J. Chem. Technol. Biotechnol.* 81, 1915–1922. doi:10.1002/jctb.1624

Cooper, D. G., Macdonald, C. R., Duff, S. J. B., and Kosaric, N. (1981). Enhanced Production of Surfactin from Bacillus Subtilis by Continuous Product Removal and Metal Cation Additions. *Appl. Environ. Microbiol.* 42, 408–412. doi:10.1128/AEM.42.3.408-412.1981

Coutte, F., Leclère, V., Béchet, M., Guez, J. S., Lecouturier, D., Chollet-Imbert, M., et al. (2010a). Effect of Pps Disruption and Constitutive Expression of srfA on Surfactin Productivity, Spreading and Antagonistic Properties of Bacillus Subtilis 168 Derivatives. *J. Appl. Microbiol.* 109, 480–491. doi:10.1111/j.1365-2672.2010.04683.x

Coutte, F., Lecouturier, D., Ait Yahia, S., Leclère, V., Béchet, M., Jacques, P., et al. (2010b). Production of Surfactin and Fengycin by Bacillus Subtilis in a Bubbleless Membrane Bioreactor. *Appl. Microbiol. Biotechnol.* 87, 499–507. doi:10.1007/s00253-010-2504-8

Coutte, F., Lecouturier, D., Dimitrov, K., Guez, J.-S., Delvigne, F., Dhulster, P., et al. (2017). Microbial Lipopeptide Production and Purification Bioprocesses, Current Progress and Future Challenges. *Biotechnol. J.* 12 (7), 1600566. doi:10.1002/biot.201600566

Coutte, F., Lecouturier, D., Leclère, V., Béchet, M., Jacques, P., and Dhulster, P. (2013). New Integrated Bioprocess for the Continuous Production, Extraction and Purification of Lipopeptides Produced by Bacillus Subtilis in Membrane Bioreactor. *Process Biochem.* 48, 25–32. doi:10.1016/J.PROCBIO.2012.10.005

Czinkóczky, R., and Németh, Á. (2020). Techno-economic Assessment of Bacillus Fermentation to Produce Surfactin and Lichenysin. *Biochem. Eng. J.* 163, 107719. doi:10.1016/j.bej.2020.107719

Deleu, M., Lorent, J., Lins, L., Brasseur, R., Braun, N., El Kirat, K., et al. (2013). Effects of Surfactin on Membrane Models Displaying Lipid Phase Separation. *Biochim. Biophys. Acta (Bba) - Biomembranes* 1828, 801–815. doi:10.1016/J.BBAMEM.2012.11.007

Demain, A. L. (2014). Importance of Microbial Natural Products and the Need to Revitalize Their Discovery. *J. Ind. Microbiol. Biotechnol.* 41, 185–201. doi:10.1007/s10295-013-1325-z

Deravel, J., Lemière, S., Coutte, F., Krier, F., Van Hese, N., Béchet, M., et al. (2014). Mycosubtilin and Surfactin Are Efficient, Low Ecotoxicity Molecules for the Biocontrol of Lettuce Downy Mildew. *Appl. Microbiol. Biotechnol.* 98, 6255–6264. doi:10.1007/s00253-014-5663-1

Desmyttere, H., Deweer, C., Muchembled, J., Sahmer, K., Jacquin, J., Coutte, F., et al. (2019). Antifungal Activities of bacillus Subtilis Lipopeptides to Two Venturia Inaequalis Strains Possessing Different Tebuconazole Sensitivity. *Front. Microbiol.* 10, 1. doi:10.3389/fmicb.2019.02327

Eeman, M., Olofsson, G., Sparr, E., Nasir, M. N., Nylander, T., and Deleu, M. (2014). Interaction of Fengycin with Stratum Corneum Mimicking Model Membranes: A Calorimetry Study. *Colloids Surf. B: Biointerfaces* 121, 27–35. doi:10.1016/J.COLSURFB.2014.05.019

Elversson, J., and Millqvist-Fureby, A. (2005). Particle Size and Density in Spray Drying-Effects of Carbohydrate Properties. *J. Pharm. Sci.* 94, 2049–2060. doi:10.1002/JPS.20418

Gong, G., Zheng, Z., Chen, H., Yuan, C., Wang, P., Yao, L., et al. (2009). Enhanced Production of Surfactin by Bacillus Subtilis E8 Mutant Obtained by Ion Beam Implantation. *Food Technol. Biotechnol.* 47, 27–31.

Grau, A., Gómez-Fernández, J. C., Peypoux, F., and Ortiz, A. (2001). Aggregational Behavior of Aqueous Dispersions of the Antifungal Lipopeptide Iturin A. *Peptides* 22, 1–5. doi:10.1016/S0196-9781(00)00350-8

Guez, J.-S., Vassaux, A., Larroche, C., Jacques, P., and Coutte, F. (2021). New Continuous Process for the Production of Lipopeptide Biosurfactants in Foam Overflowing Bioreactor. *Front. Bioeng. Biotechnol.* 9, 357. doi:10.3389/FBIOE.2021.678469

Hamley, I. W., Dehsorkhi, A., Jauregi, P., Seitsonen, J., Ruokolainen, J., Coutte, F., et al. (2013). Self-assembly of Three Bacterially-Derived Bioactive Lipopeptides. *Soft Matter* 9, 9572–9578. doi:10.1039/C3SM51514A

Jacques, P. (2011). *Surfactin and Other Lipopeptides from Bacillus Spp*. Berlin, Heidelberg: Springer, 57–91. doi:10.1007/978-3-642-14490-5_3

Jauregi, P., Coutte, F., Catiau, L., Lecouturier, D., and Jacques, P. (2013). Micelle Size Characterization of Lipopeptides Produced by B. Subtilis and Their Recovery by the Two-step Ultrafiltration Process. *Sep. Purif. Tech.* 104, 175–182. doi:10.1016/J.SEPPUR.2012.11.017

Keshani, S., Daud, W. R. W., Nourouzi, M. M., Namvar, F., and Ghasemi, M. (2015). Spray Drying: An Overview on wall Deposition, Process and Modeling. *J. Food Eng.* 146, 152–162. doi:10.1016/J.JFOODENG.2014.09.004

Kourmentza, K., Gromada, X., Michael, N., Degraeve, C., Vanier, G., Ravallec, R., et al. (2021). Antimicrobial Activity of Lipopeptide Biosurfactants against Foodborne Pathogen and Food Spoilage Microorganisms and Their Cytotoxicity. *Front. Microbiol.* 11, 1. doi:10.3389/fmicb.2020.561060

Leclère, V., Marti, R., Béchet, M., Fickers, P., and Jacques, P. (2006). The Lipopeptides Mycosubtilin and Surfactin Enhance Spreading of Bacillus Subtilis Strains by Their Surface-Active Properties. *Arch. Microbiol.* 186, 475–483. doi:10.1007/s00203-006-0163-z

Lee, G. (2002). Spray-drying of Proteins. *Pharm. Biotechnol.* 13, 135–158. doi:10.1007/978-1-4615-0557-0_6

Lee, J. K. M., Taip, F. S., and Abdullah, Z. (2018). Effectiveness of Additives in spray Drying Performance: a Review. *Food Res.* 2, 486–499. doi:10.26656/FR.2017.2(6).134

Loiseau, C., Schlusselhuber, M., Bigot, R., Bertaux, J., Berjeaud, J.-M., and Verdon, J. (2015). Surfactin from Bacillus Subtilis Displays an Unexpected Anti-Legionella Activity. *Appl. Microbiol. Biotechnol.* 99, 5083–5093. doi:10.1007/S00253-014-6317-Z

Maget-Dana, R., Thimon, L., Peypoux, F., and Ptak, M. (1992). Interfacial Properties of the Antifungal Iturins on Various Electrolyte Solutions. *J. Colloid Interf. Sci.* 149, 174–183. doi:10.1016/0021-9797(92)90402-8

Mantil, E., Buznytska, I., Daly, G., Ianoul, A., and Avis, T. J. (2019). Role of Lipid Composition in the Interaction and Activity of the Antimicrobial Compound Fengycin with Complex Membrane Models. *J. Membr. Biol.* 252, 627–638. doi:10.1007/s00232-019-00100-6

Mejri, S., Siah, A., Coutte, F., Magnin-Robert, M., Randoux, B., Tisserant, B., et al. (2018). Biocontrol of the Wheat Pathogen Zymoseptoria Tritici Using Cyclic Lipopeptides from Bacillus Subtilis. *Environ. Sci. Pollut. Res.* 25, 29822–29833. doi:10.1007/s11356-017-9241-9

Meng, X., Yu, J., Yu, M., Yin, X., and Liu, Y. (2015). Dry Flowable Formulations of Antagonistic Bacillus Subtilis Strain T429 by spray Drying to Control rice Blast Disease. *Biol. Control.* 85, 46–51. doi:10.1016/j.biocontrol.2015.03.004

Ongena, M., and Jacques, P. (2008). Bacillus Lipopeptides: Versatile Weapons for Plant Disease Biocontrol. *Trends Microbiol.* 16, 115–125. doi:10.1016/j.tim.2007.12.009

Ongena, M., Jourdan, E., Adam, A., Paquot, M., Brans, A., Joris, B., et al. (2007). Surfactin and Fengycin Lipopeptides of Bacillus Subtilis as Elicitors of Induced Systemic Resistance in Plants. *Environ. Microbiol.* 9, 1084–1090. doi:10.1111/j.1462-2920.2006.01202.x

Sen, R., and Swaminathan, T. (2005). Characterization of Concentration and Purification Parameters and Operating Conditions for the Small-Scale Recovery of Surfactin. *Process Biochem.* 40, 2953–2958. doi:10.1016/J.PROCBIO.2005.01.014

Thimon, L., Peyoux, F., Maget-Dana, R., and Michel, G. (1992). Surface-active Properties of Antifungal Lipopeptides Produced byBacillus Subtilis. *J. Am. Oil Chem. Soc.* 69, 92–93. doi:10.1007/BF02635884

Vardanega, R., Muzio, A. F. V., Silva, E. K., Prata, A. S., and Meireles, M. A. A. (2019). Obtaining Functional Powder tea from Brazilian Ginseng Roots: Effects of Freeze and spray Drying Processes on Chemical and Nutritional Quality, Morphological and Redispersion Properties. *Food Res. Int.* 116, 932–941. doi:10.1016/j.foodres.2018.09.030

Wang, Y., Zhu, X., Bie, X., Lu, F., Zhang, C., Yao, S., et al. (2014). Preparation of Microcapsules Containing Antimicrobial Lipopeptide from Bacillus Amyloliquefaciens ES-2 by spray Drying. *LWT - Food Sci. Tech.* 56, 502–507. doi:10.1016/j.lwt.2013.11.041

Wei, Y.-H., Wang, L.-C., Chen, W.-C., and Chen, S.-Y. (2010). Production and Characterization of Fengycin by Indigenous Bacillus Subtilis F29-3 Originating from a Potato Farm. *Ijms* 11, 4526–4538. doi:10.3390/ijms11114526

Yánez-Mendizábal, V., Viñas, I., Usall, J., Torres, R., Solsona, C., Abadias, M., et al. (2012). Formulation Development of the Biocontrol Agent Bacillus Subtilis Strain CPA-8 by spray-drying. *J. Appl. Microbiol.* 112, 954–965. doi:10.1111/j.1365-2672.2012.05258.x

Yu, C., Wanli, C., Dian, H., Longyu, Z., Minmin, C., Da, L., et al. (2017). Preparation and Characterization of Iturin A Microcapsules in Sodium Alginate/poly(γ-Glutamic Acid) by spray Drying. *Int. J. Polymeric Mater. Polymeric Biomater.* 66, 479–484. doi:10.1080/00914037.2016.1233417

Conflict of Interest: CF and JP from the University of Lille and University of Liège are also the two co-founders of Lipofabrik company, which markets lipopeptides from *B. subtilis*. PS is also part of Lipofabrik company.

The remaining authors declare that the research was conducted in the absence of any commercial or financial relationships that could be construed as a potential conflict of interest.

Publisher's Note: All claims expressed in this article are solely those of the authors and do not necessarily represent those of their affiliated organizations, or those of the publisher, the editors, and the reviewers. Any product that may be evaluated in this article, or claim that may be made by its manufacturer, is not guaranteed or endorsed by the publisher.

frontiers in Bioengineering and Biotechnology

REVIEW
published: 27 January 2022
doi: 10.3389/fbioe.2022.816613

Phase Behaviour, Functionality, and Physicochemical Characteristics of Glycolipid Surfactants of Microbial Origin

Karina Sałek[1]*, *Stephen R. Euston*[2] *and Tomasz Janek*[3]

[1]Institute for Life and Earth Sciences, School of Energy, Geoscience, Infrastructure and Society, Heriot-Watt University, Edinburgh, United Kingdom, [2]Institute of Biological Chemistry, Biophysics and Bioengineering, School of Engineering and Physical Sciences, Heriot-Watt University, Edinburgh, United Kingdom, [3]Department of Biotechnology and Food Microbiology, Wrocław University of Environmental and Life Sciences, Wrocław, Poland

Growing demand for biosurfactants as environmentally friendly counterparts of chemically derived surfactants enhances the extensive search for surface-active compounds of biological (microbial) origin. The understanding of the physicochemical properties of biosurfactants such as surface tension reduction, dispersion, emulsifying, foaming or micelle formation is essential for the successful application of biosurfactants in many branches of industry. Glycolipids, which belong to the class of low molecular weight surfactants are currently gaining a lot of interest for industrial applications. For this reason, we focus mainly on this class of biosurfactants with particular emphasis on rhamnolipids and sophorolipids, the most studied of the glycolipids.

Keywords: biosurfactants, glycolipids, rhamnolipids, sophorolipids, lipopeptides, global use of surfactants

OPEN ACCESS

Edited by:
Andrea Zille,
University of Minho, Portugal

Reviewed by:
Deepansh Sharma,
Amity University Jaipur, India
Sanket J. Joshi,
Sultan Qaboos University, Oman

***Correspondence:**
Karina Sałek
karina.salek@gmail.com

Specialty section:
This article was submitted to Industrial Biotechnology, a section of the journal Frontiers in Bioengineering and Biotechnology

Received: *16 November 2021*
Accepted: *10 January 2022*
Published: *27 January 2022*

Citation:
Sałek K, Euston SR and Janek T (2022) Phase Behaviour, Functionality, and Physicochemical Characteristics of Glycolipid Surfactants of Microbial Origin. Front. Bioeng. Biotechnol. 10:816613. doi: 10.3389/fbioe.2022.816613

1 INTRODUCTION

There is a high demand for surfactants across almost every sector of modern industry as they are found in a wide range of household products. The global consumption of surfactants increases every year and its global production is expected to reach US$ 28.8 billion until 2023 (Kaczerewska et al., 2020). Surfactants are used extensively in the household and personal care market, with the latter constituting approximately 14% of the global surfactant use, with the Asia-Pacific region being the largest consumer (Costello 2018). Other uses of surfactants cover the oil and gas industry, transport, industrial clean-up processes and the food industry (Shukla 2016; Costello 2018).

Many surfactants used in industry are produced synthetically from petrochemical feedstock, which is neither sustainable nor environmentally friendly. Additionally, synthetic surfactants are recognized as being relatively eco-toxic and of low biodegradability. This has led to an interest in biosurfactants as green solutions that are environmentally friendly by virtue of their low toxicity and biodegradability compared with their synthetically derived counterparts. According to Global Market Insights, Inc. (Global Market Insights Inc. 2018), by 2024 the biosurfactant demand in personal care market should reach USD 300 million, while the general U.S. biosurfactant market size may exceed even USD 600 million and for the United Kingdom the estimates are as high as USD 210 million. Due to the high demand for cleaning products (both domestic and industrial) detergent use of biosurfactants is expected to dominate the global biosurfactant applications by 2022 (Research and Markets 2017).

Despite the ever-increasing demand, the commercial production of biosurfactants is still a challenge due to high raw material costs. About 30–50% of the total cost comes solely from the preparation of culture medium for biosurfactant production secreted by microorganisms (Ebadipour et al., 2016). Thus, current research challenges include a decrease in the cost of raw materials, consumables, utilities, labor, and waste treatment and disposal (Bjerk et al., 2021). In terms of price, synthetic surfactants (priced at approximately USD 2/kg) (Kosaric and Vardar-Sukan 2015), are much cheaper compared to the pure rhamnolipids (priced range between USD 1250/kg and USD 2500/kg) (www.agaetech.com and www.sigmaaldrich.com (accessed date: 27 December 2021)). Glycolipid biosurfactants such as lactonic sophorolipids cost around USD 55 000/kg (www.carbosynth.com (accessed date: 27 December 2021)), whereas the cost of lipopeptide biosurfactant surfactin is USD 17 600/g (www.sigmaaldrich.com (accessed date: 27 December 2021)), since it is produced in lower quantities. Compared to pure commercially available biosurfactants, Ebadipour et al. (2016) described production of rhamnolipids (24 g/L) with corn steep liquor at an estimated price of USD 12/kg. According to the work of Ashby et al. (2013) production of sophorolipids using glucose and high oleic sunflower oil cost of USD 2.54/kg. According to Singh et al. (2019) cost reduction using cheaper raw materials, or agroindustrial wastes, could lead to a cost being closer to the lucrative 2 USD/kg for commercial surfactants.

Owing to the increasing customer awareness and demand for natural, vegan, organic and sustainable food additives, biosurfactants seem to represent a good candidate to replace their synthetic counterparts in food industry (Nitschke and Silva 2018). A well-studied antimicrobial and antibiofilm potential of biosurfactants enables them to be used as antiadhesive and biofilm-disrupting agents as well as food preservatives (Sambanthamoorthy et al., 2014; Nitschke and Silva 2018; Sałek and Euston 2019). Another opportunity for biosurfactant use in food industry lies within their surface-active properties, making them potentially highly valuable emulsifiers and emulsion stabilisers in not only food, but also cosmetic and pharmaceutical industry, where emulsions (especially nanoemulsions) are used as drug-delivery systems (Dalgleish 2006; Bai and McClements 2016).

Glycolipids biosurfactants have the most potential in industry with rhamnolipids and sophorolipids generating the most interest especially in detergency. Therefore, this review article focuses on the glycolipid-based biosurfactants, their functional properties, structure and applications.

2 CLASSIFICATION OF BIOSURFACTANTS OF MICROBIAL ORIGIN

Biosurfactants are classified according to molecular weight–low or high. Glycolipids, flavolipids and lipopeptides are low molecular weight (LMW) biosurfactants while lipoproteins, polysaccharides and lipopolysaccharides belong to the high molecular weight (HMW) class (Smyth et al., 2010). Currently, the LMW biosurfactants, especially glycolipids are of high interest for exploitation in the detergent and personal care markets, but have potential in the cosmetic, biomedical and food industries. A review of the major LMW biosurfactants follows in the subsequent sections, with a particular emphasis on glycolipids.

2.1 Glycolipids

Glycolipids are biosurfactants with a range of structures, made up of a sugar polar group and a lipid group. This diverse group of surfactants includes rhamnolipids, sophorolipids (including their derivatives), mannosylerythritol lipids, trehalolipids and cellobioselipids (Mulligan 2005; Franzetti et al., 2010).

A slightly different group of microbial lipids–polyol lipids, produced by yeast and fungi, are also classified as glycolipids. The two main categories of polyols–liamocins and polyol esters of fatty acids (PEFA) are less studied than the other glycolipids, however, they may present a good potential for commercialisation (Garay et al., 2018).

2.2 Lipopeptides

Lipopeptides (LPs) are a group class of biosurfactants containing a variable length fatty acid and cyclic peptide polar group. Several isoforms have been identified, with surfactin, iturin, fengycin, lichenysin among the most common, with some microorganisms excreting more than one isoform (Mnif and Dhouha 2015b). Bacteria, yeasts, molds and actinomycetes have been identified as lipopeptides producers (Mnif and Dhouha 2015b). Surfactin, a secondary metabolite of the bacterium *Bacillus subtillis*, is the most studied (Mnif and Dhouha 2015b), with reported antimicrobial and anti-mycoplasma activities, as well as cell lysate promoter and fibrin clotting properties (Chen et al., 2015). *Bacillus* sp. also produce lichenysin, iturin and fengycin, while *Pseudomonas* sp. secrete tensin, pseudofactin and viscosin. Important LP antibiotics are produced by *Streptomyces* sp. (amphotericin and laspartomycin) and *Pseudomonas* sp. (polymyxin). Amphotericin and lasapartomycin can be used as therapies for difficult to treat aspergillosis and candidiasis fungal infections as well as *Leishmania* parasites (Caffrey et al., 2001; Tollemar et al., 2001). Laspartomycin can treat antibiotic-resistant enterococci and *Staphylococcus aureus* (Borders et al., 2007; Strieker and Marahiel 2009).

Lipopeptide function is linked to their surface chemistry, with their antibiotic activity being due to their ability to adsorb to and insert into cell membranes (Carrillo et al., 2003). Lichenysin is reported to be the most surface active of the lipopeptides, with a CMC half that of surfactin (Yakimov et al., 1995), a characteristic attributed to a less polar peptide head group and longer lipid tail. Lichenysin is also reported to be highly heat, pH and salt stable (McInerney et al., 1990). The self-assembly of lipopetides such as surfactin and iturin has been studied as this will influence surface behaviour and biological activity. Surfactin has been reported to have a low critical micelle concentration (CMC) in the range 7.5–10 μM (Heerklotz and Seelig 2001; Carrillo et al., 2003), and iturin in the range 25–40 μM (Harnois et al., 1988; Maget-Dana and Peypoux 1994). Surfactin also forms unusually small micelles (Shen et al., 2009). More complex self-assembled structures have been observed, for example for mycosubtilin produced by *Bacillus*

TABLE 1 | Recent reports on possible applications glycolipids.

Biosurfactant	Biological or Physicochemical activity	Industrial sector	References
Mannosyl erythritol lipids (MELs)	Anti-melanogenic	Cosmetic	Bae et al. (2018)
MELs	Anti-bacterial	Foods Medical	Shu et al. (2019)
MELs	Anti-bacterial	Medical Food	Ceresa et al. (2020b)
MELs	Nanoparticles	Pharmaceutical	Bakur et al. (2019)
Sophorolipids	Biofilm inhibition and disruption	Pharmaceutical Food Packaging	Díaz De Rienzo et al. (2016)
Acidic sophorolipids	Anti-bacterial activity	Medical	Lydon et al. (2017)
Free acid and lactonic sophorolipids	Antimicrobial activity and inactivation mechanism against pathogenic *Escherichia coli* O157:H7	Medical Pharmaceutical Food	Zhang et al. (2017)
Lactonic sophorolipids	Solid-lipid nanoparticles	Pharmaceutical	Kanwar et al. (2018)
Sophorolipids	Anti-HIV activity Spermicidal activity	Medical	Shah et al. (2005)
Sophorolipids	Anti-bacterial Anti-biofilm	Medical Food Biomaterial	Díaz De Rienzo et al. (2015); Díaz De Rienzo et al. (2016); Ceresa et al. (2020a)
Sophorolipids	Anti-cancer (breast adenocarcinoma lines MDA-MB-231)	Medical	Ribeiro et al. (2015)
Sophorolipids	Anti-cancer	Medical	Shao et al. (2012)
Sophorolipids	Nanoparticle synthesis	Medical	Singh et al. (2009); Shikha et al. (2020)
Mono & di-RLs	Anti-microbial activity	Medical Food	Ndlovu et al. (2017)
Mono & di-RLs	Cytotoxic effect on human breast cancer cells	Medical	Rahimi et al. (2019)
Rhamnolipids	Stabilisation of oil in high water internal phase emulsions (HIPEs)	Food Medical Personal care Cosmetics	Dai et al. (2019)
Rhamnolipids	Anti-bacterial activity towards food pathogens: *B. cereus* and *L. monocytogenes*, *S. aureus*	Food Packaging	de Freitas Ferreira et al. (2018)
Rhamnolipids	Nanoemulsions for drug delivery mechanism against SCC7 tumour cells	Medical	Yi et al. (2019)
Rhamnolipids	Biodegradation of hydrophobic organic compounds	Bioremediation strategies	Zeng et al. (2018)
Rhamnolipids	Microbial-enhanced oil recovery (MEOR)	Environmental protection Petroleum	Câmara et al. (2019)
Rhamnolipid	Nanoparticle synthesis	Medical	Kumar et al. (2010); Bharali et al. (2013); Saikia et al. (2013); Kumar and Das (2018); Bayee et al. (2020)
Trehalolipids	Anti-microbial Anti-adhesive	Medical Biomaterials	Janek et al. (2018)
Trehalolipids	Immunomodulato-ry and membrano- tropic activity	Medical	Kuyukina et al. (2015); Kuyukina et al. (2020)
Trehalolipids	Anti-tumour	Medical	Christova et al. (2015)

spp. In this lipopeptide extended nanotape structures (Hamley et al., 2013) form rather than micelles. There is a recognition that lipopeptide phase behaviour has not been studied in the same detail as other biosurfactants (Hamley 2015).

2.3 Flavolipids

Flavolipids, first described by Bodour et al. (2004), are a relatively newly identified class of biosurfactants from the genus *Flavobacterium*. The surfactant isolated by the authors had a critical micelle concentration (CMC) of 300 mg/L and reduced surface tension to 26 mN/m. A strong emulsifying ability of the surfactant and successful mineralization of hexadecane was also reported. The hydrophilic moiety of flavolipids is a citric acid and two cadaverine molecules, which is unlike other lipid-based surfactants.

The ability of flavolipids to form micelles and also vesicles in the presence of iron (Martinez et al., 2000; Serrano Figueroa et al., 2016) hints at complex phase behaviour, but as far as we can determine this has not been studied in any detail.

3 GLYCOLIPIDS

The most studied group of LMW biosurfactants are the glycolipids and there is growing interest in their application for industrial applications due to this. There follows a detailed

description of selected glycolipids and recent advances in their applications. **Table 1** presents a brief summary of recent reports on the activity and potential application of glycolipids.

3.1 Rhamnolipids

Rhamnolipids (RLs) originally identified, as sugar lipids produced by the bacterium *Pseudomonas aeruginosa,* an opportunistic pathogen bacterium are one of the best-known biosurfactants. Rhamnolipids were first mentioned as novel biomolecules in 1946, when the antibacterial activity of "pyolipic acid," from *P. pyocyanea* (later *P. aeruginosa*) against *Mycobacterium tuberculosis* (Bergström et al., 1946) was reported. Three years later Jarvis and Johnson isolated and identified pyolipic acid as "an acidic, crystalline glyco-lipide" (Jarvis and Johnson 1949).

3.1.1 Structure and Production

The structures of RLs can vary significantly depending on the producing microorganism, carbon source and culture conditions. In general, RLs can be described as mono- (one rhamnose ring) or di-rhamnolipids (two rhamnose rings connected via an α-1,2-glycosidic bond). The lipid part has one, two or three saturated or unsaturated β-hydroxy fatty acids with varied chain length (C_8-C_{16}) (Lang and Wullbrandt 1999; Gunther IV et al., 2005; Abdel-Mawgoud et al., 2010).

The best-described microorganism producing rhamnolipids is *Pseudomonas aeruginosa*. Production of RLs by this organism has undergone extensive process and genetic optimization and scale-up to the point where RL products are commercially available. Despite very good functional features of RLs, the fact that they are produced by a pathogenic strain limits their applications in many consumer industries e. g personal care, food and cosmetics. Therefore, an extensive search for other, non-pathogenic RL-producers continues. Several non-pathogenic *Pseudomonas* species produce rhamnolipids, such as *P. alcaligenes* (Oliveira et al., 2009), *P. fluorescens* (Abouseoud et al., 2008), *P. chlororaphis* (Gunther IV et al., 2005), *P. putida* (Wittgens et al., 2011), and *P. stutzeri* (Celik et al., 2008; Singh and Tripathi 2013). Apart from *Pseudomonas* species, other species of bacteria such as *Burkholderia plantarii* (Andrä et al., 2006), *Burkholderia thailandensis* (Elshikh et al., 2017), *Acinetobacter calcoaceticus* (HoŠková et al., 2013; Hošková et al., 2015), *Enterobacter asburiae* (HoŠková et al., 2013; Hošková et al., 2015), and *Marinobacter* sp. (Voulgaridou et al., 2021) are also known to produce RLs.

The fermentation conditions as well as the strain selection are important for the production of the particular RLs and the number of homologues in the product. These can vary significantly even within the same species. Abalos et al. (2001) identified seven homologues of RLs isolated from *P. aeruginosa* AT10 grown on soybean oil refinery wastes. Two compounds–Rha-C_{10}-C_{10} and Rha-Rha-C_{10}-C_{10} were predominant in the isolated mixture and were characterised with very high anti-fungal activity. A total number of 15 rhamnolipid homologues in a post-fermentation mixture of *P. aeruginosa* 47T2 NCBIM 40044 (grown on waste cooking oils) were identified by Haba et al. (2003). Also, in this example, the most dominant rhamnolipid was Rha-Rha-C_{10}-C_{10} (34% relative abundance), followed by Rha-C_{10}-C_{10} (19% relative abundance) and Rha-Rha-C_{10}-C_{12} (20% relative abundance). Gong et al. (2015) presented a comparison of the yields of isolated rhamnolipids when *P. aeruginosa* TIB-R02 was grown on eight different food oil carbon sources. The di-RL Rha-Rha-C_{10}-C_{10} was identified as the most abundant (>40% relative abundance) homologue in the case of six tested oils (coconut, peanut, olive, palm, grapeseed and soybean oil), while Rha-C_{10}-C_{10} was the most dominant (>40%) for corn and frying oils. Rha-Rha-C_{12}-C_{10} was the third most abundant homologue present in all of the isolated mixtures, but its content did not exceed 20% in any of the cases (Gong et al., 2015).

Some researchers have developed methods for the chemical synthesis of RLs to overcome perceived issues with scaled up biological production (Coss et al., 2012; Palos Pacheco et al., 2017, Palos Pacheco et al., 2021; Compton et al., 2020). Whilst these can produce RLs at commercial scale and are marketed as green surfactants (www.glycosurf.com), the methods are not yet seen as economically viable compared to other synthetic surfactants (Palos Pacheco et al., 2021). They are also bio-inspired (synthetic) and not truly biological methods for RL production and thus are likely to suffer from the consumer perception that they are synthetic and not natural, even if as claimed the methods are green (Palos Pacheco et al., 2021). Scientifically, these synthesis methods have proven useful for the production of specific RL congeners that allow the effect of congener structure on surface active properties to be studied (Palos Pacheco et al., 2021).

3.1.2 Phase Behaviour

Surfactants have long been known to display complex phase behaviour in aqueous solution owing to their ability to self-assemble into various structures such as micelles, vesicles, bilayers and various liquid crystalline mesophases depending on concentration and temperature (Tadros 2005). The phase behaviour impacts on properties of the surfactants in industrial applications. Rhamnolipids, and glycolipids in general, also display this rich phase behaviour. Glycolipids, including RLs, at concentrations around the critical micelle concentration (CMC) form micelles that are spherical, disk-like or rod-like (Söderman and Johansson 1999).

Many studies characterise only the CMC of the rhamnolipids, although the micelle is only one of the potential self-association structures formed. Nitschke et al. (2011) compared CMC and surface tension (ST) of rhamnolipids isolated from various *Pseudomonas* species. According to this study, the lowest ST was for RLs isolated from *P. chlororaphis*, and varied between 25 and 30 mN/m. The RLs from *P. aeruginosa* were reported to lower ST to 27.3 mN/m and have a CMC of 13.9 mg/L. Close to that range were RLs isolated from *P. alcaligenes* with ST equal to 28 mN/m and CMC 30 mg/L. The highest ST among *Pseudomonas* species was detected for *P. fluorescens*–35 mN/m and CMC reaching 20 mg/L. In general, the CMC of rhamnolipids can vary even between 10 and 200 mg/L depending on the producing microorganisms, carbon sources, medium composition and other factors such as temperature,

aeration and pH (Nitschke et al., 2005). In practice, it has been known for some time that self-association in rhamnolipids is more complicated than just formation of micelles. Both Ishigami et al. (1987) and Champion et al. (1995) observed using cryo-TEM that rhamnolipids formed either lamellar, micelle or vesicle phases depending on the pH. Similarly, Sánchez et al. (2007), report a concentration-dependent micelle-to-vesicle transformation for diRLs at pH 7.4. Small angle neutron scattering (SANS) has revealed that both the monorhamnolipid R1 (Rha-C_{10}-C_{10}) and dirhamnolipid R2 (Rha-Rha-C_{10}-C_{10}) form small, globular, elliptical core shell micelles with the ratios of the minor-major axes in the range 1:2–10 (Chen et al., 2010) and average aggregation numbers (number of rhamnolipids per micelle) of n = 50 for R1, n = 30 for R2 and n = 40 for a mixed R1/R2 micelle. The reduced packing efficiency of the two rhamnopyranose rings in the headgroup of R2 leads to a lower curvature of the micelle surface, and so R2 micelles are more asymmetric than those of R1. Palos Pacheco and co-workers (Palos Pacheco et al., 2021) have been able to carry out detailed studies of the micellization and aggregate structure of a homologous series of monorhamnolipids with a single C14 chain, and second chain lengths of 6, 8, 10, 12 and 14 carbons. This has allowed them to study the intricacies of RL congener structure on surface properties. Surprisingly, they find that the CMC does not vary linearly with chain length. The CMC is lowest for $RlC_{14}C_{10}$ and increases for smaller and higher second lipid chain lengths. The minimum surface tension mirrors this behaviour. This behaviour suggests that interactions within the RL congener and between molecules at the interface is complex and plays a significant role in their surface behaviour. Molecular dynamics simulations of RL congeners with differing chain length ($C_{14}C_{14}$, $C_{14}C_{10}$ and $C_{10}C_{14}$) also show differing properties of the congeners suggesting complex surface interactions within the molecule (Euston et al., 2021).

Molecular simulation has been used to investigate the internal structure of RL micelles and biosurfactants in general (Euston 2017) in more detail. Schwartz and co-workers have carried out a detailed study of the structure of micelles and vesicles for both mono and di-rhamnolipids (Munusamy et al., 2017). They found that for nonionic R1, spherical, ellipsoidal, torus-like, and unilamellar vesicle structure can form depending on aggregation number (Eismin et al., 2017), with anionic R1 also forming long tubular structures (Luft et al., 2020). For non-ionic R1, the aggregation number for the micelles did not go above about n = 40, with this limited by a lack of H-bonding and a restricted size for the hydrophobic core due to the relatively small C10 alkyl chains. When a charge is present on the anionic R1, larger micelles can form due to H-bonding altering the packing of the molecules. Simulations of R2 di-rhamnolipids support the experimental evidence that they form smaller micelles (around n = 22) because of the presence of a second rhamnose group, although increasing the length of the akyl chain allows for larger micelle aggregation numbers. For di-rhamnolipids, simulation (dissipative particle dynamics, DPD) supports the formation of more complex phases at high biosurfactant concentration (Xu et al., 2018). Three multilayer structures of micelles were observed at pH < 4 depending on the concentration. At concentrations below 10% wt of diRLs, bi-layer spherical micelles formed, with their diameter increasing with increased concentration. Further increase in concentration to 15–20 wt% resulted in the formation of bi-layered rod-like micelles, which changed into net-like bi-layered lamellar phases at 25% wt. A double bi-layer was obtained when the concentration reached 40 wt% (Xu et al., 2018). At pH above 7.4, novel anisotropic morphologies were discovered. Starting from 5 to 10%, patchy spherical micelles were observed. At 11%, rod-like micelles with a helical pattern formed, and at 15% a net-like lamellar phase. Finally, the formation of vesicles was observed at concentration reaching 40 wt% (Xu et al., 2018).

This research shows that RLs have the potential to be used in preparation of advanced functional systems such as anisotropic nanomaterials, which can be applied in biomaterials, drug delivery systems, microelectronics, optoelectronics, sensors or tissue engineering (Xu et al., 2018, Xu et al., 2020).

3.1.3 Physicochemical Characterisation and Functionality

If rhamnolipids are to replace conventional surfactants in industry, their physicochemical and functional properties need to be comparable to those they replace. Pekdemir et al. (2005) studied the emulsifying ability of rhamnolipids compared to other biological surfactants (tannins, saponins, lecithin). Rhamnolipids, like all other surfactants tested, produced oil-in-water emulsions that were unstable and separated within 2 min. Rhamnolipid showed the best emulsifying properties in both distilled water and seawater. Lovaglio et al. (2011) have looked at the pH dependence of rhamnolipid emulsification. They confirm the emulsifying ability of rhamnolipids and show that the optimum properties are at basic pH, and that under these conditions rhamnolipids have as good an emulsifying ability and stability as the common anionic surfactant sodium dodecyl sulphate. Bai and McClements (2016) have noted that rhamnolipids can be used to form very fine (<0.15 μm) oil droplets with medium chain triglyceride oils and also with longer chain corn and fish oils at low surfactant to oil ratios (<1:10). Furthermore, the emulsions were stable over a wide range of pH (5–9), salt content (up to 0.1 M NaCl) and temperature (up to 90°C). Instability was observed under highly acidic conditions (pH 2–4) and high ionic strength (NaCl 0.2–0.5 M). This was explained in terms of the decrease in electrostatic repulsion between droplets at low pH (loss of charge) and at high salt (charge screening effects). Özdemir et al. (2004) have also observed that a reduced charge repulsion at low pH leads to more compact interfacial adsorbed layers of rhamnolipids, and alters the CMC, which will also change the adsorption properties. A similar effect is seen with salts (Helvaci et al., 2004) where increasing NaCl concentration up to 0.5 M leads to more dense packing of rhamnolipids at the air-water interface. Rhamnolipids are also able to emulsify vegetable oils more efficiently than hydrocarbons (Janek et al., 2013), and can form emulsions with essential oils, thus offering a way to deliver the bioactive properties of plant extracts (Haba et al., 2014). Russell et al. (2021), have looked at the combined emulsifying

ability of rhamnolipids with egg white protein (EWP). They noted that increasing the RL concentration in an emulsion homogenised at constant EWP content led to a large decrease in emulsion droplet size. In contrast, when lecithin or monoglyceride was substituted for the RL, these surfactants had little effect on droplet size. This suggests that RL interacts with protein at the interface in a different way to lecithin and monoglyceride.

Rhamnolipid adsorption at the air-water interface and the relationship to foaming properties has also been studied. Khoshdast et al. (2012) compared the ability of rhamnolipid to other common foaming agents to form froth in froth flotation separation of minerals in mining operations. The rhamnolipid outperformed all tested frothers, which was explained by its greater ability to lower surface tension and the higher interfacial elasticity due to strong inter-rhamnolipid interactions in the adsorbed film. The high surface elasticity of the rhamnolipid, however, limits foaming ability under certain conditions. During foaming through air sparging rhamnolipids only form foams between certain limiting air flow rates (Özdemir et al., 2004). Below the lower flow rate limit, foam cannot form because the high surface elasticity of the monolayer rhamnolipid resists surface film expansion. Above the upper limit of airflow, the rigid surface film fractures because the applied stress is too high, and the foam collapses immediately. The same authors also looked at the foaming properties of the individual mono- and di-rhamnolipids R1 and R2. R1 is a better foaming agent than R2 and both show a pH dependence in foaming properties, with R1 more sensitive to pH. Özdemir et al. (2004) explain this as being due to a greater screening of the carboxyl group by the two sugar groups in R2.

Despite foam being a desired feature and determinant of the commercial value of many products (especially personal care ones), making RLs a perfect candidate for commercialization, it also can be a limiting factor in the process (Rieger 1996; Bator et al., 2020). Extensive foaming poses a real challenge in sustaining high product yields along with the low production costs (Sodagari et al., 2018). Chen et al. (2010) have carried out a detailed neutron reflectivity study of the adsorbed R1 and R2 conformations. Both R1 and R2 behave as classical surfactants with a Langmuir-type isotherm. The surface area occupied per molecule is 60 $Å^2$ for R1 and 75 $Å^2$ for R2, with the latter reflecting the greater size of the di-rhamnolipid head group. When mixtures of R1 and R2 adsorb to the air-water interface, the R2 molecules are not able to compete efficiently due to steric hindrance from the larger head group, and so a mixed interface is dominated by adsorbed R1.

Due to their physicochemical and functional characteristics, rhamnolipids have already been used in many branches of industry. A lot of research has been devoted to rhamnolipid influence on the biodegradation of petroleum hydrocarbons (Nitschke et al., 2011; Kaczorek et al., 2013). This surfactant-enhanced process was extensively studied in the 90's, due to the discovery of the ability of *Pseudomonas aeruginosa* to assimilate both aromatic (including PAH–polycyclic aromatic hydrocarbons) and aliphatic hydrocarbons. Zhang and Miller reported the rhamnolipid enhanced dispersion and biodegradation of octadecane (Zhang and Miller 1992, Zhang and Miller 1994), while Deziel et al. (1996) and Arino et al. (1998) reported the growth of *P. aeruginosa* on PAH showing also the involvement of rhamnolipids in the biodegradation of those compounds. Interestingly, the use of rhamnolipids in bioremediation strategies is still investigated and due to the large amounts of reports in this topic, only a few crucial papers are mentioned.

The latest research by Fernández-Peña et al. (2020) presented the impact of four rhamnolipids (mono-RL (C10), mono-RL (C14), di-RL (C10) and di-RL (C14)) on the adsorption of hair-conditioning polymers on damaged hair in order to verify whether glycolipids such as RLs could be a good replacement for chemically derived, commercial surfactants such as SLES. The study showed that RLs increased a degree of surface coverage of surfactant-polymer composition thus enhancing the deposition and hydration efficacy on damaged hair, especially with regards to mono-RL (C10) (Fernández-Peña et al., 2020). The positive outcomes of this research suggest that rhamnolipids of short alkyl chains could be used in hair cosmetics as a replacement for SLES.

Other commercial application of rhamnolipids is in pharmaceuticals, personal care, household cleaning, petroleum recovery, pesticides and biofungicides (Sajna et al., 2015). One area that has received attention is in the synthesis of therapeutic nanoparticles, and in particular gold and silver nanoparticles (Kumar et al., 2010; Bharali et al., 2013; Saikia et al., 2013; Kumar and Das 2018; Bayee et al., 2020). Gold nanoparticles find application in the biomedical field as delivery systems for therapeutic agents, and as sensor systems in diagnostic (typically lateral flow) tests (Nejati et al., 2021). Chemical synthesis of nanoparticles requires reduction of gold (Au^{3+} or Au^{+}) or silver (Ag^{+}) to the ground state metal by reduction (Iravani et al., 2014; Daruich De Souza et al., 2019). A common reaction is the reduction of $HAuCl_4$ using the powerful reducing agent sodium borohydride. To stabilize the nanoparticles and to prevent aggregation, capping agents are added to the reaction mixture which are often surfactants. Synthetic surfactants such as cetyltrimethylammonium bromide adsorb to the nanoparticle surface and stabilize them though charge repulsion. Finding new, green synthesis methods has become a priority as many of the reducing agents and surfactants used are toxic, which presents problems when used for biomedical applications. Green synthesis methods where a single molecule can act as both reducing and capping agents are desirable. Rhamnolipids have been shown to be an effective stabilizing agent for nanoparticles but still require a reducing agent, thus only giving a partial green solution.

3.2 Sophorolipids

Sophorolipids (SLs) (**Figure 1**), first identified in the 1960's (Gorin et al., 1961), are a glycolipid with a sophorose polar group (two glucose rings linked *via* a β1-2 glycosidic bond) and a hydroxylated fatty acid lipid tail (C18 for those produced by *S. bombicola*). A number of modified sophorolipids including branched sophorolipids (Tulloch et al., 1968; Baccile et al., 2017b); acetylated sophorolipids (Baccile et al., 2017a); bolaform sophorolipids and sophorosides (Van Renterghem

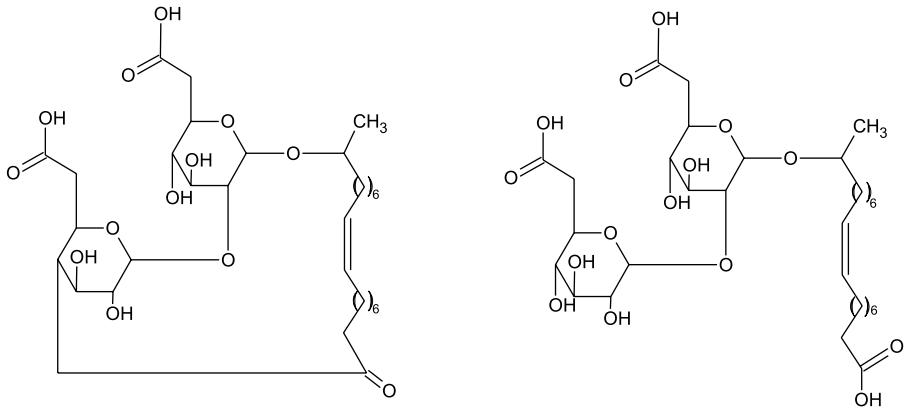

FIGURE 1 | Structure of di-acetylated lactonic and acidic sophorolipids (Hardin et al., 2007; Jezierska et al., 2018).

et al., 2018); petroselinic sophorolipids (Delbeke et al., 2016a) and chemically modified sophorolipids (Cuvier et al., 2014; Baccile et al., 2016, Baccile et al., 2019; Delbeke et al., 2016b, Delbeke et al., 2018, Delbeke et al., 2019) have been produced and studied, and will also be discussed here.

3.2.1 Structure and Production

Lactonic and acidic (**Figure 1**) are the two general forms of sophorolipid, secreted by non-pathogenic yeasts such as *Candida, Starmerella* and *Pseudohyphozyma* (Jezierska et al., 2018). These general structures are further differentiated by differing degrees of acetylation. The non-pathogenic nature of the producing organisms is advantageous for food and cosmetic application (Jezierska et al., 2018). Like the rhamnolipids, mixtures of sophorolipid congeners are produced (up to 20), but only a small number are found in significant quantities (Claus and Van Bogaert 2017).

The optimised conditions for production of sophorolipids depend on the selected strain, with some factors common to all. The suggested growth temperature of *Starmerella (Candida) bombicola* ATCC 2214 (the most commonly used strain to produce sophorolipids) is 28.8°C and pH of 3.5 in the bioreactor (Van Bogaert et al., 2007). Since yeasts are very susceptible to any oxygen limitations, especially during the exponential growth phase, a constant oxygen supply must be provided throughout the entire fermentation process (Van Bogaert et al., 2007). Interestingly, the carbon source used in the fermentation is usually a mixture of hydrophilic and hydrophobic compounds, where glucose or glycerol are commonly used as hydrophilic matter. The selection of a hydrophobic carbon source, however, is a more complicated decision, since it can enhance the production of particular type of sophorolipids over the other types. For example, the use of long-chain aliphatic hydrocarbons such as hexadecane, heptadecane or octadecane, can result in the excess formation of diacetylated lactone-based SLs, while fatty acid esters in the growth medium lead to formation of free-acid open-chain SLs (Ashby et al., 2006; Jezierska et al., 2018). The selectivity of *S. bombicola* for incorporating C18 fatty acids into sophorolipids can be exploited to produce new sophorolipids such as a petroselinic acid diacetyl sophorolipid lactone (Delbeke et al., 2016a), where the organism is grown on petroselinic acid, a positional isomer of oleic acid where the *cis* double bond is at C6 rather than the C9 in oleic acid.

In addition to the predominant C18 form of sophorolipid produced by *S. bombicola*, it is possible to promote synthesis of C16 containing sophorolipid by the organism. Geys et al. (2018) point out that the biosynthetic pathway for sophorolipid biosynthesis has a high specificity to C18 fatty acid substrate, explaining the preference for this chain length in the biosurfactant. They were able to produce C16 sophorolipids through heterologous expression of the cytochrome P450 cyp1 (1st enzyme in the sophorolipid biosynthesis pathway) gene of *Ustilago maydis,* which introduces a higher specificity to C16 fatty acids. Feeding this modified organism with palmitic acid gives rise to C16 sophorolipid production.

Branched sophorolipids have been known for several decade (Tulloch et al., 1968), and revisited recently (Baccile et al., 2017b). These are sophorolipds with a C22 behenthic acid chain with the glycosidic bond at C13 creating two branches to the lipid chain.

Genetic modification of *S. bombicola* also offers the possibility of producing novel bolaform sophorolipid derivatives, first identified at low concentration in the wild type yeast by Price et al. (2012). Bogaert et al. (2016) have described the production of bolaform sophorolipids by an engineered *S. bombicola* with the lactone esterase gene knocked-out. Bolaform surfactants have a hydrophobic moiety with hydrophilic polar groups at each end. For sophorolipids these can be composed of either a fatty acid chain with sophorose sugar moiety on each end (a symmetrical bolaform sophoroside) or one sophorose and one carboxylic acid group at the ends (a non-symmetrical bolaform sophorolipid) (Van Renterghem et al., 2018). Delbeke et al. (2018) have extended the range of bolaform sophorolipids and sophorosides through chemical modification of diacteylated lactonic sophorolipid. This allowed them to synthesise symmetrical and non-symmetrical sophorolipids and

sophorosides with longer hydrophobic linker segments and fully acetylated hydroxyl groups (peracetylated sophorolipds). Other green chemistry synthetic routes have also proven fertile ground for synthetic modification of microbially produced sophorolipids. Simple hydrogenation of the *cis* double bond of oleic sophorolipids can form the unsaturated elaidic acid derivative (Cuvier et al., 2014) leading to associated changes in self association properties. A wide range of various amino derivatives (quaternary ammonium and amine oxide derivatives) have been synthesised starting from both oleic and petroselinic sophorolipids and their biological and self-assembly properties determined (Delbeke et al., 2015, Delbeke et al., 2019; Baccile et al., 2019).

3.2.2 Phase Behaviour

In common with other biosurfactants, the sophorolipids display a rich phase behaviour in solution and this aspect of their functionality has been widely studied (Zhou et al., 2004; Penfold et al., 2011; Baccile et al., 2012, Baccile et al., 2016; Dhasaiyan et al., 2013; Cuvier et al., 2014; Manet et al., 2015). At low concentrations, sophorolipids form micelles and vesicles depending on the concentration and congener type (Baccile et al., 2012, Baccile et al., 2016; Manet et al., 2015). Penfold et al. (2011) employed small angle neutron scattering (SANS) to study phase behaviour of lactonic and acidic sophorolipid at concentrations above the CMC but below 30 mM due to the low solubility of the lactonic form. Acidic sophorolipid forms small micelles in this concentration range coexisting with a low concentration of lamellar aggregates or vesicles, whilst lactonic sophorolipids form small unilamellar vesicles at concentrations up to 3 mM, large vesicles up to 7 mM and above that tubules in the range 1–30 mM. Manet et al. (2015) have looked at the structure of acidic sophorolipid in detail using scattering (SAXS and SANS) and molecular dynamics simulations. They found that sophorolipids form prolate ellipsoids at pH < 5, where they are uncharged, with an unusual core-shell type micelle structure, where there is an uneven shell (hydrophilic group) thickness, with a very thin "shell" at the ends of the long axis of the spheroid. Baccile et al. (2016) found a complex phase behaviour of sophorolipids as a function of the degree of carboxyl group ionization/pH and position. At basic pH, both sophorolipids with an oleic or stearic acid chain form small vesicles (Baccile et al., 2016). At acid pH, however, whist the oleic congener again forms micelles, the stearic congener forms a twisted ribbon type structure.

3.2.3 Physicochemical Characterisation and Functionality

The surface and interfacial properties of SLs depend in part on their form, lactonic or acidic, and degree of acetylation. Sophorolipids have a relatively low CMC, similar to rhamnolipids, but their ability to lower the surface tension is less than for rhamnolipids, with a limiting surface tension around 35–40 mN/m (Van Bogaert et al., 2007) compared to 25 mN/m for rhamnolipids (Nitschke et al., 2005). Lactonic sophorolipids have a higher surface activity than the acidic form, and di-acetyl more than the mono-acetyl form, whilst the acid form is a better foamer (Van Bogaert et al., 2007). Sophorolipids have low foaming ability compared to rhamnolipids (Hirata et al., 2009) and this combined with their high surface activity makes them useful as detergents in cleaning applications for washing machines and dishwashers where foaming is disadvantageous (Hall et al., 1995; Furuta et al., 2004). Zhang et al. (2004) made various alkyl esters of sophorolipids by esterification of the fatty acid chain of sophorolipids with sodium alkoxides of varying chain length (methyl, ethyl, propyl and butyl) to modify the hydrophile-lipophile balance (HLB) in the molecules. An inverse relationship between the CMC and limiting surface tension was found, with the CMC reducing by half for each carbon added. This offers the opportunity to tune the surface properties of sophorolipids through chemical modification.

The potential of sophorolipids as additives in foods and cosmetics and the petroleum industry is evidenced by their emulsifying activity with hydrocarbon and triglyceride oils. Mixed lactonic and acidic and, especially, esterified sophorolipids are better emulsifiers of pure hydrocarbon oils and Arabian light crude than the non-ionic surfactant Triton-X (Koh et al., 2017). A similar set of studies highlighted the ability of sophorolipids alkyl esters to stabilise emulsions of lemon, almond and paraffin oil (Koh et al., 2016; Koh and Gross 2016). In these studies, the sophorolipid esters had a comparable interfacial tension lowering ability to a mixed lactonic and acetylated sophorolipid system at high concentration (1 mg/ml) for all oils, but noticeably they were able to maintain this surface activity to much lower concentrations. The various sophorolipid forms were able to emulsify each of the oils to varying degrees. The ethyl ester was the best emulsifier for paraffin oil, followed by the hexyl and then decyl (i.e., decreasing emulsifying ability with increasing alkyl chain length) whilst for the almond and lemon oil emulsions this order was reversed (decyl was the best emulsifier). However, even though the ethyl ester was the poorer emulsifier for lemon oil, the emulsions showed no separation after 1-week storage, unlike those made from the hexyl and decyl esters. Normally, smaller emulsion droplets would be associated with more stable emulsions, but in this case, it was found that the larger ethyl ester emulsions were more stable, which the authors attributed to extensive depletion flocculation in the longer chain ester emulsions due to formation of micelles from non-adsorbed surfactant in the continuous phase of the emulsion. For paraffin oil and almond oil emulsions made with the sophorolipid esters, precipitation was observed at higher surfactant concentrations due to the relatively low solubility of these molecules. A notable finding from these studies was that mixtures of lactonic and acetylated sophorolipid were poor emulsifiers in all oil systems compared to the esterified sophorolipids.

The chemical structure of SLs does not only influence the functional properties of the surfactant but also affects its biological activity (**Table 1**). Ma et al. (2012) studied the surface chemistry and bioactivity of lactonic and acidic SLs with different numbers of acetyl substitution, and chain length and double bond numbers of the acyl chain. They concluded that acidic SLs generally exhibited lower CMC than lactonic SLs.

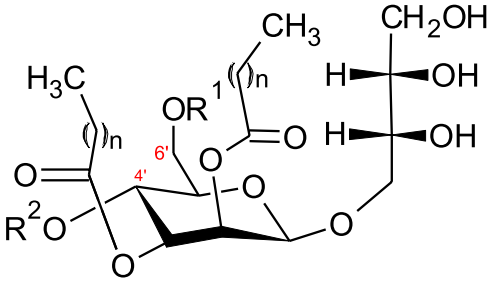

FIGURE 2 | Structure of mannosylerythritol lipids (n = 6–10) (Konishi et al., 2007a; Yu et al., 2015). MEL-A–R^1 = CH_3CO, R^2 = CH_3CO. MEL-B–R^1 = CH_3CO, R^2 = H. MEL-C–R^1 = H, R^2 = CH_3CO MEL-D–R^1 = H, R^2 = H.

Moreover, lactonic SLs showed higher cytotoxic activity against Chang liver cells (Ma et al., 2012). Similar studies conducted by Shao et al. (2012) suggest that acidic SLs showed hardly any cytotoxic activity, while lactonic SLs demonstrated significant inhibitory effect on two esophageal cancer cell lines and with the effect depending on the unsaturation degree of the hydroxyl fatty acid of SLs, where the strongest cytotoxic effect was observed for one double-bond in the fatty acid moiety.

Like rhamnolipids, sophorolipids have also been investigated for use in the green synthesis of therapeutic nanoparticles (Singh et al., 2009; Shikha et al., 2020). However, unlike rhamnolipids they are able to act both as a stabilizing and reducing agent, with the reducing ability only displayed at alkaline pH (Singh et al., 2009) suggesting a critical role for the carboxyl group in acidic sophorolipids. Thus, sophorolipids offer a cleaner option for the synthesis, negating the need for toxic reducing and capping agents.

3.3 Mannosylerythritol Lipids

A further class of glycolipids are mannosylerythritol lipids (MEL A, -B, -C and -D), composed of a polar 4-O-β-d-mannopyranosyl-meso-erythritol attached to a non-polar fatty acid chain (**Figure 2**).

The hydrophilic group can be either acetylated with a short (C_2-C_8) or medium (C_{10}-C_{18}) chain fatty acid (Jezierska et al., 2018). Four main classes of MELs are defined according to the acetylation degree at $C_{4'}$ and $C_{6'}$ (**Figure 2**)–MEL-A (diacetylated), MEL-B and MEL-C (monoacetylated) or MEL-D (non-acetylated) (Yu et al., 2015; Jezierska et al., 2018).

Yeasts, mainly of the genus *Pseudozyma* (previously *Candida*) produce MELs and their structure has been proven to be strain-dependent (Jezierska et al., 2018). Fukuoka et al. (2007) concluded that the same or very similar MELs are produced by strains closely related in the phylogenetic tree. These observations were supported by Konishi et al. (2007b), who screened 13 strains for the production of MELs. A taxonomic study together with the analyses of the MELs post-fermentation allowed the authors to classify the strains into three main groups. The first group consisted of 11 strains producing all three of MEL-A, -B and -C with the most abundant fraction being MEL-A. These strains were taxonomically closely related to each other and to *Pseudozyma antarctica* and *Pseudozyma aphidis* strains, which had already been previously identified as MEL-A dominant producers (Kitamoto et al., 2001; Rau et al., 2005). The second group with only one strain produced mainly MEL-B and was related to *Pseudozyma tsukubaensis*, known as a MEL-B exclusively producing strain (Fukuoka et al., 2008; de Andrade et al., 2017). The last group, also containing only one strain related to *Pseudozyma hubeiensis* and produced predominantly MEL-C (Konishi et al., 2011).

The main substrates for MEL-producing strains are vegetable oils, giving yields of 100 g/L and higher. However, the ability of *Pseudozyma* strains to metabolize alkanes to produce MELs was also noted (Kitamoto et al., 2001; Morita et al., 2008). A very common carbon source used for fermentations is soybean oil, but often the culture medium is also enriched with small amounts of yeast extract. Factors affecting the production of MELs can be divided into four main categories 1) the effect of yeast extract, 2) nitrogen source and its concentration, 3) carbon source and its concentrations, and 4) the effect of hydrophilic precursors (such as mannose or erythritol) (Kitamoto et al., 1990; Rau et al., 2005; Konishi et al., 2008).

The physicochemical and functional characteristics of MELs depends on their structures, for example, MEL-C, which is monoacetylated would be expected to present different functionality when compared to diacetylated MEL-A. Interestingly, when the emulsification activity of MEL-C was tested, the results were as high as those of MEL-A and higher than commercial surfactants Tween80 and SDS (Konishi et al., 2008). The CMC of MEL-C was found to be 6.0×10^{-6} M when reducing the surface tension (ST) to 25.1mN/m, which was higher than CMC of MEL-A at 2.7×10^{-6} M (ST = 28.4 mN/m) and MEL-B at 4.5×10^{-6} M (ST = 28.2 mN/m) (Kitamoto et al., 1993; Konishi et al., 2008).

The phase behaviour of glycolipid surfactants is very complex and controlled by the acyl chain type and number, and sugar head group type and stereochemistry (Kitamoto et al., 2009). At low concentrations, MELs form micelles and vesicles of varied shape (spherical, disc and rod) (Söderman and Johansson 1999), and liquid crystalline lamellar phases at higher concentrations (Imura et al., 2007). At concentrations just above the CMC, both MEL-A and MEL-B self-associate into large unilamellar vesicles (LUV) (Imura et al., 2006). At a higher concentration, associated with a second CMC, MEL-A forms a range of liquid crystalline phases depending on temperature and concentration including sponge (L_3), bicontinuous cubic (V_2), and lamella (L_R) phases (Imura et al., 2007). MEL-B, on the other hand, only exhibits one CMC above which LUVs form, with a gradual transition to multilamellar vesicles as the surfactant concentration increases (Imura et al., 2006). Konishi et al. (2008) reported that the MEL-C isolated from *Pseudozyma* KM-59 was able to self-assemble into the lyotropic liquid crystalline phases–myelines and lamella ($L\alpha$).

In general, the formation of the lyotropic liquid crystalline phases is a favourable phenomenon of surfactants due to their

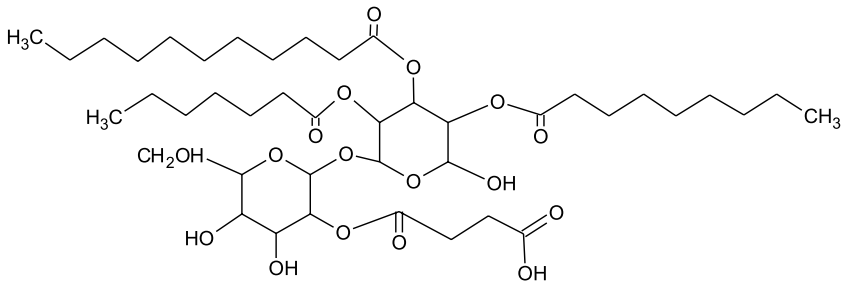

FIGURE 3 | Chemical structure of trehalolipid from *Rhodococcus* sp. (Ortiz et al., 2008).

potential applications as nanoparticles in drug delivery systems (Li et al., 2005; Imura et al., 2007).

3.4 Trehalolipids

The structure of trehalolipids (TLs) is also based on a hydrophilic sugar moiety and hydrophobic fatty acid-based tail. However, there is large diversity in the fatty acid tail, being either aliphatic fatty acids or hydroxylated fatty acids with branched-chain types (α-branched-β-hydroxy fatty acids) and of assorted chain lengths (Shao 2011). The chemical structure of TLs is strongly dependent on the producing microorganisms with differences even within the same species (**Figure 3**) (Mnif and Dhouha 2015a). The most studied trehalolipids producers are *Rhodococcus* species along with other Gram-positive species such as *Mycobacterium*, *Nocardia, Micrococcus, Gordonia, Arthrobacter* and *Corynebacterium* (Van Hamme and Ward 2001; Ortiz et al., 2008; Shao 2011).

The amount and type of trehalose lipids produced by microorganisms also depends on the carbon source used for the microbial growth. Hvidsten et al. (2017) reported a Gram-positive bacterium belonging to the genus *Dietizia–Dietzia* sp. A14101 was able to utilise various hydrocarbons that directly correlated to the variety and amounts of produced trehalolipids. This clearly suggests that physicochemical characterisation of trehalolipids cannot be generalised as it depends on many factors. Marqués et al. (2009) reported functional and physicochemical characteristics of trehalolipids from *Rhodococcus erythropolis* 51T7 isolated from crude oil-contaminated soil and grown on tetradecane (2% v/v). After 72 h of cultivation, trehalolipids were extracted as a mixture of at least six components–one major and 5 minor congeners. A multi-component trehalolipid mix was also observed by Singer and Finnety (Singer and Finnerty 1990) when they grew *Rhodococcus* strain on hexadecane, resulting in a mixture of 11 components with one major and 10 minor congeners.

The CMC and surface tension reducing ability of trehalolipids are controlled by many factors. Tuleva et al. (2009) characterised the trehalose lipids extracted from the bacterium *Micrococcus luteus* BN56 grown on hexadecane, and found a CMC of 25 mg/L. The authors also detected the formation of strong emulsions even in the early stages of the cultivation of the microorganism. On the other hand, White et al. (2013) observed a CMC of 250 mg/L for trehalose lipids extracted from *Rhodococcus* sp., strain PML026. These trehalose lipids were able to make emulsions of high stability over a wide range of pH (from pH 2 to pH 10) with the highest emulsification index (EI_{24}) at pH 8. The emulsifying ability (EI_{24}) was independent of temperature over the range from 20 to 100°C. Similarly, Marqués et al. (2009) found a CMC of trehalolipids from *Rhodococcus erythropolis* 51T7 of 37 mg/L. The authors also presented an interesting characterisation of emulsions formed in oil-trehalolipid-water (O–TL–W) systems, where isopropyl myristate was used as the oil phase. The emulsion, which was kept at room temperature for 3 months proved to be thick, stable and the microscopic evaluation showed the emulsion particles reaching the size of 5 μm, which according to Rosen and Kunjappu (Rosen and Kunjappu 2012), classifies it as a macroemulsion. Trehalose lipid-water phase behaviour was studied as a function of temperature by polarizing microscopy. Lamellar liquid-crystalline phases were detected at low concentrations and temperature, and hexagonal phases when higher concentrations and temperature (70°C and higher) were applied. These findings indicate that there is a phase inversion from anisotropic phase of the glycolipid due to the presence of the liquid crystals (Marqués et al., 2009). These observations seem to explain the stability of the emulsions described by the authors.

In all studies discussed above, the trehalolipids showed a high propensity for surface and interfacial tension reduction. Theses promising findings suggest that trehalolipids have many characteristics that are desirable in industrial applications, but the dependence of trehalose producing organisms on long chain aliphatic carbon sources, low production yields and high costs of downstream separations are limiting factors to the scale-up of their production.

Most strains producing trehalose lipids were isolated from oil-polluted sites and were very good at degrading polluting hydrocarbon. The glycolipids produced by these oil degrading bacteria improved the bioavailability of the hydrocarbon molecules by their micellization and therefore positively affected the biodegradation. For this reason, microbially enhanced oil recovery, oil-spill bioremediation and cleaning of oil storage tanks have been the main applications of trehalolipids to date (Franzetti et al., 2010). However, their reported interaction with cell membranes,

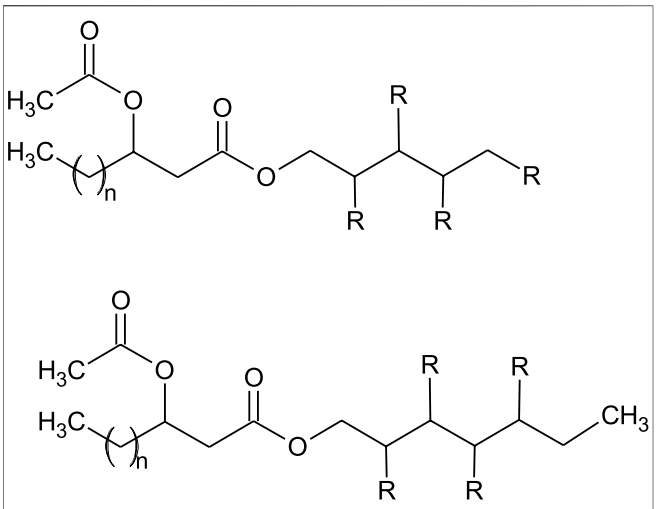

FIGURE 4 | General structure of PEFA (Garay et al., 2018). Where: R = OH or acetyl *n* = 8, 10, 12, 14, 16.

inhibition of human leukaemia cell lines, anti-fungal and anti-viral properties, and the ability to inhibit protein kinase C (PKC) activity, common in anti-tumour therapeutics, highlight their potential in medicine (Janek et al., 2018; Hirano et al., 2021).

3.5 Cellobiose Lipids

Cellobiose lipids have been known since the 1950's (Haskins 1950; Lemieux et al., 1951) and were originally named ustilagic acid after the organism (the corn smut fungus *Ustilago maydis*) that was first observed to produce these. Since then, cellobiose lipids production has been identified in other fungal species (Kulakovskaya et al., 2006, Kulakovskaya et al., 2007; Golubev et al., 2008; Teichmann et al., 2011). This class of biosurfactants comprise a cellobiose (two glucose linked β1-4) hydrophilic headgroup with differing acetylation patterns, usually attached to a hydroxypalmitic acid hydrophobic moiety (Eveleigh et al., 1964). Various other congeners have been identified including di and tri-hydroxyhexadecanoic acid chains, dehydroxy congeners, additional acetyl groups and octanoic acid replacing the palmitic acid in the hydroxylated lipid chains (Spoeckner et al., 1999; Teichmann et al., 2007, Kulakovskaya et al., 2011). Bolaform cellobiose lipids have also been observed as fermentation products with some organisms (Puchkov et al., 2002; Morita et al., 2011).

3.6 Polyol Lipids

Polyol lipids (PLs) belong to the class of extracellular fungal glycolipid biosurfactants (EFGB), however, structurally they are different from sophorolipids and mannosylerythritol lipids by not having a sugar component as the hydrophilic moiety but instead have a polyol as a polar group. Only two types of PLs have been found to date, polyol esters of fatty acids (PEFA) and liamocins (Garay et al., 2018).

3.6.1 Polyol Esters of Fatty Acids

Polyol esters of fatty acids (PEFA) are produced mainly by the yeasts of the genus *Rhodotorula* (Garay et al., 2018). As for the other microorganism-produced surfactants, the structure and yields of the produced PEFAs can significantly vary depending on the secreting strain.

Nineteen PEFAs have been identified to date, allowing a general summary of the structures to be defined (Cajka et al., 2016; Garay et al., 2017; Garay et al., 2018). Briefly, the molecules consist of a polyol head group (usually D-mannitol or D-arabitol but other polyols are also possible) esterified to an acetylated (R)-3-hydroxyacyl fatty acid via the carboxyl end (Cajka et al., 2016; Garay et al., 2017; Garay et al., 2018). **Figure 4** presents the general structure of the PEFAs with several possible variations.

The optimal conditions for PEFA production are: temperature between 24 and 27°C, pH = 6.3–6.5, and a medium known as Medium A (Garay et al., 2017; Garay et al., 2018). The carbon source most commonly used is glucose, however, glycerol, sucrose, molasses and plant-based hydrolysates can also be used (Garay et al., 2017; Garay et al., 2018).

Based on structural and physicochemical studies, PEFA seem to have potential as biosurfactants. Lyman et al. (2018) report that *Rhodotorula taiwanensis* MD1149 produces the hypoacetylated PEFA (0–4 acetylation modifications) with increased surface-active properties–mainly ST reduction to approximately 32 mN/m (Lyman et al., 2018). The isolates of *R. aff. paludigena* UCDFST 81–84 and *R. babjevae* UCDFST 04–877 were observed to reduce the ST down to 33.3 and 30.4 mN/m respectively and additionally, *R. aff. paludigena* UCDFST 81–84 isolate showed antifoam activity, which is a promising feature for the industrial application of this substance (Garay et al., 2018).

3.6.2 Liamocins

Liamocins are polyol lipids produced by various strains of Aureobasidium pullulans. The term "liamocins" was introduced by Price et al. (2013), despite the molecules being known from 1964 (Garay et al., 2018).

Structural studies have shown liamocins have a single, partially O-actetylated polyol polar group, and three or four 3,5-dihydroxy-decanoic ester group polyester tails (three in liamocin A1 and A2 and four in liamocin B1 and B2) (Price et al., 2013, Price et al., 2017).

The selection of strain and culture conditions can lead to the formation of many diverse structures of liamocins, as observed by Leathers et al. (2015). Price et al. (2017) reported a variety of different head groups of liamocins (D-galactitol, D-sorbitol, D- and L-arabitol, D-xylitol, L-threitol and glycerol), when varied polyols were used in the growth media. Interestingly, no such dependence was shown when different sugars were used in the culture medium.

In recent years liamocins were reported to exhibit antibacterial activity as well as being inhibitors of some cancer cell lines (Manitchotpisit et al., 2014; Leathers et al., 2016).

Little is still known about the physicochemical properties of liamocins and their possible application in the industry. Liamocins isolated from Aureobasidium pullulans CU 43 were reported to be fluorescent and able to reduce the ST to 27 mN/m

(Manitchotpisit et al., 2011). Kim et al. (2015) reported a glycerol-based liamocin (glycerol-liamocin) from Aureobasidium pullulans L3-GPY, which decreased the ST to 31.5 mN/m at the concentration of 1.5 mg/L.

The abovementioned findings suggest that liamocins have the potential of being used as biosurfactants, but a further, detailed investigation of their functionality is needed.

4 CONCLUSION

Glycolipids are a class of biosurfactants of high potential, not only in bioremediation and clean-up strategies, or as household-care agents, but also as very good materials for food and medical applications. Most importantly, they are all of natural origin and can mostly be produced using particular organic-wastes (waste glycerol as an example). What is more, the optimised conditions for the production of glycolipids are easy to obtain and the costs of the production may be lower when compared to the chemically-derived surfactants.

AUTHOR CONTRIBUTIONS

KS and SRE contributed in conception, design, and writing the manuscript. TJ reviewed the literature and organized the structure of the manuscript. All authors approved the final version for submission.

FUNDING

SRE acknowledges funding from European Union's Horizon 2020 research and innovation programme under grant agreement No. 635340 as part of the MARISURF project (www.marisurf.eu). The publication reflects only the author's views, and the Commission is not responsible for any use that may be made of information it contains. TJ gratefully acknowledge the financial support from the National Science Centre, Poland, project 2020/37/B/NZ9/01519. The Article Processing Charge (APC) was co-financed by Wroclaw University of Environmental and Life Sciences.

REFERENCES

Abalos, A., Pinazo, A., Infante, M. R., Casals, M., García, F., and Manresa, A. (2001). Physicochemical and Antimicrobial Properties of New Rhamnolipids Produced by *Pseudomonas aeruginosa* AT10 from Soybean Oil Refinery Wastes. *Langmuir* 17, 1367–1371. doi:10.1021/la0011735

Abdel-Mawgoud, A. M., Lépine, F., and Déziel, E. (2010). Rhamnolipids: Diversity of Structures, Microbial Origins and Roles. *Appl. Microbiol. Biotechnol.* 86, 1323–1336. doi:10.1007/s00253-010-2498-2

Abouseoud, M., Yataghene, A., Amrane, A., and Maachi, R. (2008). Biosurfactant Production by Free and Alginate Entrapped Cells of Pseudomonas Fluorescens. *J. Ind. Microbiol. Biotechnol.* 35, 1303–1308. doi:10.1007/s10295-008-0411-0

Andrä, J., Rademann, J., Howe, J., Koch, M. H. J., Heine, H., Zähringer, U., et al. (2006). Endotoxin-like Properties of a Rhamnolipid Exotoxin from Burkholderia (Pseudomonas) Plantarii: Immune Cell Stimulation and Biophysical Characterization. *Biol. Chem.* 387, 301–310. doi:10.1515/BC.2006.040

Andrade, C. J. d., Andrade, L. M. d., Rocco, S. A., Sforça, M. L., Pastore, G. M., and Jauregi, P. (2017). A Novel Approach for the Production and Purification of Mannosylerythritol Lipids (MEL) by Pseudozyma Tsukubaensis Using Cassava Wastewater as Substrate. *Sep. Purif. Tech.* 180, 157–167. doi:10.1016/j.seppur.2017.02.045

Arino, S., Marchal, R., and Vandecasteele, J. P. (1998). Involvement of a Rhamnolipid-Producing Strain of *Pseudomonas aeruginosa* in the Degradation of Polycyclic Aromatic Hydrocarbons by a Bacterial Community. *J. Appl. Microbiol.* 84, 769–776. doi:10.1046/j.1365-2672.1998.00412.x

Ashby, R. D., McAloon, A. J., Solaiman, D. K. Y., Yee, W. C., and Reed, M. (2013). A Process Model for Approximating the Production Costs of the Fermentative Synthesis of Sophorolipids. *J. Surfact Deterg* 16, 683–691. doi:10.1007/s11743-013-1466-0

Ashby, R. D., Solaiman, D. K. Y., and Foglia, T. A. (2006). The Use of Fatty Acid Esters to Enhance Free Acid Sophorolipid Synthesis. *Biotechnol. Lett.* 28, 253–260. doi:10.1007/s10529-005-5527-y

Baccile, N., Babonneau, F., Banat, I. M., Ciesielska, K., Cuvier, A.-S., Devreese, B., et al. (2017a). Development of a Cradle-To-Grave Approach for Acetylated Acidic Sophorolipid Biosurfactants. *ACS Sust. Chem. Eng.* 5, 1186–1198. doi:10.1021/acssuschemeng.6b02570

Baccile, N., Babonneau, F., Jestin, J., Pehau-Arnaudet, G., and Van Bogaert, I. (2012). Unusual, pH-Induced, Self-Assembly of Sophorolipid Biosurfactants. *ACS Nano* 6, 4763–4776. doi:10.1021/nn204911k

Baccile, N., Cuvier, A.-S., Prévost, S., Stevens, C. V., Delbeke, E., Berton, J., et al. (2016). Self-Assembly Mechanism of pH-Responsive Glycolipids: Micelles, Fibers, Vesicles, and Bilayers. *Langmuir* 32, 10881–10894. doi:10.1021/acs.langmuir.6b02337

Baccile, N., Delbeke, E. I. P., Brennich, M., Seyrig, C., Everaert, J., Roelants, S. L. K. W., et al. (2019). Asymmetrical, Symmetrical, Divalent, and Y-Shaped (Bola) amphiphiles: The Relationship between the Molecular Structure and Self-Assembly in Amino Derivatives of Sophorolipid Biosurfactants. *J. Phys. Chem. B* 123, 3841–3858. doi:10.1021/acs.jpcb.9b01013

Baccile, N., Le Griel, P., Prévost, S., Everaert, B., Van Bogaert, I. N. A., Roelants, S., et al. (2017b). Glucosomes: Glycosylated Vesicle-In-Vesicle Aggregates in Water from pH-Responsive Microbial Glycolipid. *ChemistryOpen* 6, 526–533. doi:10.1002/open.201700101

Bae, I. H., Lee, E. S., Yoo, J. W., Lee, S. H., Ko, J. Y., Kim, Y. J., et al. (2018). Mannosylerythritol Lipids Inhibit Melanogenesis via Suppressing ERK-CREB-MiTF-tyrosinase Signalling in normal Human Melanocytes and a Three-dimensional Human Skin Equivalent. *Exp. Dermatol.* 28, 738–741. doi:10.1111/exd.13836

Bai, L., and McClements, D. J. (2016). Formation and Stabilization of Nanoemulsions Using Biosurfactants: Rhamnolipids. *J. Colloid Interf. Sci.* 479, 71–79. doi:10.1016/j.jcis.2016.06.047

Bakur, A., Niu, Y., Kuang, H., and Chen, Q. (2019). Synthesis of Gold Nanoparticles Derived from Mannosylerythritol Lipid and Evaluation of Their Bioactivities. *AMB Expr.* 9, 1. doi:10.1186/s13568-019-0785-6

Bator, I., Karmainski, T., Tiso, T., and Blank, L. M. (2020). Killing Two Birds with One Stone - Strain Engineering Facilitates the Development of a Unique Rhamnolipid Production Process. *Front. Bioeng. Biotechnol.* 8, 1. doi:10.3389/fbioe.2020.00899

Bayee, P., Amani, H., Najafpour, G. D., and Kariminezhad, H. (2020). Experimental Investigations on Behaviour of Rhamnolipid Biosurfactant as a green Stabilizer for the Biological Synthesis of Gold Nanoparticles. *Ije* 33, 1. doi:10.5829/ije.2020.33.06c.02

Bergström, S., Theorell, H., and Davide, H. (1946). Pyolipic Acid, a Metabolic Product of Pseudomonas Pyocyanea Active against *Mycobacterium tuberculosis*. *Arch. Biochem. Biophys.* 10, 165–166.

Bharali, P., Saikia, J. P., Paul, S., and Konwar, B. K. (2013). Colloidal Silver Nanoparticles/rhamnolipid (SNPRL) Composite as Novel Chemotactic Antibacterial Agent. *Int. J. Biol. Macromolecules* 61, 238–242. doi:10.1016/j.ijbiomac.2013.07.006

Bjerk, T. R., Severino, P., Jain, S., Marques, C., Silva, A. M., Pashirova, T., et al. (2021). Biosurfactants: Properties and Applications in Drug Delivery,

Biotechnology and Ecotoxicology. *Bioengineering* 8, 115. doi:10.3390/bioengineering8080115

Bodour, A. A., Guerrero-Barajas, C., Jiorle, B. V., Malcomson, M. E., Paull, A. K., Somogyi, A., et al. (2004). Structure and Characterization of Flavolipids, a Novel Class of Biosurfactants Produced by Flavobacterium Sp. Strain MTN11. *Appl. Environ. Microbiol.* 70, 114–120. doi:10.1128/AEM.70.1.114-120.2004

Borders, D. B., Leese, R. A., Jarolmen, H., Francis, N. D., Fantini, A. A., Falla, T., et al. (2007). Laspartomycin, an Acidic Lipopeptide Antibiotic with a Unique Peptide Core. *J. Nat. Prod.* 70, 443–446. doi:10.1021/np068056f

Caffrey, P., Lynch, S., Flood, E., Finnan, S., and Oliynyk, M. (2001). Amphotericin Biosynthesis in Streptomyces Nodosus: Deductions from Analysis of Polyketide Synthase and Late Genes. *Chem. Biol.* 8, 713–723. doi:10.1016/S1074-5521(01)00046-1

Cajka, T., Garay, L. A., Sitepu, I. R., Boundy-Mills, K. L., and Fiehn, O. (2016). Multiplatform Mass Spectrometry-Based Approach Identifies Extracellular Glycolipids of the Yeast Rhodotorula Babjevae UCDFST 04-877. *J. Nat. Prod.* 79, 2580–2589. doi:10.1021/acs.jnatprod.6b00497

Câmara, J. M. D. A., Sousa, M. A. S. B., Barros Neto, E. L., and Oliveira, M. C. A. (2019). Application of Rhamnolipid Biosurfactant Produced by *Pseudomonas aeruginosa* in Microbial-Enhanced Oil Recovery (MEOR). *J. Petrol. Explor Prod. Technol.* 9, 2333–2341. doi:10.1007/s13202-019-0633-x

Carrillo, C., Teruel, J. A., Aranda, F. J., and Ortiz, A. (2003). Molecular Mechanism of Membrane Permeabilization by the Peptide Antibiotic Surfactin. *Biochim. Biophys. Acta (Bba) - Biomembranes* 1611, 91–97. doi:10.1016/S0005-2736(03)00029-4

Celik, G. Y., Aslim, B., and Beyatli, Y. (2008). Enhanced Crude Oil Biodegradation and Rhamnolipid Production by Pseudomonas Stutzeri Strain G11 in the Presence of Tween-80 and Triton X-100. *J. Environ. Biol.* 29, 867–870.

Ceresa, C., Fracchia, L., Williams, M., Banat, I. M., and Díaz De Rienzo, M. A. (2020a). The Effect of Sophorolipids against Microbial Biofilms on Medical-Grade Silicone. *J. Biotechnol.* 309, 34–43. doi:10.1016/j.jbiotec.2019.12.019

Ceresa, C., Hutton, S., Lajarin-Cuesta, M., Heaton, R., Hargreaves, I., Fracchia, L., et al. (2020b). Production of Mannosylerythritol Lipids (MELs) to Be Used as Antimicrobial Agents against *S. aureus* ATCC 6538. *Curr. Microbiol.* 77, 1373–1380. doi:10.1007/s00284-020-01927-2

Champion, J. T., Gilkey, J. C., Lamparski, H., Retterer, J., and Miller, R. M. (1995). Electron Microscopy of Rhamnolipid (Biosurfactant) Morphology: Effects of pH, Cadmium, and Octadecane. *J. Colloid Interf. Sci.* 170, 569–574. doi:10.1006/jcis.1995.1136

Chen, M. L., Penfold, J., Thomas, R. K., Smyth, T. J. P., Perfumo, A., Marchant, R., et al. (2010). Solution Self-Assembly and Adsorption at the Air−Water Interface of the Monorhamnose and Dirhamnose Rhamnolipids and Their Mixtures. *Langmuir* 26, 18281–18292. doi:10.1021/la1031812

Chen, W.-C., Juang, R.-S., and Wei, Y.-H. (2015). Applications of a Lipopeptide Biosurfactant, Surfactin, Produced by Microorganisms. *Biochem. Eng. J.* 103, 158–169. doi:10.1016/j.bej.2015.07.009

Christova, N., Lang, S., Wray, V., Kaloyanov, K., Konstantinov, S., and Stoineva, I. (2015). Production, Structural Elucidation, and *In Vitro* Antitumor Activity of Trehalose Lipid Biosurfactant from Nocardia Farcinica Strain. *J. Microbiol. Biotechnol.* 25, 439–447. doi:10.4014/jmb.1406.06025

Claus, S., and Van Bogaert, I. N. A. (2017). Sophorolipid Production by Yeasts: a Critical Review of the Literature and Suggestions for Future Research. *Appl. Microbiol. Biotechnol.* 101, 7811–7821. doi:10.1007/s00253-017-8519-7

Compton, A. A., Deodhar, B. S., Fathi, A., and Pemberton, J. E. (2020). Optimization of a Chemical Synthesis for Single-Chain Rhamnolipids. *ACS Sust. Chem. Eng.* 8, 8918–8927. doi:10.1021/acssuschemeng.0c00733

Coss, C., Carrocci, T., Maier, R. M., Pemberton, J. E., and Polt, R. (2012). Minimally CompetentLewisAcid Catalysts: Indium(III) and Bismuth(III) Salts Produce Rhamnosides (=6-Deoxymannosides) in High Yield and Purity. *Hca* 95, 2652–2659. doi:10.1002/hlca.201200528

Costello, H. (2018). *Global Surfactants Market 2018- Segmented by Origin, Type, Application, Geography-Growth, Trends and Forecasts to 2023*. Dallas, TX: Orbis Research, 1–285.

Cuvier, A.-S., Berton, J., Stevens, C. V., Fadda, G. C., Babonneau, F., Van Bogaert, I. N. A., et al. (2014). PH-triggered Formation of Nanoribbons from Yeast-Derived Glycolipid Biosurfactants. *Soft Matter* 10, 3950–3959. doi:10.1039/c4sm00111g

Dai, L., Yang, S., Wei, Y., Sun, C., McClements, D. J., Mao, L., et al. (2019). Development of Stable High Internal Phase Emulsions by Pickering Stabilization: Utilization of Zein-Propylene Glycol Alginate-Rhamnolipid Complex Particles as Colloidal Emulsifiers. *Food Chem.* 275, 246–254. doi:10.1016/j.foodchem.2018.09.122

Dalgleish, D. G. (2006). Food Emulsions-Their Structures and Structure-Forming Properties. *Food Hydrocolloids* 20, 415–422. doi:10.1016/j.foodhyd.2005.10.009

Daruich De Souza, C., Ribeiro Nogueira, B., and Rostelato, M. E. C. M. (2019). Review of the Methodologies Used in the Synthesis Gold Nanoparticles by Chemical Reduction. *J. Alloys Comp.* 798, 714–740. doi:10.1016/j.jallcom.2019.05.153

de Freitas Ferreira, J., Vieira, E. A., and Nitschke, M. (2019). The Antibacterial Activity of Rhamnolipid Biosurfactant Is pH Dependent. *Food Res. Int.* 116, 737–744. doi:10.1016/j.foodres.2018.09.005

Delbeke, E. I. P., Everaert, J., Lozach, O., Le Gall, T., Berchel, M., Montier, T., et al. (2018). Synthesis and Biological Evaluation of Bolaamphiphilic Sophorolipids. *ACS Sust. Chem. Eng.* 6, 8992–9005. doi:10.1021/acssuschemeng.8b01354

Delbeke, E. I. P., Everaert, J., Lozach, O., Le Gall, T., Berchel, M., Montier, T., et al. (2019). Lipid-Based Quaternary Ammonium Sophorolipid Amphiphiles with Antimicrobial and Transfection Activities. *ChemSusChem* 12, 3642–3653. doi:10.1002/cssc.201900721

Delbeke, E. I. P., Everaert, J., Uitterhaegen, E., Verweire, S., Verlee, A., Talou, T., et al. (2016a). Petroselinic Acid Purification and its Use for the Fermentation of New Sophorolipids. *AMB Expr.* 6, 1. doi:10.1186/s13568-016-0199-7

Delbeke, E. I. P., Movsisyan, M., Van Geem, K. M., and Stevens, C. V. (2016b). Chemical and Enzymatic Modification of Sophorolipids. *Green. Chem.* 18, 76–104. doi:10.1039/c5gc02187a

Delbeke, E. I. P., Roman, B. I., Marin, G. B., Van Geem, K. M., and Stevens, C. V. (2015). A New Class of Antimicrobial Biosurfactants: Quaternary Ammonium Sophorolipids. *Green. Chem.* 17, 3373–3377. doi:10.1039/c5gc00120j

Deziel, E., Paquette, G., Villemur, R., Lepine, F., Bisaillon, J., and Le, O. I. S. (1996). Biosurfactant Production by a Soil Pseudomonas Strain Growing on Polycyclic Aromatic Hydrocarbons. *Appl. Environ. Microbiol.* 62, 1908–1912. doi:10.1128/aem.62.6.1908-1912.1996

Dhasaiyan, P., Banerjee, A., Visaveliya, N., and Prasad, B. L. V. (2013). Influence of the Sophorolipid Molecular Geometry on Their Self-Assembled Structures. *Chem. Asian J.* 8, 369–372. doi:10.1002/asia.201200935

Díaz De Rienzo, M. A., Banat, I. M., Dolman, B., Winterburn, J., and Martin, P. J. (2015). Sophorolipid Biosurfactants: Possible Uses as Antibacterial and Antibiofilm Agent. *New Biotechnol.* 32, 720–726. doi:10.1016/j.nbt.2015.02.009

Díaz De Rienzo, M. A., Stevenson, P., Marchant, R., and Banat, I. M. (2016). Antibacterial Properties of Biosurfactants against Selected Gram-Positive and -negative Bacteria. *FEMS Microbiol. Lett.* 363, fnv224. doi:10.1093/femsle/fnv224

Ebadipour, N., Lotfabad, T. B., Yaghmaei, S., and RoostAazad, R. (2016). Optimization of Low-Cost Biosurfactant Production from Agricultural Residues through Response Surface Methodology. *Prep. Biochem. Biotechnol.* 46, 30–38. doi:10.1080/10826068.2014.979204

Eismin, R. J., Munusamy, E., Kegel, L. L., Hogan, D. E., Maier, R. M., Schwartz, S. D., et al. (2017). Evolution of Aggregate Structure in Solutions of Anionic Monorhamnolipids: Experimental and Computational Results. *Langmuir* 33, 7412–7424. doi:10.1021/acs.langmuir.7b00078

Elshikh, M., Funston, S., Chebbi, A., Ahmed, S., Marchant, R., and Banat, I. M. (2017). Rhamnolipids from Non-pathogenic Burkholderia Thailandensis E264: Physicochemical Characterization, Antimicrobial and Antibiofilm Efficacy against Oral hygiene Related Pathogens. *New Biotechnol.* 36, 26–36. doi:10.1016/j.nbt.2016.12.009

Euston, S. R., Banat, I. M., and Salek, K. (2021). Congener-dependent Conformations of Isolated Rhamnolipids at the Vacuum-Water Interface: A Molecular Dynamics Simulation. *J. Colloid Interf. Sci.* 585, 148–157. doi:10.1016/j.jcis.2020.11.082

Euston, S. R. (2017). Molecular Simulation of Biosurfactants with Relevance to Food Systems. *Curr. Opin. Colloid Interf. Sci.* 28, 110–119. doi:10.1016/j.cocis.2017.04.002

Eveleigh, D. E., Dateo, G. P., and Reese, E. T. (1964). Fungal Metabolism of Complex Glycosides: Ustilagic Acid. *J. Biol. Chem.* 239, 1. doi:10.1016/s0021-9258(18)51666-5

Fernández-Peña, L., Guzmán, E., Leonforte, F., Serrano-Pueyo, A., Regulski, K., Tournier-Couturier, L., et al. (2020). Effect of Molecular Structure of Eco-Friendly Glycolipid Biosurfactants on the Adsorption of Hair-Care Conditioning Polymers. *Colloids Surf. B: Biointerfaces* 185, 110578. doi:10.1016/j.colsurfb.2019.110578

Franzetti, A., Gandolfi, I., Bestetti, G., Smyth, T. J. P., and Banat, I. M. (2010). Production and Applications of Trehalose Lipid Biosurfactants. *Eur. J. Lipid Sci. Technol.* 112, 617–627. doi:10.1002/ejlt.200900162

Fukuoka, T., Morita, T., Konishi, M., Imura, T., and Kitamoto, D. (2008). A Basidiomycetous Yeast, Pseudozyma Tsukubaensis, Efficiently Produces a Novel Glycolipid Biosurfactant. The Identification of a New Diastereomer of Mannosylerythritol Lipid-B. *Carbohydr. Res.* 343, 555–560. doi:10.1016/j.carres.2007.11.023

Fukuoka, T., Morita, T., Konishi, M., Imura, T., and Kitamoto, D. (2007). Characterization of New Types of Mannosylerythritol Lipids as Biosurfactants Produced from Soybean Oil by a Basidiomycetous Yeast, Pseudozyma Shanxiensis. *J. Oleo Sci.* 56, 435–442. doi:10.5650/jos.56.435

Furuta, T., Igarashi, K., and Hirata, Y. (2004). *Low-Foaming Detergent Compositions*. U.S. Patent Application 10/481,507.

Garay, L. A., Sitepu, I. R., Cajka, T., Cathcart, E., Fiehn, O., German, J. B., et al. (2017). Simultaneous Production of Intracellular Triacylglycerols and Extracellular Polyol Esters of Fatty Acids by Rhodotorula Babjevae and Rhodotorula Aff. Paludigena. *J. Ind. Microbiol. Biotechnol.* 44, 1397–1413. doi:10.1007/s10295-017-1964-6

Garay, L. A., Sitepu, I. R., Cajka, T., Xu, J., Teh, H. E., German, J. B., et al. (2018). Extracellular Fungal Polyol Lipids: A New Class of Potential High Value Lipids. *Biotechnol. Adv.* 36, 397–414. doi:10.1016/j.biotechadv.2018.01.003

Geys, R., De Graeve, M., Lodens, S., Van Malderen, J., Lemmens, C., De Smet, M., et al. (2018). Increasing Uniformity of Biosurfactant Production in Starmerella Bombicola via the Expression of Chimeric Cytochrome P450s. *Colloids Inter.* 2, 42. doi:10.3390/colloids2040042

Global Market Insights Inc (2018). *Biosurfactants Market worth over $2.7 Bn by 2024*. Selbyville, DE: Global Market Insights. Available at: www.gminsights.com/pressrelease/biosurfactants-market-size.

Golubev, W. I., Kulakovskaya, T. v., Shashkov, A. S., Kulakovskaya, E. v., and Golubev, N. v. (2008). Antifungal Cellobiose Lipid Secreted by the Epiphytic Yeast Pseudozyma Graminicola. *Microbiology* 77, 171–175. doi:10.1134/S0026261708020082

Gong, Z., Peng, Y., and Wang, Q. (2015). Rhamnolipid Production, Characterization and Fermentation Scale-Up by *Pseudomonas aeruginosa* with Plant Oils. *Biotechnol. Lett.* 37, 2033–2038. doi:10.1007/s10529-015-1885-2

Gorin, P. A. J., Spencer, J. F. T., and Tulloch, A. P. (1961). Hydroxy Fatty Acid Glycosides of Sophorose from Torulopsis Magnoliae. *Can. J. Chem.* 39, 846–855. doi:10.1139/v61-104

Gunther, N. W., Nuñez, A., Fett, W., and Solaiman, D. K. Y. (2005). Production of Rhamnolipids by Pseudomonas Chlororaphis , a Nonpathogenic Bacterium. *Appl. Environ. Microbiol.* 71, 2288–2293. doi:10.1128/AEM.71.5.2288-2293.2005

Haba, E., Bouhdid, S., Torrego-Solana, N., Marqués, A. M., Espuny, M. J., García-Celma, M. J., et al. (2014). Rhamnolipids as Emulsifying Agents for Essential Oil Formulations: Antimicrobial Effect against Candida Albicans and Methicillin-Resistant *Staphylococcus aureus*. *Int. J. Pharmaceutics* 476, 134–141. doi:10.1016/j.ijpharm.2014.09.039

Haba, E., Pinazo, A., Jauregui, O., Espuny, M. J., Infante, M. R., and Manresa, A. (2003). Physicochemical Characterization and Antimicrobial Properties of Rhamnolipids Produced byPseudomonas Aeruginosa 47T2 NCBIM 40044. *Biotechnol. Bioeng.* 81, 316–322. doi:10.1002/bit.10474

Hall, P. J., Haverkamp, J., Van Kralingen, C. G., and Schmidt, M. (1995). *Laundry Detergent Composition Containing Synergistic Combination of Sophorose Lipid and Nonionic Surfactant*. U.S. Patent 5,520,839.

Hamley, I. W., Dehsorkhi, A., Jauregi, P., Seitsonen, J., Ruokolainen, J., Coutte, F., et al. (2013). Self-assembly of Three Bacterially-Derived Bioactive Lipopeptides. *Soft Matter* 9, 9572–9578. doi:10.1039/c3sm51514a

Hamley, I. W. (2015). Lipopeptides: From Self-Assembly to Bioactivity. *Chem. Commun.* 51, 8574–8583. doi:10.1039/c5cc01535a

Hardin, R., Pierre, J., Schulze, R., Mueller, C. M., Fu, S. L., Wallner, S. R., et al. (2007). Sophorolipids Improve Sepsis Survival: Effects of Dosing and Derivatives. *J. Surg. Res.* 142, 314–319. doi:10.1016/j.jss.2007.04.025

Harnois, I., Genest, D., Brochon, J. C., and Ptak, M. (1988). Micellization and Interactions with Phospholipid Vesicles of the Lipopeptide Iturin a, as Monitored by Time-Resolved Fluorescence of aD-Tyrosyl Residue. *Biopolymers* 27, 1403–1413. doi:10.1002/bip.360270907

Haskins, R. H. (1950). Biochemistry of the Ustilaginales: I. Preliminary Cultural Studies of Ustilago Zeae. *Can. J. Res.* 28c, 213–223. doi:10.1139/cjr50c-012

Heerklotz, H., and Seelig, J. (2001). Detergent-like Action of the Antibiotic Peptide Surfactin on Lipid Membranes. *Biophysical J.* 81, 1547–1554. doi:10.1016/S0006-3495(01)75808-0

Helvacı, Ş. Ş., Peker, S., and Özdemir, G. (2004). Effect of Electrolytes on the Surface Behavior of Rhamnolipids R1 and R2. *Colloids Surf. B: Biointerfaces* 35, 225–233. doi:10.1016/j.colsurfb.2004.01.001

Hirano, R., Kagamiya, T., Matsumoto, Y., Furuta, T., and Sakurai, M. (2021). Molecular Mechanism Underlying the Selective Attack of Trehalose Lipids on Cancer Cells as Revealed by Coarse-Grained Molecular Dynamics Simulations. *Biochem. Biophys. Rep.* 25, 100913. doi:10.1016/j.bbrep.2021.100913

Hirata, Y., Ryu, M., Oda, Y., Igarashi, K., Nagatsuka, A., Furuta, T., et al. (2009). Novel Characteristics of Sophorolipids, Yeast Glycolipid Biosurfactants, as Biodegradable Low-Foaming Surfactants. *J. Biosci. Bioeng.* 108, 142–146. doi:10.1016/j.jbiosc.2009.03.012

Hošková, M., Ježdík, R., Schreiberová, O., Chudoba, J., Šír, M., Čejková, A., et al. (2015). Structural and Physiochemical Characterization of Rhamnolipids Produced by Acinetobacter Calcoaceticus, Enterobacter Asburiae and *Pseudomonas aeruginosa* in Single Strain and Mixed Cultures. *J. Biotechnol.* 193, 45–51. doi:10.1016/j.jbiotec.2014.11.014

Hošková, M., Schreiberová, O., Ježdík, R., Chudoba, J., Masák, J., Sigler, K., et al. (2013). Characterization of Rhamnolipids Produced by Non-pathogenic Acinetobacter and Enterobacter Bacteria. *Bioresour. Tech.* 130, 510–516. doi:10.1016/j.biortech.2012.12.085

Hvidsten, I., Mjøs, S. A., Holmelid, B., Bødtker, G., and Barth, T. (2017). Lipids of Dietzia Sp. A14101. Part I: A Study of the Production Dynamics of Surface-Active Compounds. *Chem. Phys. Lipids* 208, 19–30. doi:10.1016/j.chemphyslip.2017.08.006

Imura, T., Hikosaka, Y., Worakitkanchanakul, W., Sakai, H., Abe, M., Konishi, M., et al. (2007). Aqueous-phase Behavior of Natural Glycolipid Biosurfactant Mannosylerythritol Lipid A: Sponge, Cubic, and Lamellar Phases. *Langmuir* 23, 1659–1663. doi:10.1021/la0620814

Imura, T., Ohta, N., Inoue, K., Yagi, N., Negishi, H., Yanagishita, H., et al. (2006). Naturally Engineered Glycolipid Biosurfactants Leading to Distinctive Self-Assembled Structures. *Chem. Eur. J.* 12, 2434–2440. doi:10.1002/chem.200501199

Inès, M., and Dhouha, G. (2015a). Glycolipid Biosurfactants: Potential Related Biomedical and Biotechnological Applications. *Carbohydr. Res.* 416, 59–69. doi:10.1016/j.carres.2015.07.016

Inès, M., and Dhouha, G. (2015b). Lipopeptide Surfactants: Production, Recovery and Pore Forming Capacity. *Peptides* 71, 100–112. doi:10.1016/j.peptides.2015.07.006

Iravani, S., Korbekandi, H., Mirmohammadi, S. V., and Zolfaghari, B. (2014). Synthesis of Silver Nanoparticles: Chemical, Physical and Biological Methods. *Res. Pharm. Sci.* 9, 385–406.

Ishigami, Y., Gama, Y., Nagahora, H., Yamaguchi, M., Nakahara, H., and Kamata, T. (1987). The pH-Sensitive Conversion of Molecular Aggregates of Rhamnolipid Biosurfactant. *Chem. Lett.* 16, 763–766. doi:10.1246/cl.1987.763

Janek, T., Krasowska, A., Czyżnikowska, Ż., and Łukaszewicz, M. (2018). Trehalose Lipid Biosurfactant Reduces Adhesion of Microbial Pathogens to Polystyrene and Silicone Surfaces: An Experimental and Computational Approach. *Front. Microbiol.* 9, 1–14. doi:10.3389/fmicb.2018.02441

Janek, T., Łukaszewicz, M., and Krasowska, A. (2013). Identification and Characterization of Biosurfactants Produced by the Arctic Bacterium Pseudomonas Putida BD2. *Colloids Surf. B: Biointerfaces* 110, 379–386. doi:10.1016/j.colsurfb.2013.05.008

Jarvis, F. G., and Johnson, M. J. (1949). A Glyco-Lipide Produced by Pseudomonas Aeruginosa. *J. Am. Chem. Soc.* 71, 4124–4126. doi:10.1021/ja01180a073

Jezierska, S., Claus, S., and Van Bogaert, I. (2018). Yeast Glycolipid Biosurfactants. *FEBS Lett.* 592, 1312–1329. doi:10.1002/1873-3468.12888

Kaczerewska, O., Martins, R., Figueiredo, J., Loureiro, S., and Tedim, J. (2020). Environmental Behaviour and Ecotoxicity of Cationic Surfactants towards marine Organisms. *J. Hazard. Mater.* 392, 122299. doi:10.1016/j.jhazmat.2020.122299

Kaczorek, E., Sałek, K., Guzik, U., Jesionowski, T., and Cybulski, Z. (2013). Biodegradation of Alkyl Derivatives of Aromatic Hydrocarbons and Cell Surface Properties of a Strain of Pseudomonas Stutzeri. *Chemosphere* 90, 471–478. doi:10.1016/j.chemosphere.2012.07.065

Kanwar, R., Gradzielski, M., and Mehta, S. K. (2018). Biomimetic Solid Lipid Nanoparticles of Sophorolipids Designed for Antileprosy Drugs. *J. Phys. Chem. B* 122, 6837–6845. doi:10.1021/acs.jpcb.8b03081

Khoshdast, H., Abbasi, H., Sam, A., and Noghabi, K. A. (2012). Frothability and Surface Behavior of a Rhamnolipid Biosurfactant Produced by *Pseudomonas aeruginosa* MA01. *Biochem. Eng. J.* 60, 127–134. doi:10.1016/j.bej.2011.10.015

Kim, J. S., Lee, I. K., and Yun, B. S. (2015). A Novel Biosurfactant Produced by Aureobasidium Pullulans L3-GPY from a Tiger Lily Wild Flower, Lilium Lancifolium Thunb. *PLoS ONE* 10, e0122917–12. doi:10.1371/journal.pone.0122917

Kitamoto, D., Haneishi, K., Nakahara, T., and Tabuchi, T. (1990). Production of Mannosylerythritol Lipids by Candida antarctica from Vegetable Oils. *Agric. Biol. Chem.* 54, 37–40. doi:10.1271/bbb1961.54.37

Kitamoto, D., Ikegami, T., Suzuki, G. T., Sasaki, A., Takeyama, Y.-i., Idemoto, Y., et al. (2001). Microbial Conversion of N-Alkanes into Glycolipid Biosurfactants, Manosylerythritol Lipids, by Psedozyma (Candida antarctica). *Biotechnol. Letters* 23, 1709–1714. doi:10.1023/a:1012464717259

Kitamoto, D., Morita, T., Fukuoka, T., Konishi, M.-a., and Imura, T. (2009). Self-assembling Properties of Glycolipid Biosurfactants and Their Potential Applications. *Curr. Opin. Colloid Interf. Sci.* 14, 315–328. doi:10.1016/j.cocis.2009.05.009

Kitamoto, D., Yanagishita, H., Shinbo, T., Nakane, T., Kamisawa, C., and Nakahara, T. (1993). Surface Active Properties and Antimicrobial Activities of Mannosylerythritol Lipids as Biosurfactants Produced by Candida antarctica. *J. Biotechnol.* 29, 91–96. doi:10.1016/0168-1656(93)90042-l

Koh, A., and Gross, R. (2016). A Versatile Family of Sophorolipid Esters: Engineering Surfactant Structure for Stabilization of Lemon Oil-Water Interfaces. *Colloids Surf. A: Physicochemical Eng. Aspects* 507, 152–163. doi:10.1016/j.colsurfa.2016.07.089

Koh, A., Linhardt, R. J., and Gross, R. (2016). Effect of Sophorolipid N-Alkyl Ester Chain Length on its Interfacial Properties at the Almond Oil-Water Interface. *Langmuir* 32, 5562–5572. doi:10.1021/acs.langmuir.6b01008

Koh, A., Wong, A., Quinteros, A., Desplat, C., and Gross, R. (2017). Influence of Sophorolipid Structure on Interfacial Properties of Aqueous-Arabian Light Crude and Related Constituent Emulsions. *J. Am. Oil Chem. Soc.* 94, 107–119. doi:10.1007/s11746-016-2913-7

Konishi, M., Imura, T., Fukuoka, T., Morita, T., and Kitamoto, D. (2007a). A Yeast Glycolipid Biosurfactant, Mannosylerythritol Lipid, Shows High Binding Affinity towards Lectins on a Self-Assembled Monolayer System. *Biotechnol. Lett.* 29, 473–480. doi:10.1007/s10529-006-9261-x

Konishi, M., Morita, T., Fukuoka, T., Imura, T., Kakugawa, K., and Kitamoto, D. (2008). Efficient Production of Mannosylerythritol Lipids with High Hydrophilicity by Pseudozyma Hubeiensis KM-59. *Appl. Microbiol. Biotechnol.* 78, 37–46. doi:10.1007/s00253-007-1292-2

Konishi, M., Morita, T., Fukuoka, T., Imura, T., Kakugawa, K., and Kitamoto, D. (2007b). Production of Different Types of Mannosylerythritol Lipids as Biosurfactants by the Newly Isolated Yeast Strains Belonging to the Genus Pseudozyma. *Appl. Microbiol. Biotechnol.* 75, 521–531. doi:10.1007/s00253-007-0853-8

Konishi, M., Nagahama, T., Fukuoka, T., Morita, T., Imura, T., Kitamoto, D., et al. (2011). Yeast Extract Stimulates Production of Glycolipid Biosurfactants, Mannosylerythritol Lipids, by Pseudozyma Hubeiensis SY62. *J. Biosci. Bioeng.* 111, 702–705. doi:10.1016/j.jbiosc.2011.02.004

Kosaric, N., and Vardar-Sukan, F. (2015). "Biosurfactants : Production and Utilization-Pprocesses, Technologies, and Economics," in *Biosurfactants : Production and Utilization-Pprocesses, Technologies, and Economics* (Boca Raton: CRC press).

Kulakovskaya, E. v., Golubev, V. I., and Kulaev, I. S. (2006). Extracellular Antifungal Glycolipids of Cryptococcus Humicola Yeasts. *Dokl Biol. Sci.* 410, 393–395. doi:10.1134/S0012496606050140

Kulakovskaya, E. v., Kulakovskaya, T. v., Golubev, V. I., Shashkov, A. S., Grachev, A. A., and Nifantiev, N. E. (2007). Fungicidal Activity of Cellobiose Lipids from Culture Broth of Yeast Cryptococcus Humicola and Pseudozyma Fusiformata. *Russ. J. Bioorg. Chem.* 33, 156–160. doi:10.1134/S1068162007010189

Kumar, C. G., Mamidyala, S. K., Das, B., Sridhar, B., Sarala Devi, G., and Karuna, M. S. L. (2010). Synthesis of Biosurfactant-Based Silver Nanoparticles with Purified Rhamnolipids Isolated from *Pseudomonas aeruginosa* BS-161R. *J. Microbiol. Biotechnol.* 20, 1061–1068. doi:10.4014/jmb.1001.01018

Kumar, R., and Das, A. J. (2018). "Rhamnolipid-Assisted Synthesis of Stable Nanoparticles: A Green Approach," in *Rhamnolipid Biosurfactant* (Springer), 111–124. doi:10.1007/978-981-13-1289-2_10

Kuyukina, M. S., Ivshina, I. B., Baeva, T. A., Kochina, O. A., Gein, S. V., and Chereshnev, V. A. (2015). Trehalolipid Biosurfactants from Nonpathogenic Rhodococcus Actinobacteria with Diverse Immunomodulatory Activities. *New Biotechnol.* 32, 559–568. doi:10.1016/j.nbt.2015.03.006

Kuyukina, M. S., Kochina, O. A., Gein, S. V., Ivshina, I. B., and Chereshnev, V. A. (2020). Mechanisms of Immunomodulatory and Membranotropic Activity of Trehalolipid Biosurfactants (A Review). *Appl. Biochem. Microbiol.* 56, 245–255. doi:10.1134/S0003683820030072

Lang, S., and Wullbrandt, D. (1999). Rhamnose Lipids - Biosynthesis, Microbial Production and Application Potential. *Appl. Microbiol. Biotechnol.* 51, 22–32. doi:10.1007/s002530051358

Leathers, T. D., Price, N. P. J., Bischoff, K. M., Manitchotpisit, P., and Skory, C. D. (2015). Production of Novel Types of Antibacterial Liamocins by Diverse Strains of Aureobasidium Pullulans Grown on Different Culture media. *Biotechnol. Lett.* 37, 2075–2081. doi:10.1007/s10529-015-1892-3

Leathers, T. D., Price, N. P. J., Manitchotpisit, P., and Bischoff, K. M. (2016). Production of Anti-streptococcal Liamocins from Agricultural Biomass by Aureobasidium Pullulans. *World J. Microbiol. Biotechnol.* 32, 1–7. doi:10.1007/s11274-016-2158-5

Lemieux, R. U., Thorn, J. A., Brice, C., and Haskins, R. H. (1951). Biochemistry of the Ustilaginales: Ii. Isolation and Partial Characterization of Ustilagic Acid. *Can. J. Chem.* 29, 409–414. doi:10.1139/v51-049

Li, P., Ghosh, A., Wagner, R. F., Krill, S., Joshi, Y. M., and Serajuddin, A. T. M. (2005). Effect of Combined Use of Nonionic Surfactant on Formation of Oil-In-Water Microemulsions. *Int. J. Pharmaceutics* 288, 27–34. doi:10.1016/j.ijpharm.2004.08.024

Lovaglio, R. B., dos Santos, F. J., Jafelicci, M., and Contiero, J. (2011). Rhamnolipid Emulsifying Activity and Emulsion Stability: PH Rules. *Colloids Surf. B: Biointerfaces* 85, 301–305. doi:10.1016/j.colsurfb.2011.03.001

Luft, C. M., Munusamy, E., Pemberton, J. E., and Schwartz, S. D. (2020). A Classical Molecular Dynamics Simulation Study of Interfacial and Bulk Solution Aggregation Properties of Dirhamnolipids. *J. Phys. Chem. B* 124, 814–827. doi:10.1021/acs.jpcb.9b08800

Lydon, H. L., Baccile, N., Callaghan, B., Marchant, R., Mitchell, C. A., and Banat, I. M. (2017). Adjuvant Antibiotic Activity of Acidic Sophorolipids with Potential for Facilitating Wound Healing. *Antimicrob. Agents Chemother.* 61, 1. doi:10.1128/aac.02547-16

Lyman, M., Rubinfeld, B., Leif, R., Mulcahy, H., Dugan, L., and Souza, B. (2018). Rhodotorula Taiwanensis MD1149 Produces Hypoacetylated PEFA Compounds with Increased Surface Activity Compared to Rhodotorula Babjevae MD1169. *PLoS ONE* 13, e0190373–17. doi:10.1371/journal.pone.0190373

Ma, X., Li, H., and Song, X. (2012). Surface and Biological Activity of Sophorolipid Molecules Produced by Wickerhamiella Domercqiae Var. Sophorolipid CGMCC 1576. *J. Colloid Interf. Sci.* 376, 165–172. doi:10.1016/j.jcis.2012.03.007

Maget-Dana, R., and Peypoux, F. (1994). Iturins, a Special Class of Pore-Forming Lipopeptides: Biological and Physicochemical Properties. *Toxicology* 87, 151–174. doi:10.1016/0300-483x(94)90159-7

Manet, S., Cuvier, A.-S., Valotteau, C., Fadda, G. C., Perez, J., Karakas, E., et al. (2015). Structure of Bolaamphiphile Sophorolipid Micelles Characterized with SAXS, SANS, and MD Simulations. *J. Phys. Chem. B* 119, 13113–13133. doi:10.1021/acs.jpcb.5b05374

Manitchotpisit, P., Price, N. P. J., Leathers, T. D., and Punnapayak, H. (2011). Heavy Oils Produced by Aureobasidium Pullulans. *Biotechnol. Lett.* 33, 1151–1157. doi:10.1007/s10529-011-0548-1

Manitchotpisit, P., Watanapoksin, R., Price, N. P. J., Bischoff, K. M., Tayeh, M., Teeraworawit, S., et al. (2014). Aureobasidium Pullulans as a Source of Liamocins (Heavy Oils) with Anticancer Activity. *World J. Microbiol. Biotechnol.* 30, 2199–2204. doi:10.1007/s11274-014-1639-7

Marqués, A. M., Pinazo, A., Farfan, M., Aranda, F. J., Teruel, J. A., Ortiz, A., et al. (2009). The Physicochemical Properties and Chemical Composition

of Trehalose Lipids Produced by Rhodococcus Erythropolis 51T7. *Chem. Phys. Lipids* 158, 110–117. doi:10.1016/j.chemphyslip.2009.01.001

Martinez, J. S., Zhang, G. P., Holt, P. D., Jung, H.-T., Carrano, C. J., Haygood, M. G., et al. (2000). Self-assembling Amphiphilic Siderophores from marine Bacteria. *Science* 287, 1245–1247. doi:10.1126/science.287.5456.1245

McInerney, M. J., Javaheri, M., and Nagle, D. P. (1990). Properties of the Biosurfactant Produced byBacillus Licheniformis Strain JF-2. *J. Ind. Microbiol.* 5, 95–101. doi:10.1007/BF01573858

Morita, T., Ishibashi, Y., Fukuoka, T., Imura, T., Sakai, H., Abe, M., et al. (2011). Production of Glycolipid Biosurfactants, Cellobiose Lipids, byCryptococcus humicolaJCM 1461 and Their Interfacial Properties. *Biosci. Biotechnol. Biochem.* 75, 1597–1599. doi:10.1271/bbb.110036

Morita, T., Konishi, M., Fukuoka, T., Imura, T., and Kitamoto, D. (2008). Production of Glycolipid Biosurfactants, Mannosylerythritol Lipids, by Pseudozyma Siamensis CBS 9960 and Their Interfacial Properties. *J. Biosci. Bioeng.* 105, 493–502. doi:10.1263/jbb.105.493

Mulligan, C. N. (2005). Environmental Applications for Biosurfactants. *Environ. Pollut.* 133, 183–198. doi:10.1016/j.envpol.2004.06.009

Munusamy, E., Luft, C. M., Pemberton, J. E., and Schwartz, S. D. (2017). Structural Properties of Nonionic Monorhamnolipid Aggregates in Water Studied by Classical Molecular Dynamics Simulations. *J. Phys. Chem. B* 121, 5781–5793. doi:10.1021/acs.jpcb.7b00997

Ndlovu, T., Rautenbach, M., Vosloo, J. A., Khan, S., and Khan, W. (2017). Characterisation and Antimicrobial Activity of Biosurfactant Extracts Produced by Bacillus Amyloliquefaciens and *Pseudomonas aeruginosa* Isolated from a Wastewater Treatment Plant. *AMB Expr.* 7, 1. doi:10.1186/s13568-017-0363-8

Nejati, K., Dadashpour, M., Gharibi, T., Mellatyar, H., and Akbarzadeh, A. (2021). Biomedical Applications of Functionalized Gold Nanoparticles: A Review. *J. Clust Sci.* 2021, 13. doi:10.1007/s10876-020-01955-9

Nitschke, M., Costa, S. G. V. A. O., and Contiero, J. (2005). Rhamnolipid Surfactants: An Update on the General Aspects of These Remarkable Biomolecules. *Biotechnol. Prog.* 21, 1593–1600. doi:10.1021/bp050239p

Nitschke, M., Costa, S. G. V. A. O., and Contiero, J. (2011). Rhamnolipids and PHAs: Recent Reports on Pseudomonas-Derived Molecules of Increasing Industrial Interest. *Process Biochem.* 46, 621–630. doi:10.1016/j.procbio.2010.12.012

Nitschke, M., and Silva, S. S. e. (2018). Recent Food Applications of Microbial Surfactants. *Crit. Rev. Food Sci. Nutr.* 58, 631–638. doi:10.1080/10408398.2016.1208635

Oliveira, F. J. S., Vazquez, L., de Campos, N. P., and de França, F. P. (2009). Production of Rhamnolipids by a *Pseudomonas alcaligenes* Strain. *Process Biochem.* 44, 383–389. doi:10.1016/j.procbio.2008.11.014

Ortiz, A., Teruel, J. A., Espuny, M. J., Marqués, A., Manresa, Á., and Aranda, F. J. (2008). Interactions of a Rhodococcus Sp. Biosurfactant Trehalose Lipid with Phosphatidylethanolamine Membranes. *Biochim. Biophys. Acta (Bba) - Biomembranes* 1778, 2806–2813. doi:10.1016/j.bbamem.2008.07.016

Özdemir, G., Peker, S., and Helvaci, S. S. (2004). Effect of pH on the Surface and Interfacial Behavior of Rhamnolipids R1 and R2. *Colloids Surf. A: Physicochemical Eng. Aspects* 234, 135–143. doi:10.1016/j.colsurfa.2003.10.024

Palos Pacheco, R., Eismin, R. J., Coss, C. S., Wang, H., Maier, R. M., Polt, R., et al. (2017). Synthesis and Characterization of Four Diastereomers of Monorhamnolipids. *J. Am. Chem. Soc.* 139, 5125–5132. doi:10.1021/jacs.7b00427

Palos Pacheco, R., Kegel, L. L., and Pemberton, J. E. (2021). Interfacial and Solution Aggregation Behavior of a Series of Bioinspired Rhamnolipid Congeners Rha-C14-Cx (X = 6, 8, 10, 12, 14). *J. Phys. Chem. B* 125, 13585–13596. doi:10.1021/acs.jpcb.1c09435

Pekdemir, T., Çopur, M., and Urum, K. (2005). Emulsification of Crude Oil-Water Systems Using Biosurfactants. *Process Saf. Environ. Prot.* 83, 38–46. doi:10.1205/psep.03176

Penfold, J., Chen, M., Thomas, R. K., Dong, C., Smyth, T. J. P., Perfumo, A., et al. (2011). Solution Self-Assembly of the Sophorolipid Biosurfactant and its Mixture with Anionic Surfactant Sodium Dodecyl Benzene Sulfonate. *Langmuir* 27, 8867–8877. doi:10.1021/la201661y

Price, N. P., Bischoff, K. M., Leathers, T. D., Cossé, A. A., and Manitchotpisit, P. (2017). Polyols, Not Sugars, Determine the Structural Diversity of Anti-streptococcal Liamocins Produced by Aureobasidium Pullulans Strain NRRL 50380. *J. Antibiot.* 70, 136–141. doi:10.1038/ja.2016.92

Price, N. P. J., Manitchotpisit, P., Vermillion, K. E., Bowman, M. J., and Leathers, T. D. (2013). Structural Characterization of Novel Extracellular Liamocins (Mannitol Oils) Produced by Aureobasidium Pullulans Strain NRRL 50380. *Carbohydr. Res.* 370, 24–32. doi:10.1016/j.carres.2013.01.014

Price, N. P. J., Ray, K. J., Vermillion, K. E., Dunlap, C. A., and Kurtzman, C. P. (2012). Structural Characterization of Novel Sophorolipid Biosurfactants from a Newly Identified Species of Candida Yeast. *Carbohydr. Res.* 348, 33–41. doi:10.1016/j.carres.2011.07.016

Puchkov, E. O., Zähringer, U., Lindner, B., Kulakovskaya, T. V., Seydel, U., and Wiese, A. (2002). The Mycocidal, Membrane-Active Complex of Cryptococcus Humicola Is a New Type of Cellobiose Lipid with Detergent Features. *Biochim. Biophys. Acta* 1558, 161–170. doi:10.1016/S0005-2736(01)00428-X

Rahimi, K., Lotfabad, T. B., Jabeen, F., and Mohammad Ganji, S. (2019). Cytotoxic Effects of Mono- and Di-rhamnolipids from *Pseudomonas aeruginosa* MR01 on MCF-7 Human Breast Cancer Cells. *Colloids Surf. B: Biointerfaces* 181, 943–952. doi:10.1016/j.colsurfb.2019.06.058

Rau, U., Nguyen, L. A., Schulz, S., Wray, V., Nimtz, M., Roeper, H., et al. (2005). Formation and Analysis of Mannosylerythritol Lipids Secreted by Pseudozyma Aphidis. *Appl. Microbiol. Biotechnol.* 66, 551–559. doi:10.1007/s00253-004-1672-9

Research and Markets (2017). *Biosurfactants Market by Type (Glycolipids (Sophorolipids, Rhamnolipids), Lipopeptides, Phospholipids, Polymeric Biosurfactants), Application (Detergents, Personal Care, Agricultural Chemicals, Food Processing), and Region - Global Forecast to 2022*. Dublin, Ireland: Research and Markets.

Ribeiro, I. A. C., Faustino, C. M. C., Guerreiro, P. S., Frade, R. F. M., Bronze, M. R., Castro, M. F., et al. (2015). Development of Novel Sophorolipids with Improved Cytotoxic Activity toward MDA-MB-231 Breast Cancer Cells. *J. Mol. Recognit.* 28, 155–165. doi:10.1002/jmr.2403

Rieger, M. (1996). "Foams in Personal Care Products," in *Foams Theory Measurements, and Applications*. Editors R. K. Prud'homme and S. A. Khan (New York: Routledge).

Rosen, M. J., and Kunjappu, J. T. (2012). *Surfactants and Interfacial Phenomena*. 4th Edition. John Wiley & Sons.

Russell, C., Zompra, A. A., Spyroulias, G. A., Salek, K., and Euston, S. R. (2021). The Heat Stability of Rhamnolipid Containing Egg-Protein Stabilised Oil-In-Water Emulsions. *Food Hydrocolloids* 116, 106632. doi:10.1016/j.foodhyd.2021.106632

Saikia, J. P., Bharali, P., and Konwar, B. K. (2013). Possible protection of Silver Nanoparticles against Salt by Using Rhamnolipid. *Colloids Surf. B: Biointerfaces* 104, 330–332. doi:10.1016/j.colsurfb.2012.10.069

Sajna, K. V., Gottumukkala, L. D., Sukumaran, R. K., and Pandey, A. (2015). "White Biotechnology in Cosmetics," in *Industrial Biorefineries & White Biotechnology* (Elsevier B.V.), 607–652. doi:10.1016/B978-0-444-63453-5.00020-3

Sałek, K., and Euston, S. R. (2019). Sustainable Microbial Biosurfactants and Bioemulsifiers for Commercial Exploitation. *Process Biochem.* 85, 143–155. doi:10.1016/j.procbio.2019.06.027

Sambanthamoorthy, K., Feng, X., Patel, R., Patel, S., and Paranavitana, C. (2014). Antimicrobial and Antibiofilm Potential of Biosurfactants Isolated from Lactobacilli against Multi-Drug-Resistant Pathogens. *BMC Microbiol.* 14, 1. doi:10.1186/1471-2180-14-197

Sánchez, M., Aranda, F. J., Espuny, M. J., Marqués, A., Teruel, J. A., Manresa, Á., et al. (2007). Aggregation Behaviour of a Dirhamnolipid Biosurfactant Secreted by *Pseudomonas aeruginosa* in Aqueous media. *J. Colloid Interf. Sci.* 307, 246–253. doi:10.1016/j.jcis.2006.11.041

Serrano Figueroa, L. O. m., Pitts, B., Uchida, M., and Richards, A. M. (2016). Vesicle Self-Assembly of Amphiphilic Siderophores Produced by Bacterial Isolates from Soap Lake, Washington. *Can. J. Chem.* 94, 35–43. doi:10.1139/cjc-2015-0173

Shah, V., Doncel, G. F., Seyoum, T., Eaton, K. M., Zalenskaya, I., Hagver, R., et al. (2005). Sophorolipids, Microbial Glycolipids with Anti-human Immunodeficiency Virus and Sperm-Immobilizing Activities. *Antimicrob.*

Agents Chemother. 49, 4093–4100. doi:10.1128/AAC.49.10.409310.1128/aac.49.10.4093-4100.2005

Shao, L., Song, X., Ma, X., Li, H., and Qu, Y. (2012). Bioactivities of Sophorolipid with Different Structures against Human Esophageal Cancer Cells. *J. Surg. Res.* 173, 286–291. doi:10.1016/j.jss.2010.09.013

Shao, Z. (2011). "Trehalolipids," in *Biosurfactants: From Genes to Applications*. Editor G. Soberón-Chávez (Berlin, Heidelberg: Springer Berlin Heidelberg), 121–143. doi:10.1007/978-3-642-14490-5_5

Shen, H.-H., Thomas, R. K., Chen, C.-Y., Darton, R. C., Baker, S. C., and Penfold, J. (2009). Aggregation of the Naturally Occurring Lipopeptide, Surfactin, at Interfaces and in Solution: An Unusual Type of Surfactant? *Langmuir* 25, 4211–4218. doi:10.1021/la802913x

Shikha, S., Chaudhuri, S. R., and Bhattacharyya, M. S. (2020). Facile One Pot Greener Synthesis of Sophorolipid Capped Gold Nanoparticles and its Antimicrobial Activity Having Special Efficacy against Gram Negative *Vibrio cholerae*. *Sci. Rep.* 10, 1. doi:10.1038/s41598-019-57399-3

Shu, Q., Niu, Y., Zhao, W., and Chen, Q. (2019). Antibacterial Activity and Mannosylerythritol Lipids against Vegetative Cells and Spores of Bacillus Cereus. *Food Control* 106, 106711. doi:10.1016/j.foodcont.2019.106711

Shukla, S. (2016). *Surfactants Market by Type (Cationic, Anionic, Non-ionic, Amphoteric) and Application (Household Detergents, Personal Care, Industrial & Institutional Cleaners, Emulsion Polymerization, Food Processing, Oilfield Chemicals) - Global Opportunity Analysis an*. Portland, OR: Allied Market Research, 1–130.

Singer, M. E. V., and Finnerty, W. R. (1990). Physiology of Biosurfactant Synthesis by Rhodococcus Species H13-A. *Can. J. Microbiol.* 36, 741–745. doi:10.1139/m90-127

Singh, D. N., and Tripathi, A. K. (2013). Coal Induced Production of a Rhamnolipid Biosurfactant by Pseudomonas Stutzeri, Isolated from the Formation Water of Jharia Coalbed. *Bioresour. Tech.* 128, 215–221. doi:10.1016/j.biortech.2012.10.127

Singh, P., Patil, Y., and Rale, V. (2019). Biosurfactant Production: Emerging Trends and Promising Strategies. *J. Appl. Microbiol.* 126, 2–13. doi:10.1111/jam.14057

Singh, S., Patel, P., Jaiswal, S., Prabhune, A. A., Ramana, C. v., and Prasad, B. L. V. (2009). A Direct Method for the Preparation of Glycolipid-Metal Nanoparticle Conjugates: Sophorolipids as Reducing and Capping Agents for the Synthesis of Water Re-dispersible Silver Nanoparticles and Their Antibacterial Activity. *New J. Chem.* 33, 646–652. doi:10.1039/b811829a

Smyth, T. J. P., Perfumo, A., Marchant, R., and Banat*, I. M. (2010). "Isolation and Analysis of Low Molecular Weight Microbial Glycolipids," in *Handbook of Hydrocarbon and Lipid Microbiology*. Editor K. N. Timmis (Springer-Verlag), 3705–3723. doi:10.1007/978-3-540-77587-4_291

Sodagari, M., Invally, K., and Ju, L.-K. (2018). Maximize Rhamnolipid Production with Low Foaming and High Yield. *Enzyme Microb. Tech.* 110, 79–86. doi:10.1016/j.enzmictec.2017.10.004

Söderman, O., and Johansson, I. (1999). Polyhydroxyl-based Surfactants and Their Physico-Chemical Properties and Applications. *Curr. Opin. Colloid Interf. Sci.* 4, 391–401. doi:10.1016/S1359-0294(00)00019-4

Spoeckner, S., Wray, V., Nimtz, M., and Lang, S. (1999). Glycolipids of the Smut Fungus Ustilago Maydis from Cultivation on Renewable Resources. *Appl. Microbiol. Biotechnol.* 51, 33–39. doi:10.1007/s002530051359

Strieker, M., and Marahiel, M. A. (2009). The Structural Diversity of Acidic Lipopeptide Antibiotics. *ChemBioChem* 10, 607–616. doi:10.1002/cbic.200800546

Tadros, T. F. (2005). "Applied Surfactants," in *Applied Surfactants: Principles and Applications*(Weinheim: Wiley-VCH Verlag GmbH & Co. KGaA), 53–72. doi:10.1002/3527604812

Teichmann, B., Labbé, C., Lefebvre, F., Bölker, M., Linne, U., and Bélanger, R. R. (2011). Identification of a Biosynthesis Gene Cluster for Flocculosin a Cellobiose Lipid Produced by the Biocontrol Agent Pseudozyma Flocculosa. *Mol. Microbiol.* 79, 1483–1495. doi:10.1111/j.1365-2958.2010.07533.x

Teichmann, B., Linne, U., Hewald, S., Marahiel, M. A., and Bölker, M. (2007). A Biosynthetic Gene Cluster for a Secreted Cellobiose Lipid with Antifungal Activity from Ustilago Maydis. *Mol. Microbiol.* 66, 525–533. doi:10.1111/j.1365-2958.2007.05941.x

Tollemar, J., Klingspor, L., and Ringdén, O. (2001). Liposomal Amphotericin B (AmBisome) for Fungal Infections in Immunocompromised Adults and Children. *Clin. Microbiol. Infect.* 7, 68–79. doi:10.1111/j.1469-0691.2001.tb00012.x

Tuleva, B., Christova, N., Cohen, R., Antonova, D., Todorov, T., and Stoineva, I. (2009). Isolation and Characterization of Trehalose Tetraester Biosurfactants from a Soil Strain Micrococcus Luteus BN56. *Process Biochem.* 44, 135–141. doi:10.1016/j.procbio.2008.09.016

Tulloch, A. P., Spencer, J. F. T., and Deinema, M. H. (1968). A New Hydroxy Fatty Acid Sophoroside from Candida Bogoriensis. *Can. J. Chem.* 46, 345–348. doi:10.1139/v68-057

Van Bogaert, I. N. A., Buyst, D., Martins, J. C., Roelants, S. L. K. W., and Soetaert, W. K. (2016). Synthesis of Bolaform Biosurfactants by an engineeredStarmerella Bombicolayeast. *Biotechnol. Bioeng.* 113, 2644–2651. doi:10.1002/bit.26032

Van Bogaert, I. N. A., Saerens, K., De Muynck, C., Develter, D., Soetaert, W., and Vandamme, E. J. (2007). Microbial Production and Application of Sophorolipids. *Appl. Microbiol. Biotechnol.* 76, 23–34. doi:10.1007/s00253-007-0988-7

Van Hamme, J. D., and Ward, O. P. (2001). Physical and Metabolic Interactions of Pseudomonas Sp. Strain JA5-B45 and Rhodococcus Sp. Strain F9-D79 during Growth on Crude Oil and Effect of a Chemical Surfactant on Them. *Appl. Environ. Microbiol.* 67, 4874–4879. doi:10.1128/AEM.67.10.487410.1128/aem.67.10.4874-4879.2001

Van Renterghem, L., Roelants, S. L. K. W., Baccile, N., Uyttersprot, K., Taelman, M. C., Everaert, B., et al. (2018). From Lab to Market: An Integrated Bioprocess Design Approach for New-To-Nature Biosurfactants Produced byStarmerella Bombicola. *Biotechnol. Bioeng.* 115, 1195–1206. doi:10.1002/bit.26539

Voulgaridou, G.-P., Mantso, T., Anestopoulos, I., Klavaris, A., Katzastra, C., Kiousi, D.-E., et al. (2021). Toxicity Profiling of Biosurfactants Produced by Novel marine Bacterial Strains. *Ijms* 22, 2383. doi:10.3390/ijms22052383

White, D. A., Hird, L. C., and Ali, S. T. (2013). Production and Characterization of a Trehalolipid Biosurfactant Produced by the Novel marine Bacterium Rhodococcus sp., Strain PML026. *J. Appl. Microbiol.* 115, 744–755. doi:10.1111/jam.12287

Wittgens, A., Tiso, T., Arndt, T. T., Wenk, P., Hemmerich, J., Müller, C., et al. (2011). Growth Independent Rhamnolipid Production from Glucose Using the Non-pathogenic Pseudomonas Putida KT2440. *Microb. Cell Fact* 10, 80. doi:10.1186/1475-2859-10-80

Xu, J., Sun, S., Wang, Z., Peng, S., Hu, S., and Zhang, L. (2018). PH-induced Evolution of Surface Patterns in Micelles Assembled from Dirhamnolipids: Dissipative Particle Dynamics Simulation. *Phys. Chem. Chem. Phys.* 20, 9460–9470. doi:10.1039/c8cp00751a

Xu, J., Wang, Z., Zhang, F., Peng, S., Zhang, J., and Zhang, L. (2020). Directed Self-Assembly of Patchy Microgels into Anisotropic Nanostructures. *Macromol. Rapid Commun.* 41, 1900505–1900509. doi:10.1002/marc.201900505

Yakimov, M. M., Timmis, K. N., Wray, V., and Fredrickson, H. L. (1995). Characterization of a New Lipopeptide Surfactant Produced by Thermotolerant and Halotolerant Subsurface Bacillus Licheniformis BAS50. *Appl. Environ. Microbiol.* 61, 1706–1713. doi:10.1128/aem.61.5.1706-1713.1995

Yi, G., Son, J., Yoo, J., Park, C., and Koo, H. (2019). Rhamnolipid Nanoparticles for *In Vivo* Drug Delivery and Photodynamic Therapy. *Nanomedicine: Nanotechnology, Biol. Med.* 19, 12–21. doi:10.1016/j.nano.2019.03.015

Yu, M., Liu, Z., Zeng, G., Zhong, H., Liu, Y., Jiang, Y., et al. (2015). Characteristics of Mannosylerythritol Lipids and Their Environmental Potential. *Carbohydr. Res.* 407, 63–72. doi:10.1016/j.carres.2014.12.012

Zeng, Z., Liu, Y., Zhong, H., Xiao, R., Zeng, G., Liu, Z., et al. (2018). Mechanisms for Rhamnolipids-Mediated Biodegradation of Hydrophobic Organic Compounds. *Sci. Total Environ.* 634, 1–11. doi:10.1016/j.scitotenv.2018.03.349

Zhang, L., Somasundaran, P., Singh, S. K., Felse, A. P., and Gross, R. (2004). Synthesis and Interfacial Properties of Sophorolipid Derivatives. *Colloids*

Surf. A: Physicochemical Eng. Aspects 240, 75–82. doi:10.1016/j.colsurfa.2004.02.016

Zhang, X., Ashby, R. D., Solaiman, D. K. Y., Liu, Y., and Fan, X. (2017). Antimicrobial Activity and Inactivation Mechanism of Lactonic and Free Acid Sophorolipids against *Escherichia coli* O157:H7. *Biocatal. Agric. Biotechnol.* 11, 176–182. doi:10.1016/j.bcab.2017.07.002

Zhang, Y., and Miller, R. M. (1994). Effect of a Pseudomonas Rhamnolipid Biosurfactant on Cell Hydrophobicity and Biodegradation of Octadecane. *Appl. Environ. Microbiol.* 60, 2101–2106. doi:10.1128/aem.60.6.2101-2106.1994

Zhang, Y., and Miller, R. M. (1992). Enhanced Octadecane Dispersion and Biodegradation by a Pseudomonas Rhamnolipid Surfactant (Biosurfactant). *Appl. Environ. Microbiol.* 58, 3276–3282. doi:10.1128/aem.58.10.3276-3282.1992

Zhou, S., Xu, C., Wang, J., Gao, W., Akhverdiyeva, R., Shah, V., et al. (2004). Supramolecular Assemblies of a Naturally Derived Sophorolipid. *Langmuir* 20, 7926–7932. doi:10.1021/la048590s

Conflict of Interest: The authors declare that the research was conducted in the absence of any commercial or financial relationships that could be construed as a potential conflict of interest.

frontiers in Bioengineering and Biotechnology

ORIGINAL RESEARCH
published: 19 April 2022
doi: 10.3389/fbioe.2022.794460

Rhamnolipids as Green Stabilizers of nZVI and Application in the Removal of Nitrate From Simulated Groundwater

Cinthia Cristine Moura[1], *Ana Maria Salazar-Bryam*[2], *Rodolfo Debone Piazza*[3], *Caio Carvalho dos Santos*[3], *Miguel Jafelicci Jr*[3], *Rodrigo Fernando Costa Marques*[3,4] *and Jonas Contiero*[1,2]*

[1]*Associate Laboratory of the Institute for Research in Bioenergy (IPBEN)-Unesp, São Paulo State University (Unesp), Institute for Research in Bioenergy, Rio Claro, Brazil,* [2]*Industrial Microbiology Laboratory, General and Applied Biology, Institute of Biosciences, São Paulo State University (Unesp), Rio Claro, Brazil,* [3]*Laboratory of Magnetic Materials and Colloids, Institute of Chemistry, São Paulo State University (Unesp), Araraquara, Brazil,* [4]*Monitoring and Research Center for the Quality of Fuels, Biofuels, Petroleum and Derivatives (CEMPEQC/IQ-Unesp), Araraquara, Brazil*

OPEN ACCESS

Edited by:
Murat Ozdal,
Atatürk University, Turkey

Reviewed by:
Sumeyra Gurkok,
Atatürk University, Turkey
Sonja Kubicki,
Heinrich Heine University of Düsseldorf, Germany

***Correspondence:**
Jonas Contiero
jonas.contiero@unesp.br

Specialty section:
This article was submitted to Industrial Biotechnology, a section of the journal Frontiers in Bioengineering and Biotechnology

Received: *13 October 2021*
Accepted: *07 March 2022*
Published: *19 April 2022*

Citation:
Moura CC, Salazar-Bryam AM, Piazza RD, Carvalho dos Santos C, Jafelicci M, Marques RFC and Contiero J (2022) Rhamnolipids as Green Stabilizers of nZVI and Application in the Removal of Nitrate From Simulated Groundwater. Front. Bioeng. Biotechnol. 10:794460. doi: 10.3389/fbioe.2022.794460

Environmental contamination caused by inorganic compounds is a major problem affecting soils and surface water. Most remediation techniques are costly and generally lead to incomplete removal and production of secondary waste. Nanotechnology, in this scenario with the zero-valent iron nanoparticle, represents a new generation of environmental remediation technologies. It is non-toxic, abundant, cheap, easy to produce, and its production process is simple. However, in order to decrease the aggregation tendency, the zero-iron nanoparticle is frequently coated with chemical surfactants synthesized from petrochemical sources, which are persistent or partially biodegradable. Biosurfactants (rhamnolipids), extracellular compounds produced by microorganisms from hydrophilic and hydrophobic substrates can replace synthetic surfactants. This study investigated the efficiency of a rhamnolipid biosurfactant on the aggregation of nanoscale zer-valent iron (nZVI) and its efficiency in reducing nitrate in simulated groundwater at pH 4.0. Two methods were tested: 1) adding the rhamnolipid during chemical synthesis and 2) adding the rhamnolipid after chemical synthesis of nZVI. Scanning electron microscopy field emission, X-ray diffractometry, Fourier transform infrared spectroscopy, thermogravimetric analysis, Dynamic Light Scattering, and zeta potential measurements were used to characterize bare nZVI and rhamnolipid-coated nZVI. The effects of the type of nZVI and initial NO_3 concentration were examined. Nanoscale zer-valent iron with the addition of the rhamnolipid after synthesis achieved the best removal rate of nitrate (about 78%), with an initial nitrate concentration of 25 mg L^{-1}. The results suggest that nZVI functionalized with rhamnolipids is a promising strategy for the *in situ* remediations of groundwater contaminated by NO_3, heavy metal, and inorganic carbon.

Keywords: rhamnolipids, stabilizer, NZVI, nitrate removal, groundwater

INTRODUCTION

Due to the growing demand for food and the great use of fertilizers to obtain it, the contamination of the soil and the aquifers has demanded studies to overcome the problem. Fertilizers has caused environmental pollution with threats to agricultural productivity, food security, ecosystem health, human health, and economic prosperity (Erisman et al., 2008; Klove et al., 2011; Zhang et al., 2015; Hansen et al., 2017; Velis et al., 2017). The World Health Organization and US Environmental Protection Agency have established the maximum contaminant level for nitrate (NO_3) of 10 mg L^{-1} in drinking water (WHO, International Program On Chemical Safety, 1996; EPA, 2002).

In recent years, nanoparticles have been used in environmental remediation because of their great reduction power and surface area. Nanoparticle zero-valent iron (nZVI) has been extensively implemented for groundwater remediation due to its low cost and the ability to reduce oxidized pollutants (Crane and Scott, 2012; Yirsaw et al., 2015; Stefaniuk et al., 2016; Magthalin et al., 2016). However, iron nanoparticles have some drawbacks that need to be solved such as the issue of cluster formation due to their interfacial energy and high surface reactivity (Zhang, 2003; Zhao et al., 2016), as well as their instability, which can be easily oxidized by water or oxygen in their environment, forming a passive layer on their surface. To diminish the tendency toward aggregation, nZVI is often coated with surfactants (NSET, 2003; Crane and Scott, 2012), which play major roles in improving particle mobility (Dutra, 2015), lowering interfacial tension, and preventing the coalescence of newly formed drops (Morsy, 2014). Xue et al. (2018) investigated the performance of nanoscale nZVI coated with rhamnolipids (RL) in the immobilization of cadmium and lead. They demonstrated the effectiveness of nZVI in transforming labile cadmium and lead into a stable fraction, with an increase of 56.40 and 43.10% in the maximum residual percentage of these metals after 42 days of incubation, decreasing the mobility of the metals. Nitrate may also be chemically reduced by nZVI (Huang et al., 2011). The efficiency of nitrate removal by Fe^0 is dependent on the pH value, with rapid reduction generally occurring at pH 2–4.5 (Hausmann and Syldatk, 1998; Choe et al., 2004; Huang and Zhang, 2004). nZVI is highly reactive in water, making it an excellent electron acceptor (Sturm and Morgan, 1996). Sharma et al. (2020) explored Fe_3O_4 nanoparticles prepared with a coating of rhamnolipids. These materials show to be monodispersed and stable in water under environmentally relevant pH and ionic strength values. These nanoparticles were used to remove dissolved inorganic carbons from water and showed high sorption capacity at pH 6 and pH 8 in both carbonate-free and in equilibrium with the atmosphere CO_2 systems. The nanoparticles are non-toxic, abundant, inexpensive, and easy to produce (Zhang, 2003; Cook, 2009; Keane, 2010). The core consists primarily of zero-valent iron, whereas the mixed-valent oxide shell is formed as a result of the oxidation of metallic iron (Cornell and Schwertmann, 2004; Li et al., 2006; Crane and Scott, 2014). With rapid advances in biotechnology and increased environmental awareness, synthetic surfactants are increasingly being replaced with biologically produced compounds (Banat et al., 2000; Gautam and Tyagi, 2006). The aim of green synthesis and the stabilization of metallic nanomaterial is to decrease the use of chemical methods (Park et al., 2011). Microbial biosurfactants are extracellular compounds produced by microorganisms, such as bacteria, yeast, and filamentous fungi, grown on hydrophobic/hydrophilic carbon sources (Nitschke et al., 2005; Pirôllo et al., 2008; Tese, 2011; Lovaglio et al., 2015). Biosurfactants are surface-active molecules with both hydrophilic and hydrophobic moieties, which enable these compounds to interact at interfaces and reduce the surface tension of the medium (Mishra et al., 2009; Fernandes, 2011; Tese, 2011). Rhamnolipids used in this study are produced by the bacteria *Pseudomonas aeruginosa* that have been intensively investigated and extensively reviewed for various applications (Ochsner et al., 1996; Maier and Soberón-Chávez, 2000; Nitschke et al., 2005; Akiyode and Boateng, 2018; Moutinho et al., 2021; Varjani et al., 2021; Magri and Abdel-Mawgoud, 2022). Rhamnolipids are comprised of one or two molecules of rhamnose linked to one or two molecules of β-hydroxydecanoic acid (Desai and Banat, 1997; Hausmann and Syldatk, 1998; Banat et al., 2000). Rhamnolipids are promising candidates for the stabilization of nanoparticles. These natural compounds have been used to stabilize silver nanoparticles (Xie et al., 2006; Reddy et al., 2009; Kiran et al., 2010; Kumar et al., 2010; Ravi Kumar et al., 2010; Farias et al., 2014; Salazar-Bryam et al., 2021), nickel oxide (Palanisamy, 2008; Palanisamy and Raichur, 2009), cadmium sulfide (Singhal et al., 2010), iron oxide (Liao et al., 2010) and palladium-doped nanoscale zer-valent iron particles (Basnet et al., 2013; Bhattacharjee et al., 2016). To the best of our knowledge, there are no reports in the literature of rhamnolipid-mediated synthesis, stabilization, and application of nZVI for nitrate reduction. Therefore, the aim of the present study was to report evidence for the use of a low-cost rhamnolipid biosurfactant for the stabilization of nZVI in an aqueous solution and its use for the removal of nitrate from simulated groundwater.

MATERIALS AND METHODS

Materials

Ferric chloride ($FeCl_3$ $6H_2O$, 98%), Sodium borohydride ($NaBH_4$, 97%), and Potassium bromide (KBr, 99%) were purchased from Sigma-Aldrich Chemical Corporation Sodium hydroxide (NaOH, 97%), ammonium chloride (NH_4Cl, 99%), and sodium nitrate ($NaNO_3$, 99%) were purchased from Labsynth and phosphoric acid (H_3PO_4, 95%) was purchased from J. T. Baker, Acetone (Honeyell, 100%) and deionized water were used for nZVI synthesis. For rhamnolipid production a Ca-free mineral salt medium containing glycerol as a carbon source was used (Müller et al., 2011). All of the components are of analytical grade and used without further purification. Further de-ionized water was used in all the experiments.

Production and Extraction of Rhamnolipids

The strain *Pseudomonas aeruginosa* LBI 2A1, was obtained in previous work as a part of a doctoral thesis of Lovagio (Lovaglio,

TABLE 1 | nZVI stabilization method.

Sample	RL
bare-nZVI	Without rhamnolipids
nZVI-A	Rhamnolipids addition in ferric chloride solution
nZVI-S	Stocked in rhamnolipids solution

2011). It was maintained in Lysogenic Broth (LB) plus 20% glycerol at −20°C. For pre-culture, the microorganism was inoculated into 25 ml of LB, then transferred to 200 ml of LB medium containing phosphate buffer solution (pH 6.8) and 1% (w/v) of glycerin. The system was kept on a rotary shaker for 48 h at 180 rpm and 32°C. The pre-inoculum culture (10% v/v) at an optical density of 0.08 (OD580) was transferred to 400 ml of production medium containing glycerol 2% (w/v). The pH of the medium was adjusted to 7 by adding NaOH 1 mol L^{-1}. The culture was incubated on a rotatory shaker for 120 h at 200 rpm and 32°C. Cells were separated by centrifugation at 12,000 rpm for 30 min at 4°C, and the cell pellet was discarded. To the supernatant was added 85% H_3PO_4 1:100 (v/v) to adjust of pH of about 2-3 and ethyl acetate 1:1,25 (v/v) for extraction of rhamnolipids. The mixture was shaken for 15 min and allowed to settle down until the phase separation. The inorganic phase was removed and the operation was repeated once again with the organic phase and ethyl acetate 1:1,25 for total extraction of rhamnolipids. After that, the organic phase containing the biosurfactant was concentrated using a rotary evaporator.

Surface Activity Measurements and Structural Characterization of Rhamnolipids

Surface tension was determined by the Du-Noüy ring method with a Krüss K6 Tensiometer (Krüss, Hamburg, Germany). Ultrapure water was measured to calibrate the tensiometer. Experiments were performed at room temperature; all measurements were made in triplicate.

Synthesis and Green Stabilization of nZVI

The synthesis was based on the borohydride reduction method (Wang and Zhang, 1997. The synthesis of nZVI was conducted in a beaker by adding sodium borohydride (6 mmol) dissolved in 2 ml of purified water to 40 ml ferric iron solution (4 mmol), for the reduction of ferric iron to nZVI. The solution was vigorously stirred with a magnetic bar at room temperature. The entire process was carried out in an argon atmosphere. The reduction reaction is as follows (Wang and Zhang, 1997):

$$Fe(H_2O)_6^{3+} + 3BH_4^- + 3H_2O \rightarrow Fe^0 + 3B(OH)_3 + 10.5H_2 \quad (1)$$

A black precipitate formed instantly. After 20 min of reaction, the solid was magnetically decanted and washed three times with acetone.

Two stabilization methodologies of nZVI (**Table 1**) were compared with the bare-nZVI: synthesis of nZVI with rhamnolipids addition in ferric chloride solution (nZVI-A) and nZVI stocked in rhamnolipids solution (n-ZVI-S). The rhamnolipid solution used for nZVI-A and nZVI-S was above 250 mg L^{-1} (CMC, critical micellar concentration). The separation of the generated iron particles was achieved with a magnet, followed by washing with acetone at least three times.

Nanoparticle Characterization

Characterization of the crystalline phase was determined by X-ray powder diffraction (XRD) using a Simiens D5005 diffractometer with a Cu Kα radiation source. The samples were recorded at 5–80° of 2θ, with a step of 0.02°. The Crystallographic Search-Match software was used to index the samples. Fourier transform infrared (FTIR) spectroscopy was used to confirm the obtainment of a rhamnolipid. Thermogravimetric analysis (TGA) was carried out to determine the total amount of nZVI and mass of the rhamnolipids, using the STA 409C/CD system from NETZSCH Instruments. Samples (15 mg) were analyzed from room temperature up to 700°C under 50 ml min^{-1} airflow with a heating rate of 10°C.min^{-1}. The shape and morphology of the dried nanoparticles were determined using scanning electron microscopy (SEM) model JEOL 7500F, with an acceleration of 2kV. The hydrodynamic diameter and zeta potential measurements of the particles were evaluated by Dynamic Light Scattering (DLS) and electrophoretic mobility using laser Doppler electrophoresis in a Zeta Sizer NanoZS from Malvern Instruments.

Nitrate Reduction Tests

Batch experiments were conducted using 1 L bottles at room temperature under light-excluding conditions. To create an anaerobic environment, the deionized water used for the preparation of the nitrate solution was boiled and the bottles were then purged with nitrogen gas to remove dissolved oxygen. Each bottle was filled with 1 L of initial $NaNO_3$ concentrations (C0) of about 25, 50, and 100 mg L^{-1} NO_3. At the onset of the experiment, the pH was adjusted to 4 using HCl 1 mol L^{-1} and 5 g of nZVI-S, nZVI-A, or bare nZVI were added to each bottle. Control experiments without the addition of nZVI nanoparticles were carried out in parallel. Samples (10 ml) were withdrawn every 15 min for 2 h. All experiments were performed in triplicate. The removal efficiency was calculated according to **Eq. 2**

$$removal\ efficiency\ \% = \frac{(C_0 - C_f)}{C_0} \times 100 \quad (2)$$

in which C0 is the initial NO_3 concentration and Cf is the final NO_3 concentration. Nitrate and ammonium were quantified with a Thermo Scientific™ Orion™ nitrate electrode and ammonia electrode, respectively. A kinetic model for nitrate reduction by nZVI can be described by pseudo-first-$^{order\ reaction\ kinetics}$ (kobs). According to this model, the reaction rate is proportional to the nitrate concentration, as given in the following **Eq. 3**:

$$ln\left(\frac{C}{C_0}\right) = -k_{obs} \quad (3)$$

in which C_0 is the initial NO_3 concentration and C is the NO_3 concentration at time t.

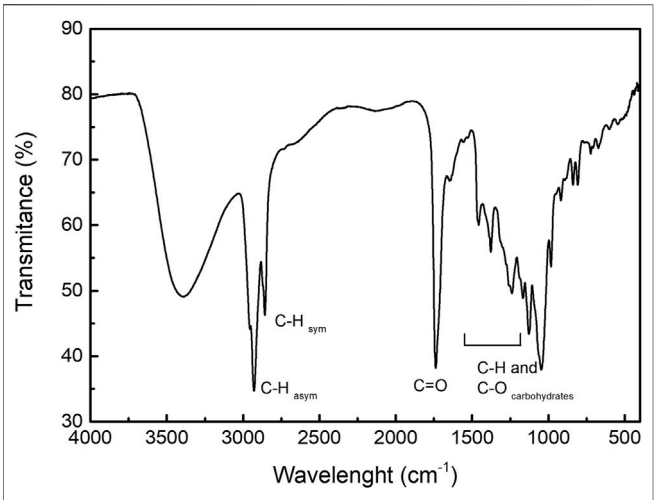

FIGURE 1 | FTIR spectrum of rhamnolipids.

RESULTS AND DISCUSSION

Rhamnolipid Production

The biosurfactant from *P. aeruginosa* LBI 2A1 was cultivated in a low-cost medium and formulated using an agro-industrial substrate based on 2% (w/v) glycerol as a carbon source. The biosurfactant was produced for 120 h at 32°C. The CMC of the crude biosurfactant was evaluated by the Du-Noüy ring method and its value was determined at 250 mg $L^{-1.}$ Although other authors have obtained 40.7 g/L, using soybean oil and ammonium nitrate (Sun et al., 2021), the use of a hydrophobic carbon source is observed, which for the strain used in this article, we have already reached up to 70.9 g/L using sunflower oil as carbon source (data not shown). This work concern to use of a by-product of the Biodiesel industry, such as glycerol. The FTIR analysis of the pure rhamnolipid is shown in **Figure 1**. The double bands at 2,922 and 2,854 cm^{-1} are assigned to C-H stretching vibrations of aliphatic groups. The band at 1,735 cm^{-1} corresponds to C=O stretching bonds of ester and carboxylic acid groups. The bands between 1,230 and 1,450 cm^{-1} are typical of C-H and O-H vibrations of carbohydrates, i.e., rhamnose units (Leitermann et al., 2008).

Characterization of nZVI

The diffractograms of the synthesized samples are shown in **Figure 2**. After synthesized, the samples were evaluated immediately and submitted to XRD analysis after 30 days. The bare nZVI sample was indexed as metallic iron (PDF 87-7194), the peaks of which correspond to (1 1 0) and (2 0 0) crystalline planes. After 30 days, it was observed the decreasing of the (1 1 0) crystalline iron plane and the arising of the (3 1 1) plane from the magnetite phase (PDF 74–419) indicates sample oxidation. The diffractogram of the nZVI-A sample revealed the presence of different crystalline phases. Besides metallic iron, magnetite (3 1 1) was also observed. Oxidation was also observed after 30 days, in which the characteristic

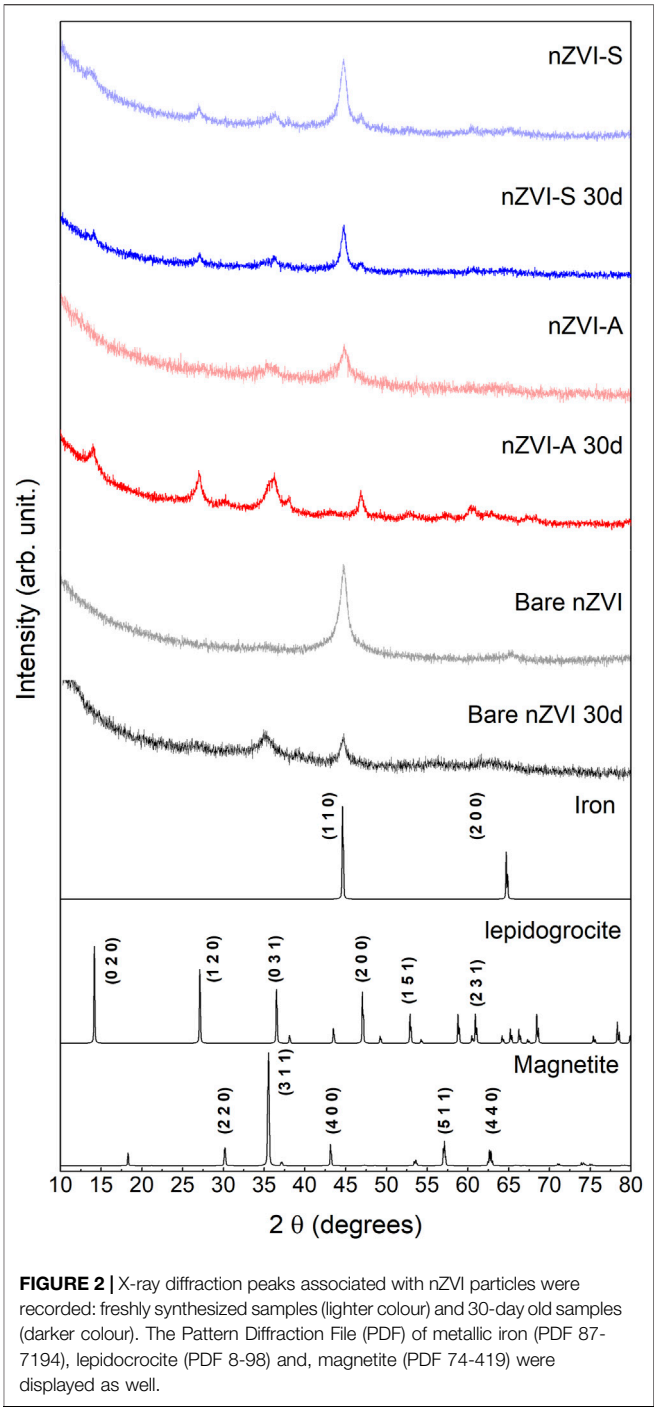

FIGURE 2 | X-ray diffraction peaks associated with nZVI particles were recorded: freshly synthesized samples (lighter colour) and 30-day old samples (darker colour). The Pattern Diffraction File (PDF) of metallic iron (PDF 87-7194), lepidocrocite (PDF 8-98) and, magnetite (PDF 74-419) were displayed as well.

peaks of metallic iron disappeared, and the sample was indexed as a mixture of magnetite and lepidocrocite (PDF 8–98) phases. On the contrary, the nZVI-S sample had better stabilization by rhamnolipids, and the metallic iron phase was present on freshly synthesized and 30-day old samples. Therefore, adding the metallic iron nanoparticles to the rhamnolipids solution results in a more effective surface functionalization protocol against oxidation. Scherrer's equation was used to calculate the average crystallite

TABLE 2 | Average crystallite diameter according to Scherrer's equation. * Crystallographic plane (1 1 0) and ** (3 1 1).

Sample	Crystallite diameter (nm)
nZVI-S	7.88 *
nZVI-S 30 d	7.16 *
nZVI-A	6.52 **
nZVI-A 30 d	4.77 *
nZVI	9.05 *
nZVI 30 d	11.3 **

diameter (D_{XRD}). **Table 2** corroborates the SEM data, demonstrating the nanometric size. The desired crystallinity phase was obtained. The estimated D_{XRD} of the nanoparticles shows different sizes among the methods used. The D_{XRD} increased as follows: nZVI-A< nZVI-S< nZVI.

The surface features of the nanoparticles were evaluated through zeta potential measurements. A zeta potential greater than ±30 mV indicates reasonably stable nanoparticles with low aggregation capacity due to charge equilibrium (Lowry et al., 2016; Hunter, 1988). **Figure 3** shows different isoelectric points according to the method used to functionalize the surface nanoparticles. The bare nZVI and nZVI-A samples exhibited the same profile curve with an isoelectric point (point of zero charge) (pHpzc) at 7.8, which is compatible with the range of values found in the literature (7.5–8.9) (Su et al., 2011; Markova et al., 2014; Wen et al., 2014; Arancibia-Miranda et al., 2016; Habish et al., 2017). However, a shift was observed for nZVI-S, with a reduction in pHpzc to 6, which shows that the nZVI-S sample had more adequate coating when the iron nanoparticle was functionalized after synthesis due to the similarity between the rhamnolipid pKa and pHpzc values. The pKa of the rhamnolipid is 5.6 (Sousa et al., 2014), while the observed pHpzc was 6, demonstrating that the surface corresponds to the rhamnolipid rather than the nanoparticles. Regarding colloidal stability, pH 4 was chosen to evaluate the zeta potential, once this is the point which materials will be applied. The results show that the bare nZVI sample had the highest value (37.2 mV), followed by nZVI-A (35.1 mV) and nZVI-S (6.3 mV). Although the nZVI-S sample had the lowest zeta potential value, the coating of the magnetic core by the rhamnolipids conferred steric stability to the compound.

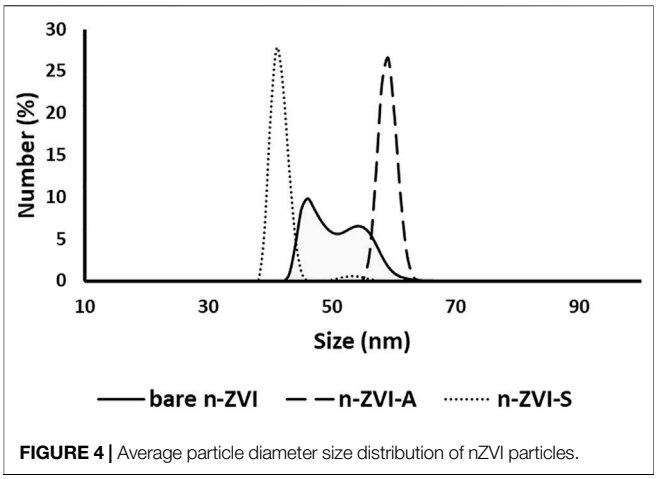

FIGURE 4 | Average particle diameter size distribution of nZVI particles.

The average diameter size of nZVI is shown in **Figure 4**. The bare nZVI had a shortened peak with a large base and an average diameter of 50 nm, while the average diameter of the nZVI-A and nZVI-S samples was approximately 60 and 42 nm, respectively. The larger average diameter for nZVI-A could be related to the addition of the rhamnolipid, as this biosurfactant has acid pH, which, in this situation, led to the formation of large aggregates, as observed by Dahrazma, et al. (2008) and Ishigami, et al. (1987). The formation of these aggregates is evidenced in the DLS analysis and SEM images (**Figure 5**).

Figure 5 displays the SEM images of bare nZVI, nZVI-A and nZVI-S. Bare nZVI was agglomerated in large clusters (**Figure 5A**). The morphology of nZVI differed depending on the time of the addition of rhamnolipids. As shown in **Figure 5B**, nZVI-S had less dispersed and smaller nanoparticles, whereas those of nZVI-A tended to be more agglomerated and

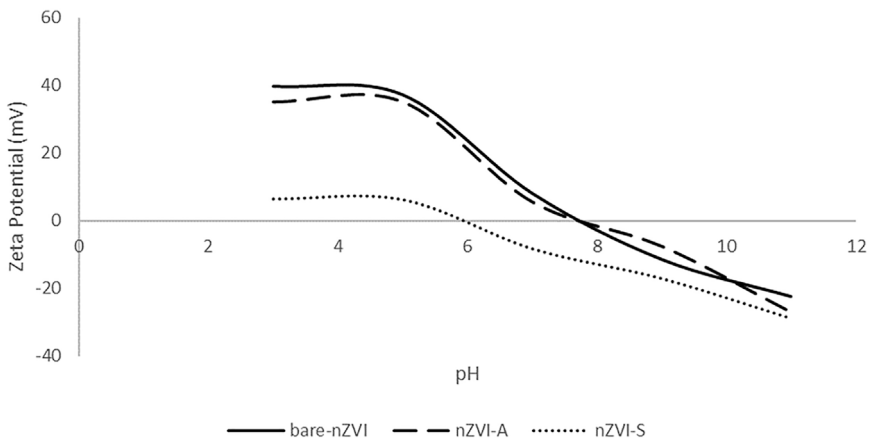

FIGURE 3 | Zeta potential and pzc of nZVI.

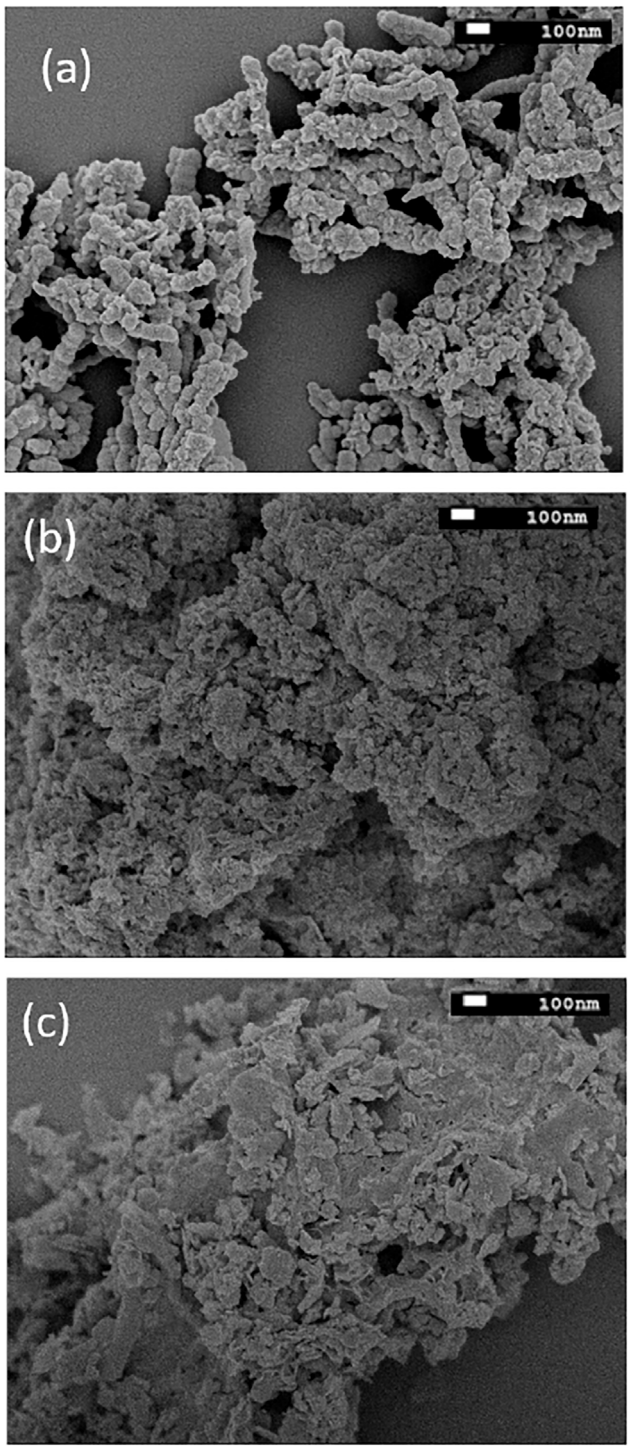

FIGURE 5 | SEM images of **(A)** bare-nZVI **(B)** nZVI-A **(C)** nZVI-S.

consequently slightly larger (**Figure 5C**). This pattern was confirmed by the DLS analysis.

The thermal behavior of samples was investigated by TGA and DTG. The results are shown in **Figure 6**.

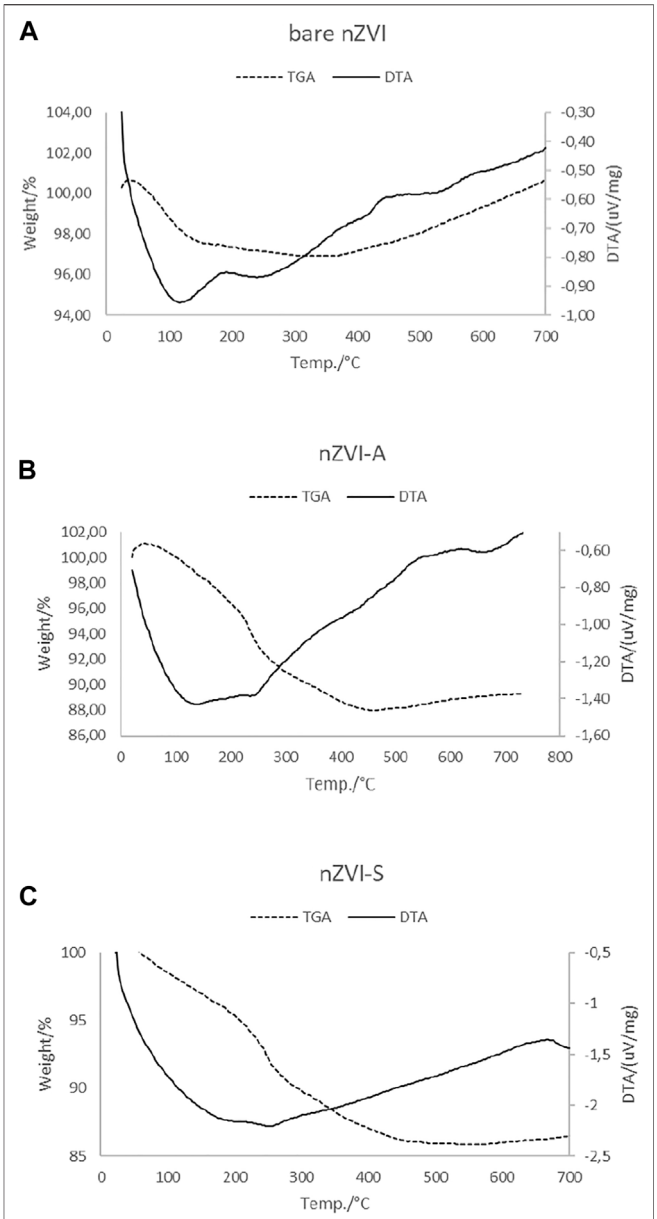

FIGURE 6 | TGA and DTA curves for **(A)** bare-nZVI, **(B)** nZVI-A and **(C)** nZVI- S.

It is possible to identify two different regions in the TGA curve for bare-nZVI. The first region between 50 and 120°C, corresponds to a weight loss, due to the removal of physically bounded water and acetone from synthesis (Habish et al., 2017). The region near 189°C

TABLE 3 | Regions of weight loss and gain (%) of nZVI-A and nZVI-S samples.

Region	Temperature °C	Weight	nZVI-A (%)	nZVI-S
I	50–230	Loss	8	9%
II	230–480	Loss	5	5%
III	480–700	Gain	1	0.5%

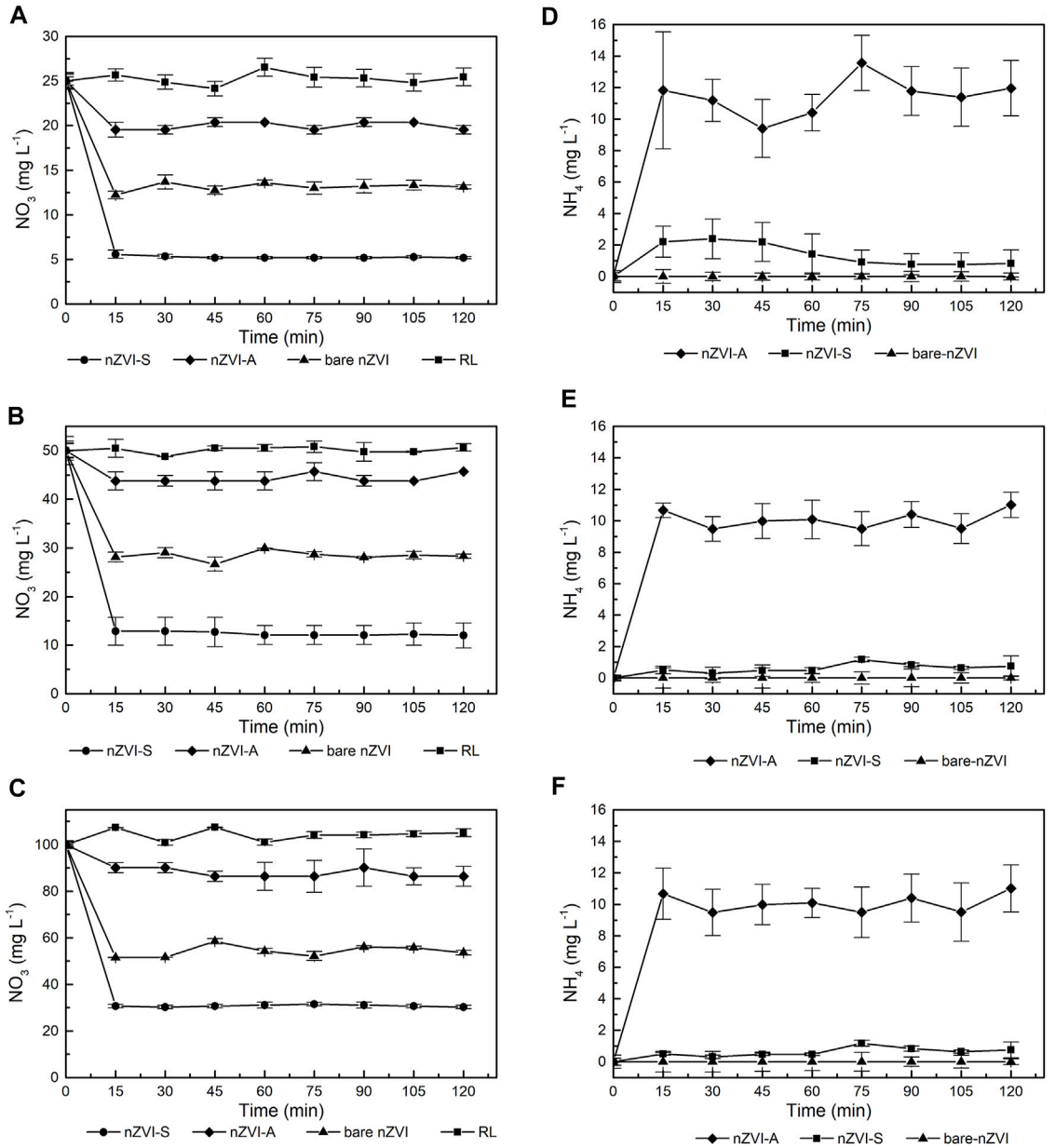

FIGURE 7 | Effect of time and initial nitrates concentration on nitrates reduction using nZVI at pH 4 **(A)** 25 mg/L NO_3 **(B)** 50 mg/L NO_3 **(C)** 100 mg/L NO_3 and effect of time and initial nitrates concentration on ammonia concentration using nZVI at pH 4 **(D)** 25 mg/L NO_3 **(E)** 50 mg/L NO_3 **(F)** 100 mg/L NO_3.

shows a slight change in the baseline without a peak and the DTA curve shows an exothermic peak, indicating the dehydration of the sample. In the second region, over 400°C, the gain mass is continuous at approximately 3%, the DTA curve presents an exothermic peak indicating oxidation on the bulk of the nanoparticle (Földvári, 2011). For the nZVI-A and nZVI-S samples, the TGA curve show three regions and the weight percentages are shown in **Table 3**.

The first region of weight loss, comprising between 40 and 230°C, corresponds to the removal of residual water and acetone from synthesis (Habish et al., 2017). In this range, the DTA curve indicates an endothermic peak at 100°C, which corresponds to a dehydration reaction. The second region of weight loss occurs with a slight change in the baseline without a peak between 230 and 480°C, due to decomposition and elimination of organic backbone from rhamnolipids (Pui et al., 2013). The third region, over 480°C, is characterized by a slight gain of weight due to the oxidation of the nZVI. The DTA curve of nZVI-A and nZVI-S samples shows endothermic peaks. The DTA curve shows exothermic signals at 230 and 480°C which is in agreement with to weight loss phenomena. Over 480°C the DTA curve also

TABLE 4 | Observed pseudo-first-order rate coefficient of nitrate reduction with nZVI.

NO_3 (mg L^{-1})	Bare-nZVI		nZVI-S		nZVI-A	
	Efficiency removal (%)	k_{obs}	Efficiency removal (%)	k_{obs}	Efficiency removal (%)	k_{obs}
25	47.57	0.043	78.62	0.107	20.18	0.015
50	43.54	0.038	77.65	0.101	12.45	0.009
100	46.29	0.041	68.89	0.078	13.62	0.010

show exothermic characteristic, that is associated with weight gain associated with the oxidation of the nZVI particles.

Nitrate Reduction by nZVI Under Low pH Conditions

Fe^0 is thermodynamically unstable in water. Dissolved oxygen is an oxidant and causes rapid corrosion of iron [**Eq. 4**]. On the other hand, under anaerobic conditions, water serves as the oxidant and corrosion takes place, producing hydrogen gas and hydroxide ions [**Eq. 5**]. The corrosion process results in an increase in pH media. Under acidic and anoxic conditions, the corrosion rate of iron is faster than iron corrosion by water [**Eq. 6**].

$$2Fe^0 + O_2 + 2H_2O \rightarrow 2Fe^{2+} + 4OH^- \quad (4)$$

$$Fe^0 + 2H_2O \rightarrow Fe^{2+} + H_2 2OH^- \quad (5)$$

$$Fe^0 + 2H^+ \rightarrow Fe^{2+} + H_2 \quad (6)$$

Several pathways of nitrate reduction by nZVI have been proposed, such as the following equations.

$$4Fe^0 + NO_3^- + 7H_2O \rightarrow NH_4^+ + 4Fe^{2+} + 10OH^- \quad (7)$$

$$5Fe^0 + 2NO_3^- + 6H_2O \rightarrow N_2^+ + 5Fe^{2+} + 12OH^- \quad (8)$$

Figure 7 compares the nitrate reduction rates achieved with bare nZVI, nZVI-S and, nZVI-A samples. The nitrate reduction was observed in the first 15 min; thereafter, the reaction remained nearly constant. The nZVI-S nanoparticles exhibited a higher kinetic constant than bare ZVI and nZVI-A, respectively, as shown in **Table 4**. In the first 15 min of the reaction, nZVI-S achieved nitrate efficiency removal of 78.62%, 77.65% and 68.89% for 25, 50, and 100 mg L^{-1} of NO_3 solution, respectively. The nitrate removal with nZVI-A was comprised between 20.18 and 12.45%, while the bare nZVI were approximately 47, 57%, and 43.54%. The control group test shows no nitrate reduction in presence of the biosurfactant.

To quantify the reaction rate, a pseudo-first-order reaction model (**Eq. 3**) was used to fit the kinetic data (Johnson et al., 1996). A high initial reduction rate was found when the initial concentration of nitrate was low. The observed surface reaction rate constant (kobs) (**Table 4**) for nZVI-S increased from 0.078 to 0.107 min^{-1} at a 15-min reaction time when the initial nitrate concentration was decreased from 100 to 25 mg L^{-1}. For bare nZVI and nZVI-A, the kobs remained nearly constant, with values of 0.043 and 0.015, respectively, when the initial concentration was 25 mg L^{-1}. The reaction did not slow down because of insufficient iron, since iron was added in stoichiometric excess in all experiments. The amount of nZVI (5 g) was not enough to react with the initial nitrate concentration according to the chemical reactions described above (**Eqs 5**, **6**). Hausmann and Syldatk (1998), found complete nitrate reduction when the Fe^0 concentration was increased to 10 g L^{-1}.

Figures 7A–D demonstrates that the nitrate removal rate diminished substantially over time. Hydroxide ions were formed as nitrate was reduced. Since no additional acid was added, the OH^- accumulated, thus reducing the nitrate removal reaction (Hausmann and Syldatk, 1998; Liu et al., 2014). This behavior is consistent with the results presented in **Figure 3**, indicating that there was a surface modification on the nanoparticle. The concentration of ammonia did not increase with an increase in the initial concentration of nitrate (**Figures 7D–F**). Approximately 45% of nitrate was transformed into ammonia using 5 g of nZVI, showing that nZVI-S followed reaction **Eqs 5**, **6**, whereas bare nZVI and nZVI-A did not transform nitrate into ammonia, probably following only **Eq. 6**.

CONCLUSION

The present study presents the potential of using the rhamnolipid biosurfactant, obtained in a sustainable way (use of glycerol as a carbon source), in the preparation of nZVI as a stabilizer, increasing its stability and performance in terms of NO_3 removal. Rhamnolipids are a promising alternative to synthetic surfactants for the synthesis and surface functionalization of zero valence iron nanoparticles. With the success achieved in this application, one more use of the rhamnolipid produced by *P. aeruginosa* LBI 2A1 is potentiated. The nanoparticles prepared with the rhamnolipid coating remained stable for 1 month, thus showing the efficiency of the process. The XRD analysis showed that the Fe^0 intensity decreased gradually over time for both bare nZVI and nZVI-A, whereas a better response was found for nZVI-S, with the rhamnolipid concentration above the CMC. Compared to bare nZVI particles, nZVI-A and nZVI-S were stable in an aqueous solution and not easily oxidized and/or aggregated. Based on the efficient removal capacity and the observed first-order coefficient (kobs), NO_3 removal by the different prepared materials followed the order of nZVI-S > bare nZVI > nZVI-A. In the presence of bare nZVI, most of the NO_3 was not converted into NH_4. For successful long-term groundwater field treatments using nZVI coated with rhamnolipids, a more detailed study of the chemical

processing as well as the application of nanoparticles *in situ* should be carried out since the focus of this study was to verify the potential of nanoparticles obtained in the removal of nitrate from the aqueous medium. The results presented lead to the conclusion that the application of rhamnolipids as a coating for zero iron nanoparticles has potential and adds to those existing in the literature for use in the removal of metals such as cadmium and lead, since there is no mention of the use of rhamnolipids in the stabilization of zero iron nanoparticles to remove NO_3 from groundwater.

DATA AVAILABILITY STATEMENT

The original contributions presented in the study are included in the article/supplementary material, further inquiries can be directed to the corresponding author.

AUTHOR CONTRIBUTIONS

CCM is responsible for conducting the rhamnolipids production experiments and nZVI. AMS-B collaborated on the bioassays carried out. RP and CCS helped in obtaining the nanoparticles as well as in the characterization analyzes of nZVI. MJ and RFCM collaborated in the discussion of obtaining the nanoparticles as well as in the analysis of the characterization of nZVI. JC wrote the manuscript, guided the students, and supported the development of the project through assistance with the Development Agencies.

FUNDING

The financial support provided by the São Paulo Research Foundation (Fapesp) and the Coordination for the Improvement of Higher Education Personnel (CAPES).

REFERENCES

Akiyode, O., and Boateng, J. (2018). Composite Biopolymer-Based Wafer Dressings Loaded with Microbial Biosurfactants for Potential Application in Chronic Wounds. *Polymers* 10 (8), 918. doi:10.3390/polym10080918

Arancibia-Miranda, N., Baltazar, S. E., García, A., Muñoz-Lira, D., Sepúlveda, P., Rubio, M. A., et al. (2016). Nanoscale Zer Valent Supported by Zeolite and Montmorillonite: Template Effect of the Removal of Lead Ion from an Aqueous Solution. *J. Hazard. Mater.* 301, 371–380. doi:10.1016/j.jhazmat.2015.09.007

Banat, I. M., Makkar, R. S., and Cameotra, S. S. (2000). Potential Commercial Applications of Microbial Surfactants. *Appl. Microbiol. Biotechnol.* 53 (5), 495–508. doi:10.1007/s002530051648

Basnet, M., Ghoshal, S., and Tufenkji, N. (2013). Rhamnolipid Biosurfactant and Soy Protein Act as Effective Stabilizers in the Aggregation and Transport of Palladium-Doped Zerovalent Iron Nanoparticles in Saturated Porous Media. *Environ. Sci. Technol.* 47 (23), 13355–13364. doi:10.1021/es402619v

Bhattacharjee, S., Basnet, M., Tufenkji, N., and Ghoshal, S. (2016). Effects of Rhamnolipid and Carboxymethylcellulose Coatings on Reactivity of Palladium-Doped Nanoscale Zer-Valent Iron Particles. *Environ. Sci. Technol.* 50 (4), 1812–1820. doi:10.1021/acs.est.5b05074

Choe, S., Liljestrand, H. M., and Khim, J. (2004). Nitrate Reduction by Zero-Valent Iron under Different PH Regimes. *Appl. Geochem.* 19 (3), 335–342. doi:10.1016/j.apgeochem.2003.08.001

Cook, S. M. (2009). *Assessing the Use and Application of Zero-Valent Iron Nanoparticle Technology for Remediation at Contaminated Sites*. Washington, DC: EPA Rep., 39. No. August.

Cornell, R. M., and Schwertmann, U. (2004). "Introduction to the Iron Oxides," in *The Iron Oxides*. doi:10.1002/3527602097.ch1

Crane, R. A., and Scott, T. B. (2012) Nanoscale Zero-Valent Iron: Future Prospects for an Emerging Water Treatment Technology. *J. Hazard. Mater.* 211-212, 112, 125. doi:10.1016/j.jhazmat.2011.11.073

Crane, R. A., and Scott, T. (2014). The Removal of Uranium onto Carbon-Supported Nanoscale Zer-Valent Iron Particles. *J. Nanopart Res.* 16 (12). doi:10.1007/s11051-014-2813-4

Dahrazma, B., Mulligan, C. N., and Nieh, M. P. (2008). Effects of Additives on the Structure of Rhamnolipid (Biosurfactant): A Small-Angle Neutron Scattering (SANS) Study. *J. Colloid Interf. Sci.* doi:10.1016/j.jcis.2007.11.0410.1016/j.jcis.2007.11.045

Desai, J. D., and Banat, I. M. (1997). Microbial Production of Surfactants and Their Commercial Potential. *Fuel Energ. Abstr* 38 (4), 221. doi:10.1128/.61.1.47-64.1997

Dutra, M. C. (20152015). *Síntese e Caracterização de Nanopartícula de Ferro-Zero Valente (Nzvi) aplicada ao tratamento de águas contaminadas com 4-Clorofenol. 78 f.* Florianópolis: Dissertação (Mestrado em Engenharia Química) - Centro Tecnológico, Universidade Federal de Santa Catarina, Florianópolis, 78.

EPA (2002). *Drinking Water from Household Wells*. Washington, DC: U.S. Environmental Protection Agency.

Erisman, J. W., Sutton, M. A., Galloway, J., Klimont, Z., and Winiwarter, W. (2008). How a Century of Ammonia Synthesis Changed the World. *Nat. Geosci* 1 (10), 636–639. doi:10.1038/ngeo325

Farias, C. B. B., Silva, A. F., Rufino, R. D., Luna, J. M., Souza, J. E. G., and Sarubbo, L. A. (2014). Synthesis of Silver Nanoparticles Using a Biosurfactant Produced in Low-Cost Medium as Stabilizing Agent. *Electron. J. Biotechnol.* 17 (3), 122–125. doi:10.1016/j.ejbt.2014.04.003

Fernandes, T. C. C. (2011). *Investigação dos efeitos tóxicos do biossurfactante ramnolipídio e suas implicações quando usado na biorremediação de águas contaminadas por petróleo*. Universidade Estadual Paulista, Instituto de Biociências de Rio Claro, 188.

Földvári, M. (2011). Handbook of the Thermogravimetric System of Minerals and its Use in Geological Practice. *Cent. Eur. Geology.* 56, 397–400. doi:10.1556/CEuGeol.56.2013.4.6

Gautam, K. K., and Tyagi, V. K. (2006). Microbial Surfactants: A Review. *J. Oleo Sci.* 55 (4), 155–166. doi:10.5650/jos.55.155

Habish, A. J., Lazarević, S., Janković-Častvan, I., Jokić, B., Kovač, J., Rogan, J., et al. (2017). Nanoscale Zer-Valent Iron (nZVI) Supported by Natural and Acid-Activated Sepiolites: the Effect of the nZVI/support Ratio on the Composite Properties and Cd2+ Adsorption. *Environ. Sci. Pollut. Res.* 24 (1), 628–643. doi:10.1007/s11356-016-7802-y

Hansen, B., Thorling, L., Schullehner, J., Termansen, M., and Dalgaard, T. (2017). Groundwater Nitrate Response to Sustainable Nitrogen Management. *Sci. Rep.* 7 (1), 1–12. doi:10.1038/s41598-017-07147-2

Hausmann, R., and Syldatk, C. (1998). "Types and Classification of Microbial Surfactants," in *Nitrate Reduction by Metallic Iron*. Editors C. P. Huang, H. W. Wang, and P. C Chiu, 32, 2257–2264. doi:10.1016/S0043-1354(97)00464-8

Huang, Y. H., and Zhang, T. C. (2004). Effects of Low PH on Nitrate Reduction by Iron Powder. *Water Res.* 38 (11), 2631–2642. doi:10.1016/j.watres.2004.03.015

Hunter, R. J. (1988). in *Zeta Potential in Colloid Science: Principles and Applications*. Editors R. H. Ottewill and R. L. Rowell. Third. (Academic Press), 2.

Hwang, Y.-H., Kim, D.-G., and Shin, H.-S. (2011). Mechanism Study of Nitrate Reduction by Nano Zero Valent Iron. *J. Hazard. Mater.* 185 (2–3), 1513–1521. doi:10.1016/j.jhazmat.2010.10.078

Ishigami, Y., Gama, Y., Nagahora, H., Yamaguchi, M., Nakahara, H., and Kamata, T. (1987). The PH-Sensitive Conversion of Molecular Aggregates of Rhamnolipid Biosurfactant. *Chem. Lett.* 16, 763–766. doi:10.1246/cl.1987.763

Johnson, T. L., Scherer, M. M., and Tratnyek, P. G. (1996). Kinetics of Halogenated Organic Compound Degradation by Iron Metal. *Environ. Sci. Technol.* 30 (8), 2634–2640. doi:10.1021/es9600901

Judia Magthalin, C., Varadharajan, A., Swarnalatha, S., and Sekaran, G. (2016). Cationic Dispersant Immobilized Matrix for Sequestering Cr (III) from Contaminated Soil. *Mater. Today Proc.* 3 (10), 3697–3702. doi:10.1016/j.matpr.2016.11.015

Keane, E. (2010). *Fate, Transport, and Toxicity of Nanoscale Zer-Valent Iron (NZVI) Used during Superfund Remediation*. Master's project, Duke University, 38. Available at: https://hdl.handle.net/10161/2172.

Kiran, G. S., Sabu, A., and Selvin, J. (2010). Synthesis of Silver Nanoparticles by Glycolipid Biosurfactant Produced from Marine Brevibacterium Casei MSA19. *J. Biotechnol.* 148 (4), 221–225. doi:10.1016/j.jbiotec.2010.06.012

Kløve, B., Ala-aho, P., Bertrand, G., Boukalova, Z., Ertürk, A., Goldscheider, N., et al. (2011). Groundwater Dependent Ecosystems. Part I: Hydroecological Status and Trends. *Environ. Sci. Pol.* 14 (7), 770–781. doi:10.1016/j.envsci.2011.04.002

Kumar, C. G., Mamidyala, K. S., Biswanath, D., Sridhar, B., Devi, G. S., and Karuna, M. S. (2010). Synthesis of Biosurfactant-Based Silver Nanoparticles with Purified Rhamnolipids Isolated from Pseudomonas Aeruginosa BS-161R. *J. Microbiol. Biotechnol.* 20 (7), 1061–1068. doi:10.4014/jmb.1001.01018

Leitermann, F., Syldatk, C., Hausmann, R., Sridhar, B., Sarala Devi, G., KarunaLeitermann, F., et al. (2008). Fast Quantitative Determination of Microbial Rhamnolipids from Cultivation Broths by ATR-FTIR Spectroscopy. *J. Biol. Eng.* 2, 1–8. doi:10.1186/1754-1611-2-13

Li, X.-q., Elliott, D. W., and Zhang, W.-x. (2006). Zero-Valent Iron Nanoparticles for Abatement of Environmental Pollutants: Materials and Engineering Aspects. *Crit. Rev. Solid State. Mater. Sci.* 31 (4), 111–122. doi:10.1080/10408430601057611

Liao, Z., Wang, H., Wang, X., Wang, C., Hu, X., Cao, X., et al. (2010). Biocompatible Surfactin-Stabilized Superparamagnetic Iron Oxide Nanoparticles as Contrast Agents for Magnetic Resonance Imaging. *Colloids Surf. A: Physicochemical Eng. Aspects* 370 (1–3), 1–5. doi:10.1016/j.colsurfa.2010.06.025

Liu, H., Guo, M., and Zhang, Y. (2014). Nitrate Removal by Fe0/Pd/Cu Nano-Composite in Groundwater. *Environ. Technol.* 35 (7), 917–924. doi:10.1080/09593330.2013.856926

Lovaglio, R. B. (2011). *Produção de Ramnolipídios Por Mutantes de Pseudomonas Aeruginosa LBI . 2011. 148f*. Rio Claro: Tese (Doutorado em Microbiologia Aplicada) - Departamento de Bioquímica e Microbiologia, Universidade Estadual Paulista, 148.

Lovaglio, R. B., Silva, V. L., Ferreira, H., Hausmann, R., and Contiero, J. (2015). Rhamnolipids Know-How: Looking for Strategies for its Industrial Dissemination. *Biotechnol. Adv.* 33 (8), 1715–1726. doi:10.1016/j.biotechadv.2015.09.002

Lowry, G. V., Hill, R. J., Harper, S., Rawle, A. F., Hendren, C. O., Klaessig, F., et al. (2016). Guidance to Improve the Scientific Value of Zeta-Potential Measurements in NanoEHS. *Environ. Sci. Nano* 3 (5), 953–965. doi:10.1039/c6en00136j

Magri, M., and Abdel-Mawgoud, A. M. (2022). Identification of Putative Producers of Rhamnolipids/glycolipids and Their Transporters Using Genome Mining. *Curr. Res. Biotechnol.* doi:10.1016/j.crbiot.2022.02.002

Maier, R. M., and Soberón-Chávez, G. (2000). Pseudomonas Aeruginosa Rhamnolipids: Biosynthesis and Potential Applications. *Appl. Microbiol. Biotechnol.* 54 (5), 625–633. doi:10.1007/s002530000443

Markova, Z., Novak, P., Kaslik, J., Plachtova, P., Brazdova, M., Jancula, D., et al. (2014). Lead Removal by Nano-Scale Zero Valent Iron: Surface Analysis and PH Effect. *Mater. Res. Bull.* 59, 341–348. doi:10.1016/j.materresbull.2014.07.045

Mishra, M., Muthuprasanna, P., Prabha, K. S., Rani, P. S., Babu, I. A. S., Chandiran, I. S., et al. (2009). Basics and Potential Applications of Surfactants - A Review. *Int. J. Pharmtech Res.* 1 (4), 1354–1365.

Morsy, S. M. I. (2014). Role of Surfactants in Nanotechnology and Their Applications. *Int. J. Curr. Microbiol. App. Sci. V.* 3 (5), 237–260.

Moutinho, L. F., Moura, F. R., Silvestre, R. C., and Romão-Dumaresq, A. S. (2021). Microbial Biosurfactants: A Broad Analysis of Properties, Applications, Biosynthesis, and Techno-Economical Assessment of Rhamnolipid Production. *Biotechnol. Prog.* 37, e3093. doi:10.1002/btpr.3093

Müller, M. M., Hörmann, B., Kugel, M., Syldatk, C., and Hausmann, R. (2011). Evaluation of Rhamnolipid Production Capacity of *Pseudomonas aeruginosa* PAO1 in Comparison to the Rhamnolipid Over-producer Strains DSM 7108 and DSM 2874. *Appl. Microbiol. Biotechnol.* 89 (3), 585–592. doi:10.1007/s00253-010-2901-z

Nitschke, M., Costa, S. G. V. A. O., Haddad, R., Goncalves, L. A. G., Eberlin, M. N., and Contiero, J. (2005). Oil Wastes as Unconventional Substrates for Rhamnolipid Biosurfactant Production by *Pseudomonas aeruginosa* LBI. *Biotechnol. Prog.* 21 (5), 1562–1566. 7 out. doi:10.1021/bp050198x

NSET (2003). "National Nanotechnology Initiative Workshop," in *Nanotechnology and the Environment* (Arlington, 53.

Ochsner, U. A., Hembach, T., and Fiechter, A. (1995). Production of Rhamnolipid Biosurfactants. *Adv. Biochem. Eng. Biotechnol.* 53, 89–118. doi:10.1007/BFb0102326

Palanisamy, P. (2008). Biosurfactant Mediated Synthesis of NiO Nanorods. *Mater. Lett.* 62 (4–5), 743–746. doi:10.1016/j.matlet.2007.06.053

Palanisamy, P., and Raichur, A. M. (2009). Synthesis of Spherical NiO Nanoparticles through a Novel Biosurfactant Mediated Emulsion Technique. *Mater. Sci. Eng. C* 29 (1), 199–204. doi:10.1016/j.msec.2008.06.008

Park, Y., Hong, Y. N., Weyers, A., Kim, Y. S., and Linhardt, R. J. (2011). Polysaccharides and Phytochemicals: A Natural Reservoir for the Green Synthesis of Gold and Silver Nanoparticles. *IET Nanobiotechnol.* 5 (3), 69. doi:10.1049/iet-nbt.2010.0033

Pirôllo, M. P. S., Mariano, A. P., Lovaglio, R. B., Costa, S. G. V. A. O., Walter, V., Hausmann, R., et al. (2008). Biosurfactant Synthesis byPseudomonas aeruginosaLBI Isolated from a Hydrocarbon-Contaminated Site. *J. Appl. Microbiol.* 105 (5), 1484–1490. doi:10.1111/j.1365-2672.2008.03893.x

Pui, A., Gherca, D., and Cornei, N. (2013). Synthesis and Characterization of MFe2O4 (M=Mg, Mn, Ni) Nanoparticles. *Mater. Res. Bull.* 48 (4), 1357–1362. doi:10.1016/j.materresbull.2012.11.088

Ravi Kumar, D. V., Kasture, M., Prabhune, A. A., Ramana, C. V., Prasad, B. L. V., and Kulkarni, A. A. (2010). Continuous Flow Synthesis of Functionalized Silver Nanoparticles Using Bifunctional Biosurfactants. *Green. Chem.* 12 (4), 609. doi:10.1039/b919550e

Reddy, A. S., Chen, C.-Y., Baker, S. C., Chen, C.-C., Jean, J.-S., Fan, C.-W., et al. (2009). Synthesis of Silver Nanoparticles Using Surfactin: A Biosurfactant as Stabilizing Agent. *Mater. Lett.* 63 (15), 1227–1230. doi:10.1016/j.matlet.2009.02.028

Salazar-Bryam, A. M., Yoshimura, I., Santos, L. P., Moura, C. C., Santos, C. C., Silva, V. L., et al. (2021). Silver Nanoparticles Stabilized by Ramnolipids: Effect of pH. *Colloids Surf. B: Biointerfaces* 205, 111883. doi:10.1016/j.colsurfb.2021.111883

Sharma, N., Ghosh, A., Fortner, J. D., and Giammar, D. E. (2020). Modeling Performance of Rhamnolipid-Coated Engineered Magnetite Nanoparticles for U(vi) Sorption and Separation. *Environ. Sci. Nano* 7 (7), 2010–2020. doi:10.1039/d0en00416b

Singhal, S., Nie, S., and Wang, M. D. (2010). Nanotechnology Applications in Surgical Oncology. *Annu. Rev. Med.* 61, 359–373. doi:10.1146/annurev.med.60.052907.094936

Sousa, J. R., Correia, J. A. C., Melo, V. M. M., Gonçalves, L. R. B., and Cruz, A. J. G. (2014). Cinética e Caracterização de Ramnolipídeos Produzidos Por Pseudomonas Aeruginosa MSIC02 Utilizando Glicerol Como Fonte de Carbono. *Quim. Nova* 37 (3), 431–441. doi:10.5935/0100-4042.2014006410.5935/0100-4042.20140064

Stefaniuk, M., Oleszczuk, P., and Ok, Y. S. (2016). Review on Nano Zerovalent Iron (NZVI): From Synthesis to Environmental Applications. *Chem. Eng. J.* 287 (1 March), 618–632. doi:10.1016/j.cej.2015.11.046

Sturm, W., and Morgan, J. (1996). in *Aquatic Chemistry Chemical Equilibria and Rates*. Editor J. J. Morgan. 3rded. (John Wiley & Sons).

Su, Y., Adeleye, A. S., Huang, Y., Sun, X., Dai, C., Zhou, X., et al. (2011). Microbial Biosurfactants: From an Environmental Application Point of View. *J. Bioremed Biodegrad* 02 (5), 1000104. doi:10.4172/2155-6199.1000104e

Sun, W., Zhu, B., Yang, F., Dai, M., Sehar, S., Peng, C., et al. (2021). Optimization of Biosurfactant Production from Pseudomonas Sp. CQ2 and its Application for Remediation of Heavy Metal Contaminated Soil. *Chemosphere* 265, 129090. doi:10.1016/j.chemosphere.2020.129090

Tese, F. (2011). *Doutorado em Biologia Celular e Molecular) - Intituto de Biociências*. Rio Claro: Universidade Estadual Paulista, 188.

Varjani, S., Rakholiya, P., Yong Ng, H., Taherzadeh, M. J., Hao Ngo, H., Chang, J.-S., et al. (2021). Bio-based Rhamnolipids Production and Recovery from Waste Streams: Status and Perspectives. *Bioresour. Technol.* 319, 124213. doi:10.1016/j.biortech.2020.124213

Velis, M., Conti, K. I., and Biermann, F. (2017). Groundwater and Human Development: Synergies and Trade-Offs within the Context of the Sustainable Development Goals. *Sustain. Sci.* 12 (6), 1007–1017. doi:10.1007/s11625-017-0490-9

Wang, C.-B., and Zhang, W.-x. (1997). Synthesizing Nanoscale Iron Particles for Rapid and Complete Dechlorination of TCE and PCBs. *Environ. Sci. Technol.* 31 (7), 2154–2156. doi:10.1021/es970039c

Wen, Z., Zhang, Y., and Dai, C. (2014). Removal of Phosphate from Aqueous Solution Using Nanoscale Zer-Valent Iron (nZVI). *Colloids Surf. A: Physicochemical Eng. Aspects* 457, 433–440. doi:10.1016/j.colsurfa.2014.06.017

WHO; International Programme on Chemical SafetyGuidelines for Drinking- Water Quality (1996). in *Volume 2: Health Criteria and Other Supporting Information*. 2nd ed. (New Jersey, USA: World Health Organization). doi:10.1016/0048-9697(87)90388-3

Xie, Y., Ye, R., and Liu, H. (2006). Synthesis of Silver Nanoparticles in Reverse Micelles Stabilized by Natural Biosurfactant. *Colloids Surf. A: Physicochemical Eng. Aspects* 279 (1–3), 175–178. doi:10.1016/j.colsurfa.2005.12.056

Xue, W., Huang, D., Zeng, G., Wan, J., Zhang, C., Xu, R., et al. (2018). Nanoscale Zer-Valent Iron Coated with Rhamnolipid as an Effective Stabilizer for Immobilization of Cd and Pb in River Sediments. *J. Hazard. Mater.* 341 (341), 381–389. doi:10.1016/j.jhazmat.2017.06.028

Yirsaw, B. D., Megharaj, M., Chen, Z., and Naidu, R. (2016). Environmental Application and Ecological Significance of Nano-Zero Valent Iron. *J. Environ. Sci.* 44, 88–98. doi:10.1016/j.jes.2015.07.016

Zhang, W.-x. (2003). Nanoscale Iron Particles for Environmental Remediation- an Overview.Pdf. *J. Nanoparticle Res.* 5, 323–332. doi:10.1023/A:1025520116015

Zhang, X., Davidson, E. A., Mauzerall, D. L., Searchinger, T. D., Dumas, P., and Shen, Y. (2015). Managing Nitrogen for Sustainable Development. *Nature* 528 (7580), 51–59. doi:10.1038/nature15743

Zhao, X., Liu, W., Cai, Z., Han, B., Qian, T., and Zhao, D. (2016). An Overview of Preparation and Applications of Stabilized Zero-Valent Iron Nanoparticles for Soil and Groundwater Remediation. *Water Res.* 100, 245–266. doi:10.1016/j.watres.2016.05.019

Conflict of Interest: The authors declare that the research was conducted in the absence of any commercial or financial relationships that could be construed as a potential conflict of interest.

Publisher's Note: All claims expressed in this article are solely those of the authors and do not necessarily represent those of their affiliated organizations, or those of the publisher, the editors and the reviewers. Any product that may be evaluated in this article, or claim that may be made by its manufacturer, is not guaranteed or endorsed by the publisher.

frontiers | Frontiers in Bioengineering and Biotechnology

ORIGINAL RESEARCH
published: 26 April 2022
doi: 10.3389/fbioe.2022.855762

Genetic Evidences of Biosurfactant Production in Two *Bacillus subtilis* Strains MB415 and MB418 Isolated From Oil Contaminated Soil

Azra Yasmin[1†], *Fozia Aslam*[1†] *and Anila Fariq*[1,2*†]

[1]*Microbiology and Biotechnology Research Lab, Department of Biotechnology, Fatima Jinnah Women University, Rawalpindi, Pakistan,* [2]*Department of Biotechnology, University of Kotli Azad Jammu and Kashmir, Kotli, Pakistan*

Biosurfactants are a diverse group of amphiphilic compounds obtained from microbes. In the present study, the genomic analysis of biosurfactant-producing *Bacillus subtilis* MB415 and MB418 obtained from oil-contaminated soil was performed. Initially, the strains were screened for biosurfactant production by hemolytic assay, emulsification index, and oil displacement. Further FTIR analysis of extracted biosurfactants revealed the presence of lipopeptides. The sequenced genomes of MB415 and MB418 were of 4.2 Mbps with 43% GC content. Among more than 4,500 protein-coding genes, many were involved in virulence, metal/multidrug resistances, flagella assembly, chemotactic response, and aromatic ring hydroxylating dioxygenases. An annotation analysis revealed that both genomes possessed non-ribosomal synthetase gene clusters for the lipopeptide synthetases *srf* and *fen* responsible for surfactin and fengycin production. Comparative studies of both genomes highlighted variability in gene operons mainly for surfactin biosynthesis.

Keywords: biosurfactant production, secondary metabolites biosynthesis, oil remediation, lipopeptides, fengycin, surfactin

OPEN ACCESS

Edited by:
Murat Ozdal,
Atatürk University, Turkey

Reviewed by:
Shaohua Chen,
South China Agricultural University, China
Vivek Sharma,
Chandigarh University, India
Furkan Orhan,
Ağrı İbrahim Çeçen University, Turkey

***Correspondence:**
Anila Fariq
neelaahmad@gmail.com

†These authors have contributed equally to this work and share first authorship

Specialty section:
This article was submitted to Industrial Biotechnology, a section of the journal Frontiers in Bioengineering and Biotechnology

Received: *15 January 2022*
Accepted: *25 March 2022*
Published: *26 April 2022*

Citation:
Yasmin A, Aslam F and Fariq A (2022) Genetic Evidences of Biosurfactant Production in Two Bacillus subtilis Strains MB415 and MB418 Isolated From Oil Contaminated Soil. Front. Bioeng. Biotechnol. 10:855762. doi: 10.3389/fbioe.2022.855762

INTRODUCTION

Natural products comprise a variety of bioactive compounds like bacteriocins, terpenoids, antibiotics, and biosurfactants (Raaijmakers et al., 2010; Anuradha, 2010). Among these, biosurfactants are surface metabolites produced by microbes during the stationary phase of growth. The broad spectrum of structurally different biosurfactants, generally glycolipids, phospholipids, lipopeptides, neutral lipids, and fatty acids, consist of hydrophobic moiety (fatty acids) of varying lengths linked to hydrophilic peptide chains of 7–10 amino acids (Geys et al., 2014). Lipopeptides are one of the major classes of lower molecular weight biosurfactants produced by microorganisms. Around 90 compounds from 26 different lipopeptide families have been identified in the last two decades (Liu et al., 2015). Microbial biosurfactants have gained special interest nowadays because of their surface and interfacial properties, eco-friendly characters, and diverse applications in industrial, health, and environmental sectors. For example, microbial glycoconjugates enhance degradation of toxic organic pollutants by increasing their bioavailability by lowering surface tension and producing a solvent interface (Bhatt et al., 2021).

Biosurfactants are encoded by several genes and synthesized by a variety of microorganisms such as *Bacillus* sp., *Pseudomonas* sp., *Acinetobacter* sp., *Candida* sp., *Cryptococcus* sp., *Penicillium* sp.,

Aspergillus sp., *Kurtzmanomyces* sp., *Rhodococcus* sp., *Sphingomonas* sp., *Arthrobacter* sp., *Lactococcus* sp., and *Pseudozyma* sp. (Borah et al., 2021). Among these, the genus *Bacillus* is the most prevalent in biosurfactant production. Carolin et al. (2021) reported on the lipopeptide biosurfactant production by *Bacillus* sp., and its significant role in the degradation of aromatic amine 4-chloroaniline compound. Similarly, biosurfactants also exhibit a promising potential to efficiently eliminate toxic heavy metal pollutants by using multiple biosurfactant-metal binding stratagems, that is, emulsification, mobilization, complexation, and solubilization (Mishra et al., 2021).

Lipopeptides are biosurfactants mainly comprise a hydrophilic peptide ring and hydrophobic fatty acid moieties. Based on their structure, they are further characterized into cyclic lipopeptides (CLPs) and linear lipopeptides. The cyclic lipopeptides, commonly produced by *Bacillus subtilis,* include fengycin, surfactin, and iturin. They are composed of a peptide ring of 7 or 10 amino acids with a long hydrophobic fatty acid chain. The fatty acid chain lengths vary in each type, that is, surfactin has a chain length of C_{13}–C_{16}, while iturin's chain is C_{14}–C_{17}, and that of fengycin is C_{14}–C_{18} (Hu et al., 2019).

Surfactin has many congeners because of the variation in the length of the fatty acid chain and the types of amino acids. The structure of surfactin offers diverse applications in several global issues such as medicine and environmental protection (Gudiña et al., 2013). It was discovered as a potent fibrin clot-inhibitor and as an antibacterial and antiviral agent. It also showed hypocholesterolemic and anti-tumor activities. Owing to its remarkable surface-, interface-, and membrane-active action, it has the ability to cross plasma membrane barriers and viral envelopes (Santos et al., 2018). It can lower the surface tension of water from 72 to 27 mN/m and is highly thermally stable and salt tolerant. Because of these properties, it possesses huge potential in the microbial enhancement of oil recovery (MEOR) and considered a good candidate for the bioremediation of contaminated soils and sub-surface environments (Hu et al., 2019).

Fengycin is another lipopeptide consisting of a decapeptide linked to a saturated or unsaturated fatty acid (C14–C18). The ring structure of its cyclic peptide is formed by linking the residue at position 3 to the C-terminal–COOH group of the amino acid at position 10 (Fanaei et al., 2021). Fengycins are predominantly produced by *Bacillus* spp. with potential bioactivities. They are active against phytopathogenic fungi and bind with their plasma membrane, thereby causing cell lysis and leakage (Gimenez et al., 2021).

The biosynthesis of these lipopeptides is governed by a complex set of proteins called non-ribosomal peptide synthetases (Wang et al., 2014). Gene clusters for the synthesis of such compounds have been found in the *Bacillus* genera (Donio et al., 2013). Several structurally and functionally diverse molecules need to be screened and characterized to create a better understanding of such biomolecules (Lu et al., 2014; Aleti et al., 2015; Singh and Tiwary, 2016).

Next-generation sequencing has revolutionized the discovery of natural products, chemicals, and biosynthetic enzymes greatly used in the fields of biotechnology and biomedicine (Luo et al., 2014). Biosurfactant production in various *Bacillus* species has been widely reported in many studies. Moreover, many *Bacillus* species are known for their metabolic capability, environmental versatility, and their ability to remove xenobiotic compounds and heavy metals via biosurfactant production (Arora, 2020). However, only limited literature is available on the genetic basis of biosurfactant production in bacteria. To this end, our research is focused on the whole genome sequencing and analysis of biosurfactant-producing and hydrocarbon-degrading indigenous *Bacillus subtilis* strains MB415 and MB418 isolated from hydrocarbon-contaminated soil. The genome analysis of both strains also indicated the gene clusters for surfactin and fengycin lipopeptides.

MATERIALS AND METHODS

Isolation and Characterization of Biosurfactant-Producing Bacteria

Soil samples were collected from the oil-contaminated site of Missa Kiswal oil field, Gujar Khan, Pakistan. Bacterial strains were isolated on Bushnell Hass mineral salt medium (Bushnell and Haas, 1941) by the spread plate method. Isolated bacterial strains were screened for biosurfactant production by a blood hemolysis assay (Mulligan et al., 1984). For this purpose, 5% defibrinated goat blood was added to the blood agar base. The emulsification activity (Cooper and Goldenberg, 1987) was determined by taking 2 ml of kerosene with an equal volume of the culture supernatant and vortexed vigorously for a few minutes. The emulsion formed was allowed to be stable for 24 h and the emulsification index was calculated as the percentage of the height of the emulsion layer (mm) divided by the total height of the liquid (mm). Furthermore, the oil-spreading technique and surface tension of culture supernatants were measured by using a torsion balance (Lin and Timasheff, 1996; Morikawa et al., 2000). Extraction and purification of biosurfactants from selected isolates were done by following the protocol of Qiao and Shao (2010). The extracted biosurfactants were analyzed through FTIR spectroscopy.

Whole Genome Sequencing

For molecular characterization, isolates were sequenced for 16S rRNAs that are submitted to NCBI. In addition, the whole genome sequence of both strains was performed to get an insight into the genetic composition. Cells were grown in Luria-Bertani (LB) broth at room temperature. The genomic DNA was extracted in the late exponential phase. The cells were collected by centrifugation at 4°C and 10,000 g for 10 min. The supernatant was discarded and the cells were suspended in 200 µL of PBS. The samples were then treated with lysozyme (1.33 mg/ml) and incubated for 5 min. Proteinase K (20 µL) was added to the cells that were incubated for 1 hour at 37°C. After this, 200 µL of buffer AL was added to the samples, mixed thoroughly, and kept at 56°C for 10 min. Furthermore, 96–100% ethanol (200 µL) was used for washing nucleic acid pellets. The mixture collected was centrifuged at 8,000 rpm for

TABLE 1 | Results of biosurfactant screening assays.

Bacterial isolates	Hemolysis	Oil spreading	Emulsification index (%)n	Surface tension (dynes/cm)
Bacillus subtilis MB415	A	+ (10s)	20 ± 2	20 ± 0.5
Bacillus subtilis MB418	B	+(2min)	15 ± 2.5	35 ± 5

α = *incomplete hemolysis* β = *complete hemolysis.*

1 min and the flow-through was discarded. Buffer AW2 (500 μL) was added to the spin column, centrifuged at 14,000 rpm, and the flow-through was discarded. Finally, the DNA was eluted with an elution buffer AE (200 μL) that was incubated for 1 min at room temperature and centrifuged at 6,000 rpm for 1 min to collect the DNA in a sterile Eppendorf tube (Aslam et al., 2018). The concentration and purity of DNA were determined by using a nanodrop spectrophotometer ND-1000 (Nanodrop Technology, Wilmington, DE). The qualitative assessment was done by visualizing genomic DNA on 1% agarose gel stained with ethidium bromide. The genomic DNA of both strains MB415 and MB418 were sequenced using the Illumina MiSeq (2 × 300 bp) platform.

Sequence Assembly and Annotation

The obtained sequence reads were assembled through SPAdes 3.1 including error correction, deBruijn graph assembly for arrangement into contigs and their scaffolding (Bankevich et al., 2012). The quality of the assembled sequence data was assessed using Quast (Gurevich et al., 2013). Finally, the genomic data were annotated through different annotation servers.

Gene prediction and functional annotation analysis was performed using three different pipelines: Integrated Microbial Genomes expert review (http://img.jgi.doe.gov), Rapid Annotation Subsystem Technology (Aziz et al., 2008), and Genome Annotation Pipeline (PGAP) by NCBI (http://www.ncbi.nlm.nih.gov/genome/annotation_prok). The genes were identified by Prodigal (Hyatt et al., 2010). The predicted CDSs were translated and searched against NCBI, non-redundant databases, UniProt, TIGRfam, Pfam, PRIAM, COG, KEGG, and interPro databases performed by the IMG ER platform that is developed by the Joint Genome Institute, Walnut Creek, CA, United States (Markowitz et al., 2009). In addition, transfer RNAs and rRNAs were identified using tRNAscan-SE (Lowe and Eddy, 1997) and RNAmmer (Lagesen et al., 2007).

RESULTS

Screening of Biosurfactant-Producing Bacteria

Fifteen hydrocarbon-degrading bacteria were isolated on Bushnell Haas Mineral salt medium from oil-polluted soil samples. Isolates with distinct morphological characteristics and competent to utilize different hydrocarbon substrates as a sole carbon source were selected, purified, and screened for biosurfactant production. Multiple screening assays were performed for the identification of potential biosurfactant producers, that is, oil spreading assay, emulsification index, and surface tension and hemolytic assays. Two isolates, that is, MB415 and MB418 showed a remarkable reduction in surface tension values, that is, 20 and 35 dyn/cm, respectively. Both strains showed distinct oil displacement and low emulsification index. Strain MB418 exhibited complete, while MB415 displayed partial hemolysis of erythrocyte cells (**Table 1**).

In the present study, the maximum emulsification activity of diesel was recorded by culture supernatants of bacterial strains. The emulsification ability is attributed to the augmented biodegradation potential of petroleum hydrocarbons. The FTIR spectrum strongly reflects that the extracted compound was a potential biosurfactant with peptide and aliphatic hydrocarbon moieties. Significant absorbance peaks of the biosurfactant isolated from *B. subtilis* MB415 and MB418 observed C-O, C-H, and C=O in the regions of 1,000–1,320/cm, 2,850–3,000/cm, and 1,665–1760/cm stretching mode, respectively, verifying the presence of glycolipids (**Figure 1**).

Genome Sequencing

The genomes of *B. subtilis* strains MB415 and MB418 were sequenced to identify their hydrocarbon degradation potential and applications in bioremediation. The genome project was deposited in the Integrated Microbial Genome (IMG ER) online database and the Genome Online Database (GOLD) (Pagani et al., 2012). The whole-genome shotgun (WGS) project of both isolates was deposited at DDBJ/EMBL/GenBank under accession numbers LYDW00000000 and MQSR00000000 for *B. subtilis* MB418 and MB415, accordingly.

Genome Properties

The genome sequences of *B. subtilis* MB415 and MB418 were generated with the help of Illumina Miseq sequenced data. For both the genomes, the paired end reads 4, 120, 685 bp and 4, 266, 089 bp respectively, were assembled into contigs and scaffolds. Genome statistics according to the NCBI Prokaryotic Genome Annotation Pipeline are summarized in **Table 2**.

Annotation Analysis and Subsystem Features

The draft genome of *B. subtilis* MB418 contains 4,543 genes containing 4,055 genes with coding sequences and 362 pseudogenes. The genome was found to have 126 RNA genes including 85 tRNAs and 35 rRNAs comprising 11 genes for 5S, 12 each for 16S and 23S rRNAs, while six were non-coding RNAs identified through RNAmmer and tRNA Scan S.E. The *B. subtilis* MB415 genome of 4, 267, 672 bps contains 4,812 genes with 4, 416 protein-coding genes and 121 rRNAs including 86 genes for

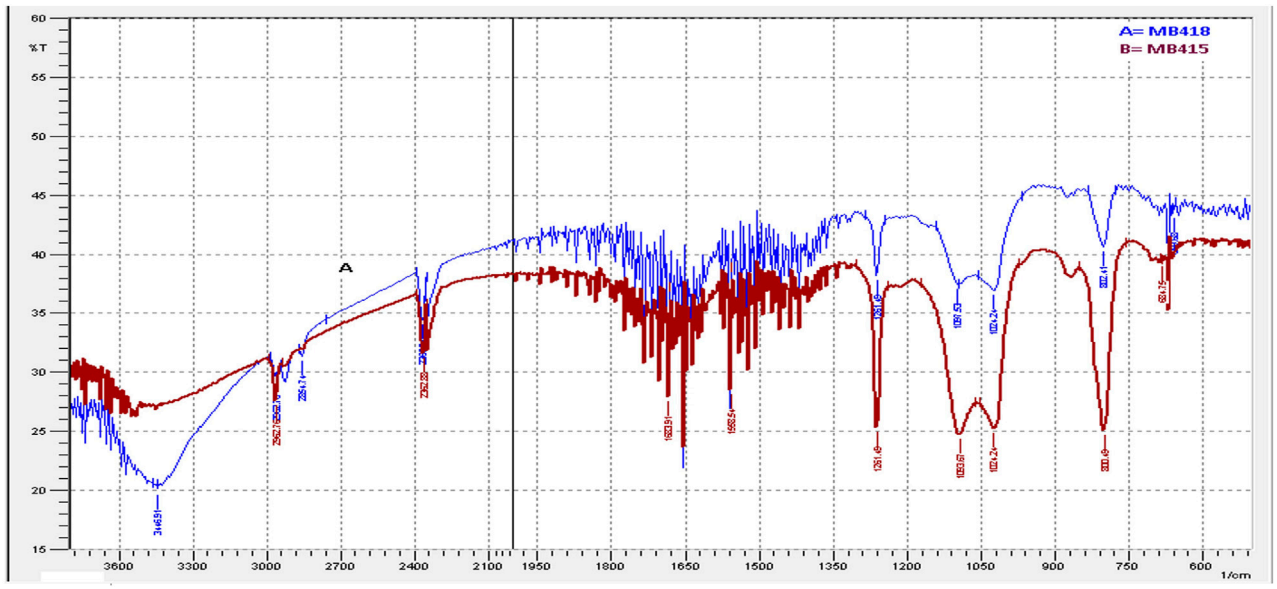

FIGURE 1 | FTIR spectra of extracted biosurfactants.

TABLE 2 | Genome characteristics of *Bacillus subtilis* MB415 and *Bacillus subtilis* MB418.

Strain	Accession number	Size Mbps	GC content	Number			
				Contigs	Subsystems	Cds	RNA
MB415	MQSR00000000	4267093	43.1	246	479	4,610	116
MB418	LYDW00000000	4118930	43.6	289	479	4,455	121

tRNAs and 11, 12, 7 genes carrying codes for 5S, 16S, and 23S respectively.

The annotation of the genome *B. subtilis* MB418 using the RAST server (Aziz et al., 2008) identified genes involved in the tolerance against metals, that is, arsenic (6 genes), copper (4 genes), and Co/Zn/Cd (4 genes). In addition, the genome has a multidrug resistance operon mdtRP mostly present in the genus *Bacillus*, and beta-lactamase, streptothricin, and vancomycin which are mostly found in gram-positive bacteria. Among 479 subsystems, 545 genes were specified for carbohydrates and 458 for amino acids and their derivatives. The genome also possesses a significant number of genes allocated for chemotaxis (15 genes) and flagellar motility (78 genes). There were around 117 genes which confer proteins for dormancy, sporulation-like genes designated for biofilm matrix protein component TsaA, sporulation gene operons, spore germination, hydrolysis, and sporulation cluster IIIA and cluster II, while in *B. subtilis* MB415, many genes involved in metal tolerance including arsenic (6), copper (5), and Co/Zn/Cd resistance (4) were identified. However, few genes were found to be involved in antibiotic resistance among multidrug resistance operon efflux pumps (8) and beta-lactamase (3), along with genes for vancomycin, streptothricin, and fosfomycin resistance. Both genomes possess genes for secondary metabolite biosynthesis that includes surfactin, fengycin, and siderophore. In addition, genes encoding enzymes involved in different aromatic compound metabolisms, that is, peripheral anaerobic and central aromatic intermediates formed during degradation were also predicted in both genomes (**Figure 2**).

Biosurfactant-Producing Genes

Emerging next-generation sequencing technology coupled with other computational efforts of annotation has enabled us to look into several potential genes simultaneously. This has improved our understanding of essential metabolic pathways and the adaptive variation of organisms in stressed environments. Similarly, bacterial diversity inhabiting soil with a high concentration of hydrocarbons (such as soil in and around oil fields) possessed certain genes for biosurfactant (surfactin, fengycin, and iturins) production.

Annotation results revealed that both genomes MB415 and MB418 carry operons responsible for the biosynthesis of secondary metabolites such as surfactin and fengycin. In *B. subtilis* MB418, surfactin-producing genes including *srf*AA codes for the surfactin family lipopeptide synthetase-A. This protein belonged to the COG1020 category of clusters of orthologous groups (COG) for the conserved protein domain family *EntF* called non-ribosomal peptide synthetase component F. In addition, it showed a close relationship with the phosphopantetheine attachment site protein (IPR006162) and

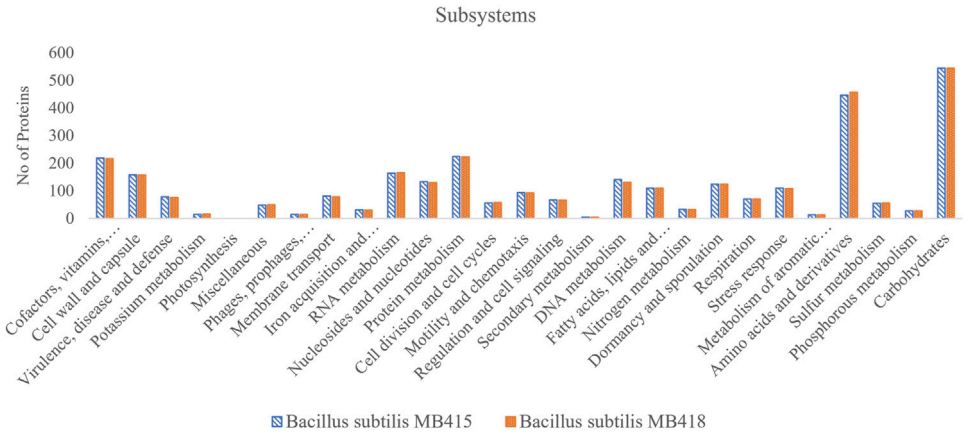

FIGURE 2 | Subsystem features of the two *Bacillus subtilis* strains (MB415 and MB418).

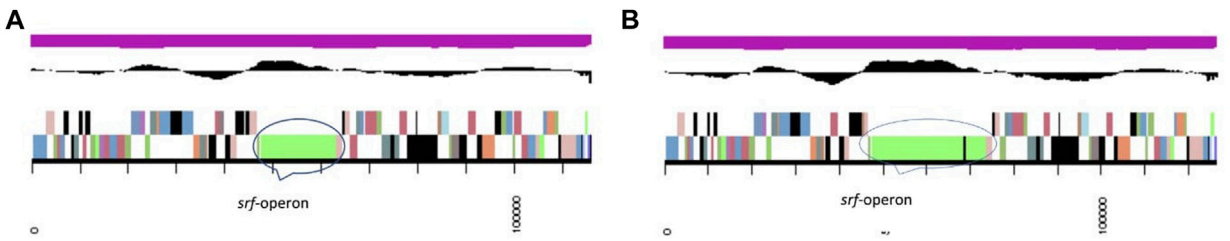

FIGURE 3 | Portion of chromosomal map having scaffold with *srf*-operon **(A)** MB418 and **(B)** MB415. From outside to the center: genes on the forward strand (color by COG categories), genes on the reverse strand (color by COG categories), RNA genes (tRNAs green, rRNAs red, other RNAs black) GC content GC skew.

acyl carrier protein of super family SSF47336 (IPR009081). It also shares similarities with the peptide chains of IPR020806 polyketide synthase, phosphopantetheine-binding domain, and others including IPR020845, SSF56801, and TIGR01720 of the non-ribosomal peptide synthase domain. It was relevant to many other protein domains including PP-binding, condensation, AMP binding_C, and pfam13745-HXXPF_rpt. Next to this is the gene *srf*AC encode for the protein surfactin family lipopeptide synthetase C. This gene of 3,828 bp is translated into a protein of 1,275 amino acids, a non-ribosomal peptide synthetase component F. This protein belongs to the phosphopantetheine attachment site (IPR006162) and other protein classes of databases InterPro, pfam, and TIGRfam like *srf*AA.

The genome also possesses gene *srf*AD (729 bp) encodes for the thioesterase domain-containing protein comprising 242 amino acids. According to clusters of orthologous groups, it belongs to the category COG3208 surfactin synthase thioesterase subunit exhibiting 91.32% similarity with alpha/beta-hydrolases of pfam00975 and SSF53474. Lastly, the gene for ycxA similar to COG2271 called sugar-phosphate permease comprises 1,227 bp and encodes for 408 amino acid sequences. The genome encodes a permease of the major facilitator superfamily (KOG2533) related to the transporter class TC: 2. A. 1 of IPR016196, IPR020846 with 85.78% alignment with pfam07690.

This gene arrangement was different in *B. subtilis* MB415. The operon starts with the gene *srf*AA of 10,764 bp encode for the surfactin family lipopeptide synthetase A (COG1020). The acyl-CoA carrier protein, also called surfactin family lipopeptide synthetase B gene *srf*AB (3329bp), was identified in the genome of *B. subtilis* MB415. This protein of 3,329 amino acids has a maximum similarity with IPR009081 (acyl carrier protein-like), IPR020845 (AMP-binding, conserved site), and SSF52777 (CoA-dependent acyltransferases). Next to this is the gene for the condensation protein SrfAB of pfam00668. In addition, it also possesses the gene *srfAC* of 3828bp, *srfAD* thioesterase domain-containing protein, and ycxA-sugar phosphate permease. The arrangement of top COG hits on the scaffold with *srf*-operon in the genome of *B. subtilis* MB418 and MB415 (**Figure 3**).

Fengycin produced by various *Bacillus* strains is expected to form a lactone between the hydroxyl group of L-Tyr3 and C-terminal carboxyl group L-II-e and fengycin synthase (FenC, FenA, and FenB). In the MB418 genome, the gene *fen*C encoding fengycin family lipopeptide synthetase A (KO: K15664 ppsA) was identified (**Figure 4**). However, in case of the *Bacillus subtilis* MB415 genome, the operon of fengycin starts with the gene *fen*B, comprising 243 bps and belonging to fengycin lipopeptide synthetase E (KO: K15668). It contains the non-ribosomal synthetase component F of COG1020. This protein of

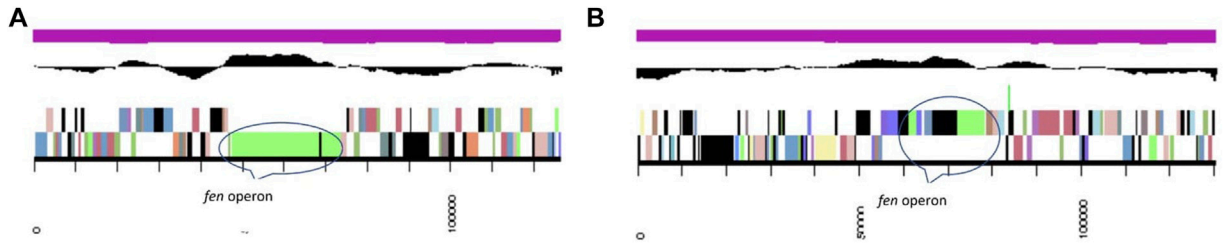

FIGURE 4 | Fengycin synthetase gene arrangement on respective scaffolds **(A)** MB418 and **(B)** MB415. From outside to the center: genes on the forward strand (color by COG categories), genes on the reverse strand (color by COG categories), RNA genes (tRNAs green, rRNAs red, other RNAs black) GC content GC skew.

2,042 amino acids consists of fengycin family lipopeptide synthetase A (KO: K15664). In between these genes, a gene for the non-ribosomal peptide synthase and condensation domain-containing protein, amino-acid adenylation domain, AMP-binding enzyme C-terminal domain, and an uncharacterized lipoprotein *yddw* were identified.

DISCUSSION

In the present study, we investigated the biosurfactant production from the hydrocarbon degraders of the Missa Kiswal oilfield. Two *B. subtilis* strains were able to produce lipopeptide biosurfactants. Similarly, a study reported the strain *B. amyloliquefaciens* An6 as a potent biosurfactant producer with diesel oil degradation efficiency (Ayed et al., 2015). Hydrocarbon-degrading bacteria possess an innate potential to produce biosurfactants which aid them in the bioavailability of hydrocarbon substrates (Antoniou et al., 2015).

The genomes of the strains isolated in the present study also decipher *Srf* operons responsible for the biosynthesis of surfactin and fengycins. In the case of *B. subtilis,* mostly fengycin and surfactin have been reported in many studies (Pereira et al., 2013). Jadeja et al. (2019) reported the *sfp* and NPRS gene in *Bacillus* sp. AKBS9 and emulsan biosynthetic gene cluster in *Acinetobactor* sp. AKBS16 for biosurfactant production through the whole genome sequence analysis of the aforementioned strains.

B. subtilis is one of the predominant lipopeptide cell factories (Steller et al., 1999). The genetic makeup of biosurfactant-producing organisms is one of the major factors governing the biosynthesis of biosurfactants. Different molecular studies demonstrated the metabolic pathways, operons, and enzymes for the extracellular production of many biosurfactants. Wang et al. (2022) identified entire core synthetic genes for bacillibactin, fengycin, and surfactin production in a novel facultative-halophilic, long-chain hydrocarbon degrader, that is, *Bacillus* sp. XT-2. Surfactin is a cyclic lipopeptide produced non-ribosomally by surfactin synthetase, a multi-enzyme peptide synthetase complex. The biosynthesis of other lipopeptides is also mediated by similar enzyme complexes. Non-ribosomal peptide synthetases (NRPSs) involved in lipopeptide biosynthesis exhibit a high degree of similarity in structural conformation even in highly distant microbial species (Dhasayan et al., 2015). Fengycin is another cyclic lipodecapeptide containing four D-amino acids and ornithine in the peptide chain. Fengycin looks like a mixture of isoforms that show differences in length and branching of the β-hydroxy fatty acid, and the amino-acid composition of the peptide ring (Hu et al., 2007).

The genomes presented in our study decrypt the *B. subtilis* sequence variation and detailed comparisons of this vital model species. Comparisons of whole-genome sequences of different bacteria revealed significant genomic variability among phylogenetically interrelated bacterial species. Even sequences with 100% homology exhibit low conservation in the total gene content. *B. subtilis* is one of the most extensively studied spore forming, non-pathogenic, gram-positive bacteria ubiquitously found in soil (Earl et al., 2007; Chen et al., 2013). Another study demonstrated the complete genome sequence analysis of polystyrene-degrading deep sea *B. paralicheniformis* G1 strain comprising 4,281,959 bp with 45.88% GC content and encoded 4,213 protein-coding genes. Numerous genes encoding monooxygenase, dioxygenase, peroxidase, esterase, and hydrolase involved in the degradation of synthetic polymers were identified along with the genes associated with flagellum-dependent motility, chemotaxis, biofilm formation, and siderophores biosynthesis (Kumar et al., 2021).

The genetic regulation of lipopeptides is governed by the four open reading frames (ORFs) in the *srfA* operon directing the surfactin synthesis including *srfAA*, *srfAB*, *srfAC,* and *srfAD* (Zhu et al., 2021). Surfactin is synthesized by a multi-enzyme synthetase complex mainly comprising *SrfA, SrfB,* and *SrfD* subunits. *Srf* operon for biosurfactant pathways consists of the gene *srfAA, -AB, -AC,* and–*AD* in *Bacillus* spp. The annotation analysis of the genome *B. subtilis* MB415 and MB418 revealed that both strains also possess this operon (**Figure 5**). According to previous studies, in the *Bacillus subtilis* species, the synthesis of surfactin is based on three amino-acid activating components of surfactin synthetase (*SrfA, -B,* and *-C*) that are activated by *SrfD*. The gene *srf*AD also possesses thioesterase that is required for the last amino acid in the growing peptide chain that results in the cyclic structure of the biosurfactant and *B. subtilis* (Vedaraman and Venkatesh, 2011).

A comparative genome analysis showed gene arrangements of surfactin-producing operon in the draft genome of *B. subtilis* MB418 shared its neighborhood region showing the same top COG hits with *Bacillus subtilis inaquosorum* BGSC 3A28 and *B. subtilis* B4143. With the difference in the SrfAA protein, in

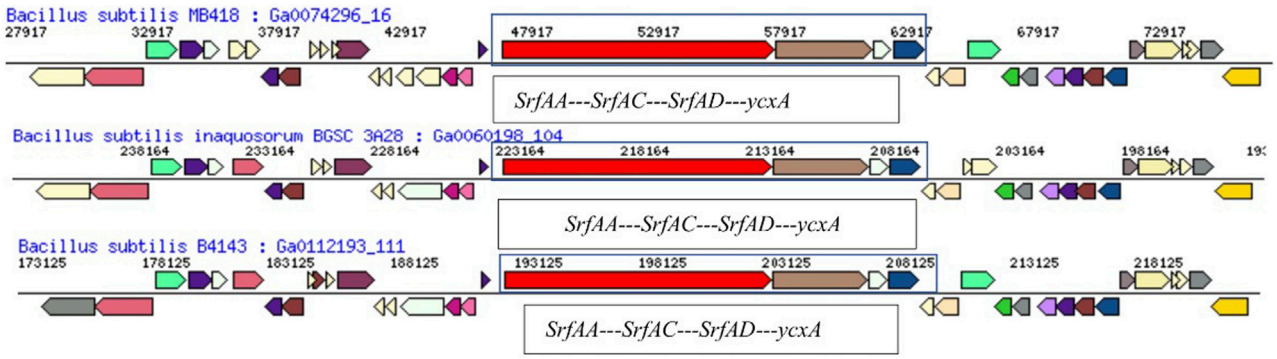

FIGURE 5 | Comparison of the hydrocarbon-degrading gene locus *srf* operon of *Bacillus subtilis* MB418 with other *Bacillus* species.

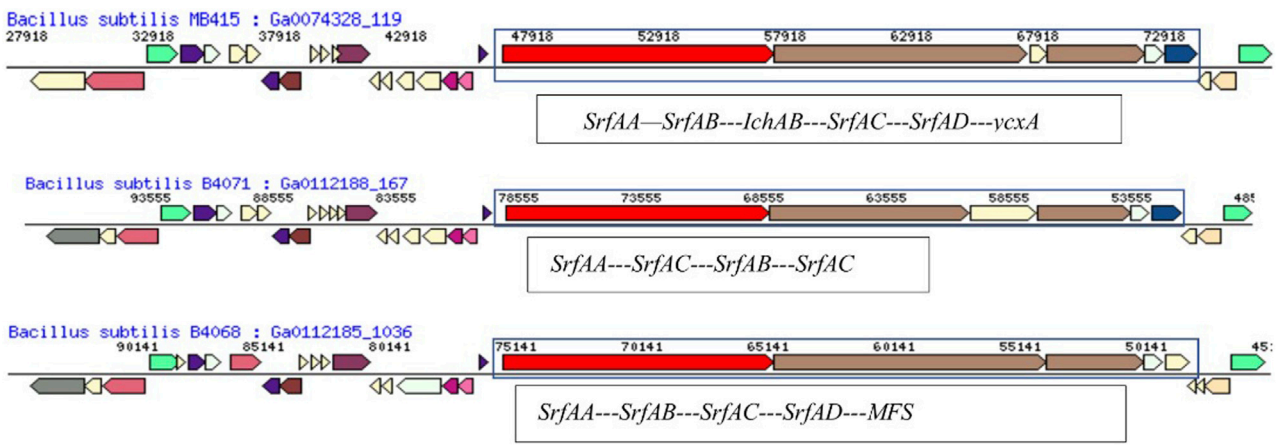

FIGURE 6 | Comparison of the hydrocarbon-degrading gene locus *srf* operon of *Bacillus subtilis* MB415 and other *Bacillus* species.

Bacillus subtilis MB418 there are 3,586 amino-acid sequences, while it is 3,587 amino acids in the rest of the two closely related genomes. However, in the case of MB415, the operon is entirely different with genes encoding for more proteins and a different arrangement as shown in **Figure 6**.

The gene *srfAB* encodes for surfactin family lipopeptide synthetase AB and consists of 3,329 amino acids. A comparison of the gene neighborhood showed maximum similarity with *B. subtilis* B4071 (Berendsen et al., 2016) having the gene for the protein SrfAB (2695aa) (**Figure 6**). With the exception, *B. subtilis* MB415 had an additional gene for non-ribosomal peptide synthase not present in the genome of B4071. The gene operon in the genome of MB415 ends at gene (*ycxA*) for sugar-phosphate permease, while in the *B. subtilis* MB4068 (Berendsen et al., 2016) operon, this gene is replaced with another gene for the major facilitator superfamily (**Figure 6**).

Furthermore, genomes which carry genes for the same proteins vary in sequence length than the ones present in the draft genome of MB415. For example, the *srf*AA gene of *B. subtilis* MB415 is of 10,764 bp codes for 3,587 amino acids. However, this gene sequence is relatively small in the previously reported surfactant-producing *B. safensis* CCMA-560 and *B. amyloliqueficiens* comprising 10, 713bps (3570aa) and 10, 701bps (3566aa), respectively. The gene *srf*AC (3828bp) sequence is the same in the genomes of *B. subtilis* MB418 and MB415 and in the rest of the *Bacillus* species. The gene encoding thioesterase in the genomes of both *B. subtilis* MB415 and MB418 comprises 3,834 bps while in *B. pumilus*, it is encoded by the *srf*AD gene (732bp) (Jiang et al., 2016). Similarly, surfactin produced by *B. subtilis* strains isolated from soil consists of seven amino acids and 13–15 lipid chains forming a cyclic lipopeptide as described previously by researchers (Sekhon et al., 2011; Sachdev and Cameotra, 2013).

The genome analysis of both isolates unveiled potential gene operons for the biosynthesis of a secondary metabolite, fengycin. Fengycin, also called plipastatin, is an anti-fungal antibiotic that inhibits filamentous fungi but is ineffective against yeast and bacteria (Volpon et al., 2000). It also has the potential to inhibit phospholipase and biofilm formation in many bacteria (Thaniyavarn et al., 2003). Fengycin is a type of lipodecapeptide with moderate surfactant activity normally produced by several strains of *Bacillus* spp. *Fen* operon

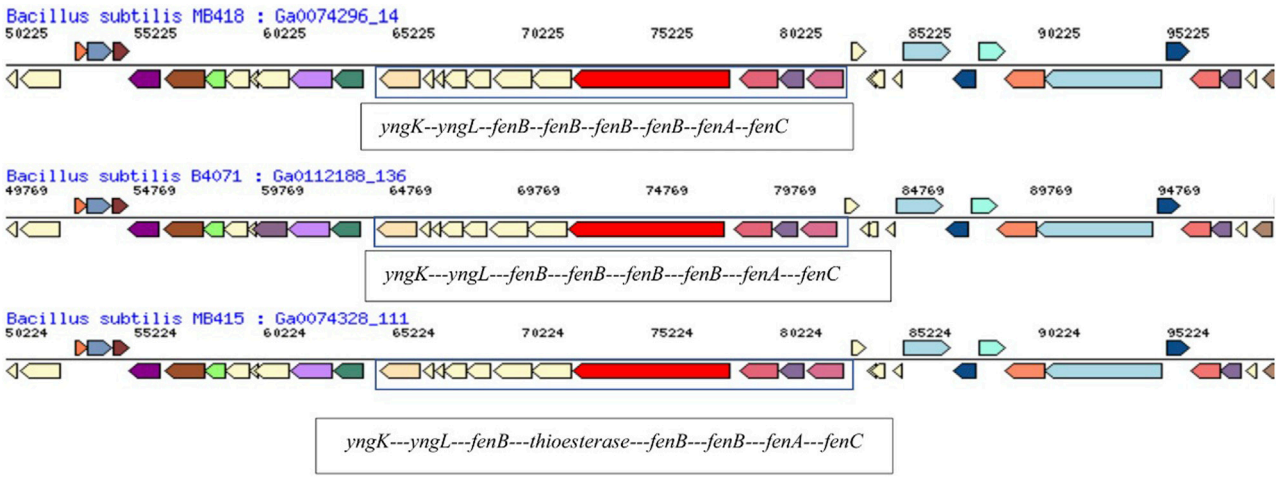

FIGURE 7 | Comparison of the hydrocarbon-degrading gene locus *fen* operon of *Bacillus subtilis* MB415, MB418, and other *Bacillus* species.

comprises an N-acyl domain at the N-terminus of *FenC* and five non-ribosomal peptide synthetase subunits assembled in a co-linear chain in the following order: *Fen*C, *Fen*D, *Fen*E, *Fen*A, and *Fen*B (Guo and Yu, 2014).

The fengycin synthetase gene operon in the draft genome of *B. subtilis* MB418 exhibited maximum similarity with *B. subtilis* B4071. However, in the genome of *B. subtilis* MB415, an esterase-producing gene is identified instead of *fenB* for fengycin lipopeptide synthetase E as indicated in other closely related *Bacillus* species (**Figure 7**). A recent study also reported three genes related to the gene cluster responsible for fengycin biosynthesis (*fenBCD*) in *B. velezensis* and *B. siamensis* (Zeng et al., 2021). Similarly, in another study, five ORFs, namely, *Fen*A, *Fen*B, *Fen*C, *Fen*D, and *Fen*E, were identified for fengycin production in the *Bacillus velezensis* strain P45 (da Rosa et al., 2022).

CONCLUSION

Indigenous bacterial strains inhabiting a polluted environment acquire tremendous potential to utilize petroleum hydrocarbons than non-native microbes. The present study demonstrated the production of lipopeptide biosurfactants from *B. subtilis* MB415 and MB418. The genome analysis of both *B. subtilis* isolates MB415 and MB418 contain a gene locus that enhanced their proficiency in degrading oil compounds. The presence of genes for flagella and secondary metabolite biosynthesis supported the experimental outcomes of emulsification and oil utilization capacities of both strains.

DATA AVAILABILITY STATEMENT

The datasets presented in this study can be found in online repositories. The names of the repository/repositories and accession number(s) can be found at: https://www.ncbi.nlm.nih.gov/genbank/, LYDW00000000, https://www.ncbi.nlm.nih.gov/genbank/, MQSR00000000.

AUTHOR CONTRIBUTIONS

The authors have contributed equally to this work. AY conceived the research idea and administered the research work. AF performed the laboratory experiments. FA performed the genome sequencing. All authors contributed to the writing of this manuscript. All authors have read and agreed to the publication of the manuscript.

REFERENCES

Aleti, G., Sessitsch, A., and Brader, G. (2015). Genome Mining: Prediction of Lipopeptides and Polyketides from Bacillus and Related Firmicutes. *Comput. Struct. Biotechnol. J.* 13, 192–203. doi:10.1016/j.csbj.2015.03.003

Antoniou, E., Fodelianakis, S., Korkakaki, E., and Kalogerakis, N. (2015). Biosurfactant Production from marine Hydrocarbon-Degrading Consortia and Pure Bacterial Strains Using Crude Oil as Carbon Source. *Front. Microbiol.* 06, 274. doi:10.3389/fmicb.2015.00274

Anuradha, S. (2010). Structural and Molecular Characteristics of Lichenysin and its Relationship With Surface Activity. *Biosurfactants* 672, 304–315. doi:10.1007/978-1-4419-5979-9_23

Arora, P. K. (2020). Bacilli-mediated Degradation of Xenobiotic Compounds and Heavy Metals. *Front. Bioeng. Biotechnol.* 8, 570307. doi:10.3389/fbioe.2020.570307

Aslam, F., Yasmin, A., and Thomas, T. (2018). Essential Gene Clusters Identified in Stenotrophomonas MB339 for Multiple Metal/antibiotic Resistance and Xenobiotic Degradation. *Curr. Microbiol.* 75 (11), 1484–1492. doi:10.1007/s00284-018-1549-2

Aziz, R. K., Bartels, D., Best, A. A., DeJongh, M., Disz, T., Edwards, R. A., et al. (2008). The RAST Server: Rapid Annotations Using Subsystems Technology. *BMC Genomics* 9 (1), 75. doi:10.1186/1471-2164-9-75

Bankevich, A., Nurk, S., Antipov, D., Gurevich, A. A., Dvorkin, M., Kulikov, A. S., et al. (2012). SPAdes: A New Genome Assembly Algorithm and its Applications to Single-Cell Sequencing. *J. Comput. Biol.* 19 (5), 455–477. doi:10.1089/cmb.2012.0021

Ben Ayed, H., Jemil, N., Maalej, H., Bayoudh, A., Hmidet, N., and Nasri, M. (2015). Enhancement of Solubilization and Biodegradation of Diesel Oil by Biosurfactant from *Bacillus Amyloliquefaciens* An6. *Int. Biodeterioration Biodegradation* 99, 8–14. doi:10.1016/j.ibiod.2014.12.009

Berendsen, E. M., Wells-Bennik, M. H., Krawczyk, A. O., de Jong, A., van Heel, A., Eijlander, R. T., et al. (2016). Draft Genome Sequences of 10 Bacillus Subtilis Strains that Form Spores with High or Low Heat Resistance. *Genome Announc* 4 (2), e00124–16. doi:10.1128/genomeA.00124-16

Bhatt, P., Verma, A., Gangola, S., Bhandari, G., and Chen, S. (2021). Microbial Glycoconjugates in Organic Pollutant Bioremediation: Recent Advances and Applications. *Microb. Cel Factories.* 20 (1), 1–18. doi:10.1186/s12934-021-01556-9

Borah, D., Chaubey, A., Sonowal, A., Gogoi, B., and Kumar, R. (2021). "Microbial Biosurfactants and Their Potential Applications: An Overview," in *Microbial Biosurfactants. Environmental and Microbial Biotechnology*. Editors Ahamed. M. I. Inamuddin and R. Prasad (Singapore: Springer). doi:10.1007/978-981-15-6607-3_5

Bushnell, L. D., and Haas, H. F. (1941). The Utilization of Certain Hydrocarbons by Microorganisms. *J. Bacteriol.* 41 (5), 653–673. doi:10.1128/jb.41.5.653-673.1941

Chen, Y., Yan, F., Chai, Y., Liu, H., Kolter, R., Losick, R., et al. (2013). Biocontrol of Tomato Wilt Disease byBacillus Subtilisisolates from Natural Environments Depends on Conserved Genes Mediating Biofilm Formation. *Environ. Microbiol.* 15 (3), 848–864. doi:10.1111/j.1462-2920.2012.02860.x

Cooper, D. G., and Goldenberg, B. G. (1987). Surface-active Agents from Two *Bacillus* Species. *Appl. Environ. Microbiol.* 53 (2), 224–229. doi:10.1128/aem.53.2.224-229.1987

Dhasayan, A., Selvin, J., and Kiran, S. (2015). Biosurfactant Production from marine Bacteria Associated with Sponge *Callyspongia Diffusa*. *3 Biotech.* 5 (4), 443–454. doi:10.1007/s13205-014-0242-9

Donio, M. B. S., Ronica, F. A., Viji, V. T., Velmurugan, S., Jenifer, J. S. C. A., Michaelbabu, M., et al. (2013). Halomonas Sp. BS4, A Biosurfactant Producing Halophilic Bacterium Isolated from Solar Salt Works in India and Their Biomedical Importance. *SpringerPlus* 2 (1), 149. doi:10.1186/2193-1801-2-149

Earl, A. M., Losick, R., and Kolter, R. (2007). *Bacillus Subtilis* Genome Diversity. *J. Bacteriol.* 189, 1163–1170. doi:10.1128/jb.01343-06

Fanaei, M., Jurcic, K., and Emtiazi, G. (2021). Detection of Simultaneous Production of Kurstakin, Fengycin and Surfactin Lipopeptides in *Bacillus Mojavensis* Using a Novel Gel- Based Method and MALDI-TOF Spectrometry. *World J. Microbiol. Biotechnol.* 37 (6), 111. doi:10.1007/s11274-021-03064-9

Femina Carolin, C., Senthil Kumar, P., Chitra, B., Fetcia Jackulin, C., and Ramamurthy, R. (2021). Stimulation of *Bacillus Sp.* By Lipopeptide Biosurfactant for the Degradation of Aromatic Amine 4-Chloroaniline. *J. Hazard. Mater.* 415, 125716. doi:10.1016/j.jhazmat.2021.125716

Ganesh Kumar, A., Hinduja, M., Sujitha, K., Nivedha Rajan, N., and Dharani, G. (2021). Biodegradation of Polystyrene by Deep-Sea Bacillus Paralicheniformis G1 and Genome Analysis. *Sci. Total Environ.* 774, 145002. doi:10.1016/j.scitotenv.2021.145002

Geys, R., Soetaert, W., and Van Bogaert, I. (2014). Biotechnological Opportunities in Biosurfactant Production. *Curr. Opin. Biotechnol.* 30, 66–72. doi:10.1016/j.copbio.2014.06.002

Gimenez, D., Phelan, A., Murphy, C., and Cobb, S. L. (2021). Fengycin A Analogues with Enhanced Chemical Stability and Antifungal Properties. *Org. Lett.* 23, 4672–4676. doi:10.1021/acs.orglett.1c01387

Gudiña, E. J., Rangarajan, V., Sen, R., and Rodrigues, L. R. (2013). Potential Therapeutic Applications of Biosurfactants. *Trends Pharmacol. Sci.* 34, 667–675. doi:10.1016/j.tips.2013.10.002

Guo, J., and Yu, J. (2014). Sorption Characteristics and Mechanisms of Pb(II) from Aqueous Solution by Using Bioflocculant MBFR10543. *Appl. Microbiol. Biotechnol.* 98 (14), 6431–6441. doi:10.1007/s00253-014-5681-z

Gurevich, A., Saveliev, V., Vyahhi, N., and Tesler, G. (2013). QUAST: Quality Assessment Tool for Genome Assemblies. *Bioinfo* 29 (8), 1072–1075. doi:10.1093/bioinformatics/btt086

Hu, F., Liu, Y., and Li, S. (2019). Rational Strain Improvement for Surfactin Production: Enhancing the Yield and Generating Novel Structures. *Microb. Cel fact.* 18 (1), 42–13. doi:10.1186/s12934-019-1089-x

Hu, L. B., Shi, Z. Q., Zhang, T., and Yang, Z. M. (2007). Fengycin Antibiotics Isolated from B-FS01 Culture Inhibit the Growth ofFusarium moniliformeSheldon ATCC 38932. *FEMS Microbiol. Let.* 272 (1), 91–98. doi:10.1111/j.1574-6968.2007.00743.x

Hyatt, D., Chen, G.-L., LoCascio, P. F., Land, M. L., Larimer, F. W., and Hauser, L. J. (2010). Prodigal: Prokaryotic Gene Recognition and Translation Initiation Site Identification. *BMC Bioinformatics* 11 (1), 119. doi:10.1186/1471-2105-11-119

Jadeja, N. B., Moharir, P., and Kapley, A. (2019). Genome Sequencing and Analysis of Strains Bacillus Sp. AKBS9 and Acinetobacter Sp. AKBS16 for Biosurfactant Production and Bioremediation. *Appl. Biochem. Biotechnol.* 187 (2), 518–530. doi:10.1007/s12010-018-2828-x

Jiang, J., Gao, L., Bie, X., Lu, Z., Liu, H., Zhang, C., et al. (2016). Identification of Novel Surfactin Derivatives from NRPS Modification of Bacillus Subtilis and its Antifungal Activity against *Fusarium Moniliforme*. *BMC Microbiol.* 16 (1), 31. doi:10.1186/s12866-016-0645-3

Lagesen, K., Hallin, P., Rødland, E. A., Stærfeldt, H.-H., Rognes, T., and Ussery, D. W. (2007). RNAmmer: Consistent and Rapid Annotation of Ribosomal RNA Genes. *Nucleic Acids Res.* 35 (9), 3100–3108. doi:10.1093/nar/gkm160

Lin, T.-Y., and Timasheff, S. N. (1996). On the Role of Surface Tension in the Stabilization of Globular Proteins. *Protein Sci.* 5 (2), 372–381. doi:10.1002/pro.5560050222

Liu, Q., Lin, J., Wang, W., Huang, H., and Li, S. (2015). Production of Surfactin Isoforms by *Bacillus Subtilis* BS-37 and its Applicability to Enhanced Oil Recovery under Laboratory Conditions. *Biochem. Eng. J.* 93, 31–37. doi:10.1016/j.bej.2014.08.023

Lowe, T. M., and Eddy, S. R. (1997). tRNAscan-SE: a Program for Improved Detection of Transfer RNA Genes in Genomic Sequence. *Nucleic Acids Res.* 25 (5), 955–964. doi:10.1093/nar/25.5.955

Lu, J., Guo, C., Zhang, M., Lu, G., and Dang, Z. (2014). Biodegradation of Single Pyrene and Mixtures of Pyrene by a Fusant Bacterial Strain F14. *Int. Biodeterioration Biodegradation* 87, 75–80. doi:10.1016/j.ibiod.2013.11.004

Luo, C., Liu, X., Zhou, H., Wang, X., and Chen, Z. (2014). Identification of Four NRPS Gene Clusters in *Bacillus Subtilis* 916 for Four Families of Lipopeptides Biosynthesis and Evaluation of Their Intricate Functions to the Typical Phenotypic Features. *Appl. Environ. Microbiol.* 81, 422–431. doi:10.1128/AEM.02921-14

Markowitz, V. M., Mavromatis, K., Ivanova, N. N., Chen, I.-M. A., Chu, K., and Kyrpides, N. C. (2009). IMG ER: a System for Microbial Genome Annotation Expert Review and Curation. *Bioinformatics* 25 (17), 2271–2278. doi:10.1093/bioinformatics/btp393

Mishra, S., Lin, Z., Pang, S., Zhang, Y., Bhatt, P., and Chen, S. (2021). Biosurfactant Is a Powerful Tool for the Bioremediation of Heavy Metals from Contaminated Soils. *J. Hazard. Mater.* 418, 126253. doi:10.1016/j.jhazmat.2021.126253

Morikawa, M., Hirata, Y., and Imanaka, T. (2000). A Study on the Structure-Function Relationship of Lipopeptide Biosurfactants. *Biochim. Biophys. Acta (Bba) - Mol. Cel Biol. Lipids* 1488 (3), 211–218. doi:10.1016/s1388-1981(00)00124-4

Mulligan, C., Cooper, D., and Neufeld, R. (1984). Selection of Microbes Producing Biosurfactants in media without Hydrocarbons. *J. Ferment. Technol.* 62, 311–314.

Pagani, I., Liolios, K., Jansson, J., Chen, I.-M. A., Smirnova, T., Nosrat, B., et al. (2012). The Genomes OnLine Database (GOLD) v.4: Status of Genomic and Metagenomic Projects and Their Associated Metadata. *Nucleic Acids Res.* 40 (D1), D571–D579. doi:10.1093/nar/gkr1100

Pereira, J. F. B., Gudiña, E. J., Costa, R., Vitorino, R., Teixeira, J. A., Coutinho, J. A. P., et al. (2013). Optimization and Characterization of Biosurfactant Production by Bacillus Subtilis Isolates towards Microbial Enhanced Oil Recovery Applications. *Fuel* 111, 259–268. doi:10.1016/j.fuel.2013.04.040

Qiao, N., and Shao, Z. (2010). Isolation and Characterization of a Novel Biosurfactant Produced by Hydrocarbon-Degrading bacteriumAlcanivorax dieseloleiB-5. *J. Appl. Microbiol.* 108, 1207–1216. doi:10.1111/j.1365-2672.2009.04513.x

Raaijmakers, J. M., De Bruijn, I., Nybroe, O., and Ongena, M. (2010). Natural Functions of Lipopeptides fromBacillusandPseudomonas: More Than Surfactants and Antibiotics. *FEMS Microbiol. Rev.* 34 (6), 1037–1062. doi:10.1111/j.1574-6976.2010.00221.x

Rosa, C. E., Pinilla, C. M. B., Stincone, P., Pereira, J. Q., Varela, A. P. M., Mayer, F. Q., et al. (2022). Genomic Characterization and Production of Antimicrobial Lipopeptides by Bacillus Velezensis P45 Growing on Feather By-products. *J. Appl. Microbiol.* 132 (3), 2067–2079. doi:10.1111/jam.15363

Sachdev, D. P., and Cameotra, S. S. (2013). Biosurfactants in Agriculture. *Appl. Microbiol. Biotechnol.* 97 (3), 1005–1016. doi:10.1007/s00253-012-4641-8

Santos, V. S. V., Silveira, E., and Pereira, B. B. (2018). Toxicity and Applications of Surfactin for Health and Environmental Biotechnology. *J. Toxicol. Environ. Health B Crit. Rev.* 21 (6-8), 382–399. doi:10.1080/10937404.2018.1564712

Sekhon, K., Khanna, S., and Cameotra, S. (2011). Enhanced Biosurfactant Production through Cloning of Three Genes and Role of Esterase in Biosurfactant Release. *Microb. Cel fact.* 10 (1), 49. doi:10.1186/1475-2859-10-49

Singh, P., and Tiwary, B. N. (2016). Isolation and Characterization of Glycolipid Biosurfactant Produced by a Pseudomonas Otitidis Strain Isolated from Chirimiri Coal Mines, India. *Bioresour. Bioproc.* 3 (1), 42. doi:10.1186/s40643-016-0119-3

Steller, S., Vollenbroich, D., Leenders, F., Stein, T., Conrad, B., Hofemeister, J., et al. (1999). Structural and Functional Organization of the Fengycin Synthetase Multienzyme System from *Bacillus Subtilis* B213 and A1/3. *Chem. Biol.* 6 (1), 31–41. doi:10.1016/s1074-5521(99)80018-0

Thaniyavarn, J., Roongsawang, N., Kameyama, T., Haruki, M., Imanaka, T., Morikawa, M., et al. (2003). Production and Characterization of Biosurfactants fromBacillus licheniformisF2.2. *Biosci. Biotechnol. Biochem.* 67 (6), 1239–1244. doi:10.1271/bbb.67.1239

Vedaraman, N., and Venkatesh, N. (2011). Production of Surfactin by *Bacillus Subtilis* MTCC 2423 from Waste Frying Oils. *Braz. J. Chem. Eng.* 28 (2), 175–180. doi:10.1590/s0104-66322011000200001

Volpon, L., Besson, F., and Lancelin, J.-M. (2000). NMR Structure of Antibiotics Plipastatins A and B fromBacillus Subtilisinhibitors of Phospholipase A2. *FEBS Lett.* 485 (1), 76–80. doi:10.1016/s0014-5793(00)02182-7

Wang, H., Fewer, D. P., Holm, L., Rouhiainen, L., and Sivonen, K. (2014). Atlas of Nonribosomal Peptide and Polyketide Biosynthetic Pathways Reveals Common Occurrence of Nonmodular Enzymes. *Proc. Natl. Acad. Sci. U.S.A.* 111 (25), 9259–9264. doi:10.1073/pnas.1401734111

Wang, X.-T., Liu, B., Li, X.-Z., Lin, W., Li, D.-A., Dong, H., et al. (2022). Biosurfactants Produced by Novel Facultative-Halophilic *Bacillus Sp.* XT-2 with Biodegradation of Long Chain N-Alkane and the Application for Enhancing Waxy Oil Recovery. *Energy* 240, 122802. doi:10.1016/j.energy.2021.122802

Zeng, Q., Xie, J., Li, Y., Chen, X., Gu, X., Yang, P., et al. (2021). Organization, Evolution and Function of Fengycin Biosynthesis Gene Clusters in the *Bacillus Amyloliquefaciens* Group. *Phytopathol. Res.* 3 (1), 1–12. doi:10.1186/s42483-021-00103-z

Zhu, Z., Zhang, B., Cai, Q., Cao, Y., Ling, J., Lee, K., et al. (2021). A Critical Review on the Environmental Application of Lipopeptide Micelles. *Bioresour. Tech.* 339, 125602. doi:10.1016/j.biortech.2021.125602

Conflict of Interest: The authors declare that the research was conducted in the absence of any commercial or financial relationships that could be construed as a potential conflict of interest.

Publisher's Note: All claims expressed in this article are solely those of the authors and do not necessarily represent those of their affiliated organizations, or those of the publisher, the editors and the reviewers. Any product that may be evaluated in this article, or claim that may be made by its manufacturer, is not guaranteed or endorsed by the publisher.

frontiers | Frontiers in Bioengineering and Biotechnology

ORIGINAL RESEARCH
published: 17 May 2022
doi: 10.3389/fbioe.2022.913362

Optimization and Kinetic Modeling of a Fed-Batch Fermentation for Mannosylerythritol Lipids (MEL) Production With *Moesziomyces aphidis*

Alexander Beck[1,2], *Franziska Vogt*[2], *Lorena Hägele*[1], *Steffen Rupp*[1,2] *and Susanne Zibek*[1,2]*

[1]Institute of Interfacial Process Engineering and Plasma Technology IGVP, University of Stuttgart, Stuttgart, Germany, [2]Fraunhofer Institute for Interfacial Engineering and Biotechnology IGB, Stuttgart, Germany

Mannosylerythritol lipids are glycolipid biosurfactants with many interesting properties. Despite the general interest in those molecules and the need for a robust process, studies on their production in bioreactors are still scarce. In the current study, the fermentative production of MEL in a bioreactor with *Moesziomyces aphidis* was performed using a defined mineral salt medium. Several kinetic process parameters like substrate consumption rates and product formation rates were evaluated and subsequently enhanced by increasing the biomass concentration through an exponential fed-batch strategy. The fed-batch approaches resulted in two to three fold increased dry biomass concentrations of 10.9–15.5 g/L at the end of the growth phase, compared with 4.2 g/L in the batch process. Consequently, MEL formation rates were increased from 0.1 g/Lh up to around 0.4 g/Lh during the MEL production phase. Thus, a maximum concentration of up to 50.5 g/L MEL was obtained when oil was added in excess, but high concentrations of residual fatty acids were also present in the broth. By adjusting the oil feeding to biomass-specific hydrolysis and MEL production rates, a slightly lower MEL concentration of 34.3 g/L was obtained after 170 h, but at the same time a very pure crude lipid extract with more than 90% MEL and a much lower concentration of remaining fatty acids. With rapeseed oil as substrate, the ideal oil-to-biomass ratio for full substrate conversion was found to be around 10 $g_{oil}/g_{biomass}$. In addition, off-gas analysis and pH trends could be used to assess biomass growth and MEL production. Finally, kinetic models were developed and compared to the experimental data, allowing for a detailed prediction of the process behavior in future experiments.

Keywords: biosurfactants, ustilaginaceae, mannosylerythritol lipids, process engineering, bioreactor, kinetic modeling

OPEN ACCESS

Edited by:
Murat Ozdal,
Atatürk University, Turkey

Reviewed by:
Eduardo J. Gudiña,
University of Minho, Portugal
Susana Marques,
Laboratório Nacional de Energia e Geologia, Portugal

***Correspondence:**
Susanne Zibek
susanne.zibek@igb.fraunhofer.de

Specialty section:
This article was submitted to Industrial Biotechnology, a section of the journal Frontiers in Bioengineering and Biotechnology

Received: *05 April 2022*
Accepted: *27 April 2022*
Published: *17 May 2022*

Citation:
Beck A, Vogt F, Hägele L, Rupp S and Zibek S (2022) Optimization and Kinetic Modeling of a Fed-Batch Fermentation for Mannosylerythritol Lipids (MEL) Production With Moesziomyces aphidis. Front. Bioeng. Biotechnol. 10:913362. doi: 10.3389/fbioe.2022.913362

INTRODUCTION

The microbial glycolipids mannosylerythritol lipids (MEL) are biosurfactants produced by various fungi of the Ustilaginaceae family. Besides their surface activity and biodegradability, which make them suitable as fully bio-based surfactants for household and personal care applications, for example, MELs also possess some additional interesting properties. These are for example the ability

to induce cell differentiation in mammalian cells (Isoda et al., 1997; Isoda and Nakahara, 1997; Wakamatsu et al., 2001), to interact with proteins or antibodies (Konishi et al., 2007; Fan et al., 2018), and to inhibit the growth of Gram-positive bacteria (Kitamoto et al., 1993; Liu et al., 2020; Shu et al., 2020). Moreover, they are reported to possess a moisturizing activity towards human skin (Morita et al., 2009b; Yamamoto et al., 2012) and hair (Morita et al., 2010a; Morita et al., 2010b). Their surface wetting ability could also make them suitable as agrochemicals (Fukuoka et al., 2015).

MEL has a hydrophilic core, 4-O-β-D-mannopyranosyl-D-erythritol, and several hydrophobic residues including two fatty acid chains at C2′ and C3′ and a different degree of acetylation at C4′ and C6'. They are traditionally classified according to their acetylation pattern into the four different congeners MEL-A, -B, -C and -D. MEL-A is the most hydrophobic congener, having two acetyl groups, while MEL-B and MEL-C are mono-acetylated at C6′ and C4' respectively. MEL-D is not acetylated and is, therefore, the most hydrophilic variant. The chain length of the two fatty acid residues is highly species-specific and can range from a combination of C_{10}-C_{10} to C_4-C_{16}. Some more unconventional and rare MEL variants, which can occur under specific process conditions or with genetically modified organisms, only have one fatty acid residue, so-called mono-acylated MELs (Fukuoka et al., 2007b; Saika et al., 2018; Saika et al., 2020), or an additional fatty acid, called tri-acylated MELs (Fukuoka et al., 2007a; Morita et al., 2008; Goossens et al., 2016; Beck et al., 2021).

The most efficient production processes for MEL use plant oils as a hydrophobic carbon source. Here, soybean, rapeseed and olive oil are among the most commonly employed substrates, but others have also been tested (see for example Beck et al. (2019b) or Morita et al. (2015) for a detailed overview). In theory, hydrocarbons like alkanes or alkenes are also possible substrates (Kitamoto et al., 2001), but they are non-renewable and thus rather for scientific purposes only. Hydrophilic carbon sources like sugars or glycerol can also be added to enhance biomass formation or MEL production, although MEL production solely from hydrophilic sources does not yield high MEL concentrations (Morita et al., 2009a; Faria et al., 2014).

The underlying metabolic pathway for MEL production has first been described in *Ustilago maydis* by Hewald et al. (2006). It comprises five essential steps that are catalyzed by respective enzymes. First, mannose and erythritol are linked by the erythritol-mannosyl-transferase Emt1. Secondly, two acylation reactions catalyzed by the acyltransferases Mac1 and Mac2 yield the basic molecule MEL-D. Selective acetylation by the acetyltransferase Mat one then generates the different congeners MEL-A, -B, -C and -D, before they are exported into the extracellular space by the transporter protein Mmf1 (Hewald et al., 2006). The necessary precursor molecules mannose and erythritol are generated from other sugars by glycolysis/gluconeogenesis, isomerization, and pentose phosphate pathway (Carly and Fickers, 2018; Masi et al., 2021). The two fatty acids are derived from the so-called chain-shortening pathway (Kitamoto et al., 1998), which is localized in cellular peroxisomes and produces fatty acids with the specific chain length (Freitag et al., 2014; Deinzer et al., 2019).

While many studies on MEL production in shake flasks, using different organisms and substrates, have been published over the last 3 decades, literature on dedicated process engineering in bioreactors is still scarce (see Beck et al. (2019b) for a detailed review). Only a few studies are dealing with MEL production in a bioreactor, and only some of them are presenting advances regarding process control and monitoring.

The first bioreactor process for MEL production was reported by Kim et al. (1999) using a 5-L glass fermenter. Process parameters for the batch cultivation with 100 g/L soybean oil were set at a temperature of 30°C, an aeration rate of one vvm (volume per volume per minute), and a stirring speed of 300 rpm. No parameter optimization was performed for this publication. Building on another study in which the process was optimized in shake flasks (Kim et al., 2002), Kim et al. (2006) later described a two-stage fed-batch fermentation using 30 g/L glucose and soybean oil (1:1 w/w) for growth and a subsequent feed of soybean oil (170 g/L in total) for MEL production. The fermentation in a 5-L bioreactor was conducted at a controlled dissolved oxygen level of 20% by varying stirrer speed (500–750 rpm) and aeration rate (0.two to two vvm) accordingly. With the optimized fed-batch approach, an increased MEL concentration of 95 g/L was obtained after 200 h, corresponding to a product yield coefficient $Y_{MEL/oil}$ of 0.45 g/g and volumetric productivity of 0.48 g/Lh. In all of their publications, an isolate called *Candida* sp. *SY16* was used, which was identified as a *P. tsukubaensis* strain (Kim et al., 2006).

Adamczak and Bednarski (2000) highlighted the importance of proper aeration for the MEL production process in bioreactors. While sufficient oxygen supply was necessary for efficient biomass growth on the one hand, it could also lead to intensive foaming when biosurfactants were produced. Since the produced foam contained not only MEL but also cells and substrate lipids, foaming should be avoided in the MEL production process. The best MEL production of 46 g/L (after 144 h) with *M. antarcticus* was found to occur during batch cultivation with 80 g/L soybean oil at 30°C, a controlled oxygen level of 50% (100–500 rpm), and an aeration rate of one vvm. A two-stage process with glucose for growth and repeated soybean oil feeding was also investigated but led to decreased MEL concentrations of only 28 g/L (Adamczak and Bednarski, 2000).

Following up on these earlier publications, Rau et al. (2005a) realized the need for a more detailed investigation of bioreactor production to establish a more economic process. Based on a previous study of MEL production in shake flasks (Rau et al., 2005b), a fed-batch process in a 72-L bioreactor with *M. aphidis* was developed (Rau et al., 2005a). The idea was to use substrate feeding to further increase cell biomass. Stirring and aeration were manually adapted to minimize foaming. In their optimized fed-batch process 30 g/L glucose, 3 g/L sodium nitrate, and 20 ml/L soybean oil were used for batch growth, followed by feeding a concentrated growth solution (glucose, nitrate, and yeast extract). Further oil addition (~126 g/L) was triggered by an anti-foam sensor every time foaming occurred. With the additional feeding of substrate, cell concentration was almost

doubled. Overall, a MEL concentration of 165 g/L after 283 h was reported for the fed-batch process, which would correlate to a product yield $Y_{MEL/substrate}$ of 0.92 g/g and overall volumetric productivity of 0.58 g/Lh (Rau et al., 2005a). The process of Rau et al. (2005a) as well as their culture medium is still one of the major references for MEL production processes and has been adapted by others, e.g. in Goossens et al. (2016).

A major drawback of all those published processes, in our opinion, is the fact that exclusively complex culture media with either peptone or yeast extract were employed. Besides being rather expensive, complex substrates such as yeast extract can generate problems during scale-up, such as lower batch-to-batch reproducibility, increased heat sensitivity during the sterilization process, and stronger foaming (Zhang and Greasham, 1999; Posch et al., 2012). Defined media, in turn, provide a better option for medium development and optimization, as all components and concentrations are known in detail. Therefore, we had established a novel defined mineral medium that was very effective for MEL production with several Ustilaginaceae species and especially *M. aphidis* in a previous work (Beck and Zibek, 2020a). Additionally, a positive correlation between biomass concentration at the end of the growth phase and subsequent oil conversion into MEL was observed in that publication, indicating that higher MEL concentrations and higher MEL production rates can be obtained when the active biomass concentration is increased during the initial cell growth phase.

With the current work, we further followed this path and successfully established a stable fermentation process with high controllability in an aerated stirred-tank bioreactor for the growth of *M. aphidis* and subsequent MEL production. The fermentation medium was based on our novel defined mineral medium (Beck and Zibek, 2020a), with glucose and rapeseed oil as carbon substrates for growth and production, respectively. The composition of the mineral medium was first characterized in terms of C/N, C/P and C/S ratios to determine the ideal ratios for efficient biomass growth and MEL production. Alternative sugar substrates for growth were also investigated. In the stirred-tank bioreactor, several process variations with either batch or fed-batch growth phase as well as different amounts of oil feeding were then examined. One aim was to demonstrate that a fed-batch growth phase led to higher biomass concentrations and subsequently faster MEL production with higher concentrations compared to the batch process. Secondly, the amount of plant oil feeding during the production phase was adapted to the biomass concentration at the end of the growth phase to enable complete conversion of the plant oil and fatty acids into MEL. This was done to use the oil substrate as efficiently as possible and to achieve a high purity of the crude lipid extract at the end of the fermentation process. This in turn facilitates subsequent downstream processing, where MEL has to be separated from excess lipids. During all these experiments in the bioreactor, key parameters like formation rates and yields for biomass and product, as well as specific oxygen requirements were systematically determined for the first time. These process values were ultimately used to create a kinetic model that adequately described the time course of the fermentations and can be exploited for further scale-up studies.

MATERIALS AND METHODS

Microorganism

Moesziomyces aphidis DSM 70725, obtained from the German Collection of Microorganisms and Cell Cultures (DSMZ; Braunschweig, Germany), was used for MEL production in all experiments.

Chemicals, Culture Media and Substrates

All chemicals were obtained from either Th. Geyer (Renningen, Germany), Merck (previously Sigma-Aldrich, Darmstadt, Germany), or Carl Roth (Karlsruhe, Germany) unless specified otherwise.

For maintenance of the microorganism, potato dextrose (PD) agar slants were used. They were prepared with 24 g/L potato dextrose broth (Bacto TM, Becton, United States) and 20 g/L agar.

Liquid culture medium for seed-culture and stirred-tank bioreactor fermentations consisted of 30 g/L glucose, 3 g/L $NaNO_3$, 1 g/L KH_2PO_4, 1 g/L $MgSO_4{*}7H_2O$, 1.1 g/L KCl, 0.15 g/L $CaCl{*}2H_2O$ as well as a vitamin and trace element solution, with an initial pH 5.5 (not adjusted) (Beck and Zibek, 2020a). Vitamin and trace element solutions were prepared as described in this previous publication, filter-sterilized, and supplemented to the bioreactor. For the fed-batch processes in the bioreactor, a concentrated feeding solution with 300 g/L glucose and 30 g/L $NaNO_3$ was used. Other salts, trace elements, and vitamins were the same concentration as in the batch medium.

Commercial food-grade rapeseed oil from a local supermarket (Kaufland, Germany) was used as the inductor and main carbon substrate for the MEL production phase. The oil was autoclaved separately and fed to the fermenter using a feeding flask and pump.

For the investigation of alternative sugar sources for growth, crystalline sugars like glucose, sucrose, fructose, xylose, arabinose, and cellobiose were bought from Carl Roth (Karlsruhe, Germany). Moreover, intermediate or side-streams from a sugar refining plant were kindly provided by Pfeifer & Langen Industrie-und Handels-KG (Köln, Germany). These were syrup, sugar beet molasses, sugar cane molasses, as well as two different process waters A and B. Except for process water B, which had a total sugar content of only 44 g/kg and contained mostly fructose and glucose, all other fractions had a sugar content of 62–74 g/kg and contained predominantly sucrose.

Seed Cultivation for Inoculum Preparation

Cryo-cultures of *M. aphidis* were thawed, plated onto PD agar plates and incubated at 30°C for 72 h. The inoculum for bioreactor fermentations was prepared in a two-step procedure, first in 100-ml and then in 1-L baffled shaking flasks. In order to ensure sufficient oxygen transfer for fast cell growth, the working volume was set to 20% v/v, i.e. 20 or 200 ml

liquid culture medium respectively. The first seed culture was inoculated with a single loop from the agar plate and incubated for 72 h at 30°C and 110 rpm to disperse and grow the cells and to achieve a homogenous suspension. The second seed culture was then inoculated with 10–20 ml of the first seed culture to a defined initial OD_{625} of 0.7 and incubated at 30°C and 110 rpm for around 24 h, until an $OD_{625} > 6$ was reached so that sufficient inoculum was available for fermentation.

Microreactor Cultivations

Screening experiments for medium composition and alternative carbon substrates were done with the BioLector I (m2p Labs GmbH, Baesweiler, Germany) microcultivation system. Cultivations were performed in flower-shaped 48-well microtiter plates (m2p Labs GmbH, Germany) sealed with adhesive gas-permeable and evaporation-reduced membranes (m2p Labs GmbH, Germany). Non-invasive online measurements of scattered light, pH and dissolved oxygen (DO) levels were recorded to assess the growth behavior as previously reported (Beck and Zibek, 2020a). The wells were filled with 1,000 µL culture medium and inoculated to an initial OD_{625} of 0.6, with the same seed cultivation procedure as for the bioreactor. Temperature and humidity in the system were controlled at 30°C and 85% relative humidity and the plates were shaken at 1,100 rpm with a diameter of 3.0 mm. Cycle time was 10 min, allowing for sequential measurement of backscatter (gain 5 and 20), pH and DO. Like in the bioreactor, MEL production was initiated after the cease of growth at around 48 h using 8% v/v of rapeseed oil (80 µL) in order to investigate the influence of growth phase on MEL production. Total process duration was 210 h.

The experimental design for the evaluation of medium composition - with regard to C/N, C/P, and C/S ratios - was based on a randomized Box-Behnken design with three factors and was created with DesignExpert 13 software (StatEase, Minneapolis, United States). The center point was performed as triplicate. This resulted in a set of 15 experiments. Two additional runs at the corners of the design space were conducted for model verification. The input variables were concentrations of $NaNO_3$ (3–6 g/L), KH_2PO_4 (1–2 g/L) and $MgSO_4{*}7H_2O$ (1-2 g/L) at a fixed glucose concentration of 30 g/L, leading to molar ratios of the respective elements (mol/mol) of 28.4–14.2 (C/N), 136-68 (C/P) and 244-122 (C/S). Output variables were biomass concentration at the end of growth (measured online as backscatter) and MEL concentration, which was quantified after the proceeding production phase on rapeseed oil (210 h process time). The 15 + 2 experiments were conducted simultaneously in a randomized order in the microcultivation system. Evaluation of the results by ANOVA was done with DesignExpert 13.

For the screening of alternative sugar sources, the experiments were performed as biological triplicates in the microcultivation system. The different carbon substrates were employed at the same total sugar concentration of 30 g/L. After the growth phase was terminated, one well of each sugar triplicate was harvested for offline analysis of sugar content, and the remaining two wells were fed with rapeseed oil to investigate a possible influence of the different sugars on subsequent MEL production.

Stirred-Tank Bioreactor (STBR) Fermentation

Fermentations in the aerated stirred-tank bioreactor (STBR) were performed in a 7-L Labfors bioreactor (Infors HT, Bottmingen, Switzerland) equipped with two rushton turbines (d = 54 mm), four baffles and probes for online measurement and control of temperature, pH and DO. The bioreactor was filled with either 4 L (batch growth) or 3 L (fed-batch growth) culture medium and inoculated with 200–400 ml of the second seed culture to an initial OD_{625} of 0.6. Temperature was controlled at 30°C. The pH was maintained at pH 6 throughout the fermentation using H_2SO_4 (1 M) and NaOH (4 M). Aeration was set at 0.7 vvm and the dissolved oxygen concentration was controlled by dynamic stirrer speed adjustment between 400–1,200 rpm to maintain a DO of 10%. Foaming was controlled by mounting mechanical foam breakers onto the stirrer shaft in the headspace of the reactor. Off-gas concentrations of O_2 and CO_2 were measured using BlueSens BCP off-gas sensors (BlueSens GmbH, Herten, Germany).

The process consists of two separate phases: a biomass growth phase with glucose as carbon source and other nutrients, as well as a subsequent MEL production phase where rapeseed oil was added after glucose depletion. The growth phase could further be divided into an initial batch growth phase and a subsequent fed-batch phase where a concentrated solution of carbon source, nitrogen source and nutrients was fed continuously. This feeding was done using the built-in programmable feeding pump of the Labfors bioreactor. The pump was calibrated for different volumetric flow rates. During fed-batch phase, an exponentially increasing flow rate was used, which was calculated from the desired specific growth rate (μ_{set}) according to the following equation (Chmiel et al., 2018):

$$F_{in}(t) = (V_L c_x)_0 \frac{\mu_{set}}{Y_{X/gluc}\left(c_{gluc,Feed} - c_{gluc}\right)} exp^{(\mu_{set} t)} \quad (1)$$

Specific growth rates μ_{set} were set at either 0.08 or 0.09 h^{-1}. Other parameters like biomass concentration at the end of the batch growth and biomass yield coefficient were derived from previous experiments (Beck and Zibek, 2020a) and set at $c_{x,0}$ = 7 g/L and $Y_{X/gluc}$ = 0.25 g/g initially.

Finally, the MEL production phase was initiated at the end of the growth phase by adding a defined amount of rapeseed oil to the fermenter. Within the production phase, individual process times and oil feeding strategies were studied to investigate the best feeding conditions (see results section).

Sampling and Analytics

For off-line analysis of optical density, dry biomass, glucose and nitrate concentrations in the bioreactor, samples of 7 ml were drawn at regular intervals and treated as follows:

OD_{625} was measured in duplicates in a photometer (Gilson Inc., Middleton, United States) after appropriate dilution. For the

quantification of dry biomass, samples of 1–5 ml, depending on the expected cell mass, were pipetted onto pre-dried and weighed filters and washed multiple times with water and ethanol to remove salts and residual substrates. After drying at 110°C for 24 h, the filters were weighed again and dry biomass was calculated from the weight difference and volume. The identical method was used to prepare samples for elemental analysis of the biomass. A correlation of dry biomass with OD_{625} values showed a linear trend during growth phase, where dry biomass [g/L] = 0.35 * OD_{625} [-]. Moreover, backscatter values obtained in the micro-cultivation system were correlated as well, showing a linear trend of backscatter gain 5 [-] = 0.14 * OD_{625} [-].

For determination of carbohydrates and sodium nitrate concentration, 1 ml of the sample was centrifuged for 10 min at 16,000 g and the supernatant was collected. An aliquot of the supernatant was diluted with 5 mM H_2SO_4, filtered with 3 kDa polyethersulfone (PES) centrifugal filters and measured by HPLC (Bischoff GmbH, Germany). Separation of the analytes was performed on a Phenomenex Rezex ROA-Organic Acid H+ (8%) column (30 cm × 7.8 mm, Phenomenex, Aschaffenburg, Germany) with 5 mM H_2SO_4 as mobile phase at a flow rate of 0.6 ml/min and 30°C column temperature. Detection of the sugars was done with a refractive index (RI) detector (Bischoff GmbH, Germany). External standards of D-glucose, D-mannose, D-mannitol, erythritol and glycerol (0.125–10 g/L each) were used for calibration. For $NaNO_3$ quantification, the supernatant was diluted with de-ionized water and analyzed with an enzymatic nitrate reductase test (R-Biopharm, Darmstadt, Germany) in a miniaturized 96-well-plate format. External $NaNO_3$ standards between 0.02–0.3 g/L were used on each plate for calibration.

For analysis of hydrophobic substances like triglycerides, fatty acids and MEL, 800 µL of culture broth was extracted with 800 µL of ethyl acetate by shaking at 1,400 rpm for 15 min, followed by centrifugation at 16,000 g and room temperature for 5 min to separate the two phases. Of the organic supernatant, 500 µL were collected and the solvent evaporated until constant weight. After weighing the crude lipid extract, it was re-suspended with pure ethanol to a total concentration of 20 g/L crude extract and analyzed by high-performance thin-layer chromatography (HPTLC). HPTLC was performed on HPTLC silica 60 plates (20 × 10 cm, Merck, Germany) using a solvent system consisting of chloroform-methanol (20:3 v/v). A sample volume of 2 µL was spotted with an ATS4 automatic TLC sampler (CAMAG, Muttenz, Switzerland). After development, the HPTLC plates were stained by dipping for one second into acetic acid/p-anisaldehyde/sulphuric acid (97:1:2 v/v/v) reagent solution, heated to 110°C and quantified densitometrically with the gel analyzer function of ImageJ. Calibration of MEL concentration between 2 and 20 g/L was done with a representative purified MEL standard from a previous *M. aphidis* cultivation, which was purified as published previously (Beck et al., 2019a). Fatty acid and residual oil concentrations were calibrated using oleic acid and commercial rapeseed oil as external standards in the range from 1–10 g/L.

Data Analysis and Calculations

Online parameters like pH, temperature T, dissolved oxygen concentration DO, stirrer speed n and the respective volumes of pH-correcting agents and feeding solution were logged by Iris fermentation software (Infors HT, Bottmingen, Switzerland). Off-gas concentrations for oxygen O_2 and carbon dioxide CO_2 were logged with FermVis software (BlueSens GmbH, Herten, Germany).

In addition to the parameters that were directly measured online or offline, other key parameters for fermentation evaluation and modeling like volumetric and biomass-specific rates as well as yields were analyzed. All equations are derived from generally accepted growth kinetics (Chmiel et al., 2018).

The specific growth rate µ was calculated from the difference in dry biomass concentration c_x:

$$\mu = \frac{1}{c_x}\frac{\Delta c_x}{\Delta t} \tag{2}$$

Volumetric substrate consumption rates r_S, yield coefficients $Y_{X/S}$ and biomass-specific substrate consumption rates q_S were determined for glucose and nitrate respectively:

$$r_S = \frac{\Delta c_S}{\Delta t}; Y_{X/S} = \frac{\Delta c_x}{\Delta c_S}; q_S = \frac{r_s}{c_x} = \frac{1}{c_x}\frac{\Delta c_S}{\Delta t} = \frac{1}{Y_{X/S}}\mu \tag{3}$$

Oxygen uptake rates (OUR), carbon dioxide emission rates (CER) and respiratory coefficients (RQ) were calculated from in- and off-gas concentrations y_{O2} and y_{CO2} (α = gas inlet, ω = exhaust) based on the following formula:

$$OUR = r_{O2} = \frac{Q_{air}p_{air}}{V_L R T} * \left(y_{O2}^{\propto} - \frac{1 - y_{O2}^{\propto} - y_{CO2}^{\propto}}{1 - y_{O2}^{\omega} - y_{CO2}^{\omega}} y_{O2}^{\omega}\right) \tag{4}$$

$$CER = r_{CO2} = \frac{Q_{air}p_{air}}{V_L R T} * \left(\frac{1 - y_{O2}^{\propto} - y_{CO2}^{\propto}}{1 - y_{O2}^{\omega} - y_{CO2}^{\omega}} y_{CO2}^{\omega} - y_{CO2}^{\propto}\right) \tag{5}$$

$$RQ = \frac{CER}{OUR} \tag{6}$$

Airflow rates Q_{air}, gas pressure p_{air} and temperature T were set as constant. The volume of liquid culture medium V_L was adjusted for the OUR/CER calculations when feeding was done during the process.

Biomass-specific oxygen uptake rates q_{O2} as well as biomass yield coefficients from oxygen $Y_{X,O2}$ were determined as follows:

$$Y_{X/O_2} = \frac{\Delta c_x}{\Delta y_{O_2}}; q_{O_2} = \frac{OUR}{c_x} = \frac{1}{Y_{X/O_2}}\mu \tag{7}$$

During the production phase, oil consumption and MEL production rates as well as the MEL yields from oil were calculated according to:

$$r_{oil} = \frac{\Delta c_{oil}}{\Delta t}; q_{oil} = \frac{r_{oil}}{c_x} = \frac{1}{c_x}\frac{\Delta c_{oil}}{\Delta t} \tag{8}$$

$$r_{MEL} = \frac{\Delta c_{MEL}}{\Delta t}; q_{MEL} = \frac{r_{MEL}}{c_x} = \frac{1}{c_x}\frac{\Delta c_{MEL}}{\Delta t} \tag{9}$$

$$Y_{MEL/oil} = \frac{\Delta c_{MEL}}{\Delta c_{oil}} \tag{10}$$

Lastly, the percentage of MEL (X_{MEL}) in the lipid fraction, which is an indicator for the conversion of the substrate lipids (oil and fatty acids) into product (MEL), was calculated from the measured concentrations of MEL, fatty acids and oil respectively:

$$X_{MEL} = \frac{c_{MEL}}{c_{oil} + c_{FA} + c_{MEL}} = \frac{c_{MEL}}{c_{crude\ extract}} \quad (11)$$

The value X_{MEL} is also equivalent to the purity of the crude lipid extract, which is obtained when the lipids (MEL, fatty acids and oil) are extracted from the broth as the first step of downstream processing.

Linear regression of experimental data was performed to determine the different rates and yields using professional graphing and analysis software (OriginPro, OriginLab Corporation, United States).

Kinetic Modeling and Simulation of the Process

For kinetic modeling of the process, several ordinary differential equations (ODEs) were designed and implemented in Microsoft Excel. According to the separation of growth and MEL production phase, two partial models were developed. Numerical solution of the ODEs based on an explicit Euler method with a step size of 0.05 h for the growth model and 0.2 h for the production model was used to simulate the respective concentrations. The model equations and input parameters are described in full detail in the results section.

RESULTS AND DISCUSSION

Based on our previous publication, the MEL fermentation process was generally divided into two stages (Beck and Zibek, 2020a). First, a growth phase was performed on glucose as sole carbon substrate to obtain high cell biomass concentrations, followed by a production phase with rapeseed oil as inductor and main carbon substrate for MEL production. The advantage of such a two-stage process is that both phases can be optimized individually and independently to a certain extent. For example, the effect of biomass concentration on MEL productivity can be studied much better than in a single-stage batch process, where many metabolic pathways are active simultaneously and are competing for the same substrate. According to our previous results, an efficient biomass formation with high cell density is a crucial step for subsequent MEL production. In the current study we therefore optimized first the biomass growth phase by evaluation of medium composition and carbon sources, and developed a batch and a subsequent fed-batch process to increase the biomass concentration in the bioreactor. The amount of oil feeding during production phase was then adapted to the biomass concentration to achieve full substrate conversion. Finally, the experimental data obtained were used to develop a kinetic model that allowed simulation of the process.

Characterization and Quantification of Cellular Biomass

As a first step, the cell growth of *M. aphidis* was characterized in detail. This is particularly important since *M. aphidis* is known to have a dimorphic growth behavior and to accumulate intracellular storage lipids, which are visible as globules inside the cells (compare Rau et al. (2005b) and Beck and Zibek (2020a)). Both phenomena made it necessary to define how biomass is quantified and how it is composed in order to establish a robust and well-defined fermentation process.

Dimorphic growth of *M. aphidis* was observed with our defined mineral medium in the bioreactor, using glucose as the sole carbon source for cell growth (**Figure 1**). During early growth phase, the cells grow as filamentous cells, which leads to large macroscopic mycelia that are visible to the naked eye. During late growth phase, when the carbon and nitrogen sources are about to be depleted, more and more elongated single cells are visible under the microscope and the broth becomes more homogenous. During production phase on oil, which is running under nitrogen-limited conditions, mostly single cells are present in the culture broth. Moreover, storage vesicles inside the cells are observed during MEL production phase on rapeseed oil, which leads to a swelling of the cells.

As mentioned before, this special behavior of the cells influences the way in which biomass needs to be measured and quantified. We thus evaluated the elemental composition of dried *M. aphidis* cells during the different process stages, i.e. growth and production phase. From a set of more than 20 samples, taken during 12 different fermentations and different process stages in the bioreactor, the average biomass composition during growth and MEL production phase was determined. It was evident that the elementary composition was considerably different between the two phases. While an average nitrogen (N) content of 6.2 ± 1.4% w/w was determined during non-limited growth on glucose and nitrate, this value dropped to only 1.3 ± 0.4% w/w during the production phase on oil (nitrogen-limited). At the same time, relative carbon (C) and hydrogen (H) levels increased (**Table 1**).

In order to set up a balance of elements, the relative C, H and N contents were multiplied with the measured dry biomass at the respective time points, yielding the total amount of each element contained within the cellular biomass. It was found that the observed increase of measured dry biomass during production phase was caused only by accumulation of C and H, while the total mass of elementary nitrogen in the dry cell mass remained constant after the depletion of $NaNO_3$ in the medium. In our culture medium using 3 g/L $NaNO_3$ as nitrogen source, a maximum of 0.49 g_N/L elementary nitrogen was available. At an average nitrogen content of 6.2 ± 1.4% in the biomass, the medium would thus allow for a theoretical maximum biomass concentration of 7.9 ± 1.9 g/L during growth. The theoretically maximum biomass yield from sodium nitrate $Y_{X/NaNO3,max}$ is thus equal to 2.6 g/g. During our experiments, an average biomass yield from nitrate $Y_{X/NaNO3}$ of 1.8 g/g (i.e. around 5.5 g/L biomass from 3 g/L $NaNO_3$) was observed during growth. The nitrogen yields were hence at 70% of the theoretical maximum. The further

FIGURE 1 | Microscope images of *M. aphidis* cells during growth (left) and MEL production (right). Arrows indicate visible storage globules inside the cells.

TABLE 1 | Average biomass composition (CHN-analysis; n > 20 samples from 12 different fermentations) of *M. aphidis* cells during growth phase (glucose, non-limited) and MEL production phase (oil addition, N-limited).

Phase and Respective Substrate	($g/100\ g_{biomass}$)				Molar Composition
	C	H	N	Others (O, S, Minerals)	
Growth (glucose)	48.5 ± 3.9	7.1 ± 0.6	6.2 ± 1.4	38.1 ± 3.7	$CH_{1.77}N_{0.112}O_{0.597}$
Production (oil)	62.2 ± 3.0	9.2 ± 0.5	1.3 ± 0.4	27.3 ± 3.3	$CH_{1.77}N_{0.018}O_{0.333}$

strong increase of biomass during production phase, which was observed up to around 30 g/L dry mass, was therefore only caused by C and H accumulation (lipid inclusion) and not by actual "growth" in terms of cell doubling, which would require additional nitrogen for DNA, RNA and amino acids synthesis.

Similar observations were made by Rau et al. (2005b), who already showed that intracellular protein levels remained constant after initial growth although dry biomass further increased. This was reported to be due to accumulation of lipid material inside the cells. An elemental composition of C 68.1, H 8.0 and N 1.9 (% w/w) was presented for *M. aphidis* DSM70725 biomass during simultaneous growth and MEL production on soybean oil (Rau et al., 2005b), which is similar to our values during production phase on oil. Moreover, Klement et al. (2012) have also shown a strong decrease in cellular nitrogen content between exponential growth and nitrogen limiting conditions for the closely related *Ustilago maydis* (N 7.35 vs 2.83% w/w) during itaconic acid production. Both references confirm our observations of a decreasing cellular nitrogen content during the nitrogen-limited MEL production phase on oil.

It was hence concluded that using lipid substrates does not only result in biomass increase by cell division but mostly due to simultaneous accumulation of lipid storage material inside the cells. This is one of the major reasons why we decided to work with separate growth and MEL production phases, allowing for a more precise analysis of biomass concentration during the fermentation process. Whenever biomass-specific rates were calculated, they were based on the biomass concentration that was achieved at the end of the growth phase ($c_{x,growth}$). It also needs to be mentioned that the lipid inclusion has implications for the modeling and simulation of biomass and lipid concentrations during the production phase, as some of the lipid substrate is accumulated in the biomass and is thus not available for MEL production.

Evaluation of Medium Composition with Regard to Biomass Formation and MEL Production

While most of the elementary nitrogen supplied in the culture medium was actually recovered in the produced biomass at the end of the growth phase, as demonstrated before, the elementary carbon was less efficiently directed into biomass formation. Of the initial 12 g_C/L elementary carbon in our medium containing 30 g/L glucose, only around 2.65 g_C/L (i.e. 22 % of the initial amount) were found in the biomass at the end of the batch growth phase. This led to a biomass yield coefficient from glucose ($Y_{X/glucose}$) of 0.18 g/g. Even when taking into account that CO_2 formation during cellular respiration can amount for up to 50% of carbon consumption in aerobic processes, there is still a considerable amount of elementary carbon not directed into either biomass formation or cellular respiration.

It was expected that increasing the concentration of the most important macro elements N, P or S in the culture medium could

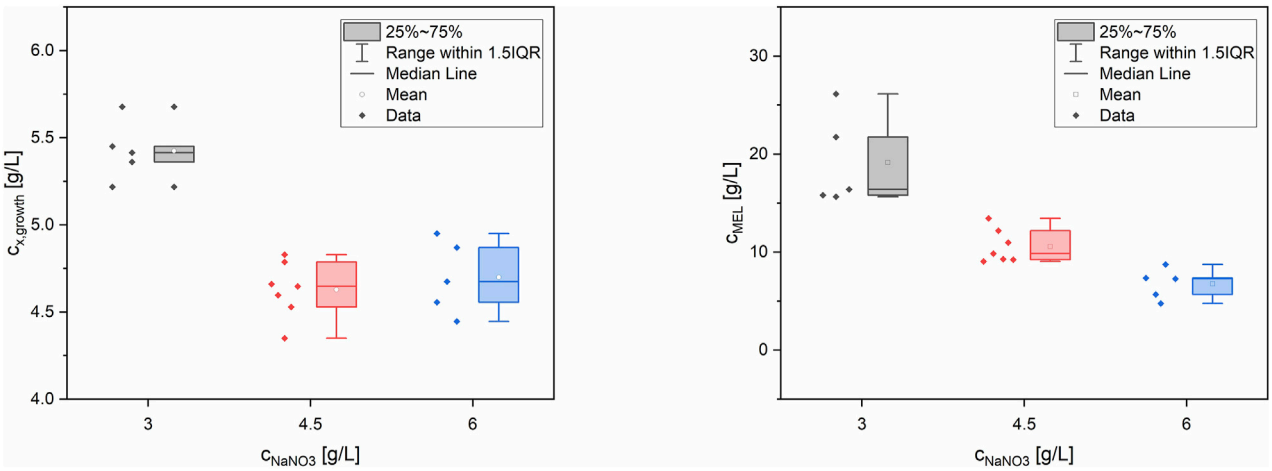

FIGURE 2 | Box-whisker plots for biomass (left) and MEL concentration (right) depending on $NaNO_3$ concentration in the medium, at a fixed glucose concentration of 30 g/L. The different concentrations of P and S were less or even not significant.

lead to a higher biomass yield from the same amount of glucose and thus a higher biomass concentration. Hence, a possible adjustment of our mineral medium was investigated. Different medium compositions with increased concentrations of N, P and S were examined at a fixed glucose concentration (30 g/L), resulting in lower C/N, C/P and C/S ratios. The experimental design was based on a randomized Box-Behnken design (**Supplementary Table S1**).

Statistical analysis of the results by ANOVA showed that nitrogen was the most significant factor ($p < 0.0001$) for biomass formation, which was quantified as dry biomass concentration at the end of the growth phase (48 h). Phosphate was less significant ($p = 0.033$), while sulfur was not significant ($p = 0.526$) and was thus excluded from the final biomass model. Biomass formation was best described by a reduced quadratic model using N^2, N and P as model terms. Comparison of experimental biomass values with those predicted by the quadratic model showed very good agreement. The two verification runs, placed at the corners of the design space, were also in agreement with the model prediction. For the MEL production, which was quantified as the MEL concentration after 210 h, only the nitrogen concentration was a significant factor ($p = 0.0002$). A reduced linear model using only N as significant parameter was the best fit for the data. Similar as for the growth model, comparison of experimental and predicted values as well as the two verification runs showed good agreement.

In summary, the lowest concentration of $NaNO_3$ (3 g/L) and thus the highest C/N ratio of 28.4 mol_C/mol_N yielded the best biomass formation ($c_{x,growth} = 5.4 \pm 0.2$ g/L) from glucose and subsequently the highest MEL production ($c_{MEL} = 19.1 \pm 4.6$ g/L) from rapeseed oil (see **Figure 2**). The maximum biomass yield coefficient from glucose $Y_{X/glucose}$ was 0.18 ± 0.01 g/L. In terms of C/P ratio, a higher P concentration slightly increased biomass but at the same time did not have a significant influence on MEL formation. The effect of P concentration was overall very small

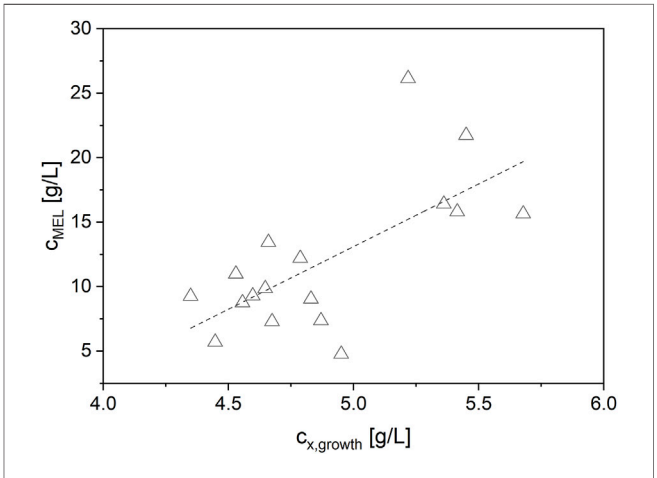

FIGURE 3 | Positive correlation between the target values biomass and MEL concentration. Higher biomass concentrations at the end of the growth phase lead to higher MEL concentrations during production phase.

compared to N. Moreover, a positive correlation between the target values biomass and MEL concentration was observed (**Figure 3**). MEL formation is enhanced when higher amounts of biomass are formed during growth phase. This is in agreement with the theory of secondary product formation, e.g. by Luedeking and Piret (1959), and similar to observations made by Kitamoto et al. (1992) using a resting cell approach with different cell concentrations. It also confirmed our prior observations using this mineral medium at different starting concentrations, where higher biomass concentrations led to subsequently higher MEL production from oil in several Ustilaginaceae species (Beck and Zibek, 2020a).

Contrary to our initial expectation, it was concluded that high C/N, C/P and C/S ratios in the medium are best to form high biomass and MEL concentrations with *M. aphidis*.

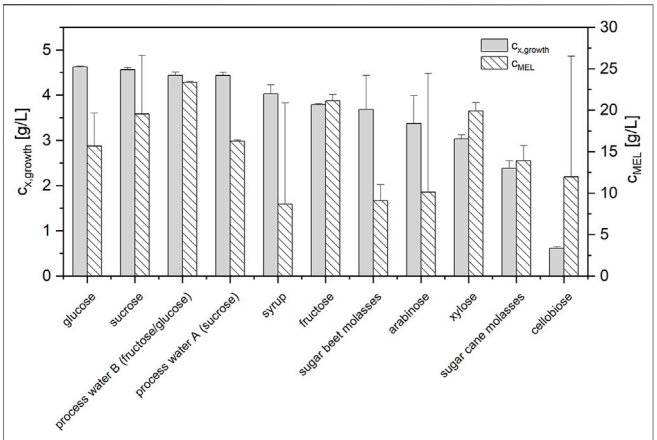

FIGURE 4 | Maximum biomass concentrations ($n = 3$) for different sugar substrates during growth and corresponding MEL concentrations ($n = 2$) after a subsequent production phase on 8% rapeseed oil. All sugar substrates were employed at a total sugar concentration of 30 g/L to ensure direct comparability.

Specifically, the high C/N ratio in our mineral medium with 30 g/L glucose and 3 g/L $NaNO_3$ proved to be ideal for biomass formation and subsequent MEL production. Most likely the resulting nitrogen limitation is beneficial for induction of MEL production as a part of the secondary lipid metabolism, which is promoted under such conditions (Hewald et al., 2006; Bolker et al., 2008; Beck and Zibek, 2020b). This holds also true for other fungal glycolipid biosurfactants like sophorolipids or cellobiose lipids (Jezierska et al., 2018). Moreover, it has been reported before that an ideal C/N ratio for the growth of *M. aphidis* DSM 70725 was around 42.5 mol_C/mol_N (30 g/L glucose and 1 g/L NH_4NO_3) and that a variation of the phosphate content between 0.1 g/L and 0.9 g/L KH_2PO_4 did not have an influence neither on cell growth nor on MEL production (Rau et al., 2005b). In Rau et al. (2005b), the C/N ratio was even higher than in our work, but it should also be noted that yeast extract was used in their culture medium, which contains additional carbon, nitrogen and phosphate compounds and thus influences these ratios to a certain extent.

According to the presented results, it was decided to continue with the mineral medium composition containing 30 g/L glucose, 3 g/L $NaNO_3$, 1 g/L KH_2PO_4 and 1 g/L $MgSO_4{*}7H_2O$ for all further experiments.

Screening of Different Sugar Substrates for Growth

After optimizing the mineral medium composition for biomass formation, different carbon substrates for cell growth were screened as well. The investigated sugars were glucose, sucrose, fructose, xylose, arabinose and cellobiose. Moreover, several fractions from the sugar refining process like syrup, two different process water A (containing mostly sucrose) and B (containing fructose and glucose) from process centrifuges, as well as sugar cane and sugar beet molasses were evaluated. Glucose was used as the reference sugar for growth. All carbon substrates were employed at the same total sugar concentration of 30 g/L.

The results showed that the crystalline sugars sucrose, fructose, xylose, and arabinose were fully consumed at the end of the growth phase and yielded biomass concentrations that were in the same range as those from the glucose reference (3.0–4.6 g/L, see **Figure 4**; **Supplementary Table S2**). The different fractions from sugar refining, which contained mostly sucrose, glucose and fructose, were also fully assimilated for growth and yielded similar biomass concentrations. Of all the investigated substrates, only cellobiose was shown to be unsuitable for cell growth. Cellobiose was not assimilated by the microorganism and resulted in much lower biomass concentrations (0.62 g/L).

In the subsequent production phase on rapeseed oil, MEL was formed in all experiments (**Figure 4**). Thus, none of the sugars inhibited subsequent MEL formation. The reference process with glucose yielded an average MEL concentration c_{MEL} of 15.7 ± 4.0 g/L. Compared to the reference, sucrose, fructose and xylose as well as process water B had even higher average c_{MEL}. Process water A was similar to glucose in terms of c_{MEL}. Syrup, arabinose and cellobiose as well as the two molasses had lower average c_{MEL}. However, there was also a high standard deviation for syrup, arabinose and cellobiose, as one experiment had a c_{MEL} comparable to the glucose reference, while the duplicate did not produce MEL. The successful production of MEL in the experiments with cellobiose, despite the absent cell growth during the growth phase, could be attributed to a combined cell growth and MEL production from rapeseed oil.

Overall, it was demonstrated that *M. aphidis* is able to assimilate a wide range of sugars for growth and that these sugars did not negatively influence or inhibit subsequent MEL formation. This is the first time that such a screening has been reported for *M. aphidis*. Nevertheless, it had been shown before that the closely related fungus *M. antarcticus* is able to use glucose, sucrose, fructose, mannose, mannitol and glycerol as carbons sources for growth, and that neither of the sugars negatively influenced subsequent MEL production from soybean oil (Kitamoto et al., 1992). Thus, it can be expected that most of the related Ustilaginaceae species that are employed for MEL production have the ability to use these carbon substrates for cell growth.

It was then decided to continue with glucose as growth substrate for further experiments, despite the equally good results for many of the investigated sugars. Glucose had been used before in other publications, which ensures comparability, and it was now shown to yield high biomass and subsequently high MEL concentrations in a reproducible manner with *M. aphidis* as the production strain.

Bioreactor Fermentations With Batch Growth Phase

The fermentation process for MEL production was then transferred to a 7-L aerated stirred-tank bioreactor and different process variations were investigated. Initially, a process with batch growth phase was established that served as a benchmark for further process optimization.

TABLE 2 | Process values for fermentations with batch growth and single or repeated oil feeding.

Process	B1	B2
growth phase	batch	batch
$c_{x,growth}$ (g/L)	4.2	n.d
$Y_{X/gluc}$ (g/g)	0.155	n.d
OUR_{max} (mmol/Lh)	24.9	25.9
production phase	single oil feed	repeated oil feed
total oil feed (%)	6	22 (6 + 4 × 4)
oil-to-biomass ratio (g/g)	12.0	n.d
$c_{MEL,max}$ (g/L)	11.2	27.1
$r_{MEL,av}$ (g/Lh)	0.105	0.101
MEL yield per total oil[#] (g/g)	0.226	0.135
X_{MEL} (%)	81	20
process duration (h)	170*/240	333

[#] *related to the total amount of oil added to the reactor.*

* *time when maximum MEL, concentration and/or purity were reached.*

The first run in the STBR was based on a simple two-staged batch (B1, see **Table 2**). Batch growth was performed on our defined mineral medium with 30 g/L glucose as carbon substrate and production was initiated with 6% v/v rapeseed oil after 48 h, when the cells entered stationary phase (**Figure 5**). The consumption of primary growth substrates glucose and nitrate resulted in formation of 4.2 g/L biomass, measured as cell dry weight. Parallel to cell growth, oxygen demand of the cells increased exponentially during growth, showing a maximum OUR of 24.9 mol/Lh after 48 h. Maximum CER at the same time was at 36.5 mmol/Lh, and the average RQ during growth phase was 1.39. The biomass specific rates q_{O2} and q_{CO2} were 4.2 and 6.5 mmol/gh respectively. Dissolved oxygen concentration in the medium decreased until the 10% set point was reached, where it was then maintained by increasing stirring speed. The growth-associated increase of pH, which resulted from a consumption of substrates, was stabilized by automated addition of acid to maintain pH 6 during growth. At 48 h, when the nitrogen source was completely consumed, rapeseed oil (6% v/v, reference volume of 4 L) was added to start the MEL production phase. Oil addition negatively influenced the offline measurement of OD and biomass during the first hours after oil addition due to the formation of a separate phase, but was again showing reasonable values during later stages when oil had been (partly) hydrolyzed. Oil hydrolysis by extracellular lipases began directly after the oil (triacylglyceride, TAG) was added to the fermenter, resulting first in an increase of free fatty acids (FFA) in the broth and then MEL production. The measured biomass concentration ultimately increased up to around 30 g/L during production phase, due to an intracellular accumulation of lipids as discussed before. A plateau of MEL concentration was reached when nearly all fatty acids were consumed after 150–170 h. At 168 h, a MEL concentration of 11.2 g/L was obtained. The share of MEL in the crude extract (X_{MEL}), which was calculated as the percentage of MEL (i.e. 11.2 g/L) in the crude lipid extract (13.9 g/L), was 81% at this time. The rest

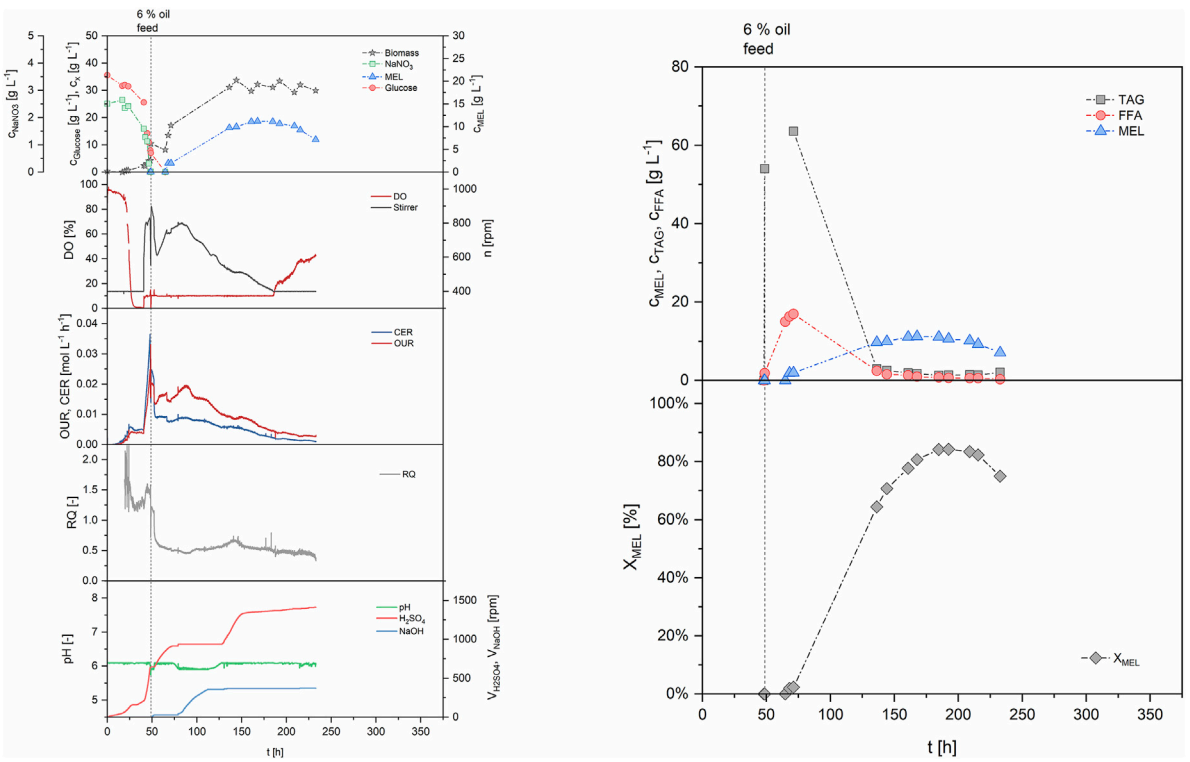

FIGURE 5 | Process data for the two-staged batch (B1). Growth was performed in batch mode, and production was initiated at 48 h using 6% v/v rapeseed oil as substrate.

was remaining substrate oil (12%) and free fatty acids (7%). The average MEL formation rate (r_{MEL}) between 48 and 168 h was calculated to 0.105 g/Lh and the yield coefficient with regard to the total amount of oil added was calculated to 0.226 g/g_{oil}. Despite the almost full consumption of oil and fatty acids, the MEL yield coefficient was relatively low. This can be explained by the previously described accumulation of storage lipids inside the cells, which leads to an increase in cell biomass, but makes them unavailable for MEL production. The process was maintained until 240 h, but there was even a decrease in MEL concentration after that point, correlating with a starvation of the microorganisms. Off-gas analysis during the production phase showed a decrease of cellular respiration, with OUR and CER values that were lower than during exponential growth and constantly decreasing with time. During the production phase the RQ was around 0.52. Hence, the oxygen uptake was higher than the emission of CO_2, which indicates that a highly oxidative pathway was active. This is for example the case during lipid metabolism, where the fatty acids are converted to acetyl-CoA by multiple cycles of β-oxidation to generate energy. The trend of pH was also an interesting indicator. As long as the oil was hydrolyzed, which correlated with a decrease in oil concentration and a release of fatty acids, the pH decreased, so base was constantly titrated to maintain the pH. At the time when oil and also fatty acid concentrations reached zero (around 130 h), pH of the broth shifted and acid was titrated. This was accompanied by a decrease in oxygen uptake and stirring speed, which can be attributed to the depletion of substrate and thus lower respiratory activity. This behavior had been observed before in the microcultivation experiments with our mineral medium, where the dissolved oxygen and pH in the broth showed the same trends (see also Beck and Zibek (2020a)). Therefore, the recorded online values (DO, stirring speed, OUR and pH) could be used to help interpret the time course of biomass growth, oil hydrolysis and MEL production.

Overall, the values for biomass and MEL concentration in this first bioreactor experiment were comparable to those obtained in the microcultivation system before. As the experiments in the microcultivation system were also performed as a two-stage batch process, the process was successfully transferred from a shake culture to the stirred-tank system.

In a second bioreactor experiment (B2, **Table 2**; **Supplementary Figure S1**), production phase was initiated again with 6% v/v oil after an initial batch growth phase, but was then prolonged by multiple additions of rapeseed oil in portions of 4% v/v after 118, 165, 215 and 286 h. Maximum oxygen uptake rate during batch growth was at 25.9 mmol/Lh and thus almost identical to the previous run, showing good reproducibility of the batch growth phase. The same was true for CER and RQ. During production phase, a maximum of 27.1 g/L MEL was achieved after 333 h, with an average MEL formation rate of 0.101 g/Lh. The MEL formation rate was thus almost identical to before, while the total MEL concentration was increased due to the longer process time and higher substrate concentration. However, the share of MEL (X_{MEL}) in the crude lipid extract at the end of the process (132.6 g/L crude extract) was only at 20%, meaning that a high amount of oil and fatty acids (32 and 48% respectively) remained in the broth. This was due to the multiple oil feeds and thus higher concentrations of fatty acids released, which could not be consumed by the microorganism and were thus accumulating in the broth over the entire production phase. Oxygen uptake rates and stirring during production phase were maintained at a higher level than before and did not show such a strong decrease, which was indicative for the maintenance of cellular activity by the still active lipid metabolism. Besides, a steady consumption of NaOH was observed to maintain the pH until the end of the process, and no acid was titrated. This correlated with the ongoing oil hydrolysis and accumulation of fatty acids in the broth.

Overall, a higher MEL concentration was achieved in the second process with repeated oil feeding, but only at the expense of an increased process time as well as higher concentrations of remaining oil and fatty acids, which in turn resulted in a reduced purity of the crude extract. Hence, the amount of oil feeding in the second process was too high for the microorganism to convert into product. MEL formation rate was similar between the two processes, regardless of the amount of oil added. This was a clear indication that the MEL formation rate mainly depends on the biomass concentration. Therefore, the biomass concentration should be increased to achieve higher productivity throughout the process. In addition, the oil dosage needs to be adjusted to the current biomass concentration to achieve good oil conversion, which in turn should lead to lower fatty acid concentrations and thus higher purity of the crude lipid extract at the end of the process.

Bioreactor Fermentations With Increased Biomass Concentration Using Fed-Batch Growth

Based on the previous results, higher biomass concentrations during growth phase were then targeted, which were expected to result in higher MEL formation rates and better oil conversion during production phase. In a first approach, the initial batch concentration of all medium components was increased to levels of 60, 90 or 120 g/L glucose respectively and the growth was examined in the microcultivation system and STBR (data not shown). Although the growth substrates (glucose and $NaNO_3$) were fully consumed and higher biomass concentrations were formed at the end of the growth phase, negative effects like oxygen limitation, growth inhibition and biomass accumulation at the reactor vessel occurred at these high medium concentrations in the batch, which in turn led to lower reproducibility and stability of the process. Similar to our observations, it had been reported before that batch concentrations of glucose and $NaNO_3$ above 30 and 3 g/L, respectively, did not lead to higher biomass concentrations and subsequently even lower MEL yields (Rau et al., 2005b).

Consequently, we focused on developing fed-batch processes with exponential substrate feeding during the growth phase. Exponential feeding ensures microbial growth at a defined and constant specific growth rate, leading to high biomass formation in a reproducible manner, while at the same time maintaining low concentrations of medium components in the reactor. The

TABLE 3 | Process values for fermentations with combined batch and fed-batch growth and repeated or continuous oil feeding.

Process	FB1	FB2	FB3	FB4
growth phase	batch + fed-batch	batch + fed-batch	batch + fed-batch	batch + fed-batch
μ_{set} (h^{-1})	0.08	0.09	0.09	0.08
feeding duration (h)	10.5	11.5	11	16.9
total medium feed (g)	460	612	708	701
$c_{x,growth}$ (g/L)	12.0	15.5	10.9	14.1
$Y_{X/gluc}$ (g/g)	0.171	0.212	0.171	0.254
OUR_{max} (mmol/Lh)	58.2	74.8	58.0	63.2
production phase	repeated oil feed	continuous oil feed	repeated oil feed	continuous oil feed
total oil feed (% v/v)	24 (6 + 6 + 6 + 6)	24 (6 + 18 cont.)	12 (6 + 6)	12 (6 + 6 cont.)
oil-to-biomass ratio (g/g)	20.2	15.7	10.9	8.8
$c_{MEL,max}$ (g/L)	50.5	43.9	35.7	34.3
$r_{MEL,av}$ (g/Lh)	0.185	0.422	0.335	0.378
MEL yield per total oil[#] (g/g)	0.208	0.181	0.294	0.275
X_{MEL} (%)	68	49	88	98
process duration (h)	502	147*/310	170*/231	169*/307

[#] *related to the total amount of oil added to the reactor.*

* *time when maximum MEL, concentration and/or purity were reached.*

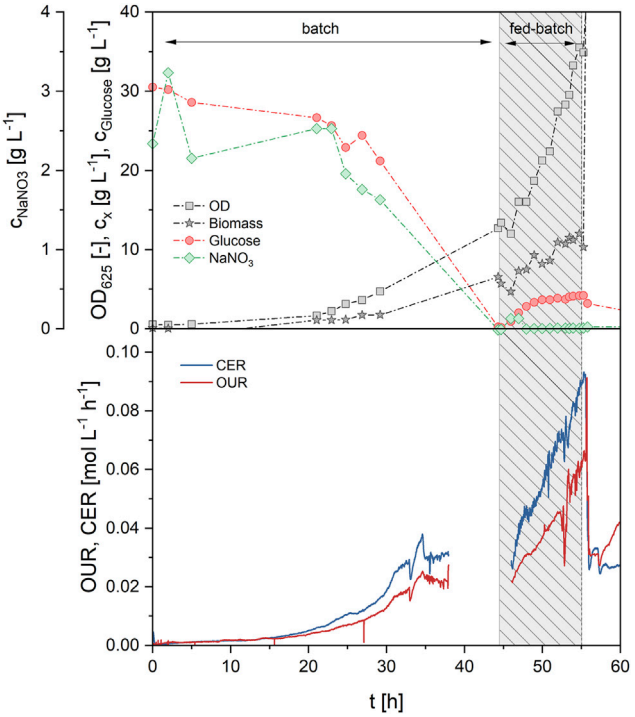

FIGURE 6 | Process data of fed-batch process 1 (FB1) during growth phase (0–55 h) showing concentrations of glucose, $NaNO_3$, biomass and OD (upper) and off-gas analysis (lower graph). Medium feeding was applied from 44.5–55 h with an exponential feed rate at μ_{set} = 0.08 h^{-1}, leading to a further increase of biomass, OUR and CER.

exponential feeding phase was always initiated after an initial batch growth phase, which was performed identically to the previous batch processes to ensure reproducibility and comparability. The aim of all fed-batch processes was to obtain a biomass concentration that was at least twice that of a simple batch growth phase, and subsequently to prove that this led to an increased MEL production rate during production phase.

In the first fed-batch process (FB1, **Table 3**; **Supplementary Figure S2**), exponential feeding with a growth rate μ_{set} of 0.08 h^{-1} was carried out after an initial batch growth phase on 30 g/L glucose. The growth rate for fed-batch was thus set at roughly 70% of the maximum growth rate μ_{max}, which was determined as 0.11 h^{-1} in the batch growth experiments before. Other parameters for the feeding equation were set at c_{x0} = 7.6 g/L and $Y_{X/S}$ = 0.25 g/g. Exponential feeding was conducted for 10.5 h between 44.5 and 55 h of process time. During that time, a total of 460 g of feeding solution were added, equivalent to 138 g glucose and 13.8 g $NaNO_3$. This led to a biomass increase from 5.7 g/L (at the end of batch growth) to 12.0 g/L (end of fed-batch), thus more than doubling the biomass concentration. The corresponding biomass yield from glucose was determined as 0.171 g/g and was constant between batch and fed-batch phase. Parallel to the biomass concentration, the OUR increased from 25.0 mmol/Lh during batch growth up to 58.2 mmol/Lh at the end of the fed-batch phase, showing the proportionality between biomass concentration and OUR (**Figure 6**). CER was simultaneously increased from 31.6 mmol/Lh up to 82.2 mmol/Lh. The specific rates q_{O2} and q_{CO2} during the fed-batch phase were at 4.3 and 6.5 mmol/gh, respectively, and the average RQ was 1.42 during both batch and fed-batch growth. Generally, off-gas data was identical with the results from batch fermentations, showing the high reproducibility and robustness of the biomass growth phase. While nitrate concentration in the broth remained at limiting levels during the feeding phase, a slight glucose accumulation up to 4.2 g/L was registered. Production phase was initiated at 55 h by adding 6% v/v rapeseed oil to the bioreactor. The first oil feed was converted very fast, showing a MEL concentration of 18.5 g/L at a X_{MEL} of 73% after 142 h. Three further oil feeds of 6% v/v each were done at 142, 190 and 242 h to maintain MEL production phase. Subsequently, a MEL

concentration of 43 g/L was reached after 310 h, but X_{MEL} was only at 40% at that time. The process was thus continued up to a process time of 500 h without further oil feeding. MEL concentration increased only a bit and reached a final value of 50.5 g/L, but the X_{MEL} was increased to 68% again, due to further consumption of remaining oil and fatty acids (8 and 24% at the end respectively). The average MEL production rate between 55 and 310 h was relatively constant at 0.185 g/Lh, and therefore almost doubled in comparison to the previous batch processes. After 310 h, the production rate decreased, which was probably caused by the long process time and reduced activity of the cells.

The second fed-batch process (FB2, **Table 3**; **Supplementary Figure S3**) was conducted at a slightly higher exponential feeding rate, equivalent to a μ_{set} of 0.09 h^{-1}. In total, 612 g of feed solution (184 g glucose and 18.4 g $NaNO_3$) were added during an 11.5 h feeding period between 42.5 and 54 h. This resulted in an increased biomass concentration of 15.5 g/L at the end of the fed-batch. The maximum OUR by that time was 74.8 mmol/Lh. Biomass concentration and OUR were therefore further increased compared to the previous run. Production phase was initiated with 6% v/v rapeseed oil at 54 h as previously, but this time the additional 18% v/v of oil were delivered as a continuous feed with a constant rate of 11 ml/h between 72 and 140 h. Compared with the previous process, the same amount of oil was added in a shorter time period. This led to a faster oil hydrolysis and high fatty acid (67 g/L) and MEL concentrations (43.9 g/L) after 147 h, when the continuous oil feeding was stopped. The average MEL formation rate between 54 and 147 h was calculated to 0.422 g/Lh. Due to the still high fatty acid concentration, however, the share of MEL in the lipid fraction X_{MEL} was only 33% at that time (15% oil and 51% fatty acids respectively). Until the end of the process, fatty acid concentration then decreased again, but MEL concentration was also slightly decreased. Overall, a final X_{MEL} of 49% (11% oil and 40% fatty acids) was obtained after 310 h of process.

Both processes with combined batch and fed-batch growth phase, FB1 and FB2, successfully achieved the goal of higher MEL concentrations and higher MEL formation rates. Compared to the batch process B2, which had a MEL concentration of 27.1 g/L, the two fed-batch processes FB1 and FB2 led to increased MEL concentrations (50.5 and 43.9 g/L). At the same time, MEL formation rate was also increased. This confirmed our hypothesis that a higher biomass concentration at the end of the growth phase leads to faster MEL production. Nevertheless, the share of MEL X_{MEL} in the lipid fraction at the end of the processes was still relatively low, due to remaining oil and fatty acids in the broth. Oil feeding with 24% v/v or around 16–20 $g_{oil}/g_{biomass}$ was thus too high, even for the increased cell biomass concentrations. It was therefore decided to decrease the amount of oil feeding to 12% v/v or around 10 $g_{oil}/g_{biomass}$, respectively, and to aim for a full conversion of the substrate oil and fatty acids into MEL. Based on an average oil hydrolysis rate of ~1 g/Lh in the process FB1, this was expected to result in full oil hydrolysis at around 150 h and subsequently a consumption of remaining fatty acids afterwards. The idea was to obtain a X_{MEL} of >80%, i.e. less than 20% remaining oil and fatty acids, similar to the first batch process with single oil feeding (B1).

The third fed-batch process (FB3, **Table 3**; **Supplementary Figure S4**) was conducted with the same feeding rate as before (μ_{set} = 0.09 h^{-1}) during growth phase (40–51 h). During 11 h of feeding, a total of 708 g feeding solution were added. This resulted in 10.9 g/L biomass and a maximum OUR of 58.0 mmol/Lh. Despite the same feeding strategy as previously, a lower biomass concentration was obtained, which also resulted in an accumulation of glucose and nitrate in the medium. By analyzing off-gas values it was observed that the transition between batch and fed-batch was initiated too late, leading to a partial lysis of cells and a decrease in OUR towards the end of the batch growth phase. Hence, the feeding rate, which was calculated based on an active biomass concentration of 6 g/L at the beginning of feeding, was over-estimated, leading to an accumulation of glucose and nitrate over the fed-batch phase. Production phase was initiated by addition of 6% v/v oil at 51 h and maintained by another 6% at 72 h. Fast oil hydrolysis and almost full consumption of residual oil and FA after 150–170 h were observed, which correlated also with the pH trend as described before. MEL concentration and X_{MEL} reached a plateau at around 170 h. After that time, a decrease in OUR and a slight decrease in biomass were observed until the process was ended at 231 h. At the end, a MEL concentration of 35.7 g/L and a X_{MEL} of 88% in the crude extract (12% fatty acids and 0% oil) were measured. Average MEL formation rate between 51 and 170 h was at 0.335 g/Lh. The MEL yield coefficient with regard to the amount of oil added was 0.294 g/g, and therefore increased from the previous processes. Although the process was ultimately terminated after 231 h, it could have been stopped already at around 170 h, where MEL concentration and X_{MEL} were at their maximum (36.8 g/L and 92% respectively). Overall, the goal of full oil conversion into MEL, while at the same time achieving a high MEL concentration and productivity, was achieved in this process.

The fourth and final fed-batch process (FB4, **Table 3**; **Supplementary Figure S5**) was combining the results from previous runs. The initial batch concentration of all medium components was lowered to an equivalent of 20 g/L glucose, respectively, and the fed-batch phase with μ_{set} = 0.08 h^{-1} was started earlier to prevent starving of cells between batch and fed-batch phase. By adding 701 g of feeding solution between 27 and 44 h of process time, a maximum biomass concentration of 14.1 g/L was reached. This time the transition between batch and fed-batch was very smooth and showed a continuous and exponential increase of OUR throughout the growth phase up to a maximum OUR of 63.2 mmol/Lh. Nitrate was fully consumed at the end of the fed-batch, while the glucose concentration remained at 12 g/L. Production phase was then initiated at 44.5 h by adding 6% of oil to the fermenter. Further oil feeding (6% v/v) was done continuously at a rate of 8 ml/h between 52 and 82 h. The total amount of oil addition was therefore 12% v/v as before. After 169 h, a maximum MEL concentration of 34.3 g/L was obtained. Average MEL formation rate was 0.378 g/Lh (45–140 h) and thus similar to FB3. The calculated yield coefficient with regard to the total amount of oil added was at 0.275 g/g. Due to remaining oil and fatty acids, the X_{MEL} at that time was at 69%. Therefore, the process

was prolonged to 307 h and the purity increased to 98% as almost all lipids were consumed (only 1% fatty acids and 1% oil remaining). MEL concentration was slightly decreased to 30.0 g/L, but remained more or less at the same level.

Overall, the last two fed-batch processes FB3 and FB4 were very comparable in terms of MEL concentrations, formation rates and yields, and they were both showing low residual oil and fatty acid concentrations at the end of the process. Both processes hence achieved a $X_{MEL} > 90\%$ in 170–200 h of process time. This was similar to the first batch process B1, but at an increased MEL concentration of around 35.7 or 34.3 g/L (FB3 and FB4) instead of 11.2 g/L (B1). The ratio of oil addition with regard to biomass concentration in those processes was in the range of 9–11 $g_{oil}/g_{biomass}$ resulting in almost full substrate conversion. When this ratio was higher, like in B2, FB1 or FB2, a higher residual amount of fatty acids and thus lower purity of the crude lipid extract at the end of the process was obtained. A ratio of around 10 $g_{oil}/g_{biomass}$ can therefore be seen as an ideal value for determining the amount of oil feeding. Although not stated explicitly, the amount of oil with regard to biomass in the publication of Rau et al. (2005a) was estimated to ~10 g/g as well, taking into account their values for cell protein concentration and overall oil feeding. This also resulted in full conversion of oil and fatty acids after 288 h (Rau et al., 2005a) and is thus in good agreement with our results.

General Observations During MEL Production in Bioreactors

Several general observations were made in all of the processes presented. First, foaming occurred towards the end of the batch growth phase and further increased during fed-batch phase when higher biomass concentrations were reached. Starting from very coarse and dry foam during early growth, the diameter of the foam bubbles decreased to only a few mm over time and became increasingly wet. It is generally hard to determine which effect is dominating the foam formation during growth phase. Parallel to the increasing concentration of cells, the stirrer speed was automatically increased to enhance the oxygen transfer, which influences the hydrodynamics and thus foam formation in the bioreactor. Moreover, medium components like nitrate are limiting towards the end of the batch and during the fed-batch growth phase, which could also have an influence on foam formation. Ultimately, the mechanical foam destruction, which had been installed in the headspace of the reactor, was no longer effective after a certain point, leading to a partial overflow of culture broth into the exhaust air tubing. Nevertheless, the addition of rapeseed oil to start the production phase caused the foam to be destroyed again. Oil could thus act not only as substrate, but also as a chemical antifoaming agent (see also Rau et al. (2005a)). During production phase, foaming was less problematic and the process remained stable. Overall, it was concluded that a smooth transition from (fed-batch) growth phase to production phase is crucial for achieving a stable process without foam overflow.

Several online-recorded values proved to be good indicators for process control and monitoring. Oxygen uptake and carbon dioxide emission rates, which were obtained from off-gas analysis, correlated with biomass growth and substrate consumption during growth phase. The biomass specific rates q_{O2} and q_{CO2} were 4.3 and 6.5 mmol/gh, respectively, and remained constant during batch and fed-batch growth. This is the first time that a biomass specific oxygen demand has been determined for a producer strain in the MEL production process. Off-gas analysis even proved a better indicator for cell growth than the off-line measurement of biomass, as it was not affected by foaming or inhomogeneity in the broth. Moreover, off-gas analysis provided real-time information on biomass concentration as well as on cellular activity. Thus, the ideal time to start the production phase can be determined without the usual offset between sampling and analysis. The recording of pH and consumption of acid and base indicated the start of oil hydrolysis and the depletion of fatty acids towards the end of the process. Overall, these conclusions can be used to develop automated process control strategies based on real-time online values and to develop an even more robust process with hindsight for scale-up.

Another common observation was the formation of so-called MEL beads in the culture broth during production phase. These are globular aggregates of MEL, fatty acids and water that have been described before when *M. aphidis* was used as the production organism (Rau et al., 2005a; Goossens et al., 2016). Their formation was observed when a certain MEL concentration and ratio of MEL to substrate lipids (oil and fatty acids) was reached. Oil addition could dissolve these globules, but they were re-appearing when oil was hydrolyzed again. Formation of MEL beads interfered with sampling during production phase, as they were sticking to probes, baffles and the reactor wall. This could be the reason for variation in offline-measured data during production phase, for example, when a slight decrease in MEL concentration was noted towards the end of the process.

The ratio of the four MEL variants MEL-A,-B,-C and–D, which is characteristic for each producer species, was relatively constant over the time course of the fermentations and also between runs. An average MEL composition of 45 ± 2% MEL-A, 21 ± 1% MEL-B, 23 ± 3% MEL-C and 11 ± 3% MEL-D was calculated over all fermentation processes. Analysis of the acyl side-chains in the MEL yielded predominantly C_8 and C_{10} acids. Overall, this is the characteristic composition of *M. aphidis* MEL, which has also been described in prior publications with this strain (Rau et al., 2005b; Onghena et al., 2011; Beck et al., 2019a)

HPLC analysis of the culture supernatants showed an increase in mannitol concentration during production phase, which has so far never been described for a MEL production process. In the fed-batch fermentations, an increase up to 35 g/L mannitol was detected. Mannitol accumulation in the broth was almost linear and correlated with oil hydrolysis. As long as hydrolysis was active and oil and fatty acids were remaining in the broth, like in FB1 and FB2, mannitol accumulated constantly. Only towards the end of the process and when all remaining fatty acids were consumed, like in FB3, mannitol concentration decreased again. We assume that mannitol is a side-product of the lipid metabolism in *M. aphidis*, as several studies have already shown that the production of polyols, like erythritol and mannitol, is a common feature in yeast (Carly and Fickers,

2018; Goncalves et al., 2019) and even in the related fungus *U. maydis* (Guevarra and Tabuchi, 1990). Ultimately, the production and accumulation of mannitol as a metabolic side-product is most likely also the reason for the occurrence of mannosylmannitol lipids (MML) along with MELs in certain Ustilaginaceae species, which has been reported by our group in a previous publication (Beck et al., 2019a).

Kinetic Modeling of the MEL Fermentation Process

Ultimately, a knowledge-based model was developed and adjusted to our experimental data to gain a better understanding of the process kinetics. The partial models for cell growth and MEL production phase are based on a system of coupled ordinary differential equations (ODEs) that were solved numerically.

For the biomass growth phase, the concentration changes of glucose, sodium nitrate and biomass are described by a feeding term and Monod kinetics with glucose and nitrate as two non-complementary limiting substrates according to Roels (1983). The specific growth rate is dominated by the most limiting compound using a minimum operator (**Eq 12**).

$$\mu = \mu_{max}\, min\left\{\frac{c_{Gluc}}{(K_{Gluc} + c_{Gluc})}; \frac{c_{NaNO3}}{(K_{NaNO3} + c_{NaNO3})}\right\} \quad (12)$$

A possible growth inhibition at high substrate concentrations was not included in the model, as the currently used concentrations are assumed to be below this level. The changes in biomass (c_x) and substrate (c_{gluc} and c_{NaNO3}) concentrations are described by **Eqs. 13–15**:

$$\frac{dc_X}{dt} = -\frac{F_{in}}{V_L}c_x + \mu\, c_X \quad (13)$$

$$\frac{dc_{gluc}}{dt} = \frac{F_{in}}{V_L}\left(c_{gluc,Feed} - c_{gluc}\right) - q_{gluc}\, c_x\,; with\, q_{gluc} = \frac{\mu}{Y_{X/gluc}} \quad (14)$$

$$\frac{dc_{NaNO3}}{dt} = \frac{F_{in}}{V_L}\left(c_{NaNO3,Feed} - c_{NaNO3}\right) - q_{NaNO3}c_x;\quad with\, q_{NaNO3} = \frac{\mu}{Y_{X/NaNO3}} \quad (15)$$

For the production phase, the concentration changes of biomass, oil, fatty acids and MEL are described by a feeding and three reaction terms in the respective model equations. All reaction terms depend on specific reaction rates q_n and the biomass concentration at the end of the growth phase ($c_{x,growth}$), thus enabling to simulate the effect of an increased biomass concentration during growth phase on the consecutive production phase. The specific reaction rates q_n are based on Michaelis-Menten kinetics with maximum reaction rates $q_{max,n}$ and substrate affinity constants $K_{m,n}$ to represent the influence of decreasing substrate concentrations on the actual reaction rates. The first reaction term ($q_{hydrolysis}$) represents the hydrolysis of oil/triglycerides into fatty acids and glycerol (**Eq 16**). A product inhibition constant $K_{i,hydrolysis}$ was included to consider the lipase inhibition by high fatty acid concentrations (compare Henkel et al. (2014)). The second reaction term (q_{MEL}) describes the conversion of fatty acids into MEL (**Eq 17**). Hence, the MEL production was simplified into a single "black-box" reaction term in a first approximation, although the MEL pathway in *M. aphidis* consists of many sequential steps in reality (Hewald et al., 2006; Lorenz et al., 2014; Günther et al., 2015). The third reaction term represents the accumulation of lipids within the cells, which removes fatty acids from the broth and converts them into intracellular lipid vesicles, thus increasing the cell biomass concentration (**Eq 18**). This was realized by simulating two types of "cell biomasses", one that was lipid-free and generated during growth phase without nitrogen limitation ($c_{x,lipid\text{-}free}$), and one that contains lipid vesicles ($c_{x,incl}$) generated during production phase (see **Eqs. 22**, **23**).

TABLE 4 | Overview of parameters used for kinetic modeling. Parameters were either calculated from experimental data, derived from reaction stoichiometry or approximated to fit the model to experimental data.

Partial Model	Parameter	Value	Based on
Growth	μ_{max} (h^{-1})	0.11	experimental data
	$q_{max,\ gluc}$ (g/gh)	0.647	experimental data
	$K_{m,Gluc}$ (g/L)	1	approximated
	$Y_{X/Gluc}$ (g/g)	0.17	experimental data
	$q_{max,\ NaNO3}$ (g/gh)	0.065	experimental data
	$K_{m,NaNO3}$ (g/L)	0.01	approximated
	$Y_{X/NaNO3}$ (g/g)	1.7	experimental data
Production	$q_{max,\ hydrolysis}$ (g/gh)	0.1	experimental data
	$K_{m,hydrolysis}$ (g/L)	5	approximated
	$K_{i,hydrolysis}$ (g/L)	20	approximated
	$Y_{FA/oil}$ (g/g)	0.957	stoichiometry
	$q_{max,MEL}$ (g/gh)	0.02	experimental data
	$K_{m,MEL}$ (g/L)	5	approximated
	$Y_{FA/MEL}$ (g/g)	1.667	experimental data
Lipid accumulation	$q_{incl,max}$ (g/gh)	0.07	approximated
	$K_{m,\ incl}$ (g/L)	1	approximated
	$Y_{X,unlim/X,incl}$ (g/g)	0.203	stoichiometry
	$Y_{FA/X,incl}$ (g/g)	1.128	stoichiometry

$$q_{hydrolysis} = q_{\,max,hydrolysis}\,\frac{c_{oil}}{c_{oil} + K_{m,hydrolysis}\left(1 + \frac{c_{FA}}{K_{i,hydrolysis}}\right)} \quad (16)$$

$$q_{MEL} = q_{\,max,MEL}\,\frac{c_{FA}}{c_{FA} + K_{m,MEL}} \quad (17)$$

$$q_{incl} = q_{\,max,incl}\,\frac{c_{FA}}{c_{FA} + K_{m,incl}} \quad (18)$$

The changes in oil, fatty acid and MEL concentrations during the production phase are thus described by **Eqs. 19–21**:

$$\frac{dc_{Oil}}{dt} = \frac{F_{in}}{V_L}\left(c_{Oil,Feed} - c_{Oil}\right) - q_{hydrolysis}\, c_{x,growth} \quad (19)$$

$$\frac{dc_{FA}}{dt} = \frac{F_{in}}{V_L}\left(c_{FA,Feed} - c_{FA}\right) + Y_{FA/oil}\, q_{hydrolysis}\, c_{x,growth} - Y_{FA/MEL}\, q_{MEL}\, c_{x,growth} - Y_{FA/X,prod}\, q_{incl}\, c_{x,growth} \quad (20)$$

$$\frac{dc_{MEL}}{dt} = \frac{F_{in}}{V_L}\left(0 - c_{MEL}\right) + q_{MEL}\, c_X \quad (21)$$

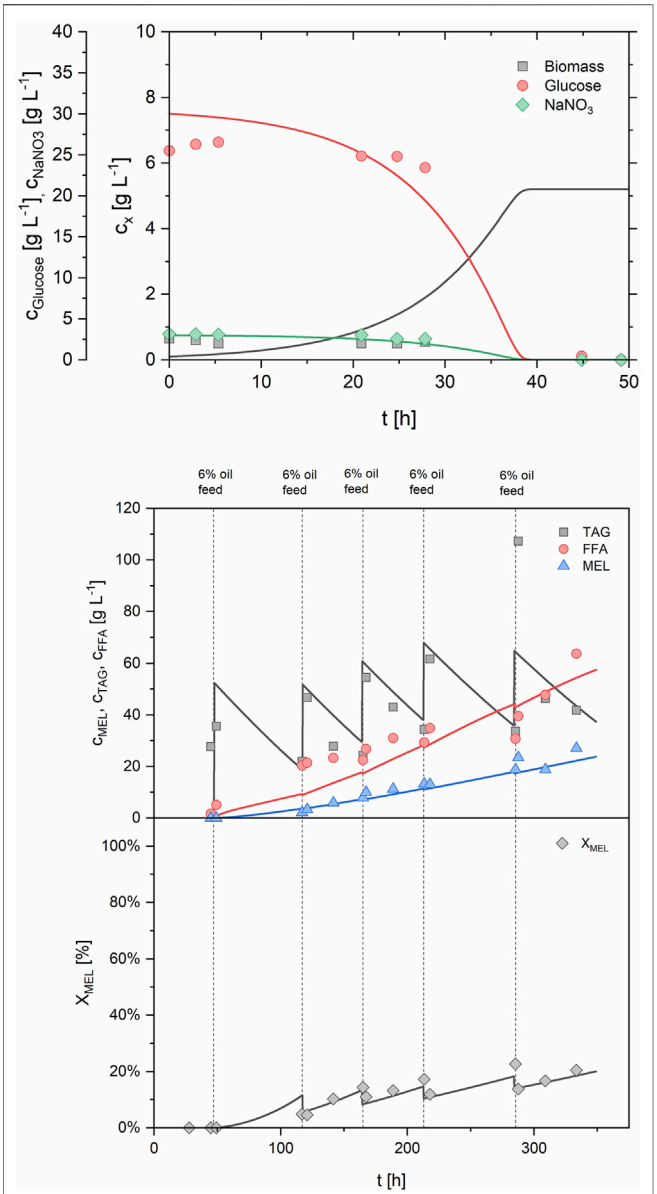

FIGURE 7 | Comparison of simulated and experimental data for process B2 using the parameters from **Table 4**. Batch growth phase (upper panel) and production phase with repeated oil feeding (lower panel) are shown.

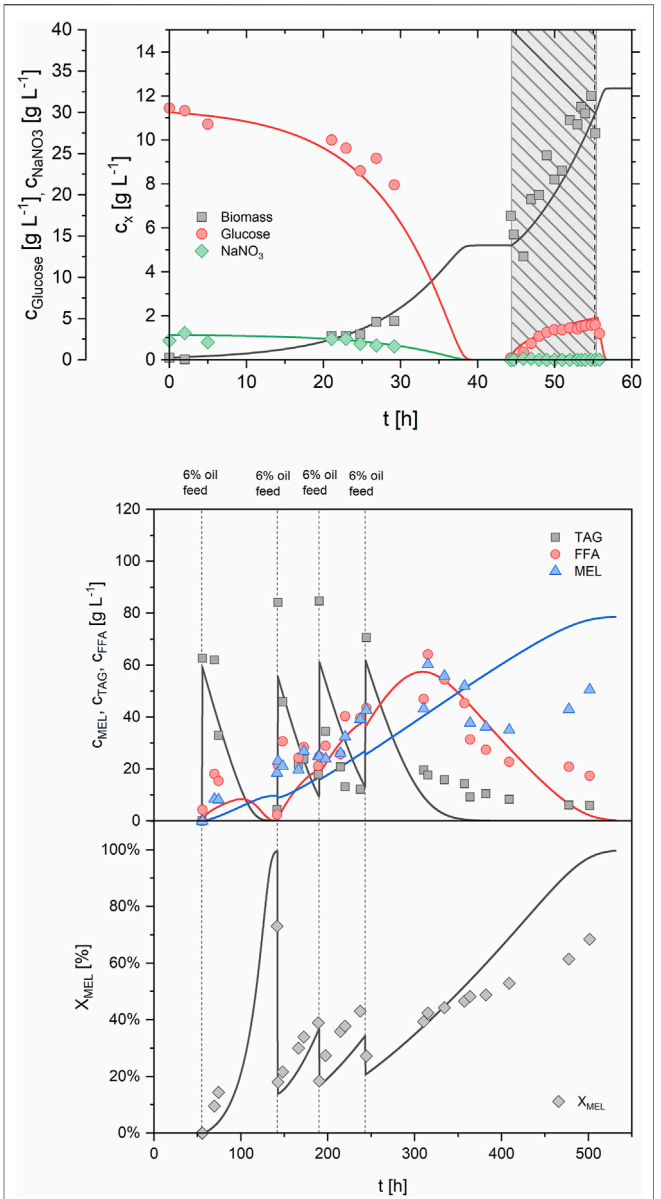

FIGURE 8 | Comparison of simulated and experimental data for process FB1 using the parameters from **Table 4**. Batch and fed-batch growth phase (upper, feeding phase is highlighted) and production phase with repeated oil feeding (lower) are shown.

The changes in biomass concentrations, modeled as a decrease in $c_{x,lipid\text{-}free}$ and an increase in $c_{x,incl}$ by inclusion of fatty acids, is described by the following equations:

$$\frac{dc_{X,incl}}{dt} = \frac{F_{in}}{V_L}\left(0 - c_{X,incl}\right) + q_{incl}\ c_{X,lipid-free} \tag{22}$$

$$\frac{dc_{X,lipid-free}}{dt} = \frac{F_{in}}{V_L}\left(0 - c_{X,lipid-free}\right) + Y_{X,lipid-free/X,incl}\ q_{incl}\ c_{X,lipid-free} \tag{23}$$

The necessary input parameters for the different model equations were yield coefficients, biomass-specific rate constants and substrate affinity constants. A summary of all parameters used for kinetic modeling are presented in **Table 4**. The yield coefficients and biomass-specific rates were calculated from our experimental data. For example, biomass yield coefficients from glucose $Y_{X/Gluc}$ and from sodium nitrate $Y_{X/NaNO3}$ were derived from the amount of consumed substrate versus produced biomass using linear regression of process data. Biomass-specific consumption rates q_n were determined from a regression of substrate consumption rates r_n versus respective biomass concentration c_x. The underlying assumption was that the biomass-specific rates and yield coefficients were constant

during the process, which was in agreement with the experimental results. The yield coefficient $Y_{FA/oil}$ was based on the reaction stoichiometry of oil hydrolysis. For simplification, "oil" was herein assumed as triolein, yielding 3 mol of oleic acid and 1 mol of glycerol during hydrolysis. The yield coefficient of biomass with lipid inclusions from fatty acids ($Y_{FA/X,incl}$), as well as the ratio of lipid-free biomass during growth to biomass with lipid inclusions during production phase ($Y_{X,lipid\text{-}free/X,incl}$) were based on a reaction stoichiometry that included the elementary compositions of the biomass during the different process stages shown in **Table 1**. The yield coefficient $Y_{FA/MEL}$ for the formation of MEL from fatty acids could not be obtained directly from experimental data, since fatty acids are an intermediate product and their concentration depends on hydrolysis, lipid inclusion and MEL production simultaneously. Consequently, $Y_{FA/MEL}$ was approximated to fit the model curves to our experimental data. The substrate affinity constants were also approximated to match the kinetic model curves to experimental data. The feeding terms in the simulations were set according to the experimental feeding rates in the respective processes.

The developed model was able to simulate the time-course of biomass and substrate concentrations during batch and fed-batch growth, as well as the substrate and product concentrations during MEL production phase. The process B2 with batch growth phase and multiple oil feeds was used to approximate the missing model parameters as described before and to demonstrate the general correlation between the model and experimental data (**Figure 7**). A MEL concentration of 22.2 g/L and a X_{MEL} of 18.5% was predicted after 333 h, which was in reasonable agreement with the experimental values of 27.1 g/L and 20.4%.

After all parameters were adjusted to the data of B2, the model was used to simulate the process FB1 with batch and fed-batch growth phase, employing the same feeding strategy as in the experiment. The growth model predicted a biomass concentration of 12.3 g/L at the end of the fed-batch phase, compared to 12.0 g/L from the experiment (**Figure 8**). As expected, the reaction rates during production phase were automatically increased according to the increased $c_{x,growth}$ in the model, and correlated well with experimental data. A MEL concentration of 40.4 g/L and a X_{MEL} of 37.6% were predicted after 310 h, compared to 43.2 g/L and 39.3% in the experiment. After 350 h, however, larger deviations between model and experimental data occurred, which could be explained by a decreased activity of lipases and cellular metabolism, which is however not included in the model. Another explanation might be the formation of MEL beads or the deposition of MEL and other hydrophobic substances at the reactor vessel and baffles, as described before. In general, it should be noted that the developed model is only valid within certain limits that are determined by the model restraints.

Overall, this is the first time that a kinetic model based on a system of ordinary differential equations has been presented for MEL production. Previously, there were only kinetic models for other biosurfactants like sophorolipids (Garcı´a-Ochoa and Casas, 1999) and rhamnolipids (Henkel et al., 2014). The rhamnolipids production model by Henkel et al. (2014) also employs a complex system of differential equations describing the cellular growth on different substrates, oil hydrolysis and rhamnolipids production. Since this is relatively similar to the MEL production process, it served as a reference for developing our model. The advantage of the here presented model is the possibility to evaluate different feeding strategies for medium and oil during growth and MEL production phase, respectively. A possible limitation of the model is the strict separation between growth and production phase models, assuming that the cells have entered stationary phase when production is started. Nevertheless, the current model is able to describe the MEL production process in detail and will be used to further optimize and evaluate MEL production.

CONCLUSION

The process for MEL production in an aerated stirred-tank bioreactor with *M. aphidis*, using a previously developed mineral salt medium, has been evaluated and enhanced by establishing an exponential fed-batch growth phase. Several experiments in the aerated STBR have shown that exponential substrate feeding of a concentrated solution containing glucose and nitrate led to a 2-3-fold increase of biomass concentration compared with a batch process. The substrate feeding, which was started after an initial batch growth phase, was conducted with defined growth rates of 0.08 or 0.09 h^{-1} and led to increased biomass concentrations of 10.9–15.5 g/L, compared with 4.2 g/L in the batch process. In the first two of the presented fed-batch processes, MEL production phase was conducted using 16–20 $g_{oil}/g_{biomass}$. This led to high MEL concentrations of 50.5 or 43.9 g/L, but at the same time to high concentrations of residual oil and fatty acids. Thus, a low MEL percentage in the crude lipid extract of 68 and 49% was obtained, respectively, even after long process times of up to 501 h. Oil feeding was therefore reduced to around 9–11 $g_{oil}/g_{biomass}$ in the last two fed-batch processes, which in turn led to slightly lower concentrations of 35.7 and 34.3 g/L MEL. At the same time however, the MEL yields from oil were increased to 0.294 and 0.275 g/g in the optimized processes and the substrate lipid was almost fully converted into product, leaving only traces of fatty acids in the broth at the end of the process. The corresponding share of MEL in the crude extract was increased to 88 and 95% respectively, and process time could be reduced to around 170 h. The increased purity of the crude lipid extract has also positive implications for the subsequent downstream processing of the broth, since, for example, a simple solvent extraction might be sufficient to obtain a product with already satisfactory purity. Flash chromatography, which is commonly employed to remove remaining oil and fatty acids from the crude extract, can be omitted if the required purity is already obtained by biological means at the end of the fermentation process.

Foaming, which has always been a common and major issue in biosurfactant production processes, was reduced by using the mineral salt medium and mechanical foam destruction in the headspace of the bioreactor, although it was still present at high biomass concentrations towards the end of the growth phase.

Several online parameters like dissolved oxygen, pH trends and off-gas analysis correlated well with biomass growth, substrate consumption and product formation, and could be used for process monitoring and control. The MEL composition was shown to be typical for *M. aphidis* and the reproducibility between the different runs was very high.

Ultimately, kinetic model equations were established for simulation and prediction of process behavior during cell growth and MEL production phase. The model was able to represent the experimental data accurately. To the best of our knowledge, this is the first time that a kinetic model based on a system of ordinary differential equations has been developed and employed for the prediction of the MEL production process. This model will be used in the future to scale the production process and perform a life-cycle assessment and techno-economic analysis that will provide a better understanding of key economic and ecological parameters for MEL production.

DATA AVAILABILITY STATEMENT

The original contributions presented in the study are included in the article/**Supplementary Material,** further inquiries can be directed to the corresponding author.

AUTHOR CONTRIBUTIONS

AB developed the concept and methodology, performed experiments, curated and analyzed experimental data, developed the kinetic model and wrote the manuscript. FV and LH performed cultivations in the bioreactor, acquired and analyzed data. SR reviewed the manuscript. SZ acquired funding, supervised the work of AB and critically reviewed and edited the manuscript. All authors read and approved the final manuscript.

FUNDING

This work was supported by a grant from the Ministry of Science, Research and the Arts of Baden-Württemberg (7533-10-5-85B) as part of the BBW ForWerts Graduate Program and a research scholarship for Alexander Beck from the German Academic Exchange Service DAAD (No. 57438025). The work moreover received funding by grants from the Federal Ministry of Education and Research, Germany as part of the 'Innovation Alliance for Functionally Optimized Biosurfactants' (031B0469P, 031B0469M, and 031B1059M). The device for micro-fermentation was funded by a grant from the Federal Ministry of Education and Research, Germany (031B0371A).

ACKNOWLEDGMENTS

The authors would like to thank Stella Radermacher, Alexander Brinkmann, Catrin Schuler, Lena Schneider, Antonia Roso, and Florian Röck who contributed to this work with their experiments, as well as Amira Oraby for her valuable comments during generation of the manuscript. We would also like to thank Dr. Thomas Hässler from Pfeifer and Langen Industrie-und Handels-KG for supplying the different sugar fractions taken from the refining process.

SUPPLEMENTARY MATERIAL

The Supplementary Material for this article can be found online at: https://www.frontiersin.org/articles/10.3389/fbioe.2022.913362/full#supplementary-material

REFERENCES

Adamczak, M., and Bednarski, W. o. (2000). Influence of Medium Composition and Aeration on the Synthesis of Biosurfactants Produced by Candida antarctica. *Biotechnol. Lett.* 22, 313–316. doi:10.1023/a:1005634802997

Beck, A., Haitz, F., Thier, I., Siems, K., Jakupovic, S., Rupp, S., et al. (2021). Novel Mannosylerythritol Lipid Biosurfactant Structures from castor Oil Revealed by Advanced Structure Analysis. *J. Ind. Microbiol. Biotechnol.* 48. doi:10.1093/jimb/kuab042

Beck, A., Haitz, F., Grunwald, S., Preuss, L., Rupp, S., and Zibek, S. (2019a). Influence of Microorganism and Plant Oils on the Structure of Mannosylerythritol Lipid (MEL) Biosurfactants Revealed by a Novel Thin Layer Chromatography Mass Spectrometry Method. *J. Ind. Microbiol. Biotechnol.* 46, 1191–1204. doi:10.1007/s10295-019-02194-2

Beck, A., Werner, N., and Zibek, S. (2019b). "Mannosylerythritol Lipids: Biosynthesis, Genetics, and Production Strategies," in *Biobased Surfactants*. Editors D.G. Hayes, D.K.Y. Solaiman, and R.D. Ashby (London: AOCS Press), 121–167. doi:10.1016/b978-0-12-812705-6.00004-6

Beck, A., and Zibek, S. (2020a). Growth Behavior of Selected Ustilaginaceae Fungi Used for Mannosylerythritol Lipid (MEL) Biosurfactant Production - Evaluation of a Defined Culture Medium. *Front. Bioeng. Biotechnol.* 8, 555280. doi:10.3389/fbioe.2020.555280

Beck, A., and Zibek, S. (2020b). Mannosylerythritollipide - mikrobielle Biotenside aus dem Bioreaktor. *BIOspektrum* 26, 100–102. doi:10.1007/s12268-020-1332-3

Bölker, M., Basse, C. W., and Schirawski, J. (2008). Ustilago Maydis Secondary Metabolism-From Genomics to Biochemistry. *Fungal Genet. Biol.* 45 (Suppl. 1), S88–S93. doi:10.1016/j.fgb.2008.05.007

Carly, F., and Fickers, P. (2018). Erythritol Production by Yeasts: a Snapshot of Current Knowledge. *Yeast* 35, 455–463. doi:10.1002/yea.3306

Casas, J. A., and García-Ochoa, F. (1999). Sophorolipid Production by Candida Bombicola: Medium Composition and Culture Methods. *J. Biosci. Bioeng.* 88, 488–494. doi:10.1016/s1389-1723(00)87664-1

Chmiel, H., Takors, R., and Weuster-Botz, D. (2018). *Bioprozesstechnik*. Berlin, Germany: Springer.

Deinzer, H.-T., Linne, U., Xie, X., Bölker, M., and Sandrock, B. (2019). Elucidation of Substrate Specificities of Decorating Enzymes Involved in Mannosylerythritol Lipid Production by Cross-Species Complementation. *Fungal Genet. Biol.* 130, 91–97. doi:10.1016/j.fgb.2019.05.003

Fan, L., Xie, P., Wang, Y., Huang, Z., and Zhou, J. (2018). Biosurfactant-Protein Interaction: Influences of Mannosylerythritol Lipids-A on β-Glucosidase. *J. Agric. Food Chem.* 66, 238–246. doi:10.1021/acs.jafc.7b04469

Faria, N. T., Santos, M. V., Fernandes, P., Fonseca, L. L., Fonseca, C., and Ferreira, F. C. (2014). Production of Glycolipid Biosurfactants, Mannosylerythritol Lipids, from Pentoses and D-glucose/D-Xylose Mixtures by Pseudozyma Yeast Strains. *Process Biochem.* 49, 1790–1799. doi:10.1016/j.procbio.2014.08.004

Freitag, J., Ast, J., Linne, U., Stehlik, T., Martorana, D., Bölker, M., et al. (2014). Peroxisomes Contribute to Biosynthesis of Extracellular Glycolipids in Fungi. *Mol. Microbiol.* 93, 24–36. doi:10.1111/mmi.12642

Fukuoka, T., Morita, T., Konishi, M., Imura, T., and Kitamoto, D. (2007a). Characterization of New Glycolipid Biosurfactants, Tri-acylated Mannosylerythritol Lipids, Produced by *Pseudozyma* Yeasts. *Biotechnol. Lett.* 29, 1111–1118. doi:10.1007/s10529-007-9363-0

Fukuoka, T., Morita, T., Konishi, M., Imura, T., Sakai, H., and Kitamoto, D. (2007b). Structural Characterization and Surface-Active Properties of a New Glycolipid Biosurfactant, Mono-Acylated Mannosylerythritol Lipid, Produced from Glucose by *Pseudozyma antarctica*. *Appl. Microbiol. Biotechnol.* 76, 801–810. doi:10.1007/s00253-007-1051-4

Fukuoka, T., Yoshida, S., Nakamura, J., Koitabashi, M., Sakai, H., Abe, M., et al. (2015). Application of Yeast Glycolipid Biosurfactant, Mannosylerythritol Lipid, as Agrospreaders. *J. Oleo Sci.* 64, 689–695. doi:10.5650/jos.ess15017

Gonçalves, C., Ferreira, C., Gonçalves, L. G., Turner, D. L., Leandro, M. J., Salema-Oom, M., et al. (2019). A New Pathway for Mannitol Metabolism in Yeasts Suggests a Link to the Evolution of Alcoholic Fermentation. *Front. Microbiol.* 10, 2510. doi:10.3389/fmicb.2019.02510

Goossens, E., Wijnants, M., Packet, D., and Lemière, F. (2016). Enhanced Separation and Analysis Procedure Reveals Production of Tri-acylated Mannosylerythritol Lipids by *Pseudozyma Aphidis*. *J. Ind. Microbiol. Biotechnol.* 43, 1537–1550. doi:10.1007/s10295-016-1838-3

Guevarra, E. D., and Tabuchi, T. (1990). Accumulation of Itaconic, 2-Hydroxyparaconic, Itatartaric, and Malic Acids by Strains of the GenusUstilago. *Agric. Biol. Chem.* 54, 2353–2358. doi:10.1080/00021369.1990.10870333

Günther, M., Grumaz, C., Lorenz, S., Stevens, P., Lindemann, E., Hirth, T., et al. (2015). The Transcriptomic Profile of Pseudozyma Aphidis during Production of Mannosylerythritol Lipids. *Appl. Microbiol. Biotechnol.* 99, 1375–1388. doi:10.1007/s00253-014-6359-2

Henkel, M., Schmidberger, A., Vogelbacher, M., Kühnert, C., Beuker, J., Bernard, T., et al. (2014). Kinetic Modeling of Rhamnolipid Production by *Pseudomonas aeruginosa* PAO1 Including Cell Density-dependent Regulation. *Appl. Microbiol. Biotechnol.* 98, 7013–7025. doi:10.1007/s00253-014-5750-3

Hewald, S., Linne, U., Scherer, M., Marahiel, M. A., Kämper, J., and Bölker, M. (2006). Identification of a Gene Cluster for Biosynthesis of Mannosylerythritol Lipids in the Basidiomycetous Fungus *Ustilago Maydis*. *Appl. Environ. Microbiol.* 72, 5469–5477. doi:10.1128/aem.00506-06

Isoda, H., Kitamoto, D., Shinmoto, H., Matsumura, M., and Nakahara, T. (1997). Microbial Extracellular Glycolipid Induction of Differentiation and Inhibition of the Protein Kinase C Activity of Human Promyelocytic Leukemia Cell Line HL60. *Biosci. Biotechnol. Biochem.* 61, 609–614. doi:10.1271/bbb.61.609

Isoda, H., and Nakahara, T. (1997). Mannosylerythritol Lipid Induces Granulocytic Differentiation and Inhibits the Tyrosine Phosphorylation of Human Myelogenous Leukemia Cell Line K562. *Cytotechnology* 25, 191–195. doi:10.1023/a:1007982909932

Jezierska, S., Claus, S., and Van Bogaert, I. (2018). Yeast Glycolipid Biosurfactants. *FEBS Lett.* 592, 1312–1329. doi:10.1002/1873-3468.12888

Kim, H.-S., Jeon, J.-W., Kim, B.-H., Ahn, C.-Y., Oh, H.-M., and Yoon, B.-D. (2006). Extracellular Production of a Glycolipid Biosurfactant, Mannosylerythritol Lipid, by Candida Sp. SY16 Using Fed-Batch Fermentation. *Appl. Microbiol. Biotechnol.* 70, 391–396. doi:10.1007/s00253-005-0092-9

Kim, H.-S., Jeon, J.-W., Lee, H.-W., Park, Y.-I., Seo, W.-T., Oh, H.-M., et al. (2002). Extracellular Production of a Glycolipid Biosurfactant, Mannosylerythritol Lipid, from Candida antarctica. *Biotechnol. Lett.* 24, 225–229. doi:10.1023/a:1014100422857

Kim, H.-S., Yoon, B.-D., Choung, D.-H., Oh, H.-M., Katsuragi, T., and Tani, Y. (1999). Characterization of a Biosurfactant, Mannosylerythritol Lipid Produced from Candida Sp. SY16. *Appl. Microbiol. Biotechnol.* 52, 713–721. doi:10.1007/s002530051583

Kitamoto, D., Fuzishiro, T., Yanagishita, H., Nakane, T., and Nakahara, T. (1992). Production of Mannosylerythritol Lipids as Biosurfactants by Resting Cells ofCandida antarctica. *Biotechnol. Lett.* 14, 305–310. doi:10.1007/bf01022329

Kitamoto, D., Ikegami, T., Suzuki, G. T., Sasaki, A., Takeyama, Y.-i., Idemoto, Y., et al. (2001). Microbial Conversion of N-Alkanes into Glycolipid Biosurfactants, Mannosylerythritol Lipids, by *Pseudozyma* (*Candida antarctica*). *Biotechnol. Lett.* 23, 1709–1714. doi:10.1023/a:1012464717259

Kitamoto, D., Yanagishita, H., Haraya, K., and Kitamoto, H. K. (1998). Contribution of a Chain-Shortening Pathway to the Biosynthesis of the Fatty Acids of Mannosylerythritol Lipid (Biosurfactant) in the Yeast *Candida antarctica*: Effect of Beta-Oxidation Inhibitors on Biosurfactant Synthesis. *Biotechnol. Lett.* 20, 813–818. doi:10.1023/a:1005347022247

Kitamoto, D., Yanagishita, H., Shinbo, T., Nakane, T., Kamisawa, C., and Nakahara, T. (1993). Surface Active Properties and Antimicrobial Activities of Mannosylerythritol Lipids as Biosurfactants Produced by Candida antarctica. *J. Biotechnol.* 29, 91–96. doi:10.1016/0168-1656(93)90042-l

Klement, T., Milker, S., Jäger, G., Grande, P. M., Domínguez de María, P., and Büchs, J. (2012). Biomass Pretreatment Affects Ustilago Maydis in Producing Itaconic Acid. *Microb. Cell. Fact.* 11, 43. doi:10.1186/1475-2859-11-43

Konishi, M., Imura, T., Fukuoka, T., Morita, T., and Kitamoto, D. (2007). A Yeast Glycolipid Biosurfactant, Mannosylerythritol Lipid, Shows High Binding Affinity towards Lectins on a Self-Assembled Monolayer System. *Biotechnol. Lett.* 29, 473–480. doi:10.1007/s10529-006-9261-x

Liu, X., Shu, Q., Chen, Q., Pang, X., Wu, Y., Zhou, W., et al. (2020). Antibacterial Efficacy and Mechanism of Mannosylerythritol Lipids-A on Listeria Monocytogenes. *Molecules* 25, 4857. doi:10.3390/molecules25204857

Lorenz, S., Guenther, M., Grumaz, C., Rupp, S., Zibek, S., and Sohn, K. (2014). Genome Sequence of the Basidiomycetous Fungus *Pseudozyma Aphidis* DSM70725, an Efficient Producer of Biosurfactant Mannosylerythritol Lipids. *Genome announc.* 2, e00053–14. doi:10.1128/genomeA.00053-14

Luedeking, R., and Piret, E. L. (1959). A Kinetic Study of the Lactic Acid Fermentation. Batch Process at Controlled pH. *Biotechnol. Bioeng.* 1, 393–412. doi:10.1002/jbmte.390010406

Masi, A., Mach, R. L., and Mach-Aigner, A. R. (2021). The Pentose Phosphate Pathway in Industrially Relevant Fungi: Crucial Insights for Bioprocessing. *Appl. Microbiol. Biotechnol.* 105, 4017–4031. doi:10.1007/s00253-021-11314-x

Morita, T., Fukuoka, T., Imura, T., and Kitamoto, D. (2015). Mannosylerythritol Lipids: Production and Applications. *J. Oleo Sci.* 64, 133–141. doi:10.5650/jos.ess14185

Morita, T., Ishibashi, Y., Fukuoka, T., Imura, T., Sakai, H., Abe, M., et al. (2009a). Production of Glycolipid Biosurfactants, Mannosylerythritol Lipids, Using Sucrose by Fungal and Yeast Strains, and Their Interfacial Properties. *Biosci. Biotechnol. Biochem.* 73, 2352–2355. doi:10.1271/bbb.90439

Morita, T., Kitagawa, M., Suzuki, M., Yamamoto, S., Sogabe, A., Yanagidani, S., et al. (2009b). A Yeast Glycolipid Biosurfactant, Mannosylerythritol Lipid, Shows Potential Moisturizing Activity toward Cultured Human Skin Cells: The Recovery Effect of MEL-A on the SDS-Damaged Human Skin Cells. *J. Oleo Sci.* 58, 639–642. doi:10.5650/jos.58.639

Morita, T., Kitagawa, M., Yamamoto, S., Sogabe, A., Imura, T., Fukuoka, T., et al. (2010a). Glycolipid Biosurfactants, Mannosylerythritol Lipids, Repair the Damaged Hair. *J. Oleo Sci.* 59, 267–272. doi:10.5650/jos.59.267

Morita, T., Kitagawa, M., Yamamoto, S., Suzuki, M., Sogabe, A., Imura, T., et al. (2010b). Activation of Fibroblast and Papilla Cells by Glycolipid Biosurfactants, Mannosylerythritol Lipids. *J. Oleo Sci.* 59, 451–455. doi:10.5650/jos.59.451

Morita, T., Konishi, M., Fukuoka, T., Imura, T., Sakai, H., and Kitamoto, D. (2008). Efficient Production of Di- and Tri-acylated Mannosylerythritol Lipids as Glycolipid Biosurfactants by Pseudozyma Parantarctica JCM 11752T. *J. Oleo Sci.* 57, 557–565. doi:10.5650/jos.57.557

Onghena, M., Geens, T., Goossens, E., Wijnants, M., Pico, Y., Neels, H., et al. (2011). Analytical Characterization of Mannosylerythritol Lipid Biosurfactants Produced by Biosynthesis Based on Feedstock Sources from the Agrofood Industry. *Anal. Bioanal. Chem.* 400, 1263–1275. doi:10.1007/s00216-011-4741-9

Posch, A. E., Spadiut, O., and Herwig, C. (2012). Switching Industrial Production Processes from Complex to Defined Media: Method Development and Case Study Using the Example of Penicillium chrysogenum. *Microb. Cell. Fact.* 11, 88. doi:10.1186/1475-2859-11-88

Rau, U., Nguyen, L. A., Roeper, H., Koch, H., and Lang, S. (2005a). Fed-batch Bioreactor Production of Mannosylerythritol Lipids Secreted by *Pseudozyma Aphidis*. *Appl. Microbiol. Biotechnol.* 68, 607–613. doi:10.1007/s00253-005-1906-5

Rau, U., Nguyen, L. A., Schulz, S., Wray, V., Nimtz, M., Roeper, H., et al. (2005b). Formation and Analysis of Mannosylerythritol Lipids Secreted by *Pseudozyma Aphidis*. *Appl. Microbiol. Biotechnol.* 66, 551–559. doi:10.1007/s00253-004-1672-9

Roels, J. A. (1983). *Energetics and Kinetics in Biotechnology*. Amsterdam: Elsevier Biomedical Press.

Saika, A., Fukuoka, T., Koike, H., Yamamoto, S., Sugahara, T., Sogabe, A., et al. (2020). A Putative Transporter Gene PtMMF1-Deleted Strain Produces Mono-Acylated Mannosylerythritol Lipids in Pseudozyma Tsukubaensis. *Appl. Microbiol. Biotechnol.* 104, 10105–10117. doi:10.1007/s00253-020-10961-w

Saika, A., Utashima, Y., Koike, H., Yamamoto, S., Kishimoto, T., Fukuoka, T., et al. (2018). Biosynthesis of Mono-Acylated Mannosylerythritol Lipid in an Acyltransferase Gene-Disrupted Mutant of *Pseudozyma Tsukubaensis*. *Appl. Microbiol. Biotechnol.* 102, 1759–1767. doi:10.1007/s00253-017-8698-2

Shu, Q., Wei, T., Lu, H., Niu, Y., and Chen, Q. (2020). Mannosylerythritol Lipids: Dual Inhibitory Modes against *Staphylococcus aureus* through Membrane-Mediated Apoptosis and Biofilm Disruption. *Appl. Microbiol. Biotechnol.* 104, 5053–5064. doi:10.1007/s00253-020-10561-8

Wakamatsu, Y., Zhao, X., Jin, C., Day, N., Shibahara, M., Nomura, N., et al. (2001). Mannosylerythritol Lipid Induces Characteristics of Neuronal Differentiation in PC12 Cells through an ERK-Related Signal Cascade. *Eur. J. Biochem.* 268, 374–383. doi:10.1046/j.1432-1033.2001.01887.x

Yamamoto, S., Morita, T., Fukuoka, T., Imura, T., Yanagidani, S., Sogabe, A., et al. (2012). The Moisturizing Effects of Glycolipid Biosurfactants, Mannosylerythritol Lipids, on Human Skin. *J. Oleo Sci.* 61, 407–412. doi:10.5650/jos.61.407

Zhang, J., and Greasham, R. (1999). Chemically Defined Media for Commercial Fermentations. *Appl. Microbiol. Biotechnol.* 51, 407–421. doi:10.1007/s002530051411

Conflict of Interest: The authors declare that the research was conducted in the absence of any commercial or financial relationships that could be construed as a potential conflict of interest.

Publisher's Note: All claims expressed in this article are solely those of the authors and do not necessarily represent those of their affiliated organizations, or those of the publisher, the editors and the reviewers. Any product that may be evaluated in this article, or claim that may be made by its manufacturer, is not guaranteed or endorsed by the publisher.

frontiers | Frontiers in Bioengineering and Biotechnology

ORIGINAL RESEARCH
published: 17 June 2022
doi: 10.3389/fbioe.2022.913351

Techno-Economic Analysis as a Driver for Optimisation of Cellobiose Lipid Fermentation and Purification

Amira Oraby[1,2], *Steffen Rupp*[1,2] *and Susanne Zibek*[1,2]*

[1]*Fraunhofer Institute for Interfacial Engineering and Biotechnology IGB, Stuttgart, Germany,* [2]*Institute of Interfacial Process Engineering and Plasma Technology IGVP, University of Stuttgart, Stuttgart, Germany*

Cellobiose lipids (CL) are glycolipids synthesized by *Ustilaginaceae* species with potential application as detergents or in cosmetics. This study identified process optimisation potential for CL fermentation based on process modelling and techno-economic analysis. Using a stoichiometric equation based on laboratory data, we calculated the maximum possible CL yield $Y_{P/S}$ of 0.45 $g_{CL} \cdot g_{glucose}^{-1}$ at the biomass yield of 0.10 $g_{Biomass} \cdot g_{glucose}^{-1}$ with an *Ustilago maydis* strain. Due to substrate inhibition that may occur at high glucose concentrations, a fed-batch process to increase biomass and CL concentrations was considered in our model. Simulation of different process scenarios showed that the choice of aeration units with high oxygen transfer rates and adaptation of power input to oxygen uptake can significantly decrease electricity consumption. We further assessed scenarios with different fermentation media and CL purification methods, suggesting additional process optimisation potential. Here the omission of vitamins from the fermentation medium proved to be a possible mean to enhance process economy, without compromising CL productivity.

Keywords: fermentation, process optimisation, techno-economic analysis (TEA), cellobiose lipids (CL), biosurfactant (BS)

OPEN ACCESS

Edited by:
Murat Ozdal,
Atatürk University, Turkey

Reviewed by:
Joachim Venus,
Leibniz Institute for Agricultural Engineering and Bioeconomy (ATB), Germany
Sathiyanarayanan Ganesan,
Université de Neuchâtel, Switzerland

***Correspondence:**
Susanne Zibek
susanne.zibek@igb.fraunhofer.de

Specialty section:
This article was submitted to Industrial Biotechnology, a section of the journal Frontiers in Bioengineering and Biotechnology

Received: *05 April 2022*
Accepted: *02 May 2022*
Published: *17 June 2022*

Citation:
Oraby A, Rupp S and Zibek S (2022) Techno-Economic Analysis as a Driver for Optimisation of Cellobiose Lipid Fermentation and Purification. Front. Bioeng. Biotechnol. 10:913351. doi: 10.3389/fbioe.2022.913351

1 INTRODUCTION

Academic and industrial interest in microbial biosurfactants, such as cellobiose lipids (CL), has continuously increased over the past decades. This is reflected in the extensive study of their characteristics and potential applications (Banat, 1995; Banat et al., 2000; Marchant and Banat, 2012; Geys et al., 2014; Günther et al., 2017), and the recent introduction of the two biosurfactants rhamnolipids and sophorolipids to products in the cosmetic industry (Moldes et al., 2020). Within an estimated global market volume of $31B in 2016 and predicted revenue growth of 3.1% per year (Ceresana, 2017), the share of biosurfactants is expected to surpass $2.5B by 2026 (Global Market Insights, Inc., 2021). Despite this positive growth forecast, the share of microbial biosurfactants is marginal. This is mainly attributed to the high production costs of microbial biosurfactants and their low concentrations (Banat et al., 2014). At the same time, ecological concerns and the thrive towards a sustainable bioeconomy highlight the ongoing need for novel microbial biosurfactants like CL.

CLs are synthesized by microorganisms from the class *Ustilaginomycetes* using sugars as the sole carbon source (Teichmann et al., 2007; Günther et al., 2017). These glycolipids are secreted as a mixture of chemical structures that vary in their variants and mixture ratios, depending on the producing microorganisms. The backbone of CL consists of a cellobiose disaccharide with different acetylation degrees, linked to a hydroxypalmitic acid via a glycosidic bond (Lemieux, 1951; Eveleigh

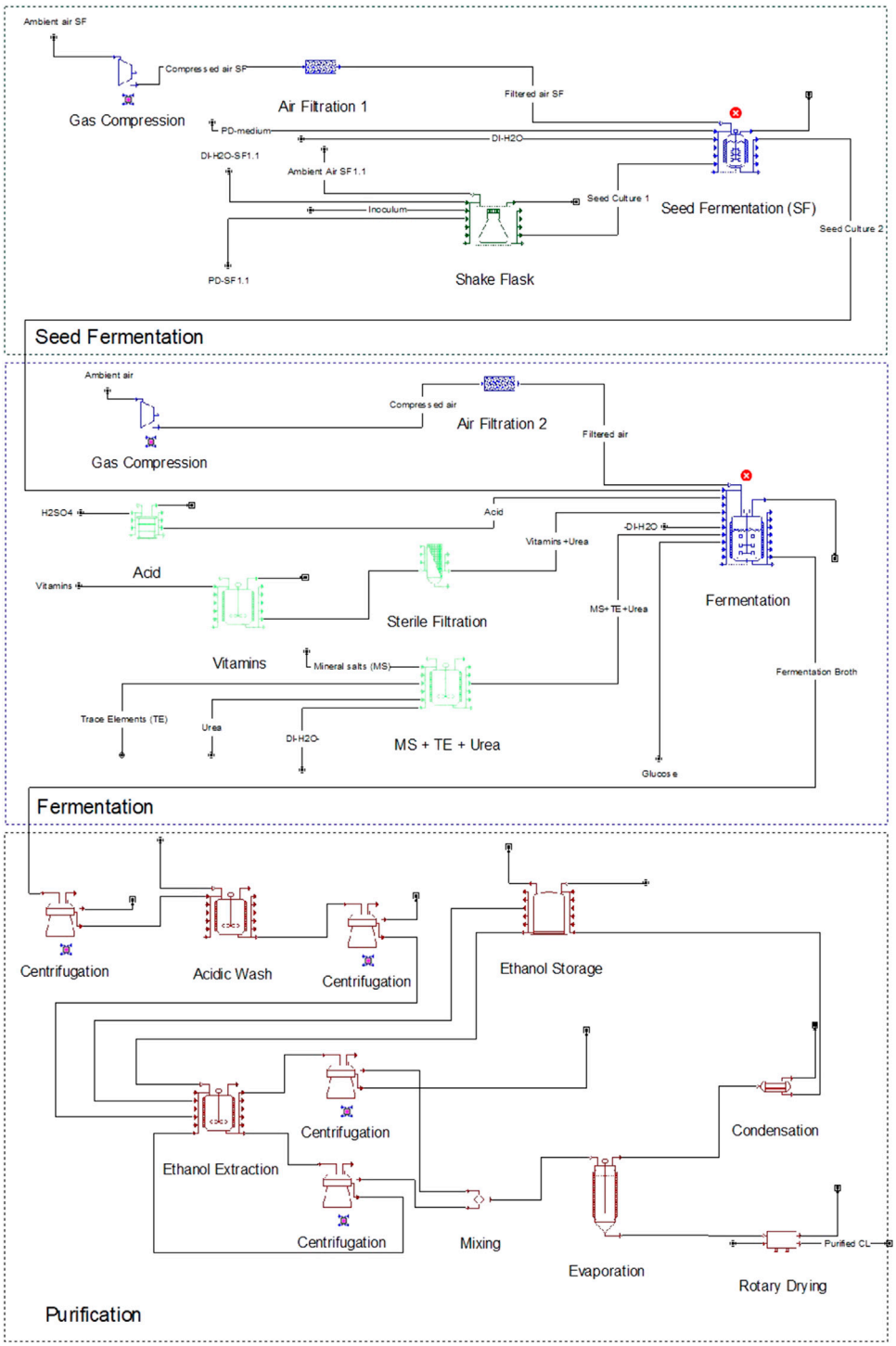

FIGURE 1 | Process flowsheet for the CL fermentation, including seed fermentation, production culture, and purification units.

et al., 1964), thus showing the typical amphiphilic structure of surfactants. Further, some CL variants are reported to show antibacterial and antifungal activity towards some Gram-positive bacteria and plant pathogens (Teichmann et al., 2007; Mimee et al., 2009).

Aiming for an optimised fermentation process, several fermentation media and parameters (Oraby et al., 2020), as well as CL purification processes, were presented in the literature (Günther, 2014). However, more systematic process optimisation needs to be done to achieve an optimised CL

fermentation and purification process with high titers that make CL an economically viable alternative to synthetic surfactants. In general, when it comes to cost-reduction of fermentative processes, three strategies can be followed (Banat et al., 2010):

1) Development of overproducing strains
2) Use of cheap and waste substrates
3) Development of more efficient bioprocesses, including optimisation of fermentation conditions, and downstream recovery processes

Our study followed the third approach, which focuses on process optimisation. In order to minimize the number of experimental procedures needed for process optimisation, we followed a simulation-based approach. We first modelled our fermentation and purification process using a flowsheet simulation software "basic scenario". Then, we simulated our fermentation in a 10 m^3 scale with several process scenarios in which different process parameters (fermentation duration, CL titer, agitation rate, aeration rate, fermentation media composition, and purification method) were varied compared to this basic scenario. Using these simulations, we conducted a techno-economic analysis (TEA) of each scenario variation to identify process bottlenecks that significantly impact the process economy. From these results, we derived the most promising process optimisation potentials that would have the most significant impact on the process economy. Others followed a similar approach for biosurfactants like sophorolipids, surfactin, rhamnolipids and other surfactants (Ashby et al., 2013; Czinkóczky and Németh, 2020; Wang et al., 2020; Ekpenyong et al., 2021; Elias et al., 2021; Moutinho et al., 2021). In comparison to their work, we present a more holistic approach that examines each process step along the whole fermentation and purification in order to identify process optimisation potential. In our approach, new scenarios were derived from the obtained results of the TEA of the basic scenario, and sensitivity analysis is only based on technical or process variations, not economic variations. This is because our aim here was to compare the effect of different variations in process parameters on the overall process economy. Using the obtained findings, we aimed at presenting recommendations that could be used for the experimental design along the process optimisation route of CL fermentation. For that purpose, relative considerations and comparisons were sufficient, whereas presenting exact economic numbers for the CL fermentation process was not within the scope of this study.

2 METHODS

CL fermentation and purification were modeled using a flowsheet simulation software to perform a TEA of the process. Process parameters for the basic scenario were approximated based on our internal laboratory results and literature data and are referenced individually in the following. Economic evaluations were performed based on (Peters and Timmerhaus, 1991), and sensitivity analysis and scenario variations were derived based on the preliminary experimental results and obtained results of the TEA of the basic scenario.

2.1 Model Development and Design

Using SuperPro Designer 11.2®, a 10 m^3 scaled fermenter was modelled for CL fermentation based on a process adapted after publications by our group (Günther, 2014; Oraby et al., 2020) and internal laboratory data in a 10 L scale. CL purification was done via centrifugation and ethanol extraction. All used media components are listed in **Supplementary Table S1** in the supplementary.

In the modelled fermentation, preparation of the seed culture consisted of two steps. The process flowsheet is illustrated in **Figure 1**. First, six 2 L shaking flasks were inoculated from potato dextrose (PD)-agar plates (Becton Dickinson, Le Pont de Claix, France) and incubated at 30°C and 120 rpm for 17 h in PD medium at pH 5.6. These were then transferred to a 300 L fermenter with PD medium to a total volume of 210 L and an optical density (OD) of 0.1. The second seed culture was agitated at 1 kW m^{-3} and aerated with 1 vvm ambient air to maintain a pO_2 level above 20% until it reached the stationary phase after 24 h. Power input and aeration rate for the seed culture and production culture were approximated based on laboratory results (data not shown) and published results by our group for a closely related microorganism (Oraby et al., 2020). This seed culture was finally used to inoculate the 10 m^3 fermenter containing a mineral salt medium (**Supplementary Table S1**) to an OD of 0.3.

0.6 g L^{-1} urea was used as nitrogen source and 100 g L^{-1} sucrose as carbon source. Sucrose is the more favourable carbon source for CL fermentation because it results in higher CL concentrations compared to glucose (Rupp et al., 2010; Oraby et al., 2020). Sucrose is hydrolysed to glucose and fructose during the first hours of fermentation and glucose is primarily consumed for CL synthesis at higher rates compared to fructose, as long as both carbon sources are available (Günther, 2014). Therefore, for approximation purposes, the hexose with highest uptake rate was used for our model and considered in the stoichiometry and yield calculations.

The production culture was agitated at 1 kW m^{-3} and aerated with 1 vvm ambient air for 14 days. 2 M H_2SO_4 and 2 M NaOH were used to adjust pH at 2.5. An air compressor was used to compress ambient air to 3 bars for aeration of both fermenters. All media components were heat sterilized separately, except for the vitamin fraction of the mineral salt medium. The vitamins were sterilized using a 0.2 μm filter at a 1000-fold concentration then added to the fermenter.

After fermentation, the culture broth was separated using a disk-stack centrifuge to a solid concentration of 200 g L^{-1} to obtain a wet pellet containing biomass and CL crystals. The pellet was then suspended in acidic water (pH 2.5 adjusted with H_2SO_4) and agitated with 1 kW m^{-3} in a stirring vessel for 30 min to wash out the remaining sugars. After the washing step, biomass

and CL crystals were separated again from the suspension. In a stirring vessel, denatured ethanol was added to the pellet at a ratio of 2 g g^{-1} and agitated with 1 kW m^{-3} for 30 min. After this step, the ethanol extract containing CL was separated from the biomass using a disk-stack centrifuge. The ethanol extraction and separation steps were performed twice to ensure the extraction of all contained CL crystals from the biomass pellet. Next, both extracts were merged, and ethanol was evaporated using a thin film evaporator (at 56.6°C and 280 mbar). The crystallized CL was then dried using a rotary dryer for 24 h at 20 kg h^{-1} m^{-3}.

Alternatively to ethanol extraction, a second downstream process (DSP) was also modelled. Here, the washed pellet containing biomass and CL was set to pH 12 using NaOH and incubated for 4 h at 50°C to hydrolyse CL to its water-soluble form CL-A (based on shaking flask experiments, results not shown). The biomass was then separated using a disk stack centrifuge, and the CL was precipitated using H_2SO_4 at a pH of 2–4. The precipitated CL-A was then separated with the disk stack centrifuge and dried for 24 h at 20 kg h^{-1} m^{-3}.

2.2 Stoichiometry of Microbial Growth and CL Formation

For modelling and simulation purposes, the dynamic reactions that happen within the fermenter were described by mathematical equations. Hereby the reaction stoichiometry quantifies the ratio of products (CL and biomass) to the used substrates, based on the material conservation law.

For aerobic, heterotrophic microorganisms, as used here, Michael (2013) approximates the microbial growth by the following general equation:

$$x_1\,C_aH_bO_c + x_2\,O_2 + x_3\,NH_3 + x_4\,HPO_4^{2-} + x_5\,K^+ + \text{other educts} \rightarrow y_1\,CH_LO_MN_NP_OK_P + y_2\,CO_2 + y_3H_2O + \text{other products} \quad (1)$$

C, H, N, and O are the major elements forming the general elemental composition of fungal biomass. With only 0.4–4.5%w/w taken up of phosphor, 0.1–0.5%w/w of sulfur, and even less potassium, it is plausible to neglect these elements for a first approximation for modelling purposes, as suggested by Chmiel (2006).

For CL fermentation using glucose ($C_6H_{12}O_6$) as carbon source and urea (CH_4N_2O) as nitrogen source, **Eq. 1** can thus be simplified to:

$$x_1\,C_6H_{12}O_6 + x_2\,O_2 + x_3\,CH_4N_2O \rightarrow y_1\,CH_{1.85}O_{0.35}N_{0.03} + y_2\,CO_2 + y_3\,H_2O + y_4\,C_{36}H_{64}O_{18} \quad (2)$$

whereas the elemental biomass composition is $CH_{1.85}O_{0.35}N_{0.03}$, and CL-B is represented by $C_{36}H_{64}O_{18}$. Biomass compositions were determined experimentally via elemental analysis in biological triplicates and analytical duplicates (performed by the Institute of Organic Chemistry, University of Stuttgart). Setting the biomass yield $Y_{X/S}$ to 0.2 and the product yield $Y_{P/S}$ to 0.2 as boundary conditions and using the material conservation, the following equation A*x = b was solved to form the stoichiometry:

TABLE 1 | Factors applied for estimation of the direct fixed capital investment, based on the equipment purchase cost (PC), the total direct investment costs (DC), and the indirect investment costs (IC). Calculation factors are based on (Peters and Timmerhaus 1991).

	Cost Item	Factor
Direct Investment Costs (DC)	Installation	0.40 * PC
	Instrumentation	0.13 * PC
	Piping	0.31 * PC
	Electrical Installation	0.13 * PC
	Insulation	0.09*PC
	Buildings	0.29*PC
	Yard Improvement	0.15*PC
	Auxiliary Facilities	0.4*PC
Indirect Investment Costs (IC)	Engineering and supervision	0.08 * DC
	Construction	0.10 * DC
Other Investment Costs (OIC)	Contractor's fee	0.04 * (DC + IC)
	Contingency	0.08 * (DC + IC)

$$\begin{array}{l} \\ \text{Elemental compositions} \\ \\ \\ \\ \text{Boundary conditions} \\ \\ \\ \end{array} \begin{array}{l} \begin{matrix} \text{Biomass} \\ \text{N-limit} \end{matrix} \\ \text{C} \\ \text{H} \\ \text{N} \\ \text{O} \\ \text{CL} = 1 \\ Y_{P/X} \\ Y_{P/S} \end{array} \begin{array}{c} \begin{matrix} CO_2 & H_2O & CL-B & C_6H_{12}O_6 & O_2 & CH_4N_2O \end{matrix} \\ \begin{pmatrix} 1 & 1 & 0 & 36 & -6 & 0 & -1 \\ 1.85 & 0 & 2 & 64 & -12 & 0 & -4 \\ 0.03 & 0 & 0 & 0 & 0 & 0 & -2 \\ 0.35 & 2 & 1 & 18 & -6 & -2 & -1 \\ 0 & 0 & 0 & 1 & 0 & 0 & 0 \\ -1 & 0 & 0 & 39.5 & 0 & 0 & 0 \\ 0 & 0 & 0 & 21.8 & -1 & 0 & 0 \end{pmatrix} \end{array} \begin{pmatrix} y_1 \\ y_2 \\ y_3 \\ y_4 \\ x_1 \\ x_2 \\ x_3 \end{pmatrix} = \begin{pmatrix} 0 \\ 0 \\ 0 \\ 0 \\ 1 \\ 0 \\ 0 \end{pmatrix} \quad (3)$$

Here A is the stoichiometric matrix, x the vector of the stoichiometric factors x_i and y_i, and B is the condition for the material conservation law (Chmiel, 2006).

For the seed culture, no CL is formed, and the nitrogen contained in the used complex medium is simplified by N_2. Further, the elemental biomass composition in the seed culture is given as $CH_{1.83}O_{0.64}N_{0.13}$. Here, the nitrogen content in the elemental composition is higher than the biomass during the production culture and nitrogen limitation, as discussed in detail by Klement and Buchs (2013). Therefore, the following equation was used for stoichiometric calculations of the seed culture with a $Y_{P/S}$ of 0.2:

$$\begin{array}{l} \\ \text{Elemental compositions} \\ \\ \\ \\ \text{Boundary conditions} \\ \\ \end{array} \begin{array}{l} \text{Biomass} \\ \text{C} \\ \text{H} \\ \text{N} \\ \text{O} \\ \text{Biomass} = 1 \\ Y_{X/S\,(SC)} \end{array} \begin{array}{c} \begin{matrix} CO_2 & H_2O & C_6H_{12}O_6 & O_2 & \begin{matrix} N_2 \text{ from} \\ \text{complex medium} \end{matrix} \end{matrix} \\ \begin{pmatrix} 1 & 1 & 0 & -6 & 0 & 0 \\ 1.83 & 0 & 2 & -12 & 0 & 0 \\ 0.13 & 0 & 0 & 0 & 0 & 2 \\ 0.64 & 2 & 1 & -6 & -2 & 0 \\ 1 & 0 & 0 & 0 & 0 & 0 \\ 0.96 & 0 & 0 & 0 & 0 & 0 \end{pmatrix} \end{array} \begin{pmatrix} y_1 \\ y_2 \\ y_3 \\ x_1 \\ x_2 \\ x_3 \end{pmatrix} = \begin{pmatrix} 0 \\ 0 \\ 0 \\ 0 \\ 1 \\ 0 \end{pmatrix} \quad (4)$$

2.3 Sensitivity Analysis of the Stoichiometry

In order to determine the maximum theoretically possible yields during CL fermentation, a sensitivity analysis of the reaction stoichiometry was conducted. Using **Eq. 3**, $Y_{P/S}$ and $Y_{X/S}$ were each set to a defined minimum of 0.1, while the theoretically possible maximum of the other yield was varied in steps of 0.05. The constraint here was a positive stoichiometric factor x_2 in vector x, guaranteeing the occurrence of aerobic fermentation. If one of the two yields used for the stoichiometric matrix resulted in a negative stoichiometric factor x_2 in vector x, that would mean that O_2 is emitted, not consumed.

TABLE 2 | Overview of all varied parameters in the simulated scenarios used to estimate theoretical optimisation potentials.

Scenario	Basic	Ferm. Duration [d]			CL conc. [g/L]			CL Yield [g/g]		Aeration rate [vvm]	Power input [kW/m^3]	CL-A	-Vita	Best
Scenario #	0	1	2	3	4	5	6	7	8	9	10	11	12	13
Duration [d]	14	10	7	5										7
Power input [kW/m^3]	1.0										0.1			0.5
Aeration rate [vvm]	1.0									0.1				0.5
CL conc. [g/L]	10				20	30	50	15	23					30
CL yield [g/g]	0.20							0.30	0.45					0.20
CL-A	—	—	—	—	—	—	—	—	—	—	—	CL-A	—	—
-Vitamins	—	—	—	—	—	—	—	—	—	—	—	-	-Vita	-Vita

2.4 Economic Evaluation

For the economic evaluation, a gate-to-gate approach was followed; hence no transportation costs were calculated. Geographical aspects of the production plant were only considered for chemical and utility prices, as well as labor charges. The plant capacity was assumed as 100%, with 330 working days per year. Depreciation was calculated using the straight-line method, at an estimated depreciation period of 11 years and a salvage value of 10% (Peters et al., 2003).

Equipment purchase cost (PC) was estimated based on equipment prices from the internal SuperPro database (year of analysis 2019), except for fermenters, vessels, and filter cartridges. Here, PC was calculated using custom cost models based on price estimates from German vendors. For total capital investment (TCI) estimation, the direct fixed capital investment (FCI) was calculated based on percentages of delivered equipment cost PC (**Table 1**) as the sum of direct investment cost (DC), indirect investment cost (IC), and other investment costs (OIC) according to the following equations:

$$\mathrm{FCI} = \mathrm{DC} + \mathrm{IC} + \mathrm{OIC} \tag{5}$$

$$\mathrm{TCI} = \mathrm{DC} + \mathrm{IC} + \mathrm{OIC} + \mathrm{WC} + \mathrm{SVC} \tag{6}$$

The working capital (WC) investment was estimated to cover expenses for 30 operation days, while startup and validation costs (SVC) were estimated as 10 % of the fixed capital investment (Peters and Timmerhaus, 1991).

Operation costs (OC) include the costs of materials, consumables, utilities including electricity and heating/cooling agents, labor-dependent costs, costs for laboratory, quality control and quality assurance, waste treatment, facility dependent costs including maintenance, repair, and depreciation, and insurance and taxes. Prices for used chemicals and media components were obtained from bulk prices of chemical providers in Germany and are listed in **Supplementary Table S1** in the supplementary. Electricity price was obtained based on the stock market price for the year 2019 in Germany, at 0.13 € kWh^{-1} (Statistische Bundesamt (Destatis), 2020). Labor costs were calculated using the built-in calculation tool of SuperPro Designer, where the total labor cost (TLC) was calculated based on the sum of labor demand per type multiplied by the labor rate per type. Here additional costs like benefits, supervision and administration were considered (Intelligen Inc., 2020). Labor demand and type were estimated based on (Peters and Timmerhaus, 1991) and calculated using average labor rates in Germany (FernUniversität Hagen, 2020). Costs for laboratory, quality control, and quality assurance were estimated as 15% of TLC. Maintenance and repair costs were estimated based on (Peters and Timmerhaus, 1991) as 6% of the TCI, while insurance accounted for 1% and local taxes for 1% of TCI, respectively.

2.5 Sensitivity Analysis

The unit production cost (UPC) per kg of CL was used as a scale to compare different process scenarios in our sensitivity analysis.

$$\mathrm{UPC} = \mathrm{OC}[\in]/\text{annual CL production}\,[\mathrm{kg}] \tag{7}$$

Based on the material and utility balances, as well as the overall process economics of the basic fermentation process (**Sections 3.2** and **3.3**), each cost category that is directly affected by process parameters was considered in more detail for a global hotspot analysis and scenario generation. Depreciation and facility-dependent expenditures, labour-dependent costs, and costs for laboratory and QC were not considered further because they are calculated based on equipment purchase cost and thus are not affected by simple process parameter variations. Costs for waste disposal were also not considered in the hotspot analysis.

Fermentation duration as a general parameter directly affecting process economics was varied to quantify its potential effect on CL production costs (scenarios 1–3, **Table 2**). Further, the CL concentration was increased to 20, 30, and 50 g L^{-1} (scenarios 4–6) at the standard yield of 0.2 g g^{-1}, and the CL yield was varied to 0.3 and 0.45 g g^{-1} (scenarios 7–8) based on the maximum possible levels determined in chapter 3.1. As the primary contributor to utility demands, the aeration rate and power input were reduced from 1 to 0.1 vvm (scenario 9) and from 1 to 0.1 kW m^{-3} (scenario 10). The purification method via alkaline modification and precipitation to CL-A (scenario 11) was compared to the ethanol extraction in the basic scenario. Additionally, a fermentation process utilising a medium containing only mineral salts and trace elements without vitamins (scenario 12) was modelled. Finally, all best parameters approximated based on the current state-of-the-art values for CL fermentation were combined and simulated in scenario 13, representing a 7 days fermentation, with a power input of 0.5 kW m^{-3}, an aeration rate

TABLE 3 | Reaction stoichiometry for the seed culture (8) and potential CL fermentations with different yields $Y_{P/S}$ and $Y_{X/S}$ (9–11).

$Y_{P/S}$	$Y_{X/S}$	Reaction stoichiometry	Equation #
–	0.20	$0.96\,C_6H_{12}O_6 + 4.62\,O_2 + 0.065\,N_2 \rightarrow 1\,C_1H_{1.83}O_{0.64}N_{0.13} + 4.75\,CO_2 + 4.84\,H_2O$	(8)
0.20	0.20	$21.78\,C_6H_{12}O_6 + 37.80\,O_2 + 0.59\,CH_4N_2O \rightarrow 39.45\,C_1H_{1.85}O_{0.35}N_{0.03} + 55.84\,CO_2 + 63.39\,H_2O + C_{36}H_{64}O_{18}$	(9)
0.10	0.40	$43.57\,C_6H_{12}O_6 + 18.78\,O_2 + 2.37\,CH_4N_2O \rightarrow 157.8\,C_1H_{1.85}O_{0.35}N_{0.03} + 69.97\,CO_2 + 88.17\,H_2O + C_{36}H_{64}O_{18}$	(10)
0.45	0.10	$9.68\,C_6H_{12}O_6 + 4.00\,O_2 + 0.13\,CH_4N_2O \rightarrow 8.77\,C_1H_{1.85}O_{0.35}N_{0.03} + 13.45\,CO_2 + 18.24\,H_2O + C_{36}H_{64}O_{18}$	(11)

of 0.5 vvm, using a fermentation medium without vitamins and producing 30 g L^{-1} CL at a yield of 0.2 g g^{-1}.

3 RESULTS AND DISCUSSION

Using TEA as a driver for the choice of process optimisation approaches is an iterative process throughout the course of process development. The choice and definition of technically feasible process scenarios is a prerequisite for enabling experimental examinations of the identified optimisation approaches. Therefore, we first considered reaction stoichiometry to define the feasible range of biomass and CL yields based on their stoichiometric compositions (**Section 3.1**). Then material and energy balances (**Section 3.2**) and overall process economics (**Section 3.3**) of the basic scenario, which was modelled as described in **Sections 2.1** and **2.2**, were used to define other potential process scenarios within the predicted feasible range. In **Section 3.4** the effects of variation in fermentation duration, CL concentration and yield (**Section 3.4.1**), aeration and agitation rates (**Section 3.4.2**), and the application of different purification methods (**Section 3.4.3**), or fermentation media (**Section 3.4.4**) on process economy are assessed and discussed. Based on the here obtained results, experimental optimisation approaches were suggested. Finally, a best-case fermentation scenario was simulated to assess the total reduction in CL production prices (**Section 3.4.5**), based on the identified optimisation potentials.

3.1 Determination of the Potential Maximal $Y_{P/S}$ and $Y_{X/S}$ Using Reaction Stoichiometry

Using **Eq. 4** (**Section 2.2**), the stoichiometric Equation 8 in **Table 3** was calculated for the seed culture, and using **Eq. 3**, the stoichiometric Equation 9 in **Table 3** was calculated for the CL production culture. These equations were implemented in our SuperPro model to calculate material conversion during the seed culture and the CL fermentation process. Further, the sensitivity analysis for $Y_{P/S}$ and $Y_{X/S}$ resulted in Equations 10 and 11 (**Table 3**).

The results in **Table 3** show that at a maximum biomass yield of $Y_{X/S}$ = 0.40 $g_{biomass}{\cdot}g_{glucose}^{-1}$, only 0.10 g CL are yielded per g glucose. On the other hand, if the biomass yield is minimised to 0.10 $g_{biomass}{\cdot}g_{glucose}^{-1}$, a maximum CL yield of up to $Y_{P/S}$ = 0.45 $g_{CL}{\cdot}g_{glucose}^{-1}$ is possible. These theoretical considerations were used to define different scenarios analysed in **Section 3.4**.

At a given glucose concentration of 50 g L^{-1} in the culture medium, as set for the basic CL fermentation scenario, a product yield of 0.45 $g_{CL}{\cdot}g_{glucose}^{-1}$ would mean that in batch fermentation, no more than 22.5 g L^{-1} CL can be produced. However, to improve the process economy, higher CL concentrations are necessary (see **Section 3.4**). At the same time, at a maximum yield of 0.45 $g_{CL}{\cdot}g_{glucose}^{-1}$, initial substrate concentration needs to increase significantly to achieve higher concentrations. An increase in initial hexose concentrations is however limited since osmotic stress, and byproduct synthesis increase with higher substrate concentrations in the medium and may result in a decrease in productivity and product yield (Krull et al., 2020). In a previous work, we showed that increasing the glucose concentration from 50 to 100 g L^{-1} resulted in a decrease in CL concentration and yield, as well as an increase in byproduct formation with *Sporisorium scitamineum*, a close relative to the strain used in this work (Oraby et al., 2020). Therefore, applying a fed-batch process, where additional carbon source, such as sucrose, is supplied during the fermentation, while the overall level of hexoses is held below 50 g L^{-1} at all times, may be the more suitable solution to obtain high concentrations without decreasing product yields (compare results in **Section 3.4.1**).

Comparing the here obtained theoretically maximum possible concentration with literature values shows that there is still optimisation potential for increasing the CL concentration. A maximum of 23 g L^{-1} CL was reported in literature by Roxburgh et al. (1954) for batch fermentation, with an initial glucose concentration of 100 g L^{-1}, resulting in a $Y_{P/S}$ of only 0.23 $g_{CL}{\cdot}g_{glucose}^{-1}$. Günther showed in his work that this maximum concentration could be increased to 33 g L^{-1}, using sucrose as the carbon source in a fed-batch process, thus illustrating the potential increase in CL concentration through substrate feeding (Günther, 2014).

3.2 Process Model and Overall Material and Utility Balances of the Basic Scenario

Implementing **Eqs 5** and **6** from **Section 2.2** to describe the fermentation stoichiometry for both the seed and production cultures, the CL basic fermentation process scenario was modelled in SuperPro Designer according to the procedure described in chapter 2.1. All equipment used for the CL model is listed in **Supplementary Table S2** in the supplementary section.

Using **Eq. 6** and an initial glucose concentration of 50 g L^{-1}, a CL concentration of 10 g L^{-1} is calculated for the basic scenario, resulting in 70 kg of CL per batch, amounting to 1,473 kg CL per year in the 10 m^3 fermenter. Equally, 71 kg biomass per batch and 1,488 kg per year are produced. When product loss during DSP is considered, a final amount of 57 kg CL per batch and 1,201 kg CL per year are yielded. These target product amounts were used for

economic calculations. 222 kg of carbon dioxide is emitted per batch due to microbial metabolism, while 109 kg of oxygen is consumed. Besides glucose (350 kg/batch), water, and sodium hydroxide, which are mainly used for CIP procedures, the other large material stream is ethanol, used for CL extraction. Here, an average of 1,534 kg ethanol is used per fermentation process, however only 248 kg of which are lost during DSP. The losses in ethanol occur mainly during the drying step of CL. The remaining 1,286 kg are regenerated during the evaporation step of the CL extract and can be used for CL extraction in proceeding batches.

Besides the material's demand, the consumption of utilities, including electricity, steam, cooling, and chilled water, was calculated for all process steps. In our model, electricity costs were the major contributor to utility costs. More than 99% of electricity was consumed by the production culture fermentation section, of which 65% were used for the compressor that provides compressed air to the fermenter for aeration, and 15% were utilized for fermenter agitation. In comparison, only 0.16% of electricity demand was utilized in the DSP section. Chilled water (5°C supply temperature and 10°C return temperature, in an assumed closed cycle loop) amounted to the second-largest cost contributor to utility costs, 97% of which were consumed by processes related to the production culture fermentation. Approximately half of the chilled water was used to temper the air compressor. The second half was used for general temperature control during fermentation and after sterilisation. Cooling water (25°C supply temperature and 30°C return temperature) was exclusively used to cool down the separators used for DSP. 70% of the consumed steam was used for fermenter heating and sterilisation processes and 28% during DSP for evaporation and drying. More than 98% of utility cost shares are attributed to the fermentation process and media preparation, with less than 2% for DSP. These results contradict with literature stating an overall major cost-share for DSP processes up to 60% (Banat et al., 2014). However, in our case, the comparably small share of DSP processes in utility costs may be due to the relatively long fermentation duration and the herewith associated high utility demand for the fermentation section. Furthermore, the purification process required to obtain CL with ethanol extraction does not need costly equipment or materials. A reduction in fermentation duration would nevertheless result in a relative increase in the cost-share of DSP.

3.3 Overall Process Economics

TCI and OC were calculated according to chapter 2.4 for our basic CL fermentation scenario in a 10 m^3 fermenter, resulting in a TCI of € 5.85 million and OC of € 1.19 million per year. These numbers are based on a pilot-scale plant and thus do not reflect realistic overall economic costs of an industrial plant; however, they are used as a baseline to compare different potential fermentation scenarios. Therefore, all further considerations will be evaluated relatively and not as absolute numbers. The pilot-scale simulation was chosen as a first scale-up step for better approximation. For further techno-economic analyses, more detailed process data needs to be obtained from pilot-scale fermentations to increase model accuracy for larger scales.

The major share of annual operation costs for the basic CL fermentation scenario was caused by the purchased equipment, expressed in depreciation and other facility-dependent costs (>70%). Labour-dependent costs were the third major contributor, accounting for 17.42% of OC. This value is within the range of traditional chemical plants and biorefineries with single output systems (Peters and Timmerhaus, 1991; Jorissen et al., 2020). Utility costs accounted for 5.47% of the OC for CL production and are considered within range compared to literature values for biorefineries, covering a wide range from 6% (e.g., Gómez-Ríos et al., 2017) up to 41% (e.g., Mussatto et al., 2013). Laboratory costs amounted to 2.61% of the OC and raw materials to 2.27%. The laboratory costs are within range, compared to chemical plants, as indicated by Peters and Timmerhaus, whereas raw material costs vary from the typical range of 10–60% of the total product cost (2003). This comparably small share in this study may be explained by the high facility-dependent costs for the modelled fermentation due to the relatively small plant scale with a fermenter scale of only 10 m^3. At a higher production and larger plant scale, raw material cost shares usually increase, with the absolute minimal production cost majorly caused by the raw material costs of the main substrates (Banat and Thavasi, 2018). An economic analysis for sophorolipid fermentation at a scale of 19,832 m^3 estimates up to 89% of the operation costs for raw materials (Ashby et al., 2013). The smallest shares of operation costs in the CL model were caused by consumables and waste disposal at 0.08% and 0.08%, respectively. However, it must be noted that only the disposal cost for the alkaline water used for reactor cleaning was considered. For consumables in biorefineries in general, values between 1% up to 14% of operation costs are usually spent (Jorissen et al., 2020).

3.4 Sensitivity Analysis (Scenarios, Derived From 3.2)

Based on the analysed overall process economics of the basic scenario, different scenario variations were simulated in order to assess the optimisation potential for CL fermentation. The effect of variation of the different parameters listed in **Table 2** on the UPC of CL is presented and discussed in relation to potential process optimisation approaches in the following.

3.4.1 Variation of Fermentation Duration, Concentration, and Yield

The fermentation duration of the production culture was set to 14 days in our basic scenario, based on our internal experimental data. The glucose fraction obtained from sucrose hydrolysis is usually consumed after approx. 5 days of fermentation at a starting level of 100 gL^{-1} sucrose. After that, fructose is metabolized at lower rates compared to glucose and is completely consumed after up to 14 days and with lower CL production rates (own experimental data, not shown). This shows that higher CL concentrations are achieved after longer fermentation durations at lower productivity rates. To design an economic process, it is therefore essential to compare the effect of a high concentration to the effect of shorter duration on process economy since a combination of both is not achievable.

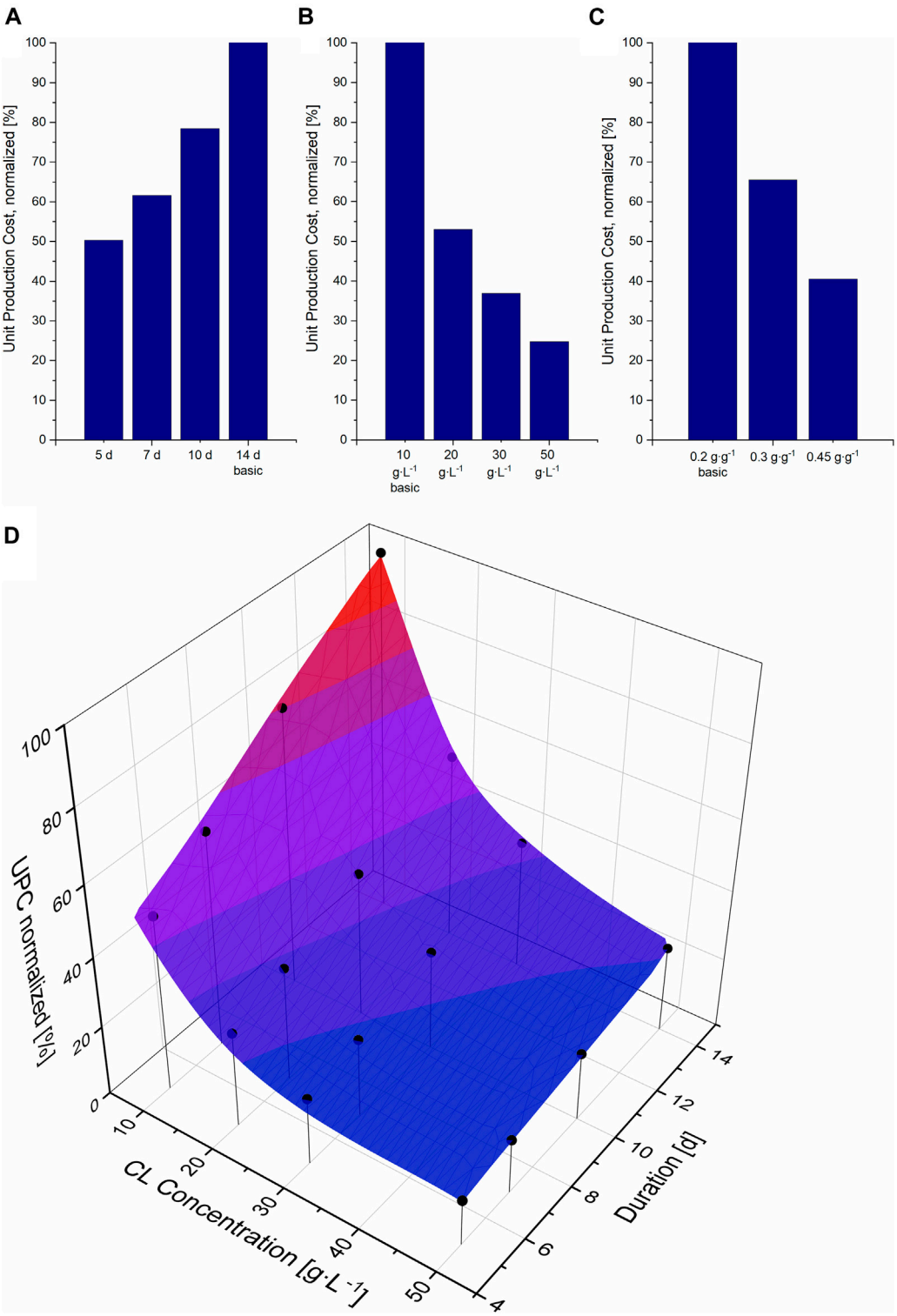

FIGURE 2 | Unit production cost (UPC) per kg CL, normalized to the UPC for the basic scenario (14 days fermentation, 10 g L^{-1} CL at a yield of 0.2 g g^{-1}), compared to different fermentation durations **(A)**, different CL concentrations **(B)** and yields **(C)**. **(D)** Surface cubic spline interpolation and simulated data points for the UPC at different fermentation durations and CL concentrations. The simulated data points are illustrated as black circles.

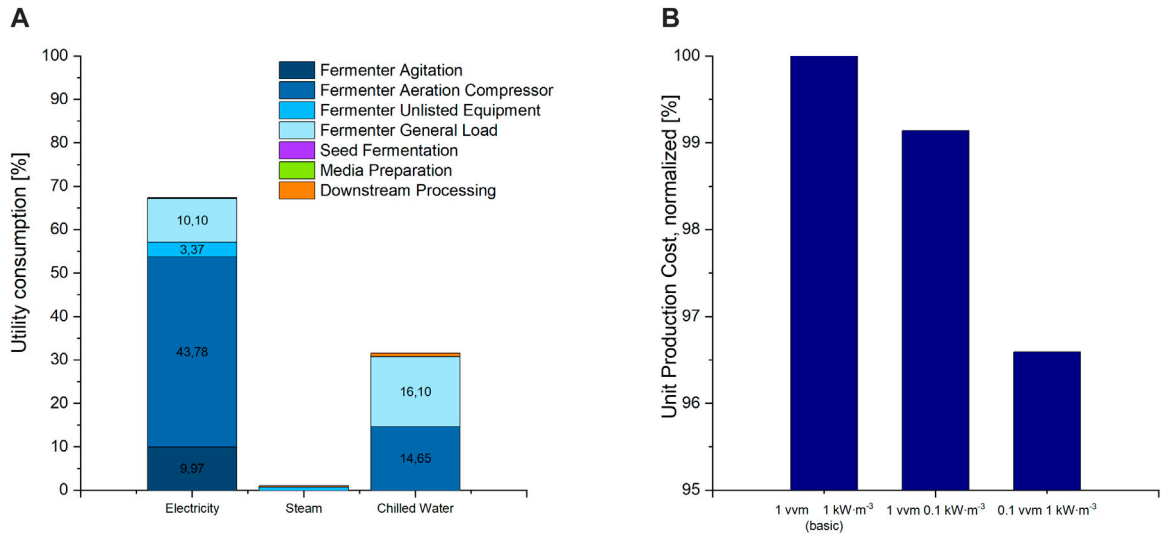

FIGURE 3 | (A) Distribution of utility costs for electricity, steam and chilled water used for cooling amongst all fermentation and purification units, as percent of overall utility consumption costs. Shares below 3% are not labelled in the diagram. **(B)** UPC of the basic scenario at a power input of 1 kW m^3 for agitation and an aeration rate of 1 vvm compressed air, compared to scenario 11 with 0.1 kW m^3 and scenario 10 with 0.1 vvm.

Reducing the fermentation duration from 14 to 5 days in our model allowed more batches per year. This increased the plant's productivity while the investment costs remained the same and only the operation costs increased, thus resulting in a reduction in UPC (**Figure 2A**). Assuming the same CL concentration of 10 g L^{-1}, an increase in fermentation duration results in a linear increase in UPC. To assess the effect of higher concentrations, three higher concentrations were further calculated for the standard fermentation duration of 14 days (**Figure 2B**). Here, a fed-batch process had to be simulated to obtain the higher concentrations at the same yield of 0.2 and with 50 g L^{-1} glucose in the initial medium. Depending on the needed feeding rate, the initial volume had to be decreased for these scenarios. An increase of CL concentration to only 20 g L^{-1} resulted in a reduction of 47% of UPC, almost as much as the reduction of fermentation duration to 5 days. A larger decrease in UPC could theoretically also be achieved, in a batch process, if the product yield was increased to 0.45 g g^{-1}, also resulting in a CL concentration of 22.5 g L^{-1} (**Figure 2C**). The decrease in UPC is higher when increasing the substrate yield instead of feeding more substrate, mainly because of the smaller vessel sizes for DSP and thus the lower PC. With a higher CL yield at the expense of biomass yield, the pellet size that needs to be purified is smaller than the pellet in a fed-batch process where the biomass yield remains the same. Thus vessels needed for DSP are smaller, the needed solvent amount for extraction and the amount of CL entrapped in the biomass pellet after extraction are less. The contribution of the additional substrate cost, in that case, has a less significant effect.

This result contradicts common literature data, where usually the substrate costs take a significant share of operation costs (Ashby et al., 2013; Cheng et al., 2017; Klein et al., 2017; Wang et al., 2020). However, the plant capacity modelled in this case study can easily explain this apparent contradiction. At a fermenter size of only 10 m^3, the revenues cannot be in a positive relation to the investment costs, especially not at such low concentrations of CL. Regular production plants would have much larger capacities, and the scaling effect would decrease the share of depreciation and PC-related expenses in favour of an increase in the share of running costs like substrate consumption. Therefore, although an increase in yield is limited to a maximum of 0.45 g g^{-1}, for future perspective, it would be advisable to aim at reaching this maximum CL yield as well. This could be achieved either by genetic modification, for instance, or by fermentation media adaptation (Banat et al., 2010).

When comparing the effect of a shorter fermentation duration to the effect of higher CL concentrations on UPC, favouring one option over the other is not trivial, and combining both aims cannot be achieved in practice. As previously shown in **Section 3.1**, CL concentrations higher than 22.5 g L^{-1} can only be achieved through a fed-batch process. On the other hand, substrate consumption rates show that the initial glucose (at a starting level of sucrose of approx. 100 g L^{-1}) is completely consumed after approx. 5 days, and the fructose even later. This means that a fed-batch process cannot be implemented for such short fermentation durations and would be only applicable for longer fermentation durations. Therefore, to identify the most promising parameter combination for an economic fermentation process that can be realised, 16 data points were simulated and a cubic spline interpolation was calculated with Origin (**Figure 2D**).

Comparing both the effect of time variation and concentration on UPC, it is apparent that an increase in CL titer results in a larger reduction in UPC compared to a decrease in fermentation duration. This is especially the case at lower CL concentrations. The higher the CL titer, the less the decrease in UPC. This is due to the additional equipment PC needed for larger DSP units like

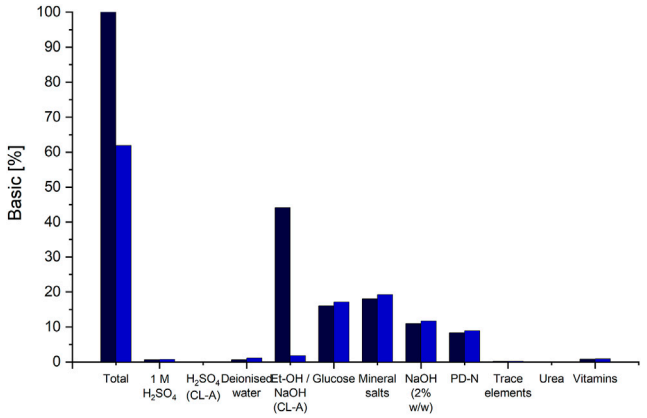

FIGURE 4 | Distribution of raw material cost-shares on the different chemicals and substrates used for fermentation and DSP. The cost shares of the basic scenario are indicated via the black columns and the cost shares for scenario 12, applying the DSP method using alkaline hydrolysis and precipitation to CL-A, are indicated in blue. The column "Et-OH/NaOH (CL-A)" indicates the cost shares of ethanol, for the basic DSP method and the cost shares for NaOH in scenario 12.

solvent vessels and extraction tanks. On the other hand, the effect of fermentation duration is linear, as no additional costs are needed for shorter fermentation durations, but more batches per year can be operated, and thus the plant's capacity can be increased. In other words: approximately the same reduction in UPC can be achieved by reducing the fermentation duration from 14 to 5 days with a titer of 10 g L^{-1} or by doubling the concentration from 10 to 20 g L^{-1} at the same fermentation duration of 14 days.

3.4.2 Variation of Aeration Rate and Power Input for Agitation

Utility costs, making up the highest share in OC of the process-parameter dependent cost categories, are mainly caused by electricity consumption during fermentation (**Figure 3**). In a TEA of a rhamnolipid production process, Moutinho et al. also showed that electricity demand makes up a major share of variable costs (2021). In our model the major share of electricity cost is taken up by the compressor used for fermenter aeration, followed by the consumption of the stirrer engine for fermenter agitation. In aerobic fermentation processes, both the agitator and stirrer are used to supply the medium with the oxygen needed by the microorganisms. Gas bubbles are introduced to the liquid via a gas sparger, the agitator. Then they are dispersed into smaller bubble sizes to provide a larger surface for oxygen transfer from the gas, into the liquid phase and to the microorganisms (Doran, 2013). The stirrer is further used for medium homogenization. The minimum power input to the stirrer and the aeration rate are limited by the oxygen demand of the microorganisms.

Based on the high contribution of both the stirrer and aeration compressor to utility consumption, a reduction in both or either should result in a reduction in operation costs. Reducing the power input from the initial 1 to 0.1 kW m^3 and the agitation rate from 1 to 0.1 vvm however resulted only in a slight decrease in UPC of less than 1% and 4%, respectively (**Figure 3**). This can be explained by the overall low share of utility costs to the overall OC of less than 5.5%. Nonetheless, considering environmental aspects, reducing electricity consumption during fermentation should be aspired. Emissions to the environment due to electricity generation seem to have a high share in environmental impact in biosurfactant fermentations (Aru and Ne, 2018; Kopsahelis et al., 2018). Therefore, for experimental optimisation, both power input and aeration rate should be adjusted to only cover the microorganism's oxygen demand without providing an excess in oxygen supply. Fermentation studies show a non-constant oxygen demand during CL fermentation (Oraby et al., 2020). Thus, a stepwise gas supply cascade can be applied, with high oxygen supply during exponential growth and reduced supply afterward and in the lag phase. This would result in an overall reduction of utility demand for oxygen supply.

To design such a gas supply cascade, maximal oxygen demand by the microorganisms (OUR_{max}) needs to be determined experimentally in a first step. Complementary to adapting the oxygen supply to the oxygen demand, the choice of a sparger unit can further result in a decrease in power consumption due to agitation and aeration. Using a ceramic sparger unit with small pore sizes, instead of traditional aeration rings, proved to be a viable option to reduce the power input in a 10 L fermenter without compromising the oxygen supply to the microorganisms (exemplary kLa values are shown in **Supplementary Table S3**). This shows that decreasing the electricity demand for agitation and aeration can easily be achieved by a better understanding of the fermentation process and adequate design of air supply cascades.

3.4.3 Comparison of Different Purification Processes

The commonly applied purification method for CL is solvent extraction (Hammami et al., 2008; Morita et al., 2011; Günther, 2014). In our basic scenario, we modelled a DSP process using ethanol to extract CL. Here, the ethanol is added to the pellet in a ratio of 2 $g_{EtOH} \cdot g_{Pellet}^{-1}$. The pellet contains after separation approx. 80% water and only about 10% CL and 10% biomass. This results in massive consumption of ethanol per g CL during extraction. Consequently, due to the large volumes, EtOH amounts for the largest share (>40%) of material costs (**Figure 4**). A reduction of the amount of used ethanol is not feasible because of the high water content in the pellet. Internal solubility examinations using a saturation shake-flask method adapted after (Baka et al., 2008) showed a decrease in CL solubility in ethanol at water contents above 40% (results not shown). Therefore, to ensure maximal CL solubility at room temperature, a minimal amount of 2 $g_{EtOH} \cdot g_{Pellet}^{-1}$ has to be used for extraction.

If an ethanol-free purification method, namely CL hydrolysis and purification via pH shift, is applied, material costs can be reduced by approx. 38% (**Figure 4**). The amount for all media components remains the same, except for NaOH and H_2SO_4, used instead of ethanol. These however result in overall lower material costs compared to the costs of ethanol. Together with an associated reduction in equipment PC, since no evaporation

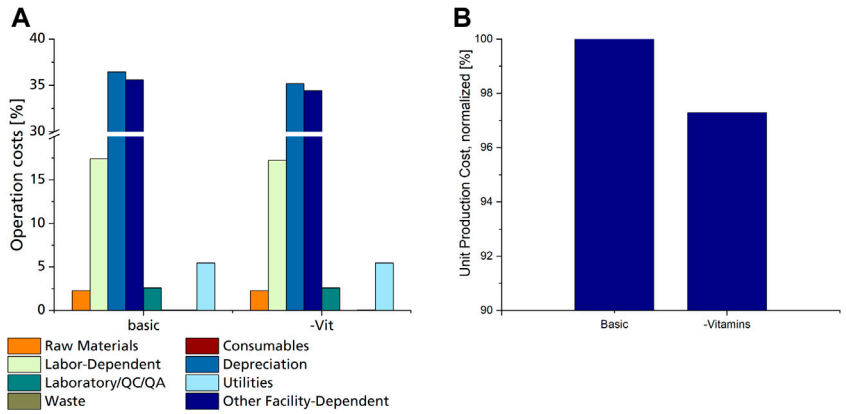

FIGURE 5 | (A) Distribution of operation costs for the basic scenario and scenario #13 utilizing a fermentation medium without vitamins, as % of overall operation costs. **(B)** Normalized UPC of the basic scenario with mineral salt medium, including vitamins, compared to scenario 13 utilizing the same mineral salt medium without vitamins.

and condensation would be needed, a total reduction in UPC by approx. 18% can be achieved by using the DSP method via pH shift. However, it has to be noted here that this would result in a different CL structure (CL-A), which needs to be considered when choosing the adequate purification method. Another means to reduce raw material costs is recirculating the evaporated ethanol after its condensation and reusing it for CL extraction.

3.4.4 Comparison of Different Fermentation Media Compositions

The choice of fermentation media components can affect both biomass growth and CL formation, as well as process economics. One approach for fermentation media optimisation is following experimental design techniques (Banat et al., 2010). Although highly beneficial, such examinations require many experiments and are very time-consuming. At the same time, economic considerations are usually neglected in such approaches. Considering economic factors of individual media constituents may limit the number of necessary experiments, especially if the omission of unnecessary media components is aspired by the experimental design. Here, the omission of more costly components first may reduce the number of needed experiments that have the most significant effect on both process economy and growth and CL formation.

The distribution of raw material cost shares shows that fermentation media components have comparably low shares (**Figure 4**), with both glucose and mineral salts contributing with approx. 16% and 18% each. Substituting glucose with other carbon sources originating from waste materials such as agro-industrial side streams may be a feasible option for cost reduction (Banat et al., 2010). However, mineral salts are necessary for both growth and CL formation and can therefore not be omitted (Oraby et al., 2020). The complex PD-N medium is needed for seed fermentation and cannot be omitted. All other media components used for the production culture have a rather small contribution to raw material costs. However, the preparation of individual media component groups may require additional equipment or consumables.

Consumable costs account for only 0.08% of OC, of which filter cartridges used for sterile filtration of media components amounted to 97%, while the rest was calculated for shaking flasks used for seed culture cultivation. Looking closer at the used media components, it is evident that only heat-labile vitamins need to be sterile filtrated, while the rest of the components can be heat sterilised. Heat sterilisation does not require any additional consumable materials and can be done in regular tanks. This means that although vitamins have a negligible share in raw material costs, their omission from the fermentation medium would result in a cost reduction since filters and filter cartridges for sterile filtration will not be needed. A decrease of up to 2.7% in unit production cost can be achieved by omitting vitamins from the fermentation medium (**Figure 5B**). However, this decrease is only valid if CL production is not affected by the lack of vitamins in the fermentation medium. This proved to be the case when comparing CL productivity with *Sporisorium scitamineum* on the same mineral salt medium with and without vitamins (Oraby et al., 2020). Here, both biomass and CL concentrations were only slightly lower when cultivated without vitamins. This also applies to other yeasts, including *Ustilago maydis*, which do not need vitamins for their growth (Burkholder et al., 1944; Kurtzman et al., 2011). Shaking flask experiments with *Sporisorium scitamineum* and *Ustilago maydis* underlined these results and showed that the omission of vitamins may decrease the side-product formation of erythritol (**Supplementary Figure S1**; **Supplementary Table S4**). These results show that omitting vitamins from the fermentation medium is a promising means to reduce production costs. It has to be noted, though, that a chelating agent, like citric acid, needs to be added to the trace element components used here to prevent the precipitation of iron after heat sterilisation.

3.4.5 Assessment of Overall Cost Optimisation Potential

Simulation of scenarios 1 to 12 show that increasing the CL concentration and yield, decreasing the fermentation duration, the agitation and aeration rate, using a DSP process without solvents, and omitting vitamins from the fermentation medium all have positive effects on the process economy. In scenario 13, variations of all these parameters were combined and defined as the best-case scenario according to the current state of the art in CL fermentation and showed a possible decrease in UPC of more than 77%. In addition to the reduction in UPC, a significant shift in OC distribution was further observed in the best-case scenario results. Especially the share of labour dependent costs and raw materials became more significant, increasing from 17 to 22% and from 2 to 8%, respectively. This highlights that the further developed/optimized the process becomes, the more important high yields and low raw material/substrate consumption get. This also applies to the scaling effect. A larger fermentation scale and production capacity would result in overall lower UPCs, but the share of raw material/substrate would become even more significant.

At this point, when process-specific optimisation approaches have been exhausted, more general optimisation approaches can lead to further cost reductions. Pinch analysis, for instance, can be performed to decrease energy consumption since the fermentation and purification processes contain various heat-consuming systems that could be used for heat recovery. Another possibility for further cost reduction is switching from batch to a continuous process. Here, less labour is required, and equipment control is simplified (Peters and Timmerhaus, 1991). However, this would require further experimental examinations. A further approach for overall cost reduction is the establishment of multiproduct systems, in which all material inputs and outputs are completely used to generate more profit (Kwan et al., 2018). In the case of CL, using the remaining biomass after CL purification as animal feed or the remaining fructose for the production of purified fructose syrup, for instance, may be a beneficial solution for additional profit generation. However, such general optimisation approaches do not target process optimisation as aimed with our approach, but rather overall economic optimisation.

4 CONCLUSION

The obtained results underline the great potential of process simulation and economic evaluation as a driver for experimental design for process optimisation in early development stages. Comparison of different scenarios of a CL fermentation in a 10 m^3 scale enabled prioritising the research directed at certain optimisation approaches. For CL, a decrease in fermentation duration, high CL concentrations and yields, a decrease in agitation and aeration rate, the choice of purification method, and utilizing a mineral salt medium with only heat sterilisable components were all identified as parameters affecting process economy. Especially the effect of the different media on the process economy could not have been predicted without economic evaluation. Furthermore, using stoichiometric calculations based on our laboratory data to describe CL fermentation with an *Ustilago maydis* strain, we were able to calculate the maximum possible CL yield $Y_{P/S}$ of 0.45 $g_{CL} \cdot g_{glucose}^{-1}$ that can be achieved at the biomass yield of 0.10 $g_{Biomass} \cdot g_{glucose}^{-1}$. This result serves as a foundation for considerations on feeding approach designs to increase CL concentrations in the fermenter.

DATA AVAILABILITY STATEMENT

The original contributions presented in the study are included in the article/**Supplementary Material**. Further inquiries can be directed to the corresponding author.

AUTHOR CONTRIBUTIONS

AO: Conceptualization; Data curation; Formal analysis; Investigation; Methodology; Visualization; Validation; Writing—original draft. SR: Writing–review and editing. SZ: Funding acquisition; Resources; Supervision; Writing—review and editing.

FUNDING

This work was partly funded by a Ph.D.-scholarship from the German Federal Environmental Foundation (DBU) AZ: 80017/333 and by Grants from the Federal Ministry of Education and Research (031B0469M, 031B0469P, and 031B1059P).

ACKNOWLEDGMENTS

The authors would like to thank Lea Maerz, Isabell Weickardt, and Daniel Hug for their assistance with the experimental work that contributed to the conceptualisation of the simulated scenarios. AO would also like to thank Prof. Dr. habil. Günter Tovar for his support and supervision during her Ph.D. research and Dr. Tobias Jorissen for his helpful advice on the economic evaluation model.

SUPPLEMENTARY MATERIAL

The Supplementary Material for this article can be found online at: https://www.frontiersin.org/articles/10.3389/fbioe.2022.913351/full#supplementary-material

REFERENCES

Aru, O. O., and Ikechukwu, N. E. O. (2018). Life Cycle Assessment of the Environmental Impact of Biosurfactant Production from Oil Waste by a Diculture of *Azotobacter vinelandii* and *Pseudomonas* Sp. *J. Bioremediat. Biodegr.* 9, 435. doi:10.4172/2155-6199.1000435

Ashby, R. D., McAloon, A. J., Solaiman, D. K. Y., Yee, W. C., and Reed, M. (2013). A Process Model for Approximating the Production Costs of the Fermentative Synthesis of Sophorolipids. *J Surfact Deterg.* 16 (5), 683–691. doi:10.1007/s11743-013-1466-0

Baka, E., Comer, J. E. A., and Takács-Novák, K. (2008). Study of Equilibrium Solubility Measurement by Saturation Shake-Flask Method Using Hydrochlorothiazide as Model Compound. *J. Pharm. Biomed. Analysis* 46, 335–341. doi:10.1016/j.jpba.2007.10.030

Banat, I. M., and Thavasi, R. (2018). *Microbial Biosurfactants and Their Environmental and Industrial Applications*. 1. Aufl. Boca Raton: CRC Press. doi:10.1201/b21950

Banat, I. M. (1995). Biosurfactants Production and Possible Uses in Microbial Enhanced Oil Recovery and Oil Pollution Remediation: A Review. *Bioresour. Technol.* 51 (1), 1–12. doi:10.1016/0960-8524(94)00101-6

Banat, I. M., Franzetti, A., Gandolfi, I., Bestetti, G., Martinotti, M. G., Fracchia, L., et al. (2010). Microbial Biosurfactants Production, Applications and Future Potential. *Appl. Microbiol. Biotechnol.* 87 (2), 427–444. doi:10.1007/s00253-010-2589-0

Banat, I. M., Makkar, R. S., and Cameotra, S. S. (2000). Potential Commercial Applications of Microbial Surfactants. *Appl. Microbiol. Biotechnol.* 53 (5), 495–508. doi:10.1007/s002530051648

Banat, I. M., Satpute, S. K., Cameotra, S. S., Patil, R., and Nyayanit, N. V. (2014). Cost Effective Technologies and Renewable Substrates for Biosurfactantsâ€ Production. *Front. Microbiol.* 5, 1–18. doi:10.3389/fmicb.2014.00697

Burkholder, P. R., McVeigh, I., and Moyer, D. (1944). Studies on Some Growth Factors of Yeasts. *J. Bacteriol.* 48 (4), 385–391. doi:10.1128/jb.48.4.385-391.1944

Ceresana (2017). *Ceresana - Marktstudie Tenside (2. Auflage)*. 2nd Edn. Editor Ceresna Consulting Konstanz: Ceresna.

Cheng, C., Zhou, Y., Lin, M., Wei, P., and Yang, S.-T. (2017). Polymalic Acid Fermentation by Aureobasidium Pullulans for Malic Acid Production from Soybean Hull and Soy Molasses: Fermentation Kinetics and Economic Analysis. *Bioresour. Technol.* 223, 166–174. doi:10.1016/j.biortech.2016.10.042

Chmiel, H. (2006). *Bioprozesstechnik*. 2. Aufl, 1. München: Elsevier GmbH.

Czinkóczky, R., and Németh, Á. (2020). Techno-Economic Assessment of Bacillus Fermentation to Produce Surfactin and Lichenysin. *Biochem. Eng. J.* 163, 107719. doi:10.1016/j.bej.2020.107719

Doran, P. M. (2013). *Bioprocess Engineering Principles*, 2. Amsterdam: Elsevier/AP Acad. Press.

Ekpenyong, M., Asitok, A., Antai, S., Ekpo, B., Antigha, R., Ogarekpe, N., et al. (2021). Kinetic Modeling and Quasi-Economic Analysis of Fermentative Glycolipopeptide Biosurfactant Production in a Medium Co-Optimized by Statistical and Neural Network Approaches. *Prep. Biochem. Biotechnol.* 51 (5), 450–466. doi:10.1080/10826068.2020.1830414

Elias, A. M., Longati, A. A., Ellamla, H. R., Furlan, F. F., Ribeiro, M. P. A., Marcelino, P. R. F., et al. (2021). Techno-Economic-Environmental Analysis of Sophorolipid Biosurfactant Production from Sugarcane Bagasse. *Ind. Eng. Chem. Res.* 60 (27), 9833–9850. doi:10.1021/acs.iecr.1c00069

Eveleigh, D. E., Dateo, G. P., and Reese, E. T. (1964). Fungal Metabolism of Complex Glycosides: Ustilagic Acid. *J. Biol. Chem.* 239 (3), 839–844. doi:10.1016/s0021-9258(18)51666-5

FernUniversität Hagen (2020). Laborcosts_pauschalsaetze_2019. FernUniversität Hagen. Available at: https://www.fernuni-hagen.de/arbeiten/personalthemen/bezahlung/pksaetze-bat200603.shtml (Accessed April 8, 2020).

Geys, R., Soetaert, W., and van Bogaert, I. (2014). Biotechnological Opportunities in Biosurfactant Production. *Curr. Opin. Biotechnol.* 30, 66–72. doi:10.1016/j.copbio.2014.06.002

Global Market Insights, Inc. (2021). Biosurfactants Market Report, 2027. Biosurfactants Market Size by Product, by Applocation, Industry Analysis Report, Regional Outlook, Application Potential, Price Trend, Competitive Market Share and Forecast, 2021-2027. Global Market Insights, Inc. Available at: https://www.gminsights.com/pressrelease/biosurfactants-market-size (Accessed September 29, 2021).

Gómez-Ríos, D., Barrera-Zapata, R., and Ríos-Estepa, R. (2017). Comparison of Process Technologies for Chitosan Production from Shrimp Shell Waste: A Techno-Economic Approach Using Aspen Plus®. *Food Bioprod. Process.* 103, 49–57. doi:10.1016/j.fbp.2017.02.010

Günther, M. (2014). *Mikrobielle Synthese, Aufarbeitung, Modifizierung und Tensideigenschaften von Mannosylerythritollipiden und Cellobioselipiden*. Stuttgart: University of Stuttgart.

Günther, M., Zibek, S., and Rupp, S. (2017). Fungal Glycolipids as Biosurfactants. *CBIOT* 6 (3), 205–218. doi:10.2174/2211550105666160822170256

Hammami, W., Labbé, C., Chain, F., Mimee, B., and Bélanger, R. R. (2008). Nutritional Regulation and Kinetics of Flocculosin Synthesis by Pseudozyma Flocculosa. *Appl. Microbiol. Biotechnol.* 80 (2), 307–315. doi:10.1007/s00253-008-1541-z

Intelligen Inc. (2020). *Super Pro Designer User Guide. v. 10*. Scotch Plain, NJ: Intelligen Inc., 1–549.

Jorissen, T., Oraby, A., Recke, G., and Zibek, S. (2020). A Systematic Analysis of Economic Evaluation Studies of Second-Generation Biorefineries Providing Chemicals by Applying Biotechnological Processes. *Biofuels Bioprod. Bioref.* 14 (5), 1028–1045. doi:10.1002/bbb.2102

Klein, B. C., Silva, J. F. L., Junqueira, T. L., Rabelo, S. C., Arruda, P. V., Ienczak, J. L., et al. (2017). Process Development and Techno-Economic Analysis of Bio-Based Succinic Acid Derived from Pentoses Integrated to a Sugarcane Biorefinery. *Biofuels Bioprod. Bioref.* 11 (6), 1051–1064. doi:10.1002/bbb.1813

Klement, T., and Büchs, J. (2013). Itaconic Acid - A Biotechnological Process in Change. *Bioresour. Technol.* 135, 422–431. doi:10.1016/j.biortech.2012.11.141

Kopsahelis, A., Kourmentza, C., Zafiri, C., and Kornaros, M. (2018). Gate-to-Gate Life Cycle Assessment of Biosurfactants and Bioplasticizers Production via Biotechnological Exploitation of Fats and Waste Oils. *J. Chem. Technol. Biotechnol.* 93 (10), 2833–2841. doi:10.1002/jctb.5633

Krull, S., Lünsmann, M., Prüße, U., and Kuenz, A. (2020). Ustilago Rabenhorstiana-An Alternative Natural Itaconic Acid Producer. *Fermentation* 6 (1), 4. doi:10.3390/fermentation6010004

Kurtzman, C. P., Fell, J. W., and Boekhout, T. (2011). "The Yeasts," in *The Yeasts. A Taxonomic Study*. 5th Edn. Amsterdam: Elsevier.

Kwan, T. H., Hu, Y., and Lin, C. S. K. (2018). Techno-Economic Analysis of a Food Waste Valorisation Process for Lactic Acid, Lactide and Poly(lactic Acid) Production. *J. Clean. Prod.* 181 (181), 72–87. doi:10.1016/j.jclepro.2018.01.179

Lemieux, R. U. (1951). The Biochemistry of the Ustilaginales. III. The Degradation Products and Proof of the Chemical Heterogeneity of Ustilagic Acid. *Can. J. Chem.* 29 (5), 415–425. doi:10.1139/v51-050

Marchant, R., and Banat, I. M. (2012). Microbial Biosurfactants: Challenges and Opportunities for Future Exploitation. *Trends Biotechnol.* 30 (11), 558–565. doi:10.1016/j.tibtech.2012.07.003

Michael, C. F. (2013). "Upstream Industrial Biotechnology," in *Expression Systems and Process Development*. 1. Aufl (Hoboken, New Jersey: WILEY Expression Systems and Process Development), 3.

Mimee, B., Pelletier, R., and Bélanger, R. R. (2009). In Vitroantibacterial Activity and Antifungal Mode of Action of Flocculosin, a Membrane-Active Cellobiose Lipid. *J. Appl. Microbiol.* 107 (3), 989–996. doi:10.1111/j.1365-2672.2009.04280.x

Moldes, A., Vecino, X., Rodríguez-López, L., Rincón-Fontán, M., and Cruz, J. M. (Editors) (2020). "Biosurfactants: the Use of Biomolecules in Cosmetics and Detergents," in *New and Future Developments in Microbial Biotechnology and Bioengineering. Microbial Biomolecules: Properties, Relevance, and Their Translational Applications* (San Diego: Elsevier), 163–185. doi:10.1016/b978-0-444-64301-8.00008-1

Morita, T., Ishibashi, Y., Fukuoka, T., Imura, T., Sakai, H., Abe, M., et al. (2011). Production of Glycolipid Biosurfactants, Cellobiose Lipids, by Cryptococcus Humicola JCM 1461 and Their Interfacial Properties. *Biosci. Biotechnol. Biochem.* 75 (8), 1597–1599. doi:10.1271/bbb.110036

Moutinho, L. F., Moura, F. R., Silvestre , R. C., and Romão-Dumaresq, A. S. (2021). Microbial Biosurfactants: A Broad Analysis of Properties, Applications, Biosynthesis, and Techno-Economical Assessment of Rhamnolipid Production. *Biotechnol. Prog.* 37 (2), e3093. doi:10.1002/btpr.3093

Mussatto, S. I., Moncada, J., Roberto, I. C., and Cardona, C. A. (2013). Techno-Economic Analysis for Brewer's Spent Grains Use on a Biorefinery Concept: the Brazilian Case. *Bioresour. Technol.* 148, 302–310. doi:10.1016/j.biortech.2013.08.046

Oraby, A., Werner, N., Sungur, Z., and Zibek, S. (2020). Factors Affecting the Synthesis of Cellobiose Lipids by Sporisorium Scitamineum. *Front. Bioeng. Biotechnol.* 8, 555647. doi:10.3389/fbioe.2020.555647

Peters, M. S., and Timmerhaus, K. D. (Editors) (1991). *Plant Design and Economics for Chemical Engineers*. 4th Edn. Singapore: McGraw-Hill Book Co.

Peters, M. S., Timmerhaus, K. D., and West, R. E. (2003). *Plant Design and Economics for Chemical Engineers*. 5th Edn. Columbia: McGraw-Hill.

Roxburgh, J. M., Spencer, J. F. T., and Sallans, H. R. (1954). Submerged Culture Fermentation, Factors Affecting the Production of Ustilagic Acid by Ustilago Zeae. *J. Agric. Food Chem.* 2 (22), 1121–1124. doi:10.1021/jf60042a007

Rupp, S., Zibek, S., Günther, M., and Hirth, T. (2010). Synthese und Optimierung von Cellobioselipiden und Mannosylerythritollipiden. *Chem. Ing. Tech.* 82 (8), 1215–1221. doi:10.1002/cite.201000078

Statistische Bundesamt (2020). *Daten zur Energiepreisentwicklung*. Lange Reihe von Januar 2005 bis Juli 2020 Germany: Statistische Bundesamt (Destatis).

Teichmann, B., Linne, U., Hewald, S., Marahiel, M. A., and Bölker, M. (2007). A Biosynthetic Gene Cluster for a Secreted Cellobiose Lipid with Antifungal Activity from Ustilago Maydis. *Mol. Microbiol.* 66 (2), 525–533. doi:10.1111/j.1365-2958.2007.05941.x

Wang, H., Tsang, C.-W., To, M. H., Kaur, G., Roelants, S. L. K. W., Stevens, C. V., et al. (2020). Techno-Economic Evaluation of a Biorefinery Applying Food Waste for Sophorolipid Production - A Case Study for Hong Kong. *Bioresour. Technol.* 303, 122852. doi:10.1016/j.biortech.2020.122852

Conflict of Interest: The authors declare that the research was conducted in the absence of any commercial or financial relationships that could be construed as a potential conflict of interest.

Publisher's Note: All claims expressed in this article are solely those of the authors and do not necessarily represent those of their affiliated organizations, or those of the publisher, the editors and the reviewers. Any product that may be evaluated in this article, or claim that may be made by its manufacturer, is not guaranteed or endorsed by the publisher.

frontiers | Frontiers in Bioengineering and Biotechnology

ORIGINAL RESEARCH
published: 09 August 2022
doi: 10.3389/fbioe.2022.917105

Synergistic Activity of Rhamnolipid Biosurfactant and Nanoparticles Synthesized Using Fungal Origin Chitosan Against Phytopathogens

Bhoomika M. Karamchandani[1], Priya A. Maurya[1], Sunil G. Dalvi[2], Samadhan Waghmode[3], Deepansh Sharma[4], Pattanathu K. S. M. Rahman[5,6], Vandana Ghormade[7] and Surekha K. Satpute[1]**

[1]Department of Microbiology, Savitribai Phule Pune University, Pune, India, [2]Tissue Culture Section, Vasantdada Sugar Institute, Pune, India, [3]Department of Microbiology, Elphinstone College, Mumbai, India, [4]Amity Institute of Microbial Technology, Amity University Rajasthan, Jaipur, India, [5]TeeGene and TARA Biologics, Life Science Accelerator, Liverpool School of Tropical Medicine, Liverpool, United Kingdom, [6]Centre for Natural Products Discovery, School of Pharmacy and Biomolecular Sciences, Liverpool John Moores University, Liverpool, United Kingdom, [7]Nanobiosciences Group, Agharkar Research Institute, Pune, India

OPEN ACCESS

Edited by:
Andrea Zille,
University of Minho, Portugal

Reviewed by:
Marcia Nitschke,
University of São Paulo, Brazil
Kamel A. Abd-Elsalam,
Agricultural Research Center , Egypt

***Correspondence:**
Sunil G. Dalvi
sgdalvi@gmail.com
Surekha K. Satpute
drsurekhasatpute@gmail.com

Specialty section:
This article was submitted to Industrial Biotechnology, a section of the journal Frontiers in Bioengineering and Biotechnology

Received: *10 April 2022*
Accepted: *24 May 2022*
Published: *09 August 2022*

Citation:
Karamchandani BM, Maurya PA, Dalvi SG, Waghmode S, Sharma D, Rahman PKSM, Ghormade V and Satpute SK (2022) Synergistic Activity of Rhamnolipid Biosurfactant and Nanoparticles Synthesized Using Fungal Origin Chitosan Against Phytopathogens. Front. Bioeng. Biotechnol. 10:917105. doi: 10.3389/fbioe.2022.917105

Phytopathogens pose severe implications in the quantity and quality of food production by instigating several diseases. Biocontrol strategies comprising the application of biomaterials have offered endless opportunities for sustainable agriculture. We explored multifarious potentials of rhamnolipid-BS (RH-BS: commercial), fungal chitosan (FCH), and FCH-derived nanoparticles (FCHNPs). The high-quality FCH was extracted from *Cunninghamella echinulata* NCIM 691 followed by the synthesis of FCHNPs. Both, FCH and FCHNPs were characterized by UV-visible spectroscopy, DLS, zeta potential, FTIR, SEM, and Nanoparticle Tracking Analysis (NTA). The commercial chitosan (CH) and synthesized chitosan nanoparticles (CHNPs) were used along with test compounds (FCH and FCHNPs). SEM analysis revealed the spherical shape of the nanomaterials (CHNPs and FCHNPs). NTA provided high-resolution visual validation of particle size distribution for CHNPs (256.33 ± 18.80 nm) and FCHNPs (144.33 ± 10.20 nm). The antibacterial and antifungal assays conducted for RH-BS, FCH, and FCHNPs were supportive to propose their efficacies against phytopathogens. The lower MIC of RH-BS (256 µg/ml) was observed than that of FCH and FCHNPs (>1,024 µg/ml) against *Xanthomonas campestris* NCIM 5028, whereas a combination study of RH-BS with FCHNPs showed a reduction in MIC up to 128 and 4 µg/ml, respectively, indicating their synergistic activity. The other combination of RH-BS with FCH resulted in an additive effect reducing MIC up to 128 and 256 µg/ml, respectively. Microdilution plate assay conducted for three test compounds demonstrated inhibition of fungi, FI: *Fusarium moniliforme* ITCC 191, FII: *Fusarium moniliforme* ITCC 4432, and FIII: *Fusarium graminearum* ITCC 5334 (at 0.015% and 0.020% concentration). Furthermore,

Abbreviations: BSs, biosurfactants; CH, chitosan; CBD, carbendazim; CHNPs, chitosan nanoparticles; CFU, colony-forming unit; DDA, degree of deacetylation; FCH, fungal chitosan; FCHNPs, fungal chitosan nanoparticles; LB, Luria–Bertani broth; MIC, minimum inhibitory concentration; MGYP, malt extract glucose yeast extract peptone; MHB/MHA, Mueller–Hinton broth/agar; NPs, nanoparticles; PBS, phosphate buffer saline; RH, rhamnolipids; SEM, scanning electron microscope; TPP, sodium tripolyphosphate.

potency of test compounds performed through the in vitro model (poisoned food technique) displayed dose-dependent (0.005%, 0.010%, 0.015%, and 0.020% w/v) antifungal activity. Moreover, RH-BS and FCHNPs inhibited spore germination (61–90%) of the same fungi. Our efforts toward utilizing the combination of RH-BS with FCHNPs are significant to develop eco-friendly, low cytotoxic formulations in future.

Keywords: agriculture, biosurfactant, *Cunninghamella*, chitosan, chitosan nanoparticles, phytopathogens

1 INTRODUCTION

The agricultural sector faces the demand for enhanced productivity to meet the ever-increasing needs of a growing population. The increased global population has disrupted the balance between production and demand, thereby affecting the availability of food. As a consequence, comprehensive agricultural production must be improved by 70% (Gu et al., 2021). Although the agricultural sector is advancing, it is still challenging to satisfy the demands of the starving population across the globe. Crop productivity is affected by a number of factors, including environmental changes, extreme weather, global warming, and disease outbreaks. Approximately $220 billion is lost annually through the outbreak of diseases caused by several pathogens (bacteria, fungi, and viruses). Population growth and an increase in the food supply have led to the enormous use of agrochemicals by farmers (Maluin and Hussein, 2020). The current market size of the agrochemical industry is USD 220 billion and expected to become USD 340 billion in 2027 (compound annual growth rate [CAGR] of ~3%) over the forecast period of 2021–2027 (Global Agrochemicals Market[1]). Nonetheless, excessive chemical use creates serious concerns, as it pollutes water and air and releases greenhouse gases (Pestovsky and Martinez-Antonio, 2017). Subsequently, this scenario generates innumerable sources of hazards for human health and the environment. In order to overcome these numerous challenges, an eco-friendly sustainable approach is obligatory for the agriculture sector.

The green approach involves the use of multifunctional biomolecules like biosurfactants (BSs), chitosan (CH), and chitosan-derived nanoparticles (CHNPs) mainly due to their biocompatible nature. The BSs (Sachdev and Cameotra, 2013), CH, and CHNPs (Malerba and Cerana, 2018; Mazzotta et al., 2022) have been explored for plant growth promotion and as biocontrol agents. BSs have been investigated for enhancing nutrient availability to plants, encouraging symbiotic associations, and improving soil health through the bioremediation of heavy metals, hydrocarbons, and other contaminants (Kumar et al., 2021). The BSs are nontoxic, biodegradable, and eco-friendly molecules that exhibit exceptional antimicrobial potential. Consequently, the wide applicability in improved crop and food safety certifies the BS-based biocontrol formulation in sustainable crop management strategies (Sharma, 2021). The antimicrobial potential of BSs can be broadened with other biomaterials like CH and CHNPs for innovative applications. Chemically, CH is the deacetylated derivative of chitin consisting of β-(1,4)-2-acetamido-2-deoxy-D-glucose and β-(1,4)-2-amino-2-deoxy-D-glucose units. The CH biopolymers originated from crustacean and fungal sources (FCH) are commercially valued product. Fungi of the Zygomycetes group efficiently convert chitin to CH by an enzyme—chitin deacetylase. FCH produced by Zygomycetes fungi is vastly recognized due to their high degree of deacetylation (DDA) and solubility. Additionally, the homogenous polymer length of FCH proposes abundant advantages over crustacean CH (Ghormade et al., 2017). CH and FCH are being explored continuously due to their broad-spectrum antimicrobial potential (Karamchandani et al., 2022). The matrix of these biopolymers functions as a shielding reservoir for the release of active ingredients by protecting them from the surrounding environment and controlling the release of agrochemicals (Cota-Arriola et al., 2013). CH biomolecule is also an active plant elicitor with massive antimicrobial potential. The well-appreciated biopolymer enables the delivery of agrochemicals and prevents postharvest decay (Karamchandani et al., 2022). Nanomaterials due to their unique structure, chemical composition, small particle size, and solubility have attracted the scientific fraternity, particularly for the purpose of agrochemicals. It is now more than past three decades that NPs have received considerable acceptance due to their exceptional functional attributes (Staroń and Długosz, 2021). Currently, nanotechnology stands as one of the most promising approaches to overcome the shortcomings of conventional agrochemicals and protecting crops successfully. The CH-derived CHNPs have superior antimicrobial action as compared to bulk materials due to their polycationic nature (Hosseinnejad and Jafari, 2016). In 2016, Sathiyabama and Parthasarathy reported that FCH and FCHNPs pose employability for formulation/products due to their adsorption abilities, biocompatibility, biodegradability, nontoxicity, and cost-effectiveness.

The agricultural sector needs to explore nano-empowered solutions to meet the food requirements in the global framework (Pestovsky and Martínez-Antonio, 2017). Our recent overview on CH and its derivatives facilitated in the realization of their promising role in averting fungal diseases of crops (Karamchandani et al., 2022). The protocols and nanoagrochemicals are to be well thought out for multifarious molecules discretely and/or in combination (Kah and Kookana, 2020). The combination of BS with FCH and/or FCHNPs undoubtedly offers superlative applications in agriculture. After a thorough literature survey, we realized that there is no

[1]https://www.prnewswire.com/news-releases/global-agrochemicals-market-2021-to-2027.

solitary report on RH-BS in combination with FCHNPs synthesized from FCH of *C. echinulata*. In view of this background, we explore the multifunctionalities of commercially available RH-BS and synthesized FCHNPs against phytopathogens associated with citrus, wheat, and sugarcane, etc. First, FCH was extracted from *C. echinulata* NCIM 691 and used for the synthesis of FCHNPs. We have also characterized FCH and FCHNPs meticulously to assure their authenticity. The antibacterial and antifungal activities of FCH and FCHNPs were investigated individually and in combination with RH-BS. Inhibition of fungal phytopathogens was also demonstrated through poisoned food technique and spore germination assays to propose innovative applications of RH-BS and FCHNPs in agriculture.

2 MATERIALS AND METHODS

2.1 Microorganisms: Fungal Culture and Phytopathogens

All the microbial cultures used in the study were procured from various repositories in India. The fungus *Cunninghamella echinulata* NCIM 691 and the bacterium *Xanthomonas campestris* NCIM 5028 were procured from the National Collection of Industrial Microorganisms (NCIM), Pune, Maharashtra, India. The ecologically heterogeneous and predominantly terrestrial fungus *C. echinulata* NCIM 691 was used for the extraction of FCH from its cell wall. Furthermore, extracted FCH was used to synthesize FCHNPs. The bacterial phytopathogen *X. campestris* NCIM 5028 was used for antibacterial assays. Other three fungal phytopathogens (labeled as FI, FII, and FIII), namely, FI: *Fusarium moniliforme* Sheldon ITCC 191, FII: *Fusarium moniliforme* Sheldon ITCC 4432, and FIII: *Fusarium graminearum* Schwabe ITCC 5334 were procured from the Indian Type Culture Collection (ITCC), Delhi, India, and used for antifungal assays (poisoned food technique and inhibition of spore germination). All the cultures were grown and maintained in media and growth conditions as per supplier's instructions.

2.2 Materials

The rhamnolipid-BS (RH-BS) was purchased from AGAE Technologies, United States. The RH-BS is composed of a mixture of mono- and di-rhamnolipid having a purity of 90%. Sodium tripolyphosphate (TPP) and commercial chitosan: CH (molecular weight = 50–190 kDa, degree of deacetylation 75%–85%) were purchased from Sigma-Aldrich (Merck KGaA, Darmstadt, Germany). The other materials used were of analytical grade. Pure quality and dehydrated media like malt extract glucose yeast extract peptone (MGYP), potato dextrose broth/agar (PDB/PDA), Mueller–Hinton broth/agar (MHB/MHA), and Luria–Bertani broth (LB) were purchased from HiMedia (Mumbai, India).

2.3 Extraction of Fungal Chitosan From *C. echinulata*

The fungal culture *C. echinulata* NCIM 691 was revived by growing in potato dextrose broth (PDB). Further conditions were set to extract FCH from the fungal mycelia using the alkali-insoluble method (Pochanavanich and Suntornsuk, 2002). First, *C. echinulata* NCIM 691 was grown on potato dextrose agar (PDA) medium for up to 7 days. Furthermore, the culture was scraped gently in phosphate buffer saline (PBS) to prepare the spore suspension (1.0×10^8 spores/ml). The spore suspension was inoculated in 250 ml Erlenmeyer flasks containing 100 ml of PDB and were incubated at 30°C for 16 h on a rotatory shaker (180 rpm). Next day, about 7.5% (v/v) of 16 h old inoculum was added aseptically to the 500 ml Erlenmeyer flasks with 200 ml of the sterile PDB. The flask was kept on a rotary shaker (180 rpm) at 29 ± 1°C for 12 days. The fungal biomass was initially separated from the media by filtration (Whatman filter paper, Grade No. 1—size 110 mm) and dried until the homogenous weight was obtained. The dry weights of the biomasses were noted, and then alkaline treatment was carried out using 1 N NaOH (1:30 w/v). This process helped in the removal of proteins and glucans from the alkali-treated supernatant. Subsequently, the solution was autoclaved at 121°C for 15 min. The alkali-insoluble material was centrifuged at 10,000 rpm for 15 min (Kubota AG-5006A, Tokyo, Japan). Post centrifugation, distilled water was added accordingly to reduce the pH up to 7.0. The obtained substance was dried further in a hot air oven at 60°C until a constant weight was achieved. This step was followed by the treatment of acetic acid (1% v/v) to the insoluble mass and was kept in a hot water bath (95°C) for 5 h. This imperative step dissolved the FCH components and was followed by centrifugation at 10,000 rpm for 20 min. The supernatant was collected and treated with 2 N NaOH to bring the pH up to 10.0. This was followed by another round of centrifugation at 10,000 rpm for 20 min, and the pellet was collected. This extracted FCH was washed multiple times with distilled water followed by 95% ethanol (1:20) and further with acetone (1:20). The extract was kept for drying in a hot air oven at 60°C until the homogenized weight could be obtained. This extract of FCH was ready for the synthesis of FCHNPs and stored at 4°C until further use.

2.3.1 Synthesis of Chitosan Nanoparticles From Fungal Chitosan of *C. echinulata*

The FCH extracted from the fungus *C. echinulata* NCIM 691 was employed to synthesize FCHNPs through the ionic gelation method as described by de Carvalho et al. (2019). Briefly, FCH was dissolved in 2 mg/ml acetic acid (1% v/v), and pH was adjusted to 5.0. The solution of sodium tripolyphosphate (TPP) was prepared in distilled water at 0.1% (w/v). About 5 ml of TPP solution was added to 15 ml of the FCH. This quantification of solutions depicts the ratio of 3:1 for CH:TPP (de Pinho Neves et al., 2014). The TPP solution was filtered through a 0.2 μm membrane filter (Pall Life Sciences, USA) and was added to FCH solution dropwise under stirring conditions using a magnetic stirrer at 700–800 rpm (room temperature) to obtain a clear solution (de Carvalho et al., 2019). After the complete addition of TPP, the solution was left under stirring for another 30 min. The positively charged amino acid group of FCH interacts with the negative charge of TPP resulting in the ionotropic gelation reaction. The ionic gelation method of FCH

synthesis initiated with meshwork formation upon TPP addition and enabled the synthesis of FCHNPs. Afterward, the solution was centrifuged at 10,000 rpm for 20 min (Khoerunnisa et al., 2021). The FCHNPs were obtained in the form of precipitate and subsequently washed twice with distilled water to remove the unreacted substances. The purified FCHNPs were then freeze-dried and stored at 4°C until further use. A similar protocol was used to synthesize CHNPs from commercial CH (Sigma-Aldrich, Merck KGaA, Darmstadt, Germany). The physicochemical characterization of FCH and FCHNPs was carried out using various analytical techniques as mentioned in the following sections. We had included commercial CH and its synthesized CHNPs as references to analyze and compare the data for FCH and FCHNPs, respectively.

2.3.2 Physicochemical Characterization of Fungal Chitosan and Chitosan Nanoparticles

The FCH and FCHNPs were characterized using the following analytical techniques: 1. UV-visible spectroscopy, 2. Dynamic Light Scattering (DLS), 3. Zeta potential, 4. Fourier Transform Infra-Red Spectroscopy (FTIR), 5. Scanning Electron Microscopy (SEM), and 6. Nanoparticle Tracking Analysis (NTA). All the samples were prepared and used as per the requirements of the corresponding technique. Appropriate reference samples were also included in the particular analytical techniques.

2.4 UV-Visible Spectroscopy

The UV-visible spectrophotometry (UV–Vis) is a routinely used technique for the quantitative determination of analytes, chemicals, and biological macromolecules. The UV-visible spectra of FCH and FCHNPs were recorded using a Jasco V-770 Spectrophotometer (JASCO Deutschland GmbH, Pfungstadt, Germany) to confirm the absorption spectra in the range of 200–800 nm (Agarwal et al., 2018; Khoerunnisa et al., 2021). This analytical tool was employed to examine FCH and FCHNPs samples which were also compared with CH and CHNPs.

2.5 Dynamic Light Scattering and Zeta Potential

Dynamic light scattering (DLS) is the most widely used technique to determine the hydrodynamic diameter of NPs and afford evidence on the aggregation state of NPs in solution. The technique determines the average particle size on a high-performance particle Zetasizer HPPS-5001 (Malvern, UK). The CH, CHNPs, FCH, and FCHNPs were analyzed in triplicate at 25°C at a scattering angle of 90°. Pure distilled water was used as a reference dispersing medium. All the samples were dissolved in 0.5% acetic acid followed by sonication for 15 min in an ultrasonicator (QSonica Sonicator, USA). Samples were then rinsed with distilled water followed by filtration using a syringe filter of 0.2 µm pore size (Pall Life Sciences, USA), and the average particle size was analyzed in triplicates (Ghadi et al., 2014).

The zeta potential of all the samples was measured using a Zetasizer Nano (Malvern, UK) to manifest the effective electric charge on the surface of NPs and quantify the charges. The property of zeta potential depends on the surface charge which is extremely significant for the stability of NPs in suspension. The zeta potential is also a key feature during the adsorption of NPs at the initial stage onto the membrane of any cell. After the adsorption of NPs on the cell surface, the rate of their uptake is dependent on the particle size. Thus, nanosize and zeta potential contribute meaningfully to the toxicity of NPs. The electrophoretic mobility of the samples assisted in depicting their zeta potential.

2.6 Fourier Transform Infra-Red Spectroscopy

Fourier transform infrared (FTIR) spectroscopy is a sensitive technique that recognizes the presence of functional groups. The technique is fairly suitable to identify and classify vital biomolecules that can be employed for diverse applications. The completely dried samples of FCH and FCHNPs were examined. The structural analysis was carried out on a spectrophotometer (Alpha II, Bruker, UK) in a wavenumber range of 400–4,000 cm^{-1}. FTIR spectra of all biomaterials were attained by using 1 mg of sample. The spectrum was then recorded and compared with the commercial CH and CHNPs (Pawlak and Mucha, 2003; Divya et al., 2017). Confirmation of scans was carried out to achieve a decent signal/noise ratio.

2.7 Scanning Electron Microscopy

The advancements in scanning electron microscopy (SEM) empower the high-resolution imaging of biomaterials. Both the nanoparticles (CHNPs and FCHNPs) were air-dried and were mounted on silicon wafers to be used to divulge their size, texture, and shape. The shape and surface morphology were determined using the SEM setup of FEI Nova NanoSEM 450, USA. The samples were dissolved in distilled water and placed on silica wafers (Sigma-Aldrich, USA), which were allowed to dry completely. Both the samples were then coated with gold and observed at an acceleration voltage of 10.0 kV with the highest magnification of ×50,000 (Anitha et al., 2009).

2.8 Nanoparticle Size Analysis

The size of the NPs was also confirmed through nanoparticle tracking analysis (NTA). This technique employs light scattering as well as Brownian motion to estimate NP size distribution of samples. The size analysis of the NPs was carried out through nanotracking analysis (NTA 2.3, UK) (Rahi et al., 2022). The sample was loaded in liquid suspension into a chamber with a laser beam for sample illumination scattering the laser light. The NTA technique needs a sample in low volumes without any sophisticated protocols for the sample preparation. The ×20 microscope objective was used to observe the images which were captured using a digital camera. The camera captures a video of the particles moving under Brownian motion. Several particles individually and simultaneously (particle-by-particle) are analyzed by NTA software. Hence, the NanoSight instrument provided NP size in high resolution, concentration, and aggregation measurements (count based) of CHNPs and

FCHNPs. Concurrently, fluorescence mode provided specific results for suitably labeled particles. The real-time monitoring process helped to scrutinize the subtle changes in the particle population characterization.

2.9 Application of Rhamnolipid Biosurfactant, Fungal Chitosan, and Synthesized Chitosan Nanoparticles in Controlling the Selected Phytopathogens

This section dealt with evaluating the efficacies of the test compounds—RH-BS (commercial), FCH (extracted), and FCHNPs (synthesized) against selected phytopathogens. The commercial CH and its synthesized CHNPs (by us in the laboratory) were tested against four phytopathogens. *X. campestris* NCIM 5028 (causative agent of black rot and bacterial wilt, etc.) and three fungi: FI (causative agent of the stalk rot, ear rot, and kernel rot of corn), FII (causative agent of the stalk rot, ear rot, and kernel rot of corn), and FIII (causative agent of the Fusarium head blight on wheat, barley, and other grains) were included in the assays. The following experiments from 1 to 3 were performed against the bacterium *X. campestris* NCIM 5028. Experiment numbers 4 to 6 were performed against three fungal pathogens (FI, FII, and FIII).

1. Determining the minimum inhibitory concentration of the test compounds against *X. campestris* using microdilution assay.
2. Determining the synergistic activity of the test compounds against *X. campestris* using checkerboard assay.
3. Evidencing antibacterial effect of the test compounds against *X. campestris* using SEM.
4. Determining the antifungal activity of the test compounds against three fungal phytopathogens using microdilution assay.
5. Determining the efficacy of the test compound dosages against three fungal phytopathogens through the poisoned food technique.
6. Determining the efficacy of the test compounds in inhibiting the spore germination of three fungal phytopathogens.

2.9.1 Determining Minimum Inhibitory Concentration of the Test Compounds Against *X. campestris* Using Microdilution Assay

The minimum inhibitory concentration (MIC) of three test compounds, viz., RH-BS, FCH, and FCHNPs, was determined against the bacterial pathogen *X. campestris* NCIM 5028. This culture was grown in LB at 30°C, and after 48 h of incubation, the bacterial suspension was prepared in MHB. The inoculum for the microdilution assay was prepared by adjusting the optical density (OD_{620}) value equivalent to 10^8 CFU/ml (determined from a calibration curve). The MIC for all the test compounds was performed by broth dilution method in separate 96-well microtiter plates (Zgoda and Porter, 2001). All three test materials were dissolved in MHB at twice the concentration of the final test compounds, with pH adjusted to 7.0. Furthermore, 100 µl of MHB was dispensed in each well of a microtiter plate (Column 3–12) containing MHB only. Column 1 contained 100 µl of dilute culture inoculum (OD adjusted) (as mentioned previously), and Column 2 contained 100 µl of the medium broth (as a negative control to monitor sterility). A multichannel pipette was then used to transfer and mix the test compounds from Columns 12 (200 µl) to 3, resulting finally a volume of 100 µl per well. The concentrations between 2 and 1,024 µg/ml were achieved for all the three test compounds through double dilutions serially from Columns 12 to 3. The absorbance of samples was measured at 620 nm at 0 and 48 h. After completing the incubation period, the MIC was identified from the well showing no visible growth in the presence of the test compound. Thus, the lowest concentration of the test compound inhibiting the visible growth of the organisms was documented as MIC. Experiments were performed in triplicate, and the mean values of three independent biological replicates were considered.

2.9.2 Determining the Synergistic Activity of the Test Compounds Against *X. campestris* Using Checkerboard Assay

The checkerboard assays were performed to investigate the synergistic activity of all three test compounds (RH-BS, FCH, and FCHNPs) against *X. campestris* NCIM 5028 by following the protocols as described by Okoliegbe et al. (2021) and Mirzaei-Najafgholi et al. (2017). Briefly, 24 h old culture of *X. campestris* NCIM 5028 was inoculated into MHB and incubated at 30°C until the exponential growth phase. Around 100 µl of each dilution of all the test compounds (2 × MIC, 1 × MIC, 1/2, 1/4, 1/8, 1/16, 1/32, and 1/64 MIC) were dispensed to each row. Furthermore, 100 µl of the second compound was added to the same or each row of the wells in the direction perpendicular to the previous compound in different dilutions in a 96-well plate. A two-fold diluted freshly prepared solution of the test compound (at different concentrations) was dispensed in a checkerboard array and inoculated with 10^8 CFU/ml of the bacterial suspension. The well without any test compound was considered the positive control. The well with the growth medium without inoculum and the test compound was used as the negative control. After incubation at 30°C, plates were examined for visual turbidity using the microplate reader (Spectra Max M2, USA). A fractional inhibitory concentration index (FICI) of both combinations (RH-BS + FCH and RH-BS + FCHNPs) is calculated (Konaté et al., 2012) using the following formula:

$$\mathrm{FICI} = \mathrm{FIC\,A} + \mathrm{FIC\,B},$$

$$\mathrm{FICI} = \frac{\text{MIC of Test Compound A combined}}{\text{MIC of Test Compound A alone}} + \frac{\text{MIC of Test Compound B combined}}{\text{MIC of Test Compound B alone}}.$$

Interaction between combinations of two test compounds is evaluated if the FIC index was: ≤0.5, synergistic; 0.5 < FICI <1, additive; 1 < FICI ≤4, indifferent and FICI >4, antagonistic.

2.9.3 Evidencing Antibacterial Effect of the Test Compounds Against *X. campestris* using SEM

The SEM was performed to evident the effect of all the three test compounds (RH-BS, FCH, and FCHNPs) on *X. campestris* NCIM

5028. The protocol for the same was adopted from Fischer et al. (2012). Cells of *X. campestris* were grown for 24 h at 30°C in MHB. About 10^8 CFU/ml cells were treated at their respective MIC of the test compound for 24 h at 30°C. The cells without the treatment of the test compounds were encompassed as a negative control. This enabled us to distinguish the morphology of the *X. campestris* NCIM 5028 cells in the presence (test) and absence (control) of the test compounds. The treated cells were washed with PBS by centrifuging at 10,000 rpm for 15 min. The cell pellet obtained after centrifugation was treated overnight with 2.5% glutaraldehyde (Sigma-Aldrich, USA) at 4°C. The next day cells were washed (to remove glutaraldehyde) with PBS by centrifugation at 10,000 rpm for 15 min followed by the ethanol treatment. The first dehydration step was achieved by taking water:ethanol in the ratio of 90:10 and incubating for 15 min, which were then centrifuged at 10,000 rpm at 4°C. The same steps were repeated several times with the different proportions of water and ethanol in the ratio of 80:20, 60:40, 40:60, 20:80, and 10:90, and finally with 100% ethanol. The treated cells were loaded on silica wafers (Sigma-Aldrich, USA), and furthermore ethanol was evaporated completely overnight. The SEM images of the dried sample were analyzed using Nova Nano SEM 450 instrumentation facility (USA) under ×50,000 magnification.

2.9.4 Determining the Antifungal Activity of the Test Compounds Against Three Fungal Phytopathogens Using Microdilution Assay

The MIC of all three test compounds (RH-BS, FCH, and FCHNPs) was evaluated against three selected fungi FI, FII, and FIII. The different concentrations (0.005%, 0.010%, 0.015%, and 0.020% w/v) of the test compounds were considered to determine their antifungal activity. In the microtiter plate, we added the test compound (20 µl) with PDB (120 µl) and 10 µl homogenous fungal suspension (1.0×10^8 spores/ml). The commercial fungicide carbendazim (CBD) (Sigma-Aldrich, USA) of similar concentrations was used as a positive control. The CBD is a commercial, broad-spectrum fungicide popular for controlling several dreaded fungi associated with cereals and fruits like citrus, pineapples, strawberries, and bananas. First, plates were placed in a refrigerator (at 4°C for 1 h) for initial prediffusion and to achieve homogeneous diffusion of the test biomaterials in the surrounding medium in the agar plate. Furthermore, plates were removed from the refrigerator and placed in an incubator (29 ± 1°C for 5 days) for optimum growth. After 5 days of completing the incubation period at 29 ± 1°C, each well was observed with naked eyes under the bright light for fungal mycelial growth (Elshikh et al., 2016; Chopra et al., 2020).

2.9.5 Determining the Efficacy of the Test Compound Dosages Against Three Fungal Phytopathogens Through the Poison Food Technique.

This technique was carried out to confirm the efficacy of all the test compounds (RH-BS, FCH, and FCHNPs) (Saharan et al., 2013) against three *Fusarium* species (FI, FII, and FIII). Different doses (0.005%, 0.010%, 0.015%, and 0.020% w/v) of all test compounds were mixed with potato dextrose broth and poured in Petri dishes (90 mm × 15 mm, HiMedia, Mumbai, India) individually. The mycelial bit of test fungal phytopathogens from the peripheral end of uniform size (diameter, 5.0 mm) were taken from 7-day-old culture and placed in the center of the Petri dishes impregnated with the test compounds individually. These Petri plates were then incubated at 29 ± 1°C for 7 days for the observation of radial mycelial growth. The inoculated plates were compared with the positive control (with commercial fungicide CBD) and negative control (without test compounds) to calculate the percentage inhibition rate of the mycelia for the respective phytopathogen.

$$\%\ \text{Inhibition rate} = \frac{M_c - M_t}{M_c} \times 100,$$

where M_c is the mycelial growth in the control plate and M_t is the mycelial growth in treatment.

2.9.6 Determining the Efficacy of the Test Compounds in Inhibiting the Spore Germination of Three Fungal Phytopathogens

All three test compounds were examined to confirm whether they affect the spore germination of fungal phytopathogens and subsequently contribute to antifungal activities. Various concentrations (0.005%, 0.010%, 0.015%, and 0.020% w/v) of the test compounds were included in the assay (Paul et al., 1993). A suspension of 1.0×10^3 spores/ml of all the fungi was prepared aseptically from a 7-day-old pure culture. The 1:1 ratio of spore suspension and the test compounds (50 µl each) were mixed in microtiter plate in 10 replicates. The plates were incubated at 29 ± 1°C for 24 h followed by microscopic observation using glass slide. The percent inhibition rate was determined by counting the number of spores germinated as compared to control using the bright-field microscope (Zeiss, Germany). The following formula described by Saharan et al. (2013) is used to calculate the inhibition percentage:

$$\%\ \text{Inhibition rate} = \frac{G_c - G_t}{G_c} \times 100,$$

where G_c is the germination in control and G_t is the germination in treatment.

2.10 Statistical Analysis

All the experiments were performed in triplicate, and the results were arranged as the mean ± standard deviation (SD). Data were then analyzed using ANOVA. The repeated measurements and differences were considered to be significant at a level of $p < 0.05$.

3 RESULTS

3.1 Biomass Production and Extraction of Chitosan From *C. echinulata*

Submerged fermentation carried out by inoculating *C. echinulata* NCIM 691 into a PDB medium (a nutritionally rich) encouraged

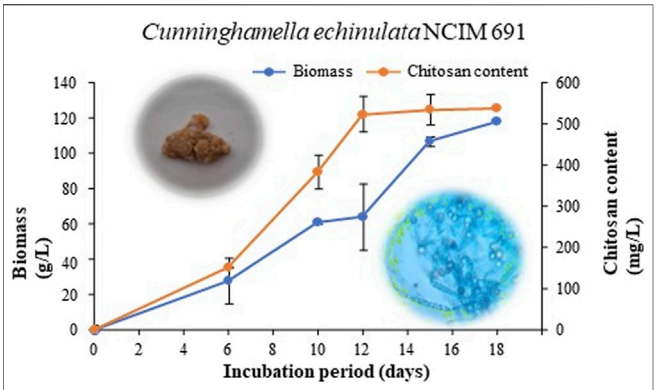

FIGURE 1 | Biomass and chitosan content of *C. echinulata* NCIM 691 grown in potato dextrose broth.

satisfactory growth of the fungal biomass. The growth curve of *C. echinulata* demonstrating the production of biomass and FCH was carried out successfully for up to 18 days (**Figure 1**). The lag and exponential phases were seen between 0 and 6 days and 6 and 12 days, respectively. After 12 days of incubation, the fungus exhibited a deceleration phase. The optimal harvesting of FCH was achieved efficaciously on the 12th day of the incubation period. Physicochemical parameters encompassing acidic pH (5.5), aeration (180 rpm), and temperature (30°C) supported a luxurious growth of *C. echinulata* NCIM 691 with a biomass of 64.2 g/L. The maximum yield of FCH found was 523 mg/L under the same cultivation parameters after the 12th day of incubation (**Figure 1**).

3.2 Physicochemical Characterization of Fungal Chitosan and Chitosan Nanoparticles

We have characterized FCH and FCHNPs through several analytical techniques. Commercial CH and its synthesized CHNPs included in the study facilitated confirmation of both test compounds under investigation. Each of the techniques being sensitive could authenticate and confirmed the presence of FCH and FCHNPs in all the test samples. The results for each of the analytical techniques are given in the following sections.

3.3 UV-Visible Spectroscopy

This technique displayed unique optical properties of FCH and FCHNPs that are sensitive to shape, size, and concentration. Additionally, the information about the agglomeration state and refractive index near the NP surface enabled the UV-Vis technique as a valued tool for detecting and characterizing the nanomaterial under investigation. The commercial CH and CHNPs depicted absorption at 300 and 290 nm, respectively. The UV-visible spectroscopic graph showed higher intensity absorption peaks in FCHNPs than FCH at 315 and 300 nm, respectively (refer **Supplementary Figure S1**). The operative technique facilitated analysis of the functional group, their energy transition, and the bandgap also helped in determining the kind of interaction in the compound. Overall, the analysis has successfully measured the extinction (scatter and absorption) of the light after passing through all the samples.

3.4 Dynamic Light Scattering and Zeta Potential

The DLS technique was performed to measure hydrodynamic diameter in the nanometer range. The size of commercial CH and the synthesized CHNPs along with FCH and FCHNPs has been illustrated in **Supplementary Table S1**. The zeta potential measurements revealed that the cationic FCHNPs (45.6 mV > 24.5 mV) possess more charges than CHNPs.

3.5 Fourier Transform Infra-Red Spectroscopy

FTIR absorption spectra of commercial CH, CHNPs, FCH, and FCHNPs are illustrated in **Figure 2**. For CH, the C-H stretching vibrations were manifested through strong peaks at around 2,869 cm^{-1}. A similar characteristic peak (at 2,864 cm^{-1}) was also obtained for extracted FCH. The FCHNPs synthesized by us also displayed the distinctive peak at 2,916 cm^{-1}. The symmetric stretch of C-O-C was observed at around 1,020–1,057 cm^{-1} in four samples. As seen in both spectra, the strong peaks in the range 3,398–3,346 cm^{-1} correspond to combined peaks of OH and intramolecular hydrogen bonding. The broadness of the peak in this region might be attributed due to the contributions from N-H bond stretches. In FCHNPs, a shift from 3,446 to 3,398 cm^{-1} was observed. A wider peak at 3,461 cm^{-1} was observed for FCH indicating an extensive hydrogen bonding. The characteristic $CO\text{-}NH_2$ peak of FCH at around 1,557 cm^{-1} was found to be shifted to 1,563 cm^{-1} in the FCHNPs, which could be due to the cross-linking of TPP with the ammonium groups present in FCHNPs. This cross-linking between the TPP and the ammonium groups might be imperative for the inter- and intra-molecular interactions.

3.6 Scanning Electron Microscopy

The SEM revealed that the particle size of FCHNPs ranges between 70 and 150 nm. The aggregation in FCHNPs occurred due to moisture entrapment. The images captured through the SEM technique showed spherical-shaped FCHNPs (**Figure 3**). The particle size of CHNPs was found to have a variable range of 200–300 nm.

3.7 Nanoparticle Size Analysis

The NTA technique assisted in estimating the average size of both NPs (CHNPs and FCHNPs) from the plot of particle size versus concentration as represented in **Figure 4**. The average size of CHNPs and FCHNPs is represented in **Supplementary Table S1**. Additionally, the particle size versus relative intensity scattered (**Figure 4B**) and 3D plot (**Figure 4C**) confirmed the nature (with respect to homogeneity) of CHNPs synthesized from commercial CH. The size versus relative intensity scattered (**Figure 4E**) and 3D plot (**Figure 4F**) demonstrated the superior homogenous

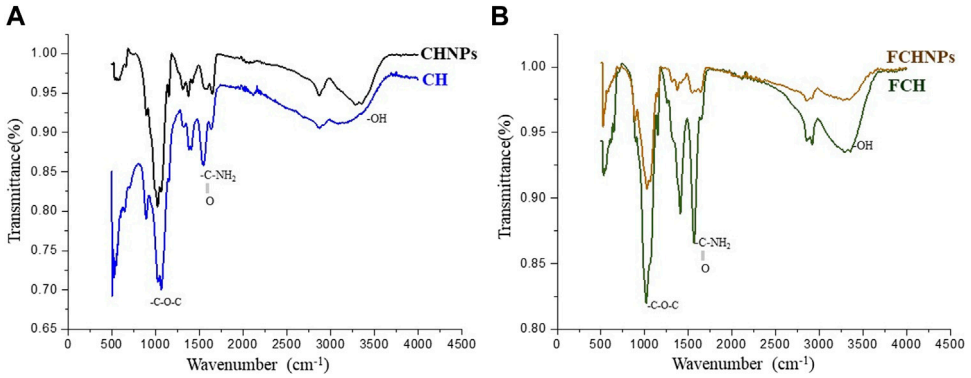

FIGURE 2 | FTIR spectra of **(A)** commercially available chitosan (CH) and synthesized nanoparticles (CHNPs). **(B)** Fungus *C. echinulata*-originated chitosan (FCH) and its synthesized chitosan nanoparticles (FCHNPs).

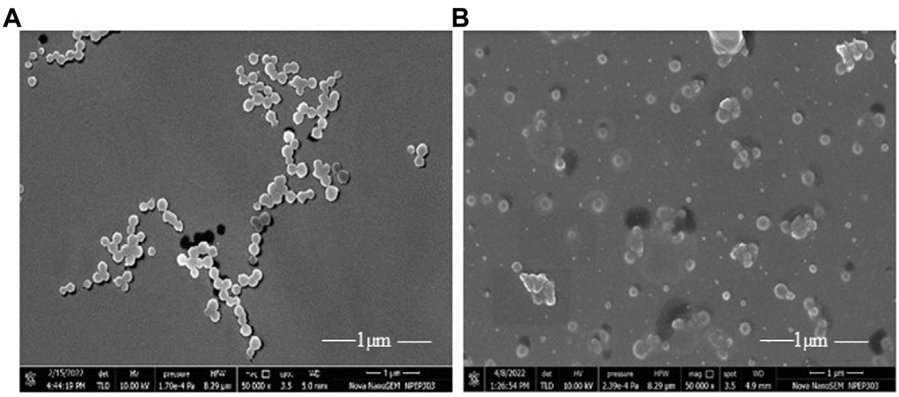

FIGURE 3 | Scanning electron micrograph of synthesized nanoparticles. **(A)** CHNPs from commercial chitosan (CH) and **(B)** FCHNPs from fungal chitosan (FCH) extracted from *C. echinulata* NCIM 691.

nature of FCHNPs as compared with CHNPs. The CHNPs were quite uneven with varied sizes (**Figure 4A–C**), while a single peak was observed for FCHNPs corresponding to homogeneous particle size (**Figure 4D–F**). Thus, the NTA methodology manifested the relationship between NP size distribution and concentration successfully.

3.7.1 Microdilution Assay for Determination of MIC of Rhamnolipid Biosurfactant, Fungal Chitosan, and Synthesized Chitosan Nanoparticles

Antibacterial activities of all the test compounds—RH-BS, FCH, and FCHNPs were inspected from MIC against Gram-negative bacterium *X. campestris* NCIM 5028. It was observed that *X. campestris* treated with RH-BS alone had the lowest MIC of 256 µg/ml among the other two test compounds. The MIC for FCH and FCHNPs was found to be > 1,024 µg/ml against the same bacterium. Therefore, the bacterium *X. campestris* NCIM 5028 used in the experiment was resistant to FCH and FCHNPs. It is important to note that the MIC is not actually a single solitary number, nevertheless a range based on the dilution series performed during its determination.

3.7.2 Synergistic Activity of Rhamnolipid Biosurfactant and Synthesized Chitosan Nanoparticles Using Fungal Chitosan Against *X. campestris*

The in vitro synergistic activity of the test compounds in two combinations (RH-BS + FCH and RH-BS + FCHNPs) was carried out against *X. campestris* NCIM 5028. The microdilution checkerboard assay enabled us to determine the synergistic or additive effect of both combinations against the test bacterium. The first combination of RH-BS with FCH could inhibit *X. campestris* at sub-MIC levels. The combination between RH-BS and FCH resulted in a reduction in the MIC of RH-BS by one-fold and FCH by more than two folds. In the case of the second combination of RH-BS with FCHNPs, the synergy was comparatively greater since the MIC of RH-BS was reduced to one-fold and of FCHNPs was more than eight folds. Thus, the highest level of synergistic effect was observed between RH-BS and FCHNPs. An FICI of both combinations is denoted in **Supplementary Table S2**. Overall, we detected a momentous decrease in MICs of RH-BS and FCHNPs suggesting a powerful synergy (FICI 0.503) between this combination. However, the MICs of FCH did not reduce down up to 8 µg/ml against *X.*

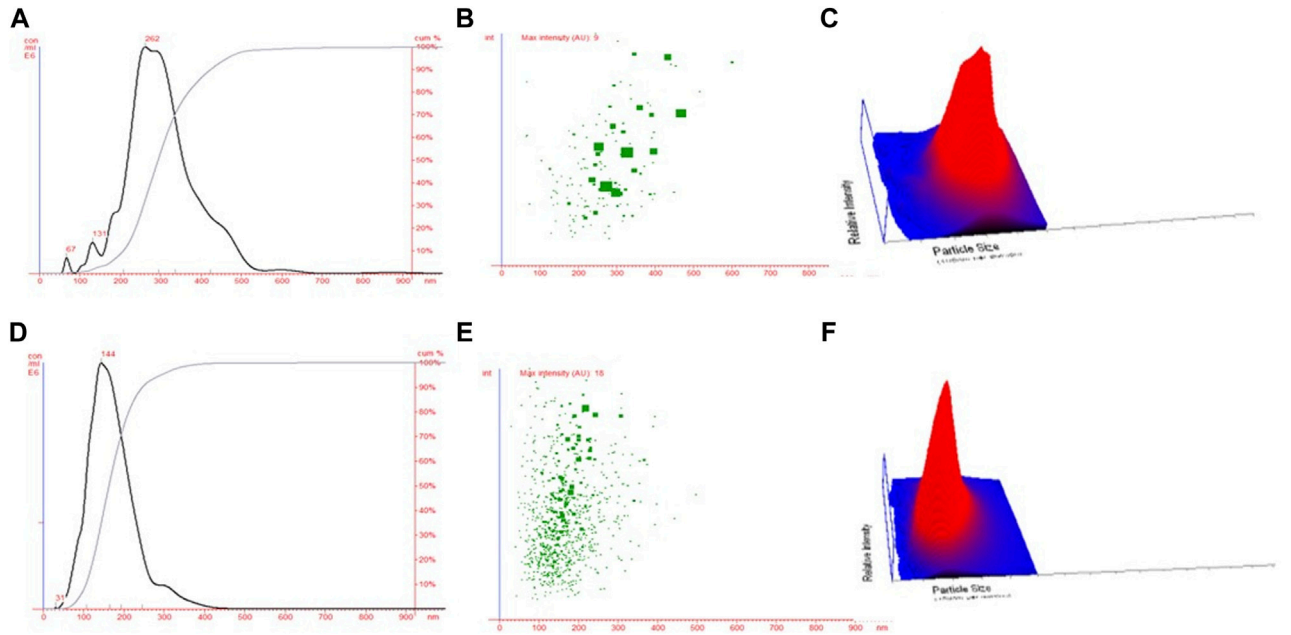

FIGURE 4 | Nanoparticle tracking analysis. **(A)** Particle size versus concentration plot estimating the average size of CHNPs synthesized from commercial CH. Particle size versus relative intensity of CHNPs synthesized using commercial CH in **(B)** scattered and **(C)** 3D plot. **(D)** Particle size versus concentration plot estimating the average size of NPs synthesized from fungal CH extracted from *C. echinulata* NCIM 691. Particle size versus relative intensity of FCHNPs synthesized using fungal CH in **(E)** scattered and **(F)** 3D plot.

campestris. Thus, the breakpoint level due to the synergy between RH-BS and FCH could have been observed if there had reduction in MIC of FCH up to 8 μg/ml.

3.7.3 Effect of the Test Compounds on Cell Morphology of *X. campestris*

The SEM technique clearly evidenced the effect of test compounds individually (FCH, RH-BS, and FCHNPs) and in both combinations (RH-BS + FCH and RH-BS + FCHNPs) on cellular morphology of *X. campestris* NCIM 5028 when treated and incubated on a rotatory shaker for 24 h (at 30°C/180 rpm) at their respective MICs. The control or the bacterial suspension in absence of the test compounds showed very distinct and intact morphology (**Figure 5A**). The slight alteration in the cell morphology of the pathogen was seen in presence of FCH (MIC: >1,024 μg/ml) (**Figure 5B**) and RH-BS (MIC: 256 μg/ml) (**Figure 5C**) during their individual treatment in comparison to control. The cell morphology was well deformed in the presence of FCHNPs when used individually (MICs: 128 μg/ml) (**Figure 5D**). The SEM manifested the distinctive morphological alteration/ destruction of the pathogen after getting treated by the first combination (RH-BS + FCH) (**Figure 5E**) and a second combination (RH-BS + FCHNPs) (**Figure 5F**). Consequently, noticeable changes in the morphology of *X. campestris* designated that cell wall, membrane permeability, and viscosity were certainly compromised by synergistic activities of the test compounds.

3.7.4 Antifungal Activity of the Test Compounds Against Selected Phytopathogens

The in vitro assessment of the MIC of all the test compounds was performed against three fungi, viz., FI, FII, and FIII through the microdilution method. The growth of FI and FII was inhibited effectively by RH-BS and FCHNPs at 0.015% concentration. However, the growth of the pathogen FIII was apparent in the presence of all the three test compounds (RH-BS, FCH, and FCHNPs) at 0.015% concentration. In comparison with RH-BS and FCHNPs, the growth of FI and FII was not inhibited effectively by FCH even at the highest concentration (0.020%). These observations were further confirmed by the poisoned food technique as described in the following section. The commercially available fungicide CBD included in the study also inhibited the growth of all three fungal pathogens at the lowest concentration (0.005%). The wells in the absence of all the three test compounds and CBD presented heavy fungal growth.

3.7.5 Poisoned Food Technique

A routinely employed in vitro poisoned food technique facilitated assessing the effect of the test compounds against three fungal phytopathogens (FI, FII, and FIII). The antifungal activity of the test compounds was evident from the reduction in the mycelial growth of the test fungi in poisoned plates as compared with the control plates (**Figure 6**). Control plates (absence of the test compounds) denoted luxuriant growth of all the three fungal pathogens on a PDA plate. In the case of FI, the application of RH-BS at the highest concentration (0.020%) hampered the

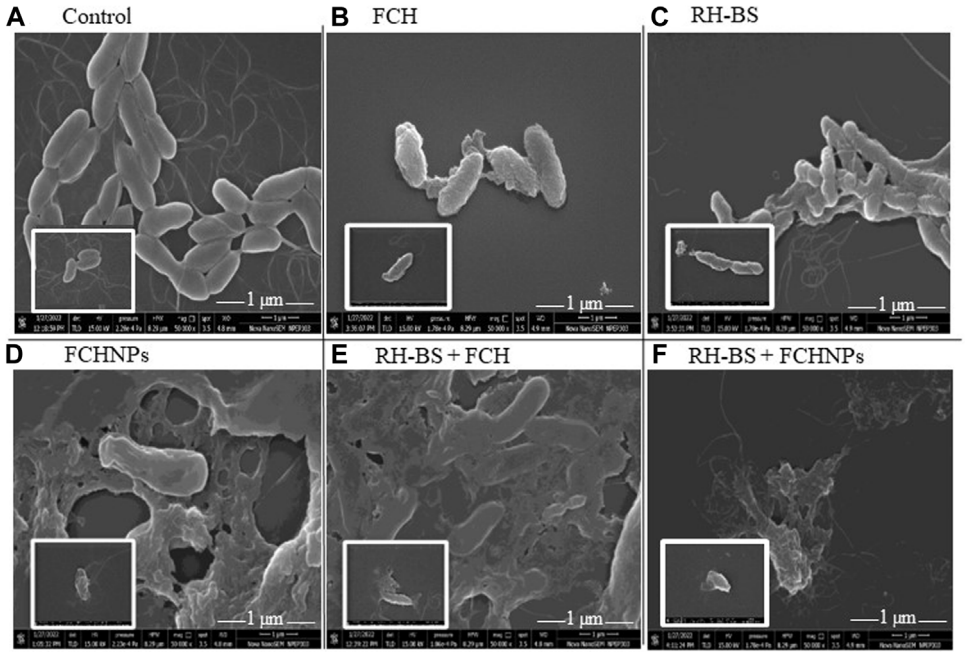

FIGURE 5 | Scanning electron microscopy images (×50,000) demonstrating the effect of three test compounds individually (FCH, RH-BS, and FCHNPs) and in two combinations (RH-BS + FCH and RH-BS + FCHNPs) at MIC (treated for 24 h and incubated at 30°C) on cellular morphology of the bacterial pathogen *Xanthomonas campestris* NCIM 5028. **(A)** Control—intact morphology of the untreated cells. **(B)** Alteration in the cell morphology of pathogen when treated with FCH at MIC (>1,024 µg/ml). **(C)** Alteration in the cell morphology of pathogen when treated with RH-BS at MIC (256 µg/ml). **(D)** Ruptured appearance of the cells of the pathogen when treated with FCHNPs at MIC (>1,024 µg/ml). **(E)** Ruptured appearance of the cells of the pathogen when treated with RH-BS (128 µg/ml) and FCH (256 µg/ml) at MIC. **(F)** Complete distortion of cells of the pathogen due to RH-BS (128 µg/ml) and FCHNPs at lower MIC (4 µg/ml) in comparison to control.

growth of the pathogen by 1.68 folds. The mycelial growth of the same pathogen (FI) was inhibited by around 1.78 folds with increased concentration (0.015–0.020%) of FCHNPs. Thus, the dose-dependent inhibition of FI was observed (**Figure 6FI**). In the case of FII, similar kinds of observations were noted. When pathogen FII was treated with RH-BS, the growth was inhibited by 1.12 folds. Around 1.75 folds inhibition in FII mycelial growth was observed in the presence of FCHNPs at 0.015% and 0.020% concentrations (**Figure 6FII**). In the case of the third pathogen FIII, both RH-BS and FCHNPs inhibited mycelial growth in around 1.40 folds (at 0.015% concentration) and 1.24 folds (at 0.020% concentration), respectively (**Figure 6FIII**). Both the fungal pathogens (FII and FIII) were found slightly resistant since their mycelial growth was not inhibited so effectually as compared with FI. The positive control—CBD—the commercial fungicide—was found to be effective against all three fungal phytopathogens even at the lowest concentration (0.005%). The complete results are summarized in **Supplementary Table S3**.

3.7.6 Spore Germination Method

The effects of RH-BS, FCH, and FCHNPs on the spore germination rate of the three fungal phytopathogens are presented in **Figure 7** as FI, FII, and FIII separately. Among three test compounds, the biomaterial FCHNPs significantly inhibited the spore germination in a dose-dependent manner.

The RH-BS prominently inhibited the spore germination of FI with 69.22% and 81.87% at concentrations of 0.015% and 0.020%, respectively, while FCH was found to be less effective in inhibiting the spore germination rate of the said fungus. The percentages of inhibition of 41.89% and 43% were observed when FCH was used at 0.015% and 0.020% concentrations, respectively, indicating the resistance of the fungal pathogen. It is important to note that among all the three test compounds, FCHNPs were found to be powerful antifungal agents exhibiting around 77.5% and 89.9% inhibition at concentrations of 0.0150% and 0.020%, respectively (**Figure 7A**).

In the case of the fungus FII, observations were similar to the FI fungal pathogen. The RH-BS inhibited the spore germination of the fungus by 56.23% and 68.32% when it was applied at a concentration of 0.015% and 0.020%, respectively, whereas FCH minimally inhibited the growth of the said pathogen by 12.62% (at 0.015% concentration) and 13.10% (at 0.020% concentration). It is noteworthy that FCHNPs are quite commanding in inhibiting the germination of spores with 65.50% and 88.56% at concentrations of 0.015% and 0.020%, respectively (**Figure 7B**).

In the case of the third fungal pathogen (FIII), the findings were the same as the first (FI) and the second (FII) pathogen. RH-BS maximally suppressed the spore germination of FIII by 58.64% (at 0.015% concentration) and 61.02% (at 0.020% concentration), whereas FCH inhibited the spore by 13.32% and 12.9% at concentrations of 0.015% and 0.020%, respectively. The

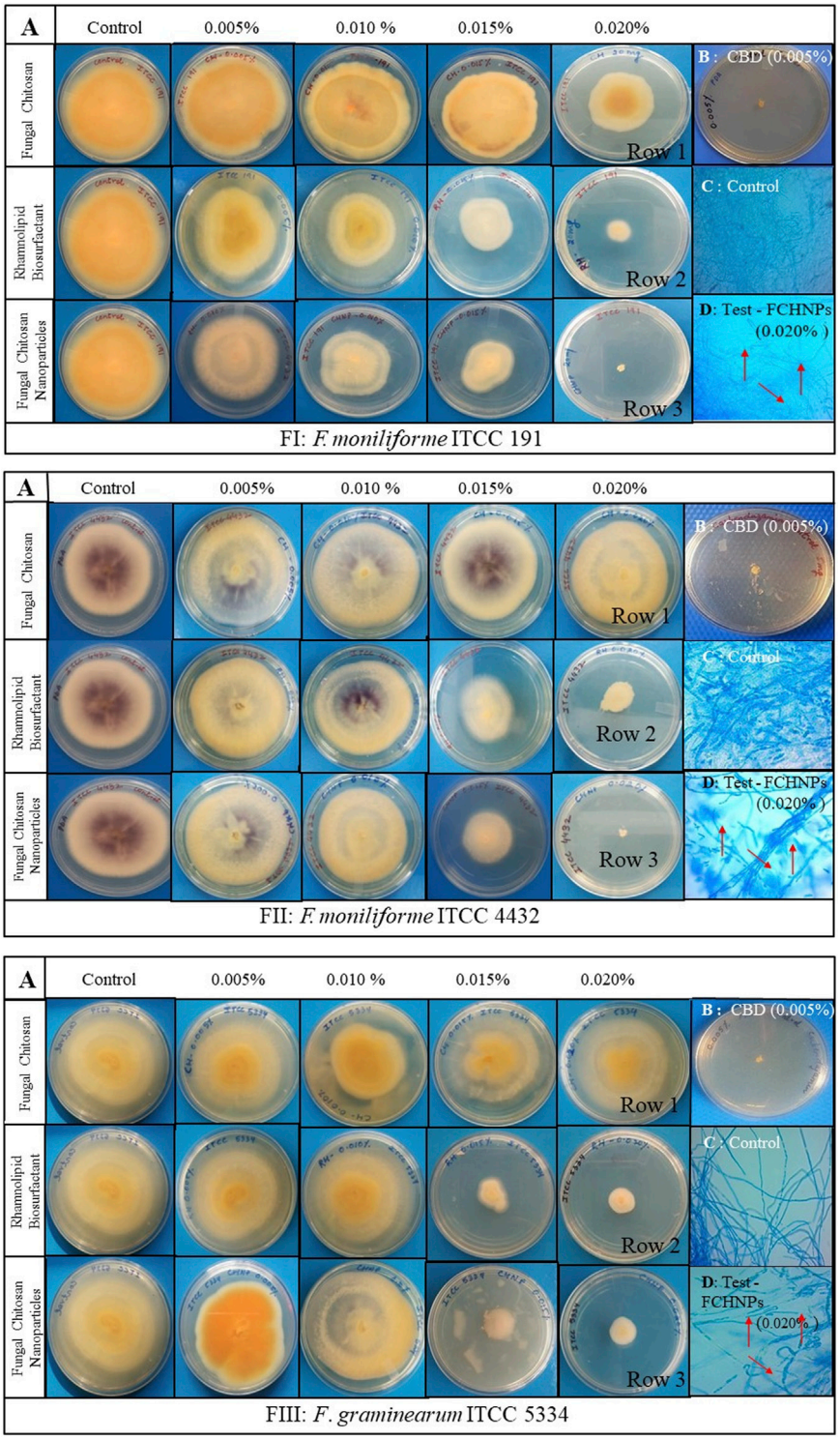

FIGURE 6 | *In vitro* interaction of rhamnolipid biosurfactant (RH-BS), fungal chitosan (FCH), and synthesized chitosan nanoparticles (FCHNPs) against three fungal phytopathogens FI: *F. moniliforme* Sheldon ITCC 191, FII: *F. moniliforme* Sheldon ITCC 4432, and FIII: *F. graminearum* Schwabe ITCC 5334 depicting the morphological alterations. **(A)** Antifungal bioassay demonstrating the effect of the test compounds on mycelial growth of FI, FII, and FIII when treated at different concentrations (0.005%, 0.010%, 0.015%, and 0.020% w/v); **(B)** CBD: 0.005% carbendazim; **(C)** Control: lactophenol cotton blue staining of fungal mycelia without any distortion in absence of the test compounds; **(D)** Test: lactophenol cotton blue staining of the distorted mycelia of fungi when treated with FCHNPs at 0.020% concentration.

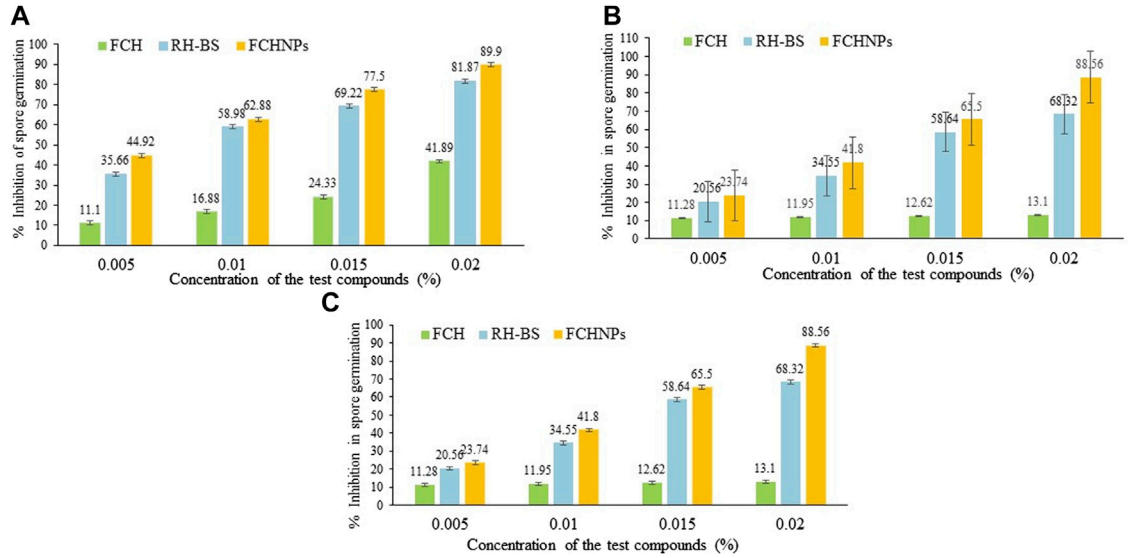

FIGURE 7 | Graphical representation of inhibition in spore germination via rhamnolipid biosurfactant (RH-BS), fungal chitosan (FCH), and synthesized chitosan nanoparticles (FCHNPs) of fungal phytopathogens. **(A)** FI: *F. moniliforme* Sheldon ITCC 191; **(B)** FII: *F. moniliforme* Sheldon ITCC 4432; and **(C)** FIII: *F. graminearum* Schwabe ITCC 5334.

FCHNPs were found to be again highly effective in inhibiting around 59.5% and 66.28% of the spore germination at a concentration of 0.015% and 0.020%, respectively (**Figure 7C**).

Overall, among the three test compounds, FCHNPs have been identified as the most potent biomaterial in inhibiting spore germination (between 59% and 90%) of all fungal phytopathogens. Followed by FCHNPs, a reasonable level of inhibition in spore germination (between 56% and 81%) was observed in all three fungi when treated with RH-BS, whereas FCH showed the lowest percentages (between 12% and 43%) in inhibition of fungal spore germination. In conclusion, all these three test biomaterials exhibited inhibition in spore germination of the fungi in a dose-dependent manner. Amongst all the three test fungi, FI was found to be affected more severely followed by FII and FIII.

4 DISCUSSION

There is a constant exploration of strategies to cope with current issues related to sustainability, food security, and climate change to provide achievable solutions for agriculture. The application of innovative biomaterials for the advancement of disease management is one such approach (Sathiyabama and Parthasarathy, 2016). In recent years, antimicrobials such as RH-BS, FCH, and FCHNPs have emerged as promising candidates for controlling disease outbreaks and pathogens. Comparatively to their synthetic counterparts, BS is an effective substitute to inhibit phytopathogens (Goswami and Deka, 2021). One of the many antimicrobial compounds available is RH-BS produced by *Pseudomonas* spp. Similar to the biomaterials (FCH and FCHNPs), surface-active agents also have a dynamic role in handling a range of pathogens (Sathiyabama and Parthasarathy, 2016). All these biomaterials are considered to be valued pesticides for controlling plant pathogens in promising ways. Considering the inevitability of the current situation, we have utilized Zygomycetes fungus—*C. echinulata*, NCIM 691—to produce FCH in nutrient-rich PDB. The fungus grew luxuriously (biomass 64.2 g/L) with a high content of FCH (523.3 mg/L) on the 12th day of submerged fermentation (**Figure 1**). The fact that the fermentation processes dedicatedly carried out for the extraction of FCH from its biomass is comparatively costlier. Nonetheless, the anticipated features like DDA, molecular weight, and viscosity of CH for the purpose of comprehensive perspective encourage the researchers to cultivate fungal biomass on large scale. Being less explored and considering the immense biotechnological applications, *C. echinulata* is a worthwhile alternative over crustacean sources (no seasonal limitations like marine sources) for the production of FCH and FCHNPs. We have carried out the characterization of CH, CHNPs, FCH, and FCHNPs through various analytical techniques (UV-visible, DLS, zeta potential, FTIR, SEM, and NTA) and confirmed their authenticity. The size of NPs and zeta potential are crucial parameters that affect the antimicrobial properties of biomaterials (Barrera-Necha et al., 2018). The characterization study through NTA revealed a nondispersive nature and small size (144.33 ± 10.20 nm) of FCHNPs and had a zeta potential value of +45.6 mV as compared to FCH (particle size via DLS 960.6 ± 57.17 nm) and zeta potential +37 mV. The NTA also confirmed the homogeneous size of FCHNPs as compared to CHNPs (refer **Figure 4**). All the observations accomplished through the physicochemical characterization of both biomaterial (FCH and FCHNPs) are well comparable with the published literature (Saharan et al., 2013; Kheiri et al., 2017; Shajahan et al., 2017; Oh et al., 2019).

After completing the characterization of FCH and FCHNPs, we continued to explore their antimicrobial potential along with

commercially available RH-BS against harmful phytopathogens. Even though the RH-BS has been studied extensively (with respect to producing organisms, production, optimization, physicochemical characterization), their innovative applications particularly as biocidal agent in agriculture are limited. We chose a bacterial pathogen *X. campestris*, which is a causative agent of citrus bacterial canker disease, banana Xanthomonas wilt, and black rot in cabbage, etc. (Leite and Mohan, 1990). Generally, the genera of *Xanthomonas* leads to postharvest diseases in several fruits and vegetables (Barth et al., 2009). Citrus fruits, banana, mango, and many other vegetables like tomato, cabbage, cauliflower, radish, turnip, and broccoli are usually spoiled by several *Xanthomonas* spp. The RH-BS is certainly effective in controlling the *X. campestris*. The outer membrane of *X. campestris* is composed of phospholipids, lipopolysaccharides, and lipoproteins which are covalently linked together with the peptidoglycan layer through hydrophobic interactions (Sikkema et al., 1995). The RH-BS inhibits pathogens through the damage to the cell membrane. A similar kind of observation has been reported for *Bacillus subtilis*. The mechanism of RH-BS involves an alteration in the lipid composition of the membrane due to an increase in the activity of cardiolipin (negatively charged phospholipid) and enhances membrane susceptibility of *B. subtilis* (Sotirova et al., 2012). The surface-active agent attacks pathogens and liberates their intracellular contents leading to the disruption and cell lysis (Kumar et al., 2021). The lower MIC (256 μg/ml) of RH-BS was observed against *X. campestris* as compared to FCH and FCHNPs (>1,024 μg/ml) when used individually. However, the two combination studies of RH-BS + FCH (128 μg/ml + 256 μg/ml) and RH-BS + FCHNPs (128 μg/ml + 4 μg/ml) resulted in additive (FICI is 0.75) and synergistic (FICI is 0.50) effects, respectively. Hence, our work significantly demonstrates a substantial decrease in MICs of RH-BS and FCHNPs suggesting a powerful synergistic activity against *X. campestris*.

Like bacteria, plant pathogenic fungi have acquired severe resistance against conventional agrochemicals (Gill and Garg, 2014). We conducted two antifungal assays (poisoned food assay and spore germination inhibition) for RH-BS, FCH, and FCHNPs against three fungal phytopathogens comprising *F. moniliforme* (two strains) that attack sugarcane, maize, rice, and fig and *F. graminearum* (single strain) that attack maize, wheat, and barley (Vishwakarma et al., 2013). Both techniques used by us have demonstrated a dose-dependent manner antifungal effect of RH-BS, FCH, and FCHNPs against the selected fungi (FI, FII, and FIII). The literature documents the noteworthy antifungal activity of RH-BS without harming the soil ecology unlike synthetic fungicides (Lahkar et al., 2018). Crouzet et al. (2020) reviewed the potential of RH-BS in a sustained agriculture framework suggesting the enhancement in plant immunity (local/systemic). The antimicrobial potential of RH-BS can be improved by combination with other biomaterials like FCH and FCHNPs. The NPs synthesized using biopolymer CH and BSs have attained flickered curiosity. The addition of RH-BS for the preparation of nanoconjugates facilitates a smaller and uniform size and the polydispersity index of CHNPs in productive ways. RH-BS stabilizes the CH particles and results in superior loading efficiency (Marangon et al. 2020). Generally, CH assembles actively at the surface of fungi/bacteria and permeabilizes the cell membrane through their electrostatic interactions (positive charges of CH and the negatively charged molecules at the cell surface of microbes). Consequently, the cell surface permeabilization leads to leakage of intracellular material leading to cell death (Palma-Guerrero et al., 2010; Krajewska et al., 2011). The other mechanisms involve the chelating action of CH, which binds to trace elements and thus becomes unavailable for the normal growth of microbe. The CH might penetrate through the fungal cell wall and inhibits protein and DNA synthesis (El-Naggar et al., 2022). The fungicidal action of FCH and FCHNPs is correlated with the modification of membrane permeability of the cell wall component of the pathogen (Dorocka-Bobkowska et al., 2003). The robust bonding of CH to the fungal cell wall decreases the negative surface charge of fungal membranes due to a decrease in K^+ concentration, and this efflux disturbs the osmotic balance of the cell wall. The FCHNPs due to small particle size result in their better uptake into microbial cells and exhibit an antimicrobial effect (de Carvalho et al., 2019). The FCHNPs synthesized by us appear to bear a strong antimicrobial activity as compared with its origin material, FCH. NPs being nano in size and surface-to-charge ratio have been greatly associated with their unique functional activity (Kutawa et al., 2021). Thus, nanomaterial proves to be highly supportive in the form of nanoformulations to use as pesticides and/or fertilizers in improving crop yield. Furthermore, the nanosensors also offer applications in protecting enormous crops through the detection of agrochemicals residues (Pestovsky and Martínez-Antonio, 2017). The research conveys that the NPs act on the nucleic acids where DNA loses replication phenomena and ultimately inactivates protein expression as well as enzymes which are imperative for ATP production (Abdel-Aliem et al., 2019). The larger surface area of NPs empowers them to get adsorb firmly onto the microbial surfaces resulting in cell disruption by altering the membrane integrity. Thus, these NPs diffuse into fungal cells and inhibit the synthesis of DNA, RNA, mitochondrial function, and protein synthesis (Kutawa et al., 2021).

Most of the fungi exhibit pathogenicity and long-term survival due to their spore-forming abilities. Germination of spores is the crucial step to recruit vegetative growth and results in perilous diseases by many fungal pathogens (Ortiz et al., 2019). The unique morphology of the fungal spores is a precise target for designing and developing innovative antifungal drugs. Our study on RH-BS, FCH, and FCHNPs documents inhibition in spore germination of the selected fungi in a dose-dependent manner (0.005%, 0.010%, 0.015%, and 0.020% w/v). The inhibition of the spore germination was initiated for RH-BS and FCHNPs at 0.010% and 0.015% concentrations, respectively. Thus, RH-BS and FCHNPs pose promising applications in controlling the growth of spore-forming dreaded fungal phytopathogens. RH-BS has a repressive effect on the breeding and growth of pathogenic fungi through inhibition in spore germination (Yan et al., 2015). Recent studies have recognized the antifungal potential of RH-BS through zoospore lysis, spore

germination abortion, and mycelial growth inhibition. The amphiphilic nature of BS enables them to interact with plasma membranes (Crouzet et al., 2020). The mode of action of BS is via lysis of mycelial cells resulting in their destabilization through their intercalation with the bilayers of phosphatidylcholine and phosphatidylethanolamine. Thus, the effect on membrane permeabilization is significant due to the cell lysis of the fungal pathogen. The RH-BS explicates defense responses that are induced by other elicitors like CH. Thus, these molecules cause local resistance in hemibiotrophic fungus *Leptosphaeria maculans* ultimately protecting *Brassica napus* (Monnier et al., 2020). Recently, a few members of our research group (Chopra et al., 2020) have reported promising antimicrobial activity of *P. aeruginosa* RTE4 origin RH-BS against phytopathogens *X. campestris*, *F. solani*, and *Corticium invisum*. Thus, the strain RTE4-derived RH-BS has an application as a powerful biofungicide. Through the present work, we have extended our efforts to utilize the antimicrobial potential of RH-BS with FCHNPs (from CH of fungus origin) in controlling phytopathogens. The RH-BS coupled with FCHNPs has positively improved their efficacy. The amended antimicrobial activity is related to the augmented delivery of RH-BS and FCHNPs at the cell surface of the pathogen. A similar kind of work has been reported by Marangon et al. (2020) for CHNPs (synthesized using CH of crustacean origin) in combination with RH-BS to improve antibacterial efficacy through greater electrostatic interactions and more effective disruption of the pathogen's cell membrane. The mechanism involves the high density of polycationic NPs over the cell envelope. The stated combination study of these two biomaterials offers a promising strategy to design a biological low cytotoxic nanoformulation for the agriculture sector. When these biomaterials are used individually, they are less effective against selected pathogens; however, their synergistic activities certainly raise inquisitiveness among the research community to explore diverse innovative applications. Furthermore, in vivo assays are in the process to examine the influence of RH-BS and FCHNPs against phytopathogens.

5 CONCLUSION

In the present work, we have successfully produced the stable, valuable, and high-quality FCH from the fungal mycelia of *C. echinulata* NCIM 691. Furthermore, FCHNPs were synthesized magnificently using *C. echinulata*-originated FCH through the ionic gelation method. Matricular physicochemical characterization of FCH and FCHNPs assured their authenticity. The improvised antibacterial activity of RH-BS and FCHNPs was observed in combination against *X. campestris*. Promising antimicrobial activity of RH-BS with FCHNPs against selected phytopathogens encouraged us to recommend these types of novel bioformulation for the future. Plenty of monitoring protocols is obligatory to utilize nanoagrochemicals as active substance, coformulants, with or without other adjuvants. The difficulty in tracking the role/mechanism of these nanocarriers in food and the environment gratifies the use of biologically originated NPs. It is important to highlight that not much work has been reported so far in deliberating the biocontrol potential of RH-BS with FCH and FCHNPs for their synergistic and additive activity against phytopathogens associated with staple (rice, wheat, maize, and barley) and commercially important crops (citrus fruits, mango, banana, date palm fruits, cruciferous vegetables, and turfgrass, etc.). Our work demonstrating the synergistic activity of RH-BS with FCHNPs is crucial in facilitating eco-friendly formulations against harmful phytopathogens.

DATA AVAILABILITY STATEMENT

The raw data supporting the conclusion of this article will be made available by the authors, without undue reservation.

AUTHOR CONTRIBUTIONS

BK performed all the laboratory experiments and was involved in writing the preliminary draft. PM assisted in the conduct of the experiments. SW, DS, PR, and VG analyzed the data and were involved in editing the manuscript. SD and SS contributed to conceptualization, designing the methodology, interpretations, and review and editing of the manuscript. All authors read carefully and approved the final version of the manuscript.

ACKNOWLEDGMENTS

The authors acknowledge the financial support received from Savitribai Phule Pune University and Rashtriya Uchchatar Shiksha Abhiyan (Ref. No: RUSA-CBS-TH-3.2) and the technical support from the Vasantdada Sugar Institute (VSI), Pune.

SUPPLEMENTARY MATERIAL

The Supplementary Material for this article can be found online at: https://www.frontiersin.org/articles/10.3389/fbioe.2022.917105/full#supplementary-material

REFERENCES

Abdel-Aliem, H. A., Gibriel, A. Y., Rasmy, N. M. H., Sahab, A. F., El-Nekeety, A. A., and Abdel-Wahhab, M. A. (2019). Antifungal Efficacy of Chitosan Nanoparticles against Phytopathogenic Fungi and Inhibition of Zearalenone Production by *Fusarium graminearum*. *Com. Sci.* 10, 338–345. doi:10.14295/cs.v10i3.1899

Agarwal, M., Agarwal, M. K., Shrivastav, N., Pandey, S., Das, R., and Gaur, P. (2018). Preparation of Chitosan Nanoparticles and Their *In-Vitro* Characterization. *Ijlssr* 4, 1713–1720. doi:10.21276/ijlssr.2018.4.2.17

Anitha, A., Divya Rani, V. V., Krishna, R., Sreeja, V., Selvamurugan, N., and Nair, S. V. (2009). Synthesis, Characterization, Cytotoxicity and Antibacterial Studies of Chitosan, O-Carboxymethyl and N, O-Carboxymethyl Chitosan Nanoparticles. *Carbohydr. Polym.* 78, 672–677. doi:10.1016/J.CARBPOL.2009.05.028

Barrera-Necha, L. L., Correa-Pacheco, Z. N., Bautista-Baños, S., Hernández-López, M., Jiménez, J. E. M., and Mejía, A. F. M. (2018). Synthesis and Characterization of Chitosan Nanoparticles Loaded Botanical Extracts with Antifungal Activity on *Colletotrichum gloeosporioides* and *Alternaria* species. *Adv. Microbiol.* 8, 286. doi:10.4236/aim.2018.84019

Barth, M., Hankinson, T. R., Zhuang, H., and Breidt, F. (2009). in *Microbiological Spoilage of Fruits and Vegetables" in* Compendium Of the Microbiological Spoilage of Foods and Beverages. Editors W. H. Sperber and M. P. Doyle (New York: Springer), 135–183. doi:10.1007/978-1-4419-0826-1_6

Chopra, A., Bobate, S., Rahi, P., Banpurkar, A., Mazumder, P. B., and Satpute, S. (2020). *Pseudomonas aeruginosa* RTE4: A Tea Rhizobacterium with Potential for Plant Growth Promotion and Biosurfactant Production. *Front. Bioeng. Biotechnol.* 8, 861. doi:10.3389/fbioe.2020.00861

Cota-Arriola, O., Onofre Cortez-Rocha, M., Burgos-Hernández, A., Marina Ezquerra-Brauer, J., and Plascencia-Jatomea, M. (2013). Controlled Release Matrices and Micro/nanoparticles of Chitosan with Antimicrobial Potential: Development of New Strategies for Microbial Control in Agriculture. *J. Sci. Food Agric.* 93, 1525–1536. doi:10.1002/jsfa.6060

Crouzet, J., Arguelles-Arias, A., Dhondt-Cordelier, S., Cordelier, S., Pršić, J., Hoff, G., et al. (2020). Biosurfactants in Plant Protection against Diseases: Rhamnolipids and Lipopeptides Case Study. *Front. Bioeng. Biotechnol.* 8, 1014. doi:10.3389/FBIOE.2020.01014

de Carvalho, F. G., Magalhaes, T. C., Teixeira, N. M., Gondim, B. L. C., Carlo, H. L., Dos Santos, R. L., et al. (2019). Synthesis and Characterization of TPP/chitosan Nanoparticles: Colloidal Mechanism of Reaction and Antifungal Effect on *C. albicans* Biofilm Formation. *Mat. Sci. Eng. C* 104, 109885. doi:10.1016/J.MSEC.2019.109885

de Pinho Neves, A. L., Milioli, C. C., Müller, L., Riella, H. G., Kuhnen, N. C., and Stulzer, H. K. (2014). Factorial Design as Tool in Chitosan Nanoparticles Development by Ionic Gelation Technique. *Colloids Surf. A* 445, 34–39. doi:10.1016/j.colsurfa.2013.12.058

Divya, K., Vijayan, S., George, T. K., and Jisha, M. S. (2017). Antimicrobial Properties of Chitosan Nanoparticles: Mode of Action and Factors Affecting Activity. *Fibers Polym.* 18, 221–230. doi:10.1007/S12221-017-6690-1

Dorocka-Bobkowska, B., Konopka, K., and Düzgüneş, N. (2003). Influence of Antifungal Polyenes on the Adhesion of *Candida albicans* and *Candida glabrata* to Human Epithelial Cells *In Vitro*. *Arch. Oral Biol.* 48, 805–814. doi:10.1016/S0003-9969(03)00174-2

El-Naggar, N. E. A., Saber, W. I., Zweil, A. M., and Bashir, S. I. (2022). An Innovative Green Synthesis Approach of Chitosan Nanoparticles and Their Inhibitory Activity against Phytopathogenic *Botrytis cinerea* on Strawberry Leaves. *Sci. Rep.* 12, 1–20. doi:10.1038/s41598-022-07073-y

Elshikh, M., Ahmed, S., Funston, S., Dunlop, P., McGaw, M., Marchant, R., et al. (2016). Resazurin-based 96-well Plate Microdilution Method for the Determination of Minimum Inhibitory Concentration of Biosurfactants. *Biotechnol. Lett.* 38, 1015–1019. doi:10.1007/s10529-016-2079-2

Fischer, E. R., Bryan, T. H., Nair, V., Hoyt, F. H., and Dorward, D. W. (2012). Scanning Electron Microscopy. *Curr. Protoc. Microbiol.* (May). doi:10.1002/9780471729259.mc02b02s25

Ghadi, A., Mahjoub, S., Tabandeh, F., and Talebnia, F. (2014). Synthesis and Optimization of Chitosan Nanoparticles: Potential Applications in Nanomedicine and Biomedical Engineering. *Casp. J. Intern. Med.* 5, 156.

Ghormade, V., Pathan, E. K., and Deshpande, M. V. (2017). Can Fungi Compete with Marine Sources for Chitosan Production? *Int. J. Biol. Macromol.* 104, 1415–1421. doi:10.1016/J.IJBIOMAC.2017.01.112

Gill, H. K., and Garg, H. (2014). "Pesticide: Environmental Impacts and Management Strategies," in *Pesticides-Toxic Aspects*. Editors M. L. Larramendy and S. Solonesky (Rijeka: Croatia: In Tech), 187. doi:10.5772/57399

Goswami, M., and Deka, S. (2021). "Biosurfactant-Mediated Biocontrol of Pathogenic Microbes of Crop Plants," in *Biosurfactants for a Sustainable Future: Production and Applications in the Environment and Biomedicine*. Editors H. Sarma and M. N. V. Prasad (United States: Wiley), 491–509. doi:10.1002/9781119671022.ch22

Gu, D., Andreev, K., and Dupre, M. E. (2021). Major Trends in Population Growth Around the World. *China CDC Wkly.* 3, 604. doi:10.46234/ccdcw2021.160

Hosseinnejad, M., and Jafari, S. M. (2016). Evaluation of Different Factors Affecting Antimicrobial Properties of Chitosan. *Int. J. Biol. Macromol.* 85, 467–475. doi:10.1016/j.ijbiomac.2016.01.022

Kah, M., and Kookana, R. (2020). Emerging Investigator Series: Nanotechnology to Develop Novel Agrochemicals: Critical Issues to Consider in the Global Agricultural Context. *Environ. Sci. Nano.* 7, 1867–1873. doi:10.1039/D0EN00271B

Karamchandani, B. M., Chakraborty, S., Dalvi, S. G., and Satpute, S. K. (2022). Chitosan and its Derivatives: Promising Biomaterial in Averting Fungal Diseases of Sugarcane and Other Crops. *J. Basic Microbiol.*, 1–22. doi:10.1002/jobm.202100613

Kheiri, A., Jorf, S. M., Malihipour, A., Saremi, H., and Nikkhah, M. (2017). Synthesis and Characterization of Chitosan Nanoparticles and Their Effect on Fusarium Head Blight and Oxidative Activity in Wheat. *Int. J. Biol. Macromol.* 102, 526–538. doi:10.1016/j.ijbiomac.2017.04.034

Khoerunnisa, F., Nurhayati, M., Dara, F., Rizki, R., Nasir, M., Aziz, H. A., et al. (2021). Physicochemical Properties of TPP-Crosslinked Chitosan Nanoparticles as Potential Antibacterial Agents. *Fibers Polym.* 22, 2954–2964. doi:10.1007/S12221-021-0397-Z

Konaté, K., Mavoungou, J. F., Lepengué, A. N., Aworet-Samseny, R. R., Hilou, A., Souza, A., et al. (2012). Antibacterial Activity against β-lactamase Producing Methicillin and Ampicillin-Resistant *Staphylococcus aureus*: Fractional Inhibitory Concentration Index (FICI) Determination. *Ann. Clin. Microbiol. Antimicrob.* 11, 1–12. doi:10.1186/1476-0711-11-18

Krajewska, B., Wydro, P., and Jańczyk, A. (2011). Probing the Modes of Antibacterial Activity of Chitosan. Effects of pH and Molecular Weight on Chitosan Interactions with Membrane Lipids in Langmuir Films. *Biomacromol* 12, 4144–4152. doi:10.1021/bm2012295

Kumar, A., Singh, S. K., Kant, C., Verma, H., Kumar, D., Singh, P. P., et al. (2021). Microbial Biosurfactant: a New Frontier for Sustainable Agriculture and Pharmaceutical Industries. *Antioxid* 10, 1472. doi:10.3390/antiox10091472

Kutawa, A. B., Ahmad, K., Ali, A., Hussein, M. Z., Abdul Wahab, M. A., Adamu, A., et al. (2021). Trends in Nanotechnology and its Potentialities to Control Plant Pathogenic Fungi: A Review. *Biol* 10, 881. doi:10.3390/biology10090881

Lahkar, J., Goswami, D., Deka, S., and Ahmed, G. (2018). Novel Approaches for Application of Biosurfactant Produced by *Pseudomonas aeruginosa* for Biocontrol of *Colletotrichum capsici* Responsible for Anthracnose Disease in Chilli. *Eur. J. Plant Pathol.* 150, 57–71. doi:10.1007/s10658-017-1252-3

Leite, R. P., Jr, and Mohan, S. K. (1990). Integrated Management of the Citrus Bacterial Canker Disease Caused by *Xanthomonas campestris* Pv. *citri* in the State of Paraná. *Braz. Crop Prot.* 9, 3–7. doi:10.1016/0261-2194(90)90038-9

Malerba, M., and Cerana, R. (2018). Recent Advances of Chitosan Applications in Plants. *Polymers* 10, 118. doi:10.3390/polym10020118

Maluin, F. N., and Hussein, M. Z. (2020). Chitosan-based Agronanochemicals as a Sustainable Alternative in Crop Protection. *Mol* 25, 1611. doi:10.3390/molecules25071611

Marangon, C. A., Martins, V. C., Ling, M. H., Melo, C. C., Plepis, A. M. G., Meyer, R. L., et al. (2020). Combination of Rhamnolipid and Chitosan in Nanoparticles Boosts Their Antimicrobial Efficacy. *ACS Appl. Mat. Interfaces* 12, 5488–5499. doi:10.1021/ACSAMI.9B19253

Mazzotta, E., Muzzalupo, R., Chiappetta, A., and Muzzalupo, I. (2022). Control of the Verticillium Wilt on Tomato Plants by Means of Olive Leaf Extracts Loaded on Chitosan Nanoparticles. *Microorganisms* 10, 136. doi:10.3390/microorganisms10010136

Mirzaei-Najafgholi, H., Tarighi, S., Golmohammadi, M., and Taheri, P. (2017). The Effect of Citrus Essential Oils and Their Constituents on Growth of *Xanthomonas citri* Subsp. *Citri. Mol.* 22, 591. doi:10.3390/molecules22040591

Monnier, N., Cordier, M., Dahi, A., Santoni, V., Guénin, S., Clément, C., et al. (2020). Semipurified Rhamnolipid Mixes Protect *Brassica napus* against *Leptosphaeria maculans* Early Infections. *Phytopathology* 110, 834–842. doi:10.1094/PHYTO-07-19-0275-R

Oh, J. W., Chun, S. C., and Chandrasekaran, M. (2019). Preparation and *In Vitro* Characterization of Chitosan Nanoparticles and Their Broad-Spectrum Antifungal Action Compared to Antibacterial Activities against Phytopathogens of Tomato. *Agronomy* 9, 21. doi:10.3390/agronomy9010021

Okoliegbe, I. N., Hijazi, K., Cooper, K., Ironside, C., and Gould, I. M. (2021). Antimicrobial Synergy Testing: Comparing the Tobramycin and Ceftazidime Gradient Diffusion Methodology Used in Assessing Synergy in Cystic Fibrosis-Derived Multidrug-Resistant *Pseudomonas aeruginosa*. *Antibiot* 10, 967. doi:10.3390/ANTIBIOTICS10080967

Ortiz, S. C., Huang, M., and Hull, C. M. (2019). Spore Germination as a Target for Antifungal Therapeutics. *Antimicrob. Agents Chemother.* 63, e00994–19. doi:10.1128/AAC.00994-19

Palma-Guerrero, J., Lopez-Jimenez, J. A., Pérez-Berná, A. J., Huang, I. C., Jansson, H. B., Salinas, J., et al. (2010). Membrane Fluidity Determines Sensitivity of Filamentous Fungi to Chitosan. *Mol. Microbiol.* 75, 1021–1032. doi:10.1111/j.1365-2958.2009.07039.x

Paul, G. C., Kent, C. A., and Thomas, C. R. (1993). Viability Testing and Characterization of Germination of Fungal Spores by Automatic Image Analysis. *Biotechnol. Bioeng.* 42, 11–23. doi:10.1002/bit.260420103

Pawlak, A., and Mucha, M. (2003). Thermogravimetric and FTIR Studies of Chitosan Blends. *Thermochim. Acta.*, 153–166. doi:10.1016/S0040-6031(02)00523-3

Pestovsky, Y. S., and Martinez-Antonio, A. (2017). The Use of Nanoparticles and Nanoformulations in Agriculture. *J. Nanosci. Nanotechnol.* 17, 8699–8730. doi:10.1166/jnn.2017.15041

Pochanavanich, P., and Suntornsuk, W. (2002). Fungal Chitosan Production and its Characterization. *Lett. Appl. Microbiol.* 35, 17–21. doi:10.1046/J.1472-765X.2002.01118.X

Rahi, S., Lanjekar, V., and Ghormade, V. (2022). Development of a Rapid Dot-Blot Assay for Ochratoxin A (OTA) Detection Using Peptide Conjugated Gold Nanoparticles for Bio-Recognition and Detection. *Food control.* 136, 108842. doi:10.1016/j.foodcont.2022.108842

Sachdev, D. P., and Cameotra, S. S. (2013). Biosurfactants in Agriculture. *Appl. Microbiol. Biotechnol.* 97, 1005–1016. doi:10.1007/s00253-012-4641-8

Saharan, V., Mehrotra, A., Khatik, R., Rawal, P., Sharma, S. S., and Pal, A. (2013). Synthesis of Chitosan-Based Nanoparticles and Their *In Vitro* Evaluation against Phytopathogenic Fungi. *Int. J. Biol. Macromol.* 62, 677–683. doi:10.1016/J.IJBIOMAC.2013.10.012

Sathiyabama, M., and Parthasarathy, R. (2016). Biological Preparation of Chitosan Nanoparticles and It's *In Vitro* Antifungal Efficacy against Some Phytopathogenic Fungi. *Carbohydr. Polym.* 151, 321–325. doi:10.1016/j.carbpol.2016.05.033

Shajahan, A., Shankar, S., Sathiyaseelan, A., Narayan, K. S., Narayanan, V., Kaviyarasan, V., et al. (2017). Comparative Studies of Chitosan and its Nanoparticles for the Adsorption Efficiency of Various Dyes. *Int. J. Biol. Macromol.* 104, 1449–1458. doi:10.1016/j.ijbiomac.2017.05.128

Sharma, D. (2021). "Role of Biosurfactants in Agriculture and Soil Reclamation," in *Biosurfactants:* Greener Surface Active Agents For Sustainable Future (Singapore: Springer). doi:10.1007/978-981-16-2705-7_5

Sikkema, J., de Bont, J. A., and Poolman, B. (1995). Mechanisms of Membrane Toxicity of Hydrocarbons. *Microbiol. Rev.* 59, 201–222. doi:10.1128/mr.59.2.201-22210.1128/mr.59.2.201-222.1995

Sotirova, A., Avramova, T., Stoitsova, S., Lazarkevich, I., Lubenets, V., Karpenko, E., et al. (2012). The Importance of Rhamnolipid-Biosurfactant-Induced Changes in Bacterial Membrane Lipids of *Bacillus subtilis* for the Antimicrobial Activity of Thiosulfonates. *Curr. Microbiol.* 65, 534–541. doi:10.1007/s00284-012-0191-7

Staroń, A., and Długosz, O. (2021). Antimicrobial Properties of Nanoparticles in the Context of Advantages and Potential Risks of Their Use. *J. Environ. Sci. Health. Part A.* 56, 680–693. doi:10.1080/10934529.2021.1917936

Vishwakarma, S. K., Kumar, P., Nigam, A., Singh, A., and Kumar, A. (2013). Pokkah Boeng: An Emerging Disease of Sugarcane. *J. Plant Pathol. Microbiol.* 4, 2. doi:10.4172/2157-7471.1000170

Yan, F., Xu, S., Guo, J., Chen, Q., Meng, Q., and Zheng, X. (2015). Biocontrol of Post-harvest *Alternaria alternata* Decay of Cherry Tomatoes with Rhamnolipids and Possible Mechanisms of Action. *J. Sci. Food Agric.* 95, 1469–1474. doi:10.1002/jsfa.6845

Zgoda, J. R., and Porter, J. R. (2001). A Convenient Microdilution Method for Screening Natural Products against Bacteria and Fungi. *Pharm. Biol.* 39, 22. doi:10.1076/phbi.39.3.221.5934

Conflict of Interest: Author PR was employed by TeeGene and TARA Biologics.

The remaining authors declare that the research was conducted in the absence of any commercial or financial relationships that could be construed as a potential conflict of interest.

Advantages of publishing in Frontiers

OPEN ACCESS
Articles are free to read for greatest visibility and readership

FAST PUBLICATION
Around 90 days from submission to decision

HIGH QUALITY PEER-REVIEW
Rigorous, collaborative, and constructive peer-review

TRANSPARENT PEER-REVIEW
Editors and reviewers acknowledged by name on published articles

Frontiers
Avenue du Tribunal-Fédéral 34
1005 Lausanne | Switzerland

Visit us: www.frontiersin.org
Contact us: frontiersin.org/about/contact

REPRODUCIBILITY OF RESEARCH
Support open data and methods to enhance research reproducibility

DIGITAL PUBLISHING
Articles designed for optimal readership across devices

FOLLOW US
@frontiersin

IMPACT METRICS
Advanced article metrics track visibility across digital media

EXTENSIVE PROMOTION
Marketing and promotion of impactful research

LOOP RESEARCH NETWORK
Our network increases your article's readership